FU JEN STUDIES

SCIENCE AND ENGINEERING

No.45, May 2012

CONTENTS

輔仁學誌 — 理工類

中華民國101年5月　　第四十五期

目　錄

頁次

Maximum Likelihood Estimator of the Three-Parameter Generalized Beta Distribution

Sy-Mien Chen

Department of Mathematics
Fu-Jen Catholic University, Taiwan, R. O. C.

Abstract

This research investigates the maximum likelihood estimators for the three-parameter Generalized Beta distribution. It lays out the conditions for the central limit theorem of MLE besides the Fisher information matrix. Statistical inferences are also discussed. A simulation study is carried out to explore the bias and standard error of the maximum likelihood estimator. In addition, the hazard function is studied when all the three parameters are unknown.

Key words: words: CLT; Digamma function; Trigamma function; Incomplete Beta function; Simulated annealing; MLE.

*E-mail address:smchen@math.fju.edu.tw

1. Introduction

The three-parameter generalized beta distribution was also named the Sahinoglu-Libby (SL) distribution due to the fact that the distribution was pioneered in 1981 by Sahinoglu[14]. In 1982, Libby and Novick [8] proposed a multivariate generalized beta distribution of the first kind with applications to utility assessment. For the univariate case, the three-parameter generalized beta distribution is denoted as G3B (α, β, γ) or G3B for short. Apart from being more flexible than the regular Beta distribution, the three-parameter generalized beta distribution is very versatile and is capable of modeling a variety of uncertainties. Gelfand (1987)[4] applied the distribution to the problem of Bayesian estimation of the ratio of two variances. Sahinoglu (2000)[15] used the distribution to study the reliability of integrated software network when the software failure and recovery data are insufficient. Sahinoglu and Libby (2003)[16] formulated the density function of the unavailability or variability random variables by G3B distribution in order to estimate the network reliability and quality indices for engineering and utility considerations. By assuming that the forced outage ratio of an embedded hardware component follows G3B, Sahinoglu, Libby and Das (2005)[17] evaluated availability index with small samples for component and network reliability. Nadarajah (2005a)[10] discussed some probability properties of G3B, which includes the moment generation function, expectation, variance and the Rényi entropy. Nadarajah (2005b)[11] also considered the densities of the sums, products and ratio of two random variates from G3B. Chen and Chen (2008)[3] discussed G3B from Bayesian point of view. See Pham-Gia (1989) [12], Kegan and West (2005)[5], Chen and Lin (2005)[2], Verheijen (2001)[20], Bandourian *et. al.* (2002)[1], Kleiber (2005)[6], Tunaru and Albota (2005)[19], Sepanski and Kong (2007) [18] for more applications.

So far most of the results in the literature about G3B(α, β, γ) are probability properties. However, in the real world, the knowledge of the objects which we are interested in is estimated from data collected, and it is important to know the statistical properties of the estimator in order to prevent from misinterpretation. In this paper, we study the inference problem except the sampling distribution of G3B. In section 2, the three parameter generalized beta distribution is reviewed. Some of its properties are derived. In section 3, the

maximum likelihood estimator (MLE) is considered. A numerical and simulation study is presented in section 4. Conclusions are given in section 5.

2. Maximum Likelihood Approach

A random variable X is said to follow a Libby- Novick (or Sahinoglu-Libby) three-parameter Generalized Beta distribution G3B(α, β, γ), if it has the probability density function

$$f_X(x) = \frac{\gamma^{\alpha} x^{\alpha-1}(1-x)^{\beta-1}}{B(\alpha,\beta)\{1-(1-\gamma)x\}^{\alpha+\beta}}, \text{ for } 0<x<1, \quad \alpha,\beta,\gamma>0.$$

The shape of the density functions of G3B(α, β, γ) varies under different values of parameters, see Fig 1.

The hazard function of G3B is defined as

$$h_X(t) = \frac{\gamma^{\alpha} t^{\alpha-1}(1-t)^{\beta-1}}{B(\alpha,\beta)\{1-I_{\frac{\gamma t}{1+(\gamma-1)t}}(\alpha,\beta)\}\{1-(1-\gamma)t\}^{\alpha+\beta}}$$ which is increasing in t,

where $B(\alpha,\beta)=\int_0^1 u^{\alpha-1}(1-u)^{\beta-1}du$ is the complete beta function and

$I_z(\alpha,\beta)=\dfrac{\int_0^z u^{\alpha-1}(1-u)^{\beta-1}du}{B(\alpha,\beta)}$ is the incomplete beta function.

Let $X_1, X_2, ..., X_n$ be a sample with sample size n from G3B (α, β, γ) distribution, then the log likelihood function is defined by

$$l(\alpha,\beta,\gamma \mid x) = \alpha n \ln(\gamma) + (\alpha-1)\sum_{i=1}^{n}\ln(x_i) + (\beta-1)\sum_{i=1}^{n}\ln(1-x_i) - n\ln B(\alpha,\beta) - (\alpha+\beta)\sum_{i=1}^{n}\ln[1-(1-\gamma)x_i].$$

By differentiating the log likelihood function with respect to α, β and γ respectively and

setting the results to zeros, we have the following estimating equations:

$$\left.\begin{aligned} \frac{\partial l}{\partial \alpha} &= n\ln\gamma - n\{\Psi_0(\alpha)-\Psi_0(\alpha+\beta)\} + \sum_{i=1}^{n}\ln[\frac{x_i}{1-(1-\gamma)x_i}] = 0 \\ \frac{\partial l}{\partial \beta} &= -n\{\Psi_0(\beta)-\Psi_0(\alpha+\beta)\} + \sum_{i=1}^{n}\ln[\frac{1-x_i}{1-(1-\gamma)x_i}] = 0 \\ \frac{\partial l}{\partial \gamma} &= \frac{\alpha n}{\gamma} - (\alpha+\beta)\sum_{i=1}^{n}\frac{x_i}{1-(1-\gamma)x_i} = 0 \end{aligned}\right\} \quad (2)$$

where Ψ_0 is the digamma function defined by $\Psi_0(m) = \frac{d}{dm}\ln\Gamma(m)$.

Let Ψ_1 be the trigamma function defined by $\Psi_1(m) = \frac{d^2}{dm^2}\ln\Gamma(m)$.

Lemma 1: Let $X_1, X_2, ..., X_n$ be a random sample from G3B (α, β, γ) distribution with parameters α, β, γ. Then with probability tending to 1 as n tends to infinity, there exist solutions of the likelihood equations.

Proof: It is easy to see that the pdf of G3B (α, β, γ) meets the regularity conditions (A0)~(A2) in section 6.3 and (A)~(B) in section 6.5 of Lehmann and Casella (1998). Furthermore, since the trigamma function $\Psi_1(m)$ is decreasing in m, the regularity conditions (C) and (D) in section 6.5 of Lehmann and Casella hold by Lemma 3, Lemma 4, Lemma 8.

Theorem: Let $X_1, X_2, ..., X_n$ be a random sample from G3B (α, β, γ) distribution with parameters α, β, γ. Let $\hat{\alpha}_M, \hat{\beta}_M, \hat{\gamma}_M$ be themaximum likelihood estimator of α, β, γ, respectively.

(1-1) $\hat{\alpha}_M$ is consistent for estimating α and is asymptotically efficient in the sense that

$$\sqrt{n}(\hat{\alpha}_M - \alpha) \text{ is AN } \left(0, \frac{1}{\Psi_1(\alpha)-\Psi_1(\alpha+\beta)}\right)$$

(1-2) $\hat{\beta}_M$ is consistent for estimating β and is asymptotically efficient in the sense that

$$\sqrt{n}(\hat{\beta}_M - \beta) \text{ is AN } \left(0, \frac{1}{\Psi_1(\beta)-\Psi_1(\alpha+\beta)}\right)$$

(1-3) $\hat{\gamma}_M$ is consistent for estimating γ and is asymptotically efficient in the sense that

$\sqrt{n}(\hat{\gamma}_M - \gamma)$ is AN $(0, \frac{(\alpha+\beta+1)\gamma^2}{\alpha\beta})$.

(2-1) $\sqrt{n}[(\hat{\alpha}_M, \hat{\beta}_M) - (\alpha, \beta)]$ is asymptotically normal with mean zero vector and covariance matrix

$$\frac{1}{D_{12}}\begin{pmatrix} \Psi_1(\beta) - \Psi_1(\alpha+\beta) & \Psi_1(\alpha+\beta) \\ \Psi_1(\alpha+\beta) & \Psi_1(\alpha) - \Psi_1(\alpha+\beta) \end{pmatrix},$$

where $D_{12} = \Psi_1(\alpha)\Psi_1(\beta) - \Psi_1(\alpha+\beta)(\Psi_1(\alpha) + \Psi_1(\beta))$.

(2-2) $\sqrt{n}[(\hat{\alpha}_M, \hat{\gamma}_M) - (\alpha, \gamma)]$ is asymptotically normal with mean zero vector and covariance matrix

$$\frac{1}{D_{13}}\begin{pmatrix} \frac{\alpha\beta}{\gamma^2(\alpha+\beta+1)} & \frac{\beta}{\gamma(\alpha+\beta)} \\ \frac{\beta}{\gamma(\alpha+\beta)} & \Psi_1(\alpha) - \Psi_1(\alpha+\beta) \end{pmatrix}, \text{ where}$$

$$D_{13} = \frac{\alpha\beta}{(\alpha+\beta+1)\gamma^2}[\Psi_1(\alpha) - \Psi_1(\alpha+\beta)] - \left[\frac{\beta}{(\alpha+\beta)\gamma}\right]^2.$$

(2-3) $\sqrt{n}[(\hat{\beta}_M, \hat{\gamma}_M) - (\beta, \gamma)]$ is asymptotically normal with mean zero vector and covariance matrix

$$\frac{1}{D_{23}}\begin{pmatrix} \frac{\alpha\beta}{\gamma^2(\alpha+\beta+1)} & -\frac{\alpha}{\gamma(\alpha+\beta)} \\ -\frac{\alpha}{\gamma(\alpha+\beta)} & \Psi_1(\beta) - \Psi_1(\alpha+\beta) \end{pmatrix}, \text{ where}$$

$$D_{23} = \frac{\alpha\beta}{(\alpha+\beta+1)\gamma^2}[\Psi_1(\beta) - \Psi_1(\alpha+\beta)] - \left[\frac{\alpha}{(\alpha+\beta)\gamma}\right]^2.$$

(3) $\sqrt{n}((\hat{\alpha}_M, \hat{\beta}_M, \hat{\gamma}_M) - (\alpha, \beta, \gamma))$ is AN((0,0,0), $\begin{bmatrix} \sigma_{11} & \sigma_{12} & \sigma_{13} \\ \sigma_{21} & \sigma_{22} & \sigma_{23} \\ \sigma_{31} & \sigma_{32} & \sigma_{33} \end{bmatrix}$), and

$$\sigma_{11} = \frac{1}{\det(I)}\left\{\frac{\alpha\beta}{\gamma^2(\alpha+\beta+1)}[\Psi_1(\beta) - \Psi_1(\alpha+\beta)] - \frac{\alpha^2}{\gamma^2(\alpha+\beta)^2}\right\}$$

$$\sigma_{22} = \frac{1}{\det(I)}\left\{\frac{\alpha\beta}{\gamma^2(\alpha+\beta+1)}[\Psi_1(\alpha)-\Psi_1(\alpha+\beta)]-\frac{\beta^2}{\gamma^2(\alpha+\beta)^2}\right\}$$

$$\sigma_{33} = \frac{1}{\det(I)}\{\Psi_1(\alpha)\Psi_1(\beta)-\Psi_1(\alpha+\beta)[\Psi_1(\alpha)+\Psi_1(\beta)]\}$$

$$\sigma_{12} = \sigma_{21} = \frac{-1}{\det(I)}\left\{\frac{\alpha\beta}{\gamma^2(\alpha+\beta+1)}\Psi_1(\alpha+\beta)-\frac{\alpha\beta}{\gamma^2(\alpha+\beta)^2}\right\}$$

$$\sigma_{13} = \sigma_{31} = \frac{1}{\det(I)}\left\{\frac{1}{\gamma(\alpha+\beta)}[\beta\cdot\Psi_1(\beta)-(\alpha+\beta)\Psi_1(\alpha+\beta)]\right\}$$

$$\sigma_{23} = \sigma_{32} = \frac{-1}{\det(I)}\left\{\frac{1}{\gamma(\alpha+\beta)}[\alpha\cdot\Psi_1(\alpha)-(\alpha+\beta)\Psi_1(\alpha+\beta)]\right\}.$$

Proof: The parameter γ has no effect on the conditions for eigenvalues to be positive. By a numerical study viaMATLAB, all three functions with $\alpha, \beta > 0$,

$\Psi_1(\alpha)\Psi_1(\beta)-\Psi_1(\alpha+\beta)[\Psi_1(\alpha)+\Psi_1(\beta)]$,

$\frac{-\beta}{(\alpha+\beta)^2}+\frac{\alpha}{[(\alpha+\beta+1)]}[\Psi_1(\alpha)-\Psi_1(\alpha+\beta)]$ and

$\frac{-\alpha}{(\alpha+\beta)}+\frac{\beta}{(\alpha+\beta+1)}[\Psi_1(\beta)-\Psi_1(\alpha+\beta)]$ are all positive. The theorem is therefore proved by Lemma 2 ~ Lemma 8 in the Appendix and by theorem 5.1 in Lehmann and Casella (1998) [7].

Corrolary 1:Under the same conditions as inTheorem,

(1-1) An approximate 100(1- α^*)% confidence interval of α is given by $\left(\hat{\alpha}_M - z_{\alpha^*/2}\cdot\sigma_{11}/\sqrt{n}, \hat{\alpha}_M + z_{\alpha^*/2}\cdot\sigma_{11}/\sqrt{n}\right)$;

(1-2) An approximate 100(1- α^*)% confidence interval of β is given by $\left(\hat{\beta}_M - z_{\alpha^*/2}\cdot\sigma_{22}/\sqrt{n}, \hat{\beta}_M + z_{\alpha^*/2}\cdot\sigma_{22}/\sqrt{n}\right)$;

(1-3) An approximate 100(1- α^*)% confidence interval of γ is given by $\left(\hat{\gamma}_M - z_{\alpha^*/2}\cdot\sigma_{33}/\sqrt{n}, \hat{\gamma}_M + z_{\alpha^*/2}\cdot\sigma_{33}/\sqrt{n}\right)$.

(2-1) An approximate 100(1- α^*)% Bonferroni joint confidence intervals of (α , β)are given by

$\left(\hat{\alpha}_M - z_{\alpha^*/4} \cdot \sigma_{11} / \sqrt{n}, \hat{\alpha}_M + z_{\alpha^*/4} \cdot \sigma_{11} / \sqrt{n}\right)$ and

$\left(\hat{\beta}_M - z_{\alpha^*/4} \cdot \sigma_{22} / \sqrt{n}, \hat{\beta}_M + z_{\alpha^*/4} \cdot \sigma_{22} / \sqrt{n}\right)$

(2-2) An approximate 100(1- α^*)% Bonferroni joint confidence intervals of (β , γ) are given by

$\left(\hat{\beta}_M - z_{\alpha^*/4} \cdot \sigma_{22} / \sqrt{n}, \hat{\beta}_M + z_{\alpha^*/4} \cdot \sigma_{22} / \sqrt{n}\right)$ and

$\left(\hat{\gamma}_M - z_{\alpha^*/4} \cdot \sigma_{33} / \sqrt{n}, \hat{\gamma}_M + z_{\alpha^*/4} \cdot \sigma_{33} / \sqrt{n}\right)$

(2-3) An approximate 100(1- α^*)% Bonferroni joint confidence intervals of (α , γ) are given by

$\left(\hat{\alpha}_M - z_{\alpha^*/4} \cdot \sigma_{11} / \sqrt{n}, \hat{\alpha}_M + z_{\alpha^*/4} \cdot \sigma_{11} / \sqrt{n}\right)$ and

$\left(\hat{\gamma}_M - z_{\alpha^*/4} \cdot \sigma_{33} / \sqrt{n}, \hat{\gamma}_M + z_{\alpha^*/4} \cdot \sigma_{33} / \sqrt{n}\right)$

(3) An approximate 100(1- α^*)% Bonferroni joint confidence intervals of (α , β , γ) are given by

$\left(\hat{\alpha}_M - z_{\alpha^*/6} \cdot \sigma_{11} / \sqrt{n}, \hat{\alpha}_M + z_{\alpha^*/6} \cdot \sigma_{11} / \sqrt{n}\right)$,

$\left(\hat{\beta}_M - z_{\alpha^*/6} \cdot \sigma_{22} / \sqrt{n}, \hat{\beta}_M + z_{\alpha^*/6} \cdot \sigma_{22} / \sqrt{n}\right)$ and

$\left(\hat{\gamma}_M - z_{\alpha^*/6} \cdot \sigma_{33} / \sqrt{n}, \hat{\gamma}_M + z_{\alpha^*/6} \cdot \sigma_{33} / \sqrt{n}\right)$.

Proof: By Theorem.

Corollary 2: Under the same conditions as inTheorem,

(1-1) The decision rule of an approximate size α^* test of testing $H_0 : \alpha = \alpha_0$ versus $H_1 : \alpha \neq \alpha_0$ is rejecting H_0 if

$|\hat{\alpha}_M - \alpha_0| \geq \sigma_{11} / \sqrt{n} \cdot z_{\alpha^*/2}$.

(1-2) The decision rule of an approximate size α^* test of testing $H_0 : \beta = \beta_0$ versus $H_1 : \beta \neq \beta_0$ is rejecting H_0 if

$|\hat{\beta}_M - \beta_0| \geq \sigma_{22} / \sqrt{n} \cdot z_{\alpha^*/2}$.

(1-3) The decision rule of an approximate size α^* test of

testing $H_0: \gamma = \gamma_0$ versus $H_1: \gamma \neq \gamma_0$ is rejecting H_0 if $|\hat{\gamma}_M - \gamma_0| \geq \sigma_{33}/\sqrt{n} \cdot z_{\alpha^*/2}$.

(2-1) The decision rule of an approximate size α^* test for testing $H_0:(\alpha,\beta)=(\alpha_0,\beta_0)$ versus $H_1:(\alpha,\beta) \neq (\alpha_0,\beta_0)$ is rejecting H_0 if $|\hat{\alpha}-\alpha_0| \geq \sigma_{11}/\sqrt{n} \cdot z_{\alpha^*/4}$ or $|\hat{\beta}-\beta_0| \geq \sigma_{22}/\sqrt{n} \cdot z_{\alpha^*/4}$.

(2-2) The decision rule of an approximate size α^* test for testing $H_0:(\alpha,\gamma)=(\alpha_0,\gamma_0)$ versus $H_1:(\alpha,\gamma) \neq (\alpha_0,\gamma_0)$ is rejecting H_0 if $|\hat{\alpha}-\alpha_0| \geq \sigma_{11}/\sqrt{n} \cdot z_{\alpha^*/4}$ or $|\hat{\gamma}-\gamma_0| \geq \sigma_{33}/\sqrt{n} \cdot z_{\alpha^*/4}$.

(2-3) The decision rule of an approximate size α^* test for testing $H_0:(\beta,\gamma)=(\beta_0,\gamma_0)$ versus $H_1:(\beta,\gamma) \neq (\beta_0,\gamma_0)$ is rejecting H_0 if $|\hat{\beta}-\beta_0| \geq \sigma_{22}/\sqrt{n} \cdot z_{\alpha^*/4}$ or $|\hat{\gamma}-\gamma_0| \geq \sigma_{33}/\sqrt{n} \cdot z_{\alpha^*/4}$.

(3) The decision rule of an approximate size α^* test for testing $H_0:(\alpha,\beta,\gamma)=(\alpha_0,\beta_0,\gamma_0)$ versus $H_1:(\alpha,\beta,\gamma) \neq (\alpha_0,\beta_0,\gamma_0)$ is rejecting H_0 if $|\hat{\alpha}-\alpha_0| \geq \sigma_{11}/\sqrt{n} \cdot z_{\alpha^*/6}$, $|\hat{\beta}-\beta_0| \geq \sigma_{22}/\sqrt{n} \cdot z_{\alpha^*/6}$ or $|\hat{\gamma}-\gamma_0| \geq \sigma_{33}/\sqrt{n} \cdot z_{\alpha^*/6}$.

Proof: By Theorem.

4. Simulation study

4.1 Parameter Setting

Since the explicite form of MLEs involves solving a highly non-linear optimization problem, a numerical method is therefore required. On the other hand, since the positive function Ψ_0 is involved, therefore Simulated Annealing method (Robert and Casella 2004)[13] is preferred over the Newton - Raphson method in finding MLE. While applying the Simulated Annealing method, the temperature function we use to control the cooling is $W(t) = \dfrac{1}{100\ln(1+t)}$ and the size of the interval around the current point is 0.5.

To generate random sample from G3B(α,β,γ) we first generate random numbers W

from Beta(α,β), then take the transformation $\frac{W}{(1-\gamma)W+\gamma}$ (by Lemma 2). About the sample size, when one or two of the parameters are unknown, 50, 100, 300, 500 are considered. When all the three parameters are unknown, the sample sizes used are 300, 500, 1000 and 2000. Based on the time consumption, for small sample sizes the number of iteration is 500 and 100 for large sample. Different combinations of parameters are chosen from 0.3, 0.6, 0.8, 1.2, 1.5, 1.8, 2.0, 2.5, 3.0 and 3.5. For each different combination of parameters, the simulations are repeated 50000 times. All the computations and graphs are done by MATLAB with a PC.

4.2. Simulation Results

Through a Monte Carlo simulation study, the asymptotic results in section 3 are verified. The accuracy is up to the fourth decimal point. Note that the trigamma function $\Psi_1(m)$ decreases to zero as $m \to \infty$, this may render the Fisher information matrix only semi-positive definite. But in practice, huge values of α,β are seldom encountered, so the asymptotic properties of the maximum likelihood estimator in the Theorem can still provide valuable information.

From Fig 2, when only one parameter is unknown, the sampling distributions of the maximum likelihood estimators are skewed to the right for small sample sizes. But when the sample size is large enough, the sampling distributions become more and more symmetric. The bias listed in Table 1 shows that the estimators are asymptotically unbiased. The standard errors decrease as the sample size increases, and are quite close to the theoretical root Cramer Rao Lower bound. These results fit the results we got from section 3. Note that from formula (4)(5)(6) in Lemma 6, the regularity conditions for the asymptotically results to hold are independent from the parameter γ. To reach the same accuracy and precision of each parameter, the sample size needed for γ is larger than those needed for α and β. On the other hand, when the sample size is fixed, the variances of the estimators are $\frac{1}{n[\Psi_1(\alpha)-\Psi_1(\alpha+\beta)]}$, $\frac{1}{n[\Psi_1(\beta)-\Psi_1(\alpha+\beta)]}$ and $\frac{(\alpha+\beta+1)\gamma^2}{n\alpha\beta}$, which are increasing functions of $\alpha,\beta\ \gamma$ respectively. Therefore, the larger the true value of the parameter the larger the sample size is needed.

When two of the parameters are unknown, the scatter plots in Fig 3 show that the estimator $\hat{\alpha}$ and $\hat{\beta}$, $\hat{\alpha}$ and $\hat{\gamma}$ are positive correlated, but $\hat{\beta}$ and $\hat{\gamma}$ are negative correlated, this

agrees with the results in Theorem that $Cov(\hat{\alpha},\hat{\beta}) = c_1\Psi_1(\alpha+\beta)$, $Cov(\hat{\alpha},\hat{\gamma}) = c_2\frac{\beta}{\gamma(\alpha+\beta)}$, $Cov(\hat{\beta},\hat{\gamma}) = -c_3\frac{\alpha}{\gamma(\alpha+\beta)}$ where $c_i > 0$, i=1, 2, 3. The elliptical shapes agree with the asymptotic normality of Theorem. From Table 2, the bias, the standard error and the sum of root mean squared error decrease as the sample size increases.

It is not surprising that one needs a larger sample size to achieve better estimating results when all the three parameters are unknown. The bias, the standard error and the sum of root mean squared error of the estimators of the three unknown parameters are given in Table 3. Both characters decrease as the sample size increases; Again, all the results shown in the table support the Theorem. In addition, the maximum likelihood estimator of the hazard function can be obtained by the invariance property of maximum likelihood estimator. From what we have in the table, the mle of the hazard function is also asymptotically unbiased and the standard error of the estimator of the hazard function decreases as the sample size increases.

5. Conclusions

We have studied the maximum likelihood estimators of the parameters of the three-parameter generalized beta distribution. The conditions for the central limit theorem of the estimators are given. In addition, Bonferroni joint confidence intervals and hypotheses testing problem are also discussed. From the expressions of the system of non-linear equations, we can see that it is not an easy task to solve them analytically. Through a Monte Carlo simulation study, the asymptotic results in section 3 are verified. Simulated annealing method is used to get the maximum likelihood estimators. The accuracy is up to the forth decimal point. For each different combination of parameters, the simulations are repeated 50000 times. The results show that the effect of sample size on the accuracy and precision of estimation, especially on the parameter γ, is quite significant. The effect on the hazard function when all three parameters are unknown is also very significant. Also, the larger the value of unknown parameters, the more difficult the convergence of the simulated annealing technique, eased (in one way among others) by an increase of the sample size.

Even though the trigamma function $\Psi_1(m)$ decreases to zero as $m \to \infty$, which may cause the Fisher information matrix only semi-positive definite. But in real world, huge values of α, β are seldom encountered, so the asymptotic properties of MLE derived in this research is still a valuable information.

Appendix

Lemma 2: Let $X = \dfrac{W}{(1-\gamma)W + \gamma}$. Then $X \sim G3B(\alpha, \beta, \gamma)$ iff $W \sim Beta(\alpha, \beta)$.

Lemma 3: (1) The Fisher information of G3B(α, β, γ) is

$$I(\alpha,\beta,\gamma) = \begin{pmatrix} \Psi_1(\alpha) - \Psi_1(\alpha+\beta) & -\Psi_1(\alpha+\beta) & \dfrac{-\beta}{(\alpha+\beta)\gamma} \\ -\Psi_1(\alpha+\beta) & \Psi_1(\beta) - \Psi_1(\alpha+\beta) & \dfrac{\alpha}{(\alpha+\beta)\gamma} \\ \dfrac{-\beta}{(\alpha+\beta)\gamma} & \dfrac{\alpha}{(\alpha+\beta)\gamma} & \dfrac{\alpha\beta}{(\alpha+\beta+1)\gamma^2} \end{pmatrix} \quad (1)$$

where $\Psi_1(m) = \dfrac{d^2}{dm^2}\ln\Gamma(m) = \int_0^\infty \dfrac{t\, e^{-mt}}{1-e^{-t}}\, dt$, $m > 0$, is the trigamma function, and is decreasing to zero as $m \to \infty$.

(2) The determinant of the Fisher information matrix $I(\alpha, \beta, \gamma)$ is

$$\det(I) = \frac{1}{\gamma^2}\left\{ \begin{array}{l} \dfrac{\alpha\beta}{\alpha+\beta+1}[\Psi_1(\alpha)\Psi_1(\beta) - \Psi_1(\alpha+\beta)(\Psi_1(\alpha)+\Psi_1(\beta))] \\ +\Psi_1(\alpha+\beta) - \dfrac{1}{(\alpha+\beta)^2}[\alpha^2\Psi_1(\alpha) + \beta^2\Psi_1(\beta)] \end{array} \right\}$$

(3) The value of the determinant of the Fisher information matrix $I(\alpha, \beta, \gamma)$ may tend to zero as $\alpha \to \infty$ or $\beta \to \infty$. But for small to moderate large value of α and β, is always positive.

Lemma 4: Let $\Psi_2(m) = \frac{d}{dm}\Psi_1(m) = \frac{d^3}{dm^3}\ln\Gamma(m)$, $m > 0$. Then for given α, β

$$\left|\frac{\partial^3 \ln f(X;\alpha,\beta,\gamma)}{\partial\alpha^3}\right| = \left|-\Psi_2(\alpha) + \Psi_2(\alpha+\beta)\right|;$$

$$\left|\frac{\partial^3 \ln f(X;\alpha,\beta,\gamma)}{\partial\beta^3}\right| = \left|-\Psi_2(\beta) + \Psi_2(\alpha+\beta)\right|;$$

$$\left|\frac{\partial^3 \ln f(X;\alpha,\beta,\gamma)}{\partial\gamma^3}\right| = \left|\frac{2\alpha}{\gamma^3} - (\alpha+\beta)\frac{2X^3}{[1-(1-\gamma)X]^3}\right|;$$

$$\left|\frac{\partial^3 \ln f(X;\alpha,\beta,\gamma)}{\partial\alpha^2\partial\beta}\right| = \left|\frac{\partial^3 \ln f(X;\alpha,\beta,\gamma)}{\partial\beta^2\partial\alpha}\right| = \left|\Psi_2(\alpha+\beta)\right|;$$

$$\left|\frac{\partial^3 \ln f(X;\alpha,\beta,\gamma)}{\partial\alpha^2\partial\gamma}\right| = \left|\frac{\partial^3 \ln f(X;\alpha,\beta,\gamma)}{\partial\beta^2\partial\gamma}\right| = \left|\frac{\partial^3 \ln f(X;\alpha,\beta,\gamma)}{\partial\alpha\,\partial\beta\,\partial\gamma}\right| = 0;$$

$$\left|\frac{\partial^3 \ln f(X;\alpha,\beta,\gamma)}{\partial\gamma^2\partial\alpha}\right| = \left|-\frac{1}{\gamma^2} + \left(\frac{X}{1-(1-\gamma)X}\right)^2\right|$$

$$\left|\frac{\partial^3 \ln f(X;\alpha,\beta,\gamma)}{\partial\gamma^2\partial\beta}\right| = \left(\frac{X}{1-(1-\gamma)X}\right)^2;$$

Lemma 5: The characteristic polynomial of the Fisher information matrix is

$$-\lambda^3 + \{\Psi_1(\alpha) + \Psi_1(\beta) - 2\Psi_1(\alpha+\beta) + \frac{\alpha\beta}{\gamma^2(\alpha+\beta+1)}\}\lambda^2 - \{$$

$$\frac{\alpha\beta}{\gamma^2(\alpha+\beta+1)}[\Psi_1(\alpha) + \Psi_1(\beta) - 2\Psi_1(\alpha+\beta)] +$$

$$[\Psi_1(\alpha) - \Psi_1(\alpha+\beta)][\Psi_1(\beta) - \Psi_1(\alpha+\beta)] - \frac{\alpha^2+\beta^2}{[\gamma(\alpha+\beta)]^2} - (\Psi_1(\alpha+\beta))^2\}\lambda$$

$$+\frac{\alpha\beta}{\gamma^2(\alpha+\beta+1)}[\Psi_1(\alpha)\Psi_1(\beta) - \Psi_1(\alpha+\beta)(\Psi_1(\alpha) + \Psi_1(\beta))]$$

$$+\frac{1}{[\gamma(\alpha+\beta)]^2}[2\alpha\beta\Psi_1(\alpha+\beta) - \beta^2(\Psi_1(\beta) - \Psi_1(\alpha+\beta)) - \alpha^2(\Psi_1(\alpha) - \Psi_1(\alpha+\beta))]. \quad (3)$$

The eigenvalues are

$$\lambda_1 = S + T - \frac{a_1}{3},$$

$$\lambda_2 = -\frac{1}{2}(S+T) - \frac{a_1}{3} + i\frac{\sqrt{3}(S-T)}{2},$$

$$\lambda_3 = -\frac{1}{2}(S+T) - \frac{a_1}{3} - i\frac{\sqrt{3}(S-T)}{2},$$

where

$$S = \sqrt[3]{R + \sqrt{Q^3 + R^2}}, \qquad T = \sqrt[3]{R - \sqrt{Q^3 + R^2}},$$

$$Q = \frac{3a_2 - a_1^2}{9}, \qquad R = \frac{9a_1a_2 - 27a_3 - 2a_1^3}{54},$$

and

$$-a_1 = \Psi_1(\alpha) + \Psi_1(\beta) - 2\Psi_1(\alpha+\beta) + \frac{\alpha\beta}{\gamma^2(\alpha+\beta+1)},$$

$$-a_2 = \frac{-\alpha\beta}{\gamma^2(\alpha+\beta+1)}[\Psi_1(\alpha) + \Psi_1(\beta) - 2\Psi_1(\alpha+\beta)] -$$

$$[\Psi_1(\alpha) - \Psi_1(\alpha+\beta)][\Psi_1(\beta) - \Psi_1(\alpha+\beta)] + \frac{\alpha^2+\beta^2}{[\gamma(\alpha+\beta)]^2} + (\Psi_1(\alpha+\beta))^2\}$$

$$-a_3 = \frac{\alpha\beta}{\gamma^2(\alpha+\beta+1)}[\Psi_1(\alpha)\Psi_1(\beta) - \Psi_1(\alpha+\beta)(\Psi_1(\alpha) + \Psi_1(\beta))]$$

$$+\frac{1}{[\gamma(\alpha+\beta)]^2}[2\alpha\beta\Psi_1(\alpha+\beta) - \beta^2(\Psi_1(\beta) - \Psi_1(\alpha+\beta)) - \alpha^2(\Psi_1(\alpha) - \Psi_1(\alpha+\beta))].$$

Lemma 6 :

(a) The characteristic Polynomial of $\begin{bmatrix} I_{11} & I_{12} \\ I_{21} & I_{22} \end{bmatrix}$ is given by

$$\lambda^2 - [\Psi_1(\alpha) + \Psi_1(\beta) - 2\Psi_1(\alpha+\beta)]\lambda + \Psi_1(\alpha)\Psi_1(\beta) - \Psi_1(\alpha+\beta)[\Psi_1(\alpha) + \Psi_1(\beta)] .$$

The eigen values

$$\lambda = \frac{[\Psi_1(\alpha) + \Psi_1(\beta) - 2\Psi_1(\alpha+\beta)] \pm \sqrt{[\Psi_1(\alpha) - \Psi_1(\beta)]^2 + 4[\Psi_1(\alpha+\beta)]^2}}{2} \text{ are}$$

positive provided that $\Psi_1(\alpha)\Psi_1(\beta) - \Psi_1(\alpha+\beta)[\Psi_1(\alpha) + \Psi_1(\beta)] > 0.$ (4)

(b)The characteristic polynomial of the matrix $\begin{bmatrix} I_{11} & I_{13} \\ I_{31} & I_{33} \end{bmatrix}$ is

$$\lambda^2 - [\Psi_1(\alpha) - \Psi_1(\alpha+\beta) + \frac{\alpha\beta}{\gamma^2(\alpha+\beta+1)}]\lambda - [\frac{\beta}{\gamma(\alpha+\beta)}]^2$$

$$+ \frac{\alpha\beta}{[\gamma^2(\alpha+\beta+1)]}[\Psi_1(\alpha) - \Psi_1(\alpha+\beta)].$$

The eigenvalues are

$$\lambda = \frac{[\Psi_1(\alpha) - \Psi_1(\alpha+\beta) + \frac{\alpha\beta}{\gamma^2(\alpha+\beta+1)}] \pm \sqrt{[\Psi_1(\alpha) - \Psi_1(\alpha+\beta) - \frac{\alpha\beta}{\gamma^2(\alpha+\beta+1)}]^2 + [\frac{2\beta}{\gamma(\alpha+\beta)}]^2}}{2}$$

are positive provided that $\frac{-\beta}{(\alpha+\beta)^2} + \frac{\alpha}{[(\alpha+\beta+1)]}[\Psi_1(\alpha) - \Psi_1(\alpha+\beta)] > 0.$ (5)

(c) The characteristic polynomial of the matrix $\begin{bmatrix} I_{22} & I_{23} \\ I_{32} & I_{33} \end{bmatrix}$ is

$$\lambda^2 - [\Psi_1(\beta) - \Psi_1(\alpha+\beta) + \frac{\alpha\beta}{\gamma^2(\alpha+\beta+1)}]\lambda - [\frac{\alpha}{\gamma(\alpha+\beta)}]^2 + \frac{\alpha\beta}{[\gamma^2(\alpha+\beta+1)]}[\Psi_1(\beta) - \Psi_1(\alpha+\beta)].$$

The eigenvalues are

$$\lambda = \frac{[\Psi_1(\beta) - \Psi_1(\alpha+\beta) + \frac{\alpha\beta}{\gamma^2(\alpha+\beta+1)}] \pm \sqrt{[\Psi_1(\beta) - \Psi_1(\alpha+\beta) - \frac{\alpha\beta}{\gamma^2(\alpha+\beta+1)}]^2 + [\frac{2\alpha}{\gamma(\alpha+\beta)}]^2}}{2}$$

are positive provided that $\frac{-\alpha}{(\alpha+\beta)^2} + \frac{\beta}{(\alpha+\beta+1)}[\Psi_1(\beta) - \Psi_1(\alpha+\beta)] > 0.$ (6)

Lemma 7: (R. Tunaru and G. Albota (2005)) A matrix has an inverse $\Leftrightarrow$ zero is not an eigenvalue.

Lemma 8: (Magnus and Neudecker 2007) A symmetric matrix A_{SXS} is positive definite
$\Leftrightarrow$ All its eigenvalues are positive
$\Leftrightarrow$ All principal minors $|\ A_K\ |$ are positive for $k=1,2,...,s$.

Table 1: The bias, standard error and root mean square error of the maximum likelihood estimator when only one parameter is unknown

A	0.3			1.5			1.8			3		
N	bias	s.e.	rmse	bias	s.e.	rmse	bias	s.e.	rmse	bias	s.e.	rmse
50	.0037	.0424	.0422	.0148	.1970	.1976	.0197	.2417	.2425	.0175	.3663	.3668
100	.0035	.0300	.0299	.0109	.1378	.1384	.0156	.1646	.1655	.0156	.2665	.2669
300	.0015	.0173	.0175	.0047	.0775	.0775	.0071	.0917	.0917	.0062	.1490	.1491
500	.0008	.0141	.0134	.0010	.0616	.0620	-.0008	.0728	.0726	.0019	.1175	.1174
$\sqrt{\text{C.R.L.B}}$	.0132			.0608			.0721			.1170		

(a) α is unknown ($\beta=1.5, \gamma=0.6$)

B	0.6			1.5			2.5			3.5		
N	bias	s.e.	rmse	bias	s.e.	rmse	bias	s.e.	rmse	bias	s.e.	rmse
50	.0093	.0843	.0847	.0234	.1960	.1973	.0354	.3124	.3145	.0760	.4750	.4810
100	.0054	.0566	.0571	.0160	.1439	.1449	.0131	.2191	.2194	.0380	.3148	.3171
300	.0025	.0346	.0344	.0055	.0781	.0781	.0077	.1273	.1277	.0120	.1825	.1830
500	.0010	.0265	.0257	.0013	.0624	.0621	.0027	.0933	.0934	.0002	.1386	.1385
$\sqrt{\text{C.R.L.B}}$	.0257			.0608			.0985			.1353		

(b) β is unknown ($\alpha=1.5, \gamma=2.0$)

Γ	0.8			1.8			2			3		
N	bias	s.e.	rmse	bias	s.e.	rmse	bias	s.e.	rmse	bias	s.e.	rmse
50	.0186	.2071	.2080	.0555	.4825	.4857	.0557	.5525	.5553	.1062	.8490	.8556
100	.0152	.1530	.1538	.0123	.3365	.3367	.0237	.3715	.3722	.0264	.5904	.5910
300	.0055	.0849	.0852	.0113	.2015	.2017	.0170	.2186	.2194	.0171	.3161	.3165
500	-.0002	.0648	.0648	.0075	.1507	.1508	.0103	.1661	.1665	.0195	.2439	.2448
$\sqrt{\text{C.R.L.B}}$	.0663			.1493			.1661			.2490		

(c) γ is unknown ($\alpha=1.5, \beta=0.6$)

Remark: $\sqrt{\text{C.R.L.B}}$ is the root of the Cramar-Rao Lower Bound when the sample size is 500.

Table 2: The biases, standard errors and the sum of root mean square errors when two of the parameters are unknown

	α=0.3; β=0.8				α=0.3; β=2.5			
	$\hat{\alpha}$		$\hat{\beta}$		$\hat{\alpha}$		$\hat{\beta}$	
n	bias	s.e.	bias	s.e.	srmse	bias	s.e.	bias	s.e.	srmse
50	.0134	.0539	.0381	.1375	.1986	.0142	.0529	.2911	.7671	.8751
100	.0067	.0387	.0140	.0922	.1324	.0080	.0361	.1266	.4969	.5491
300	.0016	.0200	.0073	.0500	.0701	.0017	.0200	.0328	.2713	.2930
500	.0018	.0141	.0031	.0387	.0553	.0018	.0141	.0276	.2114	.2283

	α=1.2; β=0.8				α=1.2; β=1.5			
	$\hat{\alpha}$		$\hat{\beta}$		$\hat{\alpha}$		$\hat{\beta}$	
n	bias	s.e.	bias	s.e.	srmse	bias	s.e.	bias	s.e.	srmse
50	.0591	.2587	.0368	.1612	.4306	.0578	.2435	.0738	.3071	.5660
100	.0434	.1741	.0244	.1077	.2899	.0346	.1679	.0436	.2218	.3974
300	.0103	.1020	.0054	.0600	.1625	.0117	.0922	.0189	.1212	.2157
500	.0042	.0735	.0008	.0458	.1195	.0095	.0700	.0098	.0927	.1641

(a) α, β are unknown (γ =0.6)

	α=0.8; γ=0.6				α=0.8; γ=3			
	$\hat{\alpha}$		$\hat{\gamma}$		$\hat{\alpha}$		$\hat{\gamma}$	
n	bias	s.e.	bias	s.e.	srmse	bias	s.e.	bias	s.e.	srmse
50	.0803	.2496	.1213	.3351	.6185	.0774	.2400	.5311	1.565	1.905
100	.0381	.1533	.0556	.2081	.3733	.0336	.1487	.2474	.9852	1.168
300	.0101	.0787	.0112	.1044	.1844	.0106	.0812	.0780	.5383	.6261
500	.0063	.0583	.0102	.0787	.1382	.0026	.0592	.0206	.3861	.4462

	α=1.8; γ=0.6				α=1.8; γ=1.5			
	$\hat{\alpha}$		$\hat{\gamma}$		$\hat{\alpha}$		$\hat{\gamma}$	
n	bias	s.e.	bias	s.e.	srmse	bias	s.e.	bias	s.e.	srmse
50	.4940	1.394	.2323	.6598	2.178	.5270	1.440	.6068	1.635	3.278
100	.1541	.5929	.0747	.2691	.8918	.1951	.6712	.2719	.9359	1.674
300	.0743	.2816	.0354	.1330	.4290	.0774	.2795	.0896	.3219	.6242
500	.0403	.1975	.0217	.0954	.2996	.0301	.2064	.0349	.2362	.4472

(b) α , γ are unknown(β =1.5)

	β=0.6; γ=0.3				β=0.6; γ=3.5			
	$\hat{\beta}$		$\hat{\gamma}$		$\hat{\beta}$		$\hat{\gamma}$	
n	bias	s.e.	bias	s.e.	srmse	bias	s.e.	bias	s.e.	srmse
50	.0462	.1584	.0064	.1292	.2942	.0417	.1446	.0065	1.405	1.555
100	.0242	.1030	.0031	.0933	.1993	.0176	.1010	.0875	1.090	1.197
300	.0043	.0520	.0027	.0490	.1010	.0045	.0520	.0450	.5838	.6380
500	.0022	.0387	.0021	.0387	.0783	.0047	.0424	.0163	.4688	.5116

	β=1.2; γ=0.3				β=1.2; γ=1.8			
	$\hat{\beta}$		$\hat{\gamma}$		$\hat{\beta}$		$\hat{\gamma}$	
n	bias	s.e.	bias	s.e.	srmse	bias	s.e.	bias	s.e.	srmse
50	.1732	.5303	.0011	.1334	.6912	.1865	.6463	.0080	.8055	1.478
100	.0804	.2777	.0000	.0949	.3837	.0602	.2867	.0283	.5648	.8585
300	.0228	.1425	-.0001	.0520	.1963	.0207	.1418	-.0012	.3129	.4561
500	.0131	.1054	-.0002	.0387	.1457	.0108	.1063	.0079	.2400	.3469

(c) β , γ are unknown(α =1.5)

Table 3: when all three parameters are unknown.

		α= 0.3; β=1.5; γ=0.6					α= 1.5; β=1.5; γ=0.6				
n		$\hat{\alpha}$	$\hat{\beta}$	$\hat{\gamma}$	srmse	$\hat{h}(0.5)$	$\hat{\alpha}$	$\hat{\beta}$	$\hat{\gamma}$	srmse	$\hat{h}(0.5)$
	bias	.0016	.2793	.0043		-.1034	.0474	.0433	.0455		.1955
300	s.e.	.0239	.9122	.2987	1.235	.8436	.2491	.2432	.2481	.7404	.9848
	bias	.0006	.1158	.0143		-.0322	.0251	.0300	.0212		.0784
500	s.e.	.0173	.4238	.2337	.6907	.6462	.1855	.1857	.1769	.5535	.4025
	bias	-.0003	.0503	.0023		-.0274	.0144	.0140	.0118		.0376
1000	s.e.	.0141	.2490	.1559	.4221	.4396	.1233	.1237	.1183	.3682	.2467
	bias	.0003	.0180	.0062		.0008	.0093	.0054	.0078		.0215
2000	s.e.	.0100	.1568	.1105	.2779	.3041	.0854	.0860	.0812	.2531	.1610

		α= 3; β=1.5; γ=0.6					α= 1.5; β=0.6; γ=0.6				
n		$\hat{\alpha}$	$\hat{\beta}$	$\hat{\gamma}$	srmse	$\hat{h}(0.5)$	$\hat{\alpha}$	$\hat{\beta}$	$\hat{\gamma}$	srmse	$\hat{h}(0.5)$
	bias	.3129	.0189	.1092		16.50	.1070	.0066	.0883		792
300	s.e.	.9859	.2073	.3606	1.619	374.9	.4851	.0583	.3761	.9415	25041
	bias	.1658	.0137	.0544		2.348	.0568	.0017	.0470		.0448
500	s.e.	.7242	.1520	.2516	1.153	63.85	.2500	.0436	.1987	.5045	.1521
	bias	.0725	.0037	.0257		.0461	.0249	.0029	.0187		.0185
1000	s.e.	.4119	.1077	.1446	.6724	.1929	.1830	.0316	.1432	.3598	.0949
	bias	.0283	.0033	.0112		.0198	.0097	.0016	.0062		.0058
2000	s.e.	.2903	.0742	.1015	.4686	.0894	.1149	.0224	.0900	.2271	.0581

α= 1.5; β=1.2; γ=0.6 α= 1.5; β=2; γ=0.6

n		$\hat{\alpha}$	$\hat{\beta}$	$\hat{\gamma}$	srmse	$\hat{h}(0.5)$	$\hat{\alpha}$	$\hat{\beta}$	$\hat{\gamma}$	srmse	$\hat{h}(0.5)$
	bias	.0501	.0249	.0483		.1429	.0508	.0666	.0504		.2895
300	s.e.	.2680	.1713	.2456	.6960	.5790	.2359	.3934	.2529	.8982	1.130
	bias	.0377	.0112	.0362		.0859	.0251	.0497	.0226		.1330
500	s.e.	.1997	.1249	.1817	.5141	.3309	.1729	.2895	.1865	.6564	.6909
	bias	.0105	.0135	.0073		.0225	.0100	.0268	.0086		.0487
1000	s.e.	.1269	.0849	.1145	.3284	.1771	.1187	.2059	.1261	.4536	.3795
	bias	.0058	.0073	.0013		.0052	.0060	.0126	.0046		.0233
2000	s.e.	.0883	.0574	.0781	.2241	.1163	.0806	.1393	.0860	.3075	.2504

α= 1.5; β=0.6; γ=1.2 α= 1.5; β=0.6; γ=3

n		$\hat{\alpha}$	$\hat{\beta}$	$\hat{\gamma}$	srmse	$\hat{h}(0.5)$	$\hat{\alpha}$	$\hat{\beta}$	$\hat{\gamma}$	srmse	$\hat{h}(0.5)$
	bias	.0887	.0070	.1389		.6741	.1112	.0063	.4354		30.13
300	s.e.	.3444	.0579	.5518	.9831	2.284	.4012	.0573	1.616	2.148	182.0
	bias	.0699	.0026	.1038		.3850	.0643	.0036	.2449		5.419
500	s.e.	.2638	.0436	.4128	.7416	1.480	.2602	.0458	1.054	1.396	31.52
	bias	.0336	.0021	.0520		.1490	.0331	.0011	.1258		1.712
1000	s.e.	.1697	.0316	.2700	.4801	.5249	.1744	.0316	.6923	.9120	6.356
	bias	.0139	.0012	.0214		.0595	.0186	.0007	.0672		.6737
2000	s.e.	.1122	.0224	.1806	.3168	.2996	.1082	.0200	.4286	.5641	2.442

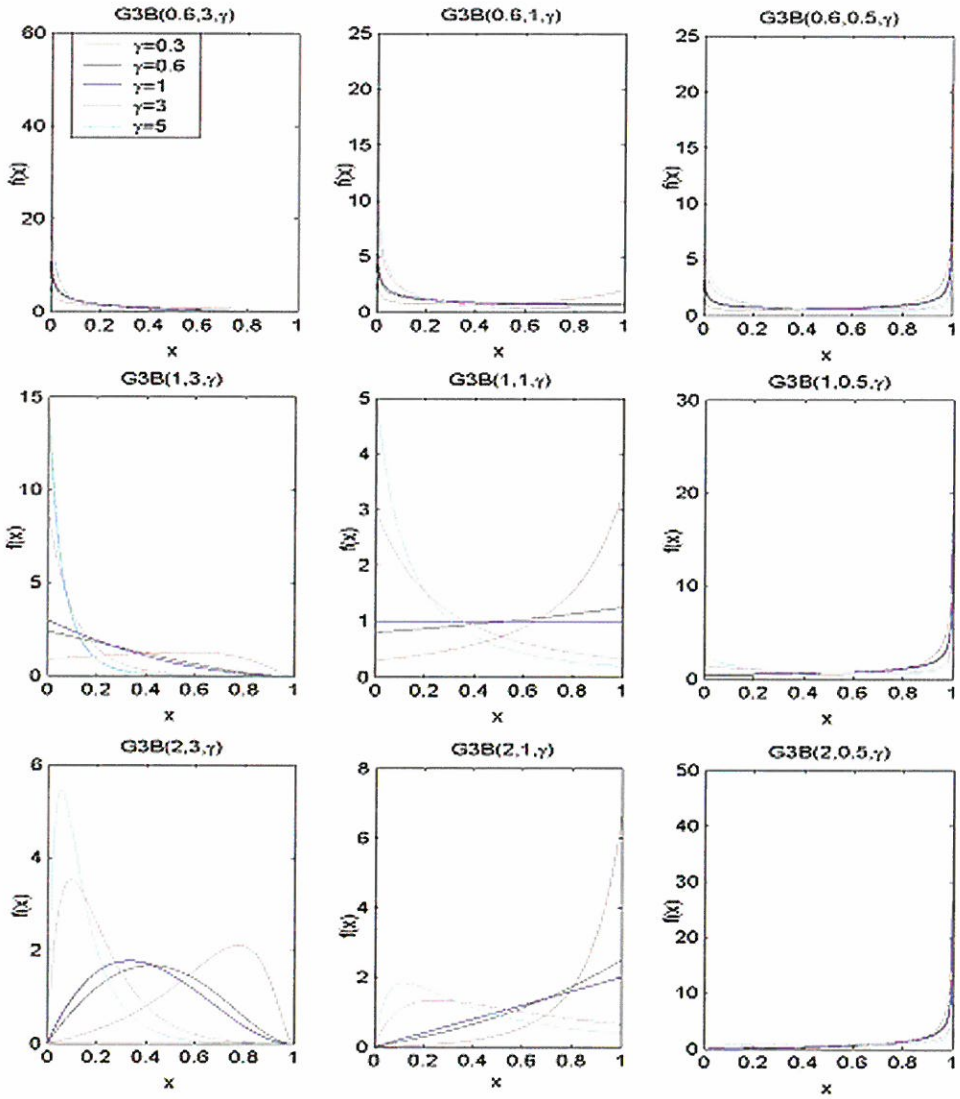

Fig 1: Density for G3B(α , β , γ)

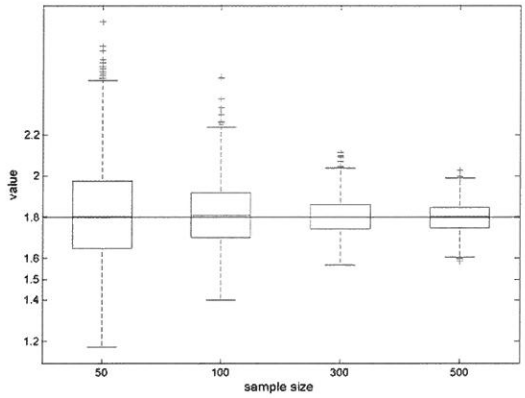

(a): Box plots for $\hat{\alpha}$

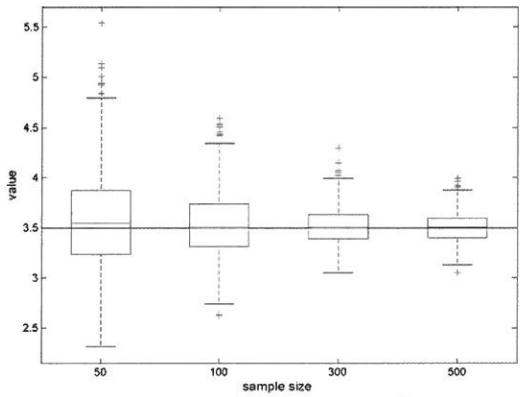

(b): Box plots for $\hat{\beta}$

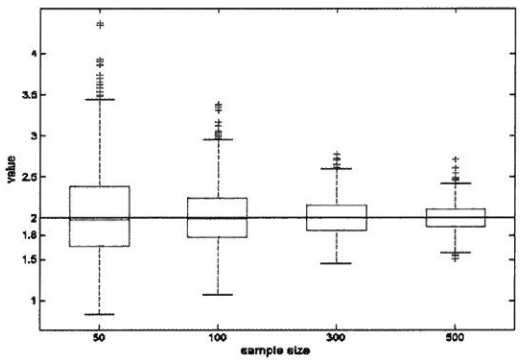

(c): Box plots for $\hat{\gamma}$

Fig 2: Box plots under different sample size .

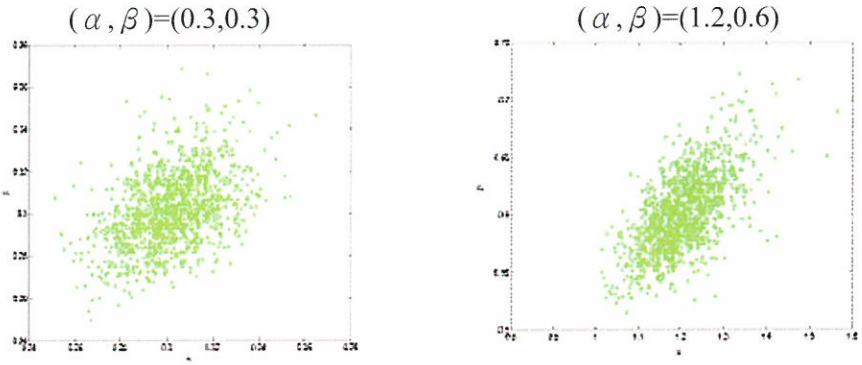

(a) When α and β are unknown and $\gamma = 0.6$;

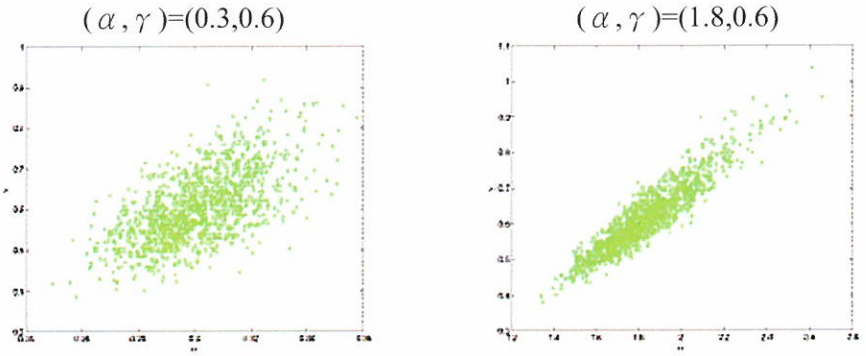

(b) When α and γ are unknown and $\beta = 1.5$;

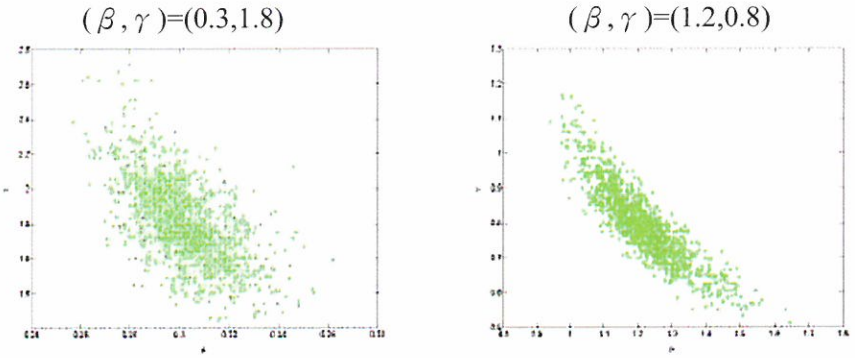

(c) When β and γ are unknown and $\alpha = 1.5$;

Fig 3: The scatter plots of MLE when the sample size is 500.

Reference

1. Bandourian R., McDonald J. B. and Turley R. S. (2002), "A Comparison of Parametric Models of Income Distribution Across Countries and Over Time", *Luxembourg Income Study Working Papers*, No 305, 1-47.
2. Chen K.Y. and Lin C. T. (2005), "A note on infinite-armed Bernoulli bandit problems with generalized beta prior distributions", *Statistical Papers*, 46, 129-140.
3. Chen W. T. and Chen S. M. (2008), "An estimating problem on Generalized Beta Distribution", Fu Jen Studies, Science and Engineering, No 42, 31-52.
4. Gelfand A. (1987), " Estimation of a restricted variance ratio", *In Proceedings of the Second International Tampere Conference in Statistics*, (Edited by T. Pukkila and S. Puntanen), 457-466, Tampere, Finland.
5. Kegan B. and West R. W. (2005), "Modeling the simple epidemic with deterministic differential equations and random initial conditions", *Mathematical Biosciences*, 195, 179-193.
6. Kleiber C. (2005), "The Lorenz Curve in Economics and Econometrics", *Gini-Lorenz Centennial Conference, Siena,* May 23-26.
7. Lehmann E. L. and Casella G., *Theory of Point Estimation*, 2nd Ed. Springer, 1998.
8. Libby, D. L. and Novick, M. R. (1982), "Multivariate Generalized Beta Distributions with Applications to Utility Assessment", *Journal of Educational Statistics*, 7(4), 271-294.
9. Magnus J. R. and Neudecker H. (2007), *Maxtrix Differential Calculus with applications in Statistics and Economics.* 3rd Ed. John Weleys and Sons.
10. Nadarajah S.(2005a), "Exponentiated beta distributions", *Computers and Mathematics with Applications* 49, 1029-1035.
11. Nadarajah S. (2005b), Sums, "Products and Ratios of Generalized Beta Variables", *Statistical Papers*, 49, 69-90.
12. Pham-Gia T. (1989), WorkSamp (software survey section), *Mathl. Comput. Modelling* 12(2), I.
13. Robert, C. P. and Casella, G. (2004). *Monte Carlo Statistical Methods*, 2nd Ed; Springer.
14. Sahinoglu M. (1981), *Statistical Inference on the Reliability Performance Index for Electric Power Generation Systems.* PhD dissertation, Institute of statistics, College Station, Texas A&M University.
15. Sahinoglu M. (2000), *Reliability Index Evaluations of Integrated Software Systems (Internet) for Insufficient Software Failure and Recovery Data.* SpringerLink, 363-373.
16. Sahinoglu M. and Libby D. L. (2003), Sahinoglu-Libby (SL)," Probability Density Function Component Reliability Applications in Integrated Networks", *2003 Proceedings Annual Reliability and Maintainability Symposium*, 280-287.
17. Sahinoglu M., Libby D. L. and Das S.R., "Measuring Availability Indexes with Small Samples for Component and Network Reliability Using the Sahinoglu-Libby Probability Model", *IEEE Transactions on Instrumentation and Measurement,* 54(3) : 1283-1295, 2005.
18. Sepanski J. H. and Kong L. (2007), A Family of Generalized Beta Distributions for Income. Cornell University Library arxiv.org > stat > arxiv:0710.4614
19. Tunaru R. and Albota G. (2005), Estimating Risk Neutral Density with a Generealized Gamma Distribution. www.cass.city.ac.uk/facfin/papers/WP2005.
20. Verheijen P. J. T. (2001), Statistical Distributions in Particle Technology.

Received August 17,2011
Revised January 3,2012
Accepted January 9,2012

廣義三參數貝它分佈之最大概似估計式之研究

陳思勉

輔仁大學數學系

摘　要

本研究探討三參數貝他分佈之最大概似估計式之近似信賴區間及假設檢定，此外本文也透過模擬冶金法討論最大概似估計式之偏差及標準誤。

關鍵詞：中央極限定理；不完整貝它函數；模擬冶金法。

網路應用在偏鄉教育－遠距課輔無遠弗屆 以數位學伴線上課業輔導服務計畫為例

林宏彥　楊志田

輔仁大學資訊中心 台灣省新北市新莊區

摘　要

電腦與網路科技進步快速，造就學習機會之多元化。透過網路進行遠距離的線上教育，能有效解決傳統面對面上課方式所衍生的交通安全與時間效率問題。本文藉由執行教育部數位學伴線上課業輔導服務計畫之系統維運經驗，研究建立有效管理大量配對同時進行遠距網路課輔之機制，並分析討論執行過程中的問題與解決辦法，最後提出感想與建議。

偏鄉遠距網路課輔的核心工作有三：輔導面、教學面、數位技術面，缺一不可。其中數位技術面的部份，雖然是屬於基礎建設，但卻也是造就輔導面與教學面可以成功的重要推手。我們認為所建立的機制是可行且有效的，我們將繼續修訂檢討此機制，也非常樂意與大家分享經營的經驗，希望能有更多的學童與大學生在這樣教學模式中受惠且成長。

關鍵詞：數位學伴、系統維運、偏鄉遠距網路課輔。

1. 前 言

偏鄉教育長期以來為社會與教育單位關心的主題，相關計畫例如有：教育部的攜手計畫 [1]、博幼社會福利基金會的課輔方案 [2]、永齡教育慈善基金會的永齡希望小學課輔計畫 [3]、教育部發展原住民族教育五年中程個案計畫 [4]，還有許多院校系所社團與社服單位也在各角落持續經營。無論哪種方案，依循的還是傳統的教學方式，採現場面對面直接教學。這對於偏遠的地區，在往返途中面對的交通安全與時間問題是個非常重要的挑戰；也因如此，多半是集中於假期或寒暑假，難以在平時例行性執行。

基於「縮減城鄉數位落差」政策，行政院 91 年核定「挑戰 2008：國家發展重點計畫（2002-2007）」[5]。全案共建構十項計畫，當中第六項為「數位台灣 (e-Taiwan) 計畫」[6]，主要任務在推動國家資訊通信基礎建設與電子化政府。「數位台灣計畫」為落實「數位人權」，行政院國家資訊通信發展推動小組於 93 年度提出「縮減數位落差四年計畫」(94-97 年)，行政院將之列為國家重大政策，為人民創造一個公平運用資訊通信科技的環境與機會 e-Opportunity)。接著，並更積極的在 97~100 年間實施「創造數位機會四年計畫」，其中包括 2.4 萬台的「國民電腦計畫」，協助低收入戶學童等弱勢族群使用。並逐年推動「創造偏鄉數位機會推動計畫」[7]。接著，在「新世紀第三期國家建設計畫」(民國 98 至 101 年四年計畫)[8] 之教科文建設之教育篇的規劃策略中，將「強化弱勢扶助，縮短城鄉差距，均衡資源分配」，列為「公義關懷」執行要項，並在該計畫中的第 3 年實施「100 年國家建設計畫」[9]，其中在教科文建設之教育篇規劃了一項 招募大專校院志工線上課後輔導，服務偏鄉弱勢學童 ，而這項計畫在之前的 95 年就開始進行實驗。

教育部在 95 年起推動「偏鄉地區中小學網路課業輔導服務計畫」，運用網路教學方式，由大學生輔導偏鄉地區的國中、國小學生，提升偏鄉學生學習成效，促成學習機會均等，97 年全面推廣到全國，委由輔仁大學擔任總計畫 [10] 及北區輔導中心 [11]。99 年將課輔對象擴及於家庭經濟弱勢學童，計畫方向調整為「數位學伴線上課業輔導服務」[12]。教育部 數位學伴線上課業輔導服務計畫 中，輔仁大學擔任「總計畫暨北一區輔導中心」[13][14] 及「系統維運」[15][16]，每學期偕同國內 28 所大學校院約 1500 名大學生，為散佈國內各偏鄉、離島 80 餘所中小學 1000 多名學童，進行一對一網路課業輔導。

教育部電算中心主任何榮桂說， 當硬體設備都到位，需要有系統的執行和長時間的關注 [17]。教育部電算中心前主任趙涵捷則提到：「電腦及網路已被視為是縮減城鄉差距，拓展偏鄉學生學習與溝通的有效方法。因此目前各縣市政府及偏鄉學校皆殷切期望，能夠透過網路課輔來改善學童的學習困境。但是網路課輔有其設備環境管理

及遠距輔導專業之挑戰，實施品質亦不易掌控」[18]。這些都一再的說明，要經營如此大規模的網路課輔同時進行，除了設備之外，還需要有具體的運作機制模式與認真經營的態度。

本論文在第二部分提出建立有效管理大量配對同時進行遠距網路課輔之機制，首先規劃營運的機制，再來是推動營運的核心概念，最後是執行營運的機制。在第三部分，我們分析與討論執行的重要結果，並在最後提出感想與建議。

2. 營運方法

1. 規劃營運機制

依據教育部 99 年數位學伴線上課業輔導服務計畫 [12] 之執行與管理的需求，規劃營運機制的架構，如圖一。

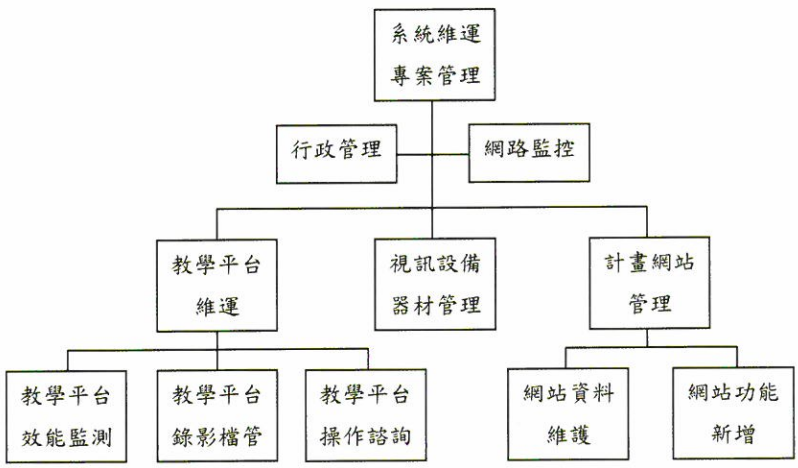

圖一 系統維運營運機制

2. 推動營運機制

在營運機制中，首先要推動認識兩個部分：系統、維運，以利之後各層面互相配合之進行過程，茲說明如下：

(1) 系統

本案之系統，分成網路、設備與應用軟體三部分，如圖二。圖二當中虛線框所指的協助管理部分，包含：對於無管轄權的網路設備，提供技術偵測，協助發掘問題與通知管轄單位進行障礙排除；而在設備部分，耳麥視訊置放於計畫中各夥伴單位，基本上由使用單位保管，我方提供線上登錄及故障通報機制與汰換更新。

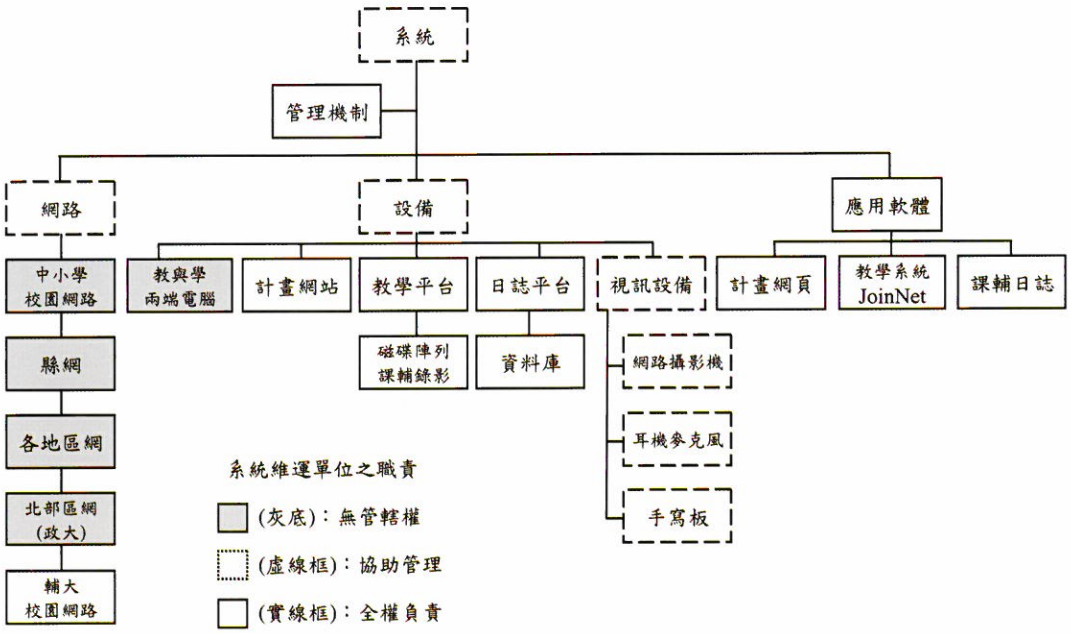

圖二 系統分類

圖二說明當網路課輔過程中發生了連線溝通上的問題時候，可能是因為網路的問題、設備的問題，也可能是應用軟體的問題，大家認識此說明有助於之後了解問題的責任歸屬。其中，網路問題的責任歸屬常常是被誤判的一項，所以應和本案所有成員介紹說明圖三的網路訊號傳輸概念。在圖三當中，可看出中間的教學平台相當類似於資料的中間轉換站，但是各使用端到教學平台之間，尚須經過許多單位的網路，因此當連不上教學平台的時候，不一定表示問題發生在教學平台的所處網路，而可能是當中的任何一段，此時須進一步判斷才可確定。

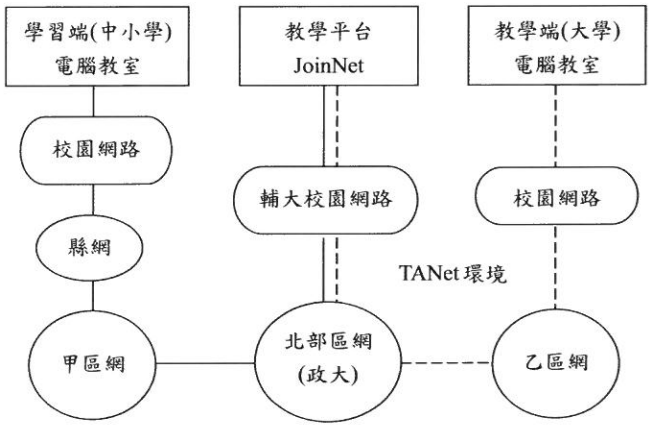

圖三 網路課輔過程之訊號傳輸示意圖

(2) 維運

維運的過程是本案所有成員應當共同配合完成的，所以也應推動讓大家知道，以利之後按部就班進行。茲將程序列述於下：

A. 環境建置：

大中小學伴的電腦教室設備、網路運作，在開課前應該先準備、測試妥當。

(a) 由各區輔導中心，召集夥伴大學，示範系統檢測、安裝、測試等步驟。

(b) 夥伴大學派員到其輔導的中小學，協助電腦教室的檢測、軟體設定安裝、以及網路連線測試。

(c) 若安裝過程碰到障礙，除了找輔導中心外，亦可向系統維運單位尋求協助。

(d) 每學期初，列為必須執行的基本任務。

B. 教育訓練：

系統維運協助各區輔導中心，執行相關技術操作講習之訓練。

(a) 建置教學文件、使用手冊，與各項 Q&A，並放置在計畫網站。

(b) 安排區輔導中心助理或技術人員、夥伴大學種子教師、夥伴中小學帶班老師，講授教學平台的操作、課輔日誌撰寫程序，以及安排技術專業課程：教學平台、課輔日誌、設備維護。

(c) 夥伴大學種子教師，召集該校全體課輔老師，轉達相關的系統操作方式，與注意事項。

(d) 夥伴中小學帶班老師，回校後，亦召集參與計畫之學童，教導如何操作教學平台功能，及檢測相關環境。
(e) 發展線上教育訓練機制。所有計畫成員，無須聚集於特定地點，可在各自工作崗位，以教學平台特定帳號，進行線上同步教學。

C. 同步協調：
教與學雙方，依照協調之上課時間，各就定位。
(a) 教師端，先以主控身份，登錄進系統等待。
(b) 學童端，由螢幕畫面，判斷老師是否已登錄？確定後，以訪客身份，等待主控端的同意後，進入課輔教室共用版面。

D. 障礙辨識：
網路課輔進行當中，多台電腦同時上網進行影音、文字訊號的傳輸，難免偶而出現設備問題。因此，必須訓練使用者判斷問題的可能出處後，能當場解決最好，若問題依舊，便須向上一層通報，尋求協助。
(a) 若是集體性無法連上教學平台，且全區狀況相同，則可能是北區區網到系統維運單位間的網路故障，或是教學平台主機故障。若是全班狀況相同，但同區其他學校正常，則可能是所屬校園網路到縣網間網路系統故障。
(b) 若是單一個案無法連上教學平台，例如班上少數幾部電腦無法連上教學平台、或雜音、無聲：應屬個別電腦的問題，可能網路卡、音效卡、耳麥故障，或相關設定有誤。

E. 障礙排除：
先辨識障礙最可能原因後，針對不同情況，有不同的處理方式：
(a) 集體性問題，且全區狀況相同：向系統維運通報處理，再向輔導中心備案。
(b) 集體性問題，全班狀況相同，但同區其他學校正常：向 ISP 電信業者通報檢修，再向輔導中心備案。
(c) 單一個案問題：現場處理，若短時間內解決不了，啟動備用機器。

F. 以課輔日誌系統，作品質管制：
日誌系統屬於計畫網站的核心功能之一，目的在記錄與觀察大小學伴的成長與學習過程。透過共通平台達到訊息交流、經驗傳承、數據分析。主要功能有各項基本資料建立、大學學伴課輔日誌、帶班老師日誌、各項出缺勤紀錄與統計、學童學習資料與成效評估、交流園地、教材分享與線上試卷等。

3. 執行營運機制

(1) 決定網路課輔平台

各種產品通常都會有所優點與主要規劃的對象群與功能導向，所以在評估平台之前，必須先設定清楚所要的功能方向。以本案之網路課輔所需，主要需求功能有：

A. 即時語音對傳功能：以便能以語音直接溝通。

B. 視訊影音對傳功能：上課進行中即時影像的傳輸，視訊更新率不需要太高，約二至三秒更新一次即可。

C. 共享電子白板：可以利用數位板模擬實際臨場課輔時的筆式溝通環境，以書寫或繪圖的方式加強課輔效果。匯入教材或圖層時，可於教材或圖層畫面上教學，擦拭教學痕跡後教材或圖層資料不會有所影響。

D. 共享網頁功能：以便利教學端引導學習端學習既有線上教材。

E. 圖片共享功能：可將掃描器掃描結果、各種軟硬體呈現之畫面，或轉成圖片檔之數位教材上傳至線上互動平台供討論用。

F. 遠端操控功能：以利教學端協助學習端排除電腦之簡易故障，並可瞭解學生現階段畫面。

G. 全程錄影功能：可將陪伴過程的影音、筆式溝通等事件完整記錄下來，作為之後考核之依據。

H. 錄影檔案管理功能：方便整理與調閱特定時段與特定對象的學習紀錄。

基於上述需求，針對三種平台做測試比較，整理幾項比較關鍵性差異的結果如下表一，其他關於 J 系統與 C 系統的比較可參考 [19][20]，J 系統與 A 系統的比較可參考 [21]。

表一 各種視訊平台之關鍵差異比較

	J 系統(本案採用)	C 系統	A 系統
電子白板	● 可接受手繪、文字輸入、文字與圖片剪貼、上傳圖片，與虛擬印表機方式輸入內容。 ● 文字輸入為文字方塊概念，可調整文字方塊大	● 可手繪、文字輸入、上傳圖片。 ● 文字輸入時，每次一行，無法自動換行。 ● 僅能以橡皮擦功能進行內容清除。	● 可手繪、文字輸入、上傳圖片、ppt、pptx。 ● 手繪功能無法呈現過程，只能呈現最後結果。 ● 各圖形各一物件，但是無法只擦拭某圖形的一部

電子白板	小並有自動換行功能。 ● 手繪線條、上傳文字或圖片均成為繪圖物件，可以選取方式清除特定物件。且清除時不會影響到背景圖片。 ● 透過虛擬印表機功能，各種格式之教材檔亦可選擇列印至 J 系統印表機即完成上傳。	若有背景圖片，也會被破壞掉。(98.07.開始開發，將「上傳圖片」與「手繪+文字輸入」圖層分開，橡皮擦功能不再同時擦去上傳圖片。) ● 若有教材需上傳，僅先轉為 JPG、GIF、BMP、PNG 圖片格式，再以上傳圖片達成。Word 等文件直接上傳功能於 98.07.開始開發。	分。 ● 若有文件教材需上傳，需先轉為 JPG、ppt、pptx 等格式上傳達成。
錄影	● 聲音、視訊、對話框、電子白板同時錄製。 ● 其專屬錄影格式在播放時，仍可調整各框架大小，比如是否顯示視訊框、捲動電子白板內容或全螢幕播放。 ● 使用者可下載錄影檔，透過 J 系統程式即可播放。管理者亦可統一管理所有錄影檔，比如置於 FTP 供下載。	● 只能錄對話框與電子白板。 ● 電子白板錄影檔無法下載，只能線上觀看。但可多段調整播放速度。	● 錄影檔可線上觀看 ● 但是下載錄影檔則必須一個一個下載分類到本地端電腦。
動態視訊頻寬	● 可預設控制頻寬需求在 48Kb/s。	● 需要較高頻寬需求，據經驗測試，同時線上人數 5 人以上即有明顯的狀況產生。	● 老師機的上傳流量約為 30Kb/s，但是學生端的上傳頻寬則需要兩倍以上，這對較偏鄉學校的網路環境是個負擔。
管理者影響	● 由主機管理者統一開設教室與密碼，志工與學生亦無須學習教室的開設功能。 ● 必要時可隨時調閱任一教室之錄影檔案，也可另行備份存查。	● 若大量應用到遠距課輔的需求，勢必需要開放或再行開發部分管理功能。例如帳號群組功能或是錄影檔管理功能等等。	● 若大量應用到遠距課輔的需求，勢必需要開放或再行開發部分管理功能。例如開設大量帳號功能、帳號群組功能或是上述錄影檔之異地集體備份管理功能等等。

綜上分析，不論是在 1. 電子白板書寫過程的呈現功能 (有助於了解例如學童端書寫筆順的過程，或是數學計算的過程)、2. 錄影檔案的下載管理功能 (有助於事後分析學童之學習過程或是提供再次複習的功能)、3. 整體頻寬需求、4. 管理者端的相關功能 (大量開帳號、錄影檔案備份)，都是 J 系統較為適合，所以我們選擇 J 系統作為本案的平台。

(2) 建置網路課輔平台效能監測

為了掌控每一主機在同時多組的網路課輔能正常進行，必須特別注意主機的相關系統資源，以及網路使用流量，尤其針對某些中小學的網路頻寬本就不寬鬆的情況下，更須注意觀察。

本計畫架設即時監測系統，監督課輔平台之各項資源情況，以利了解問題發生與即時因應，並可作為事後追蹤之判斷依據。平時設定在發生所預設的條件下即時以 E_mail 傳送到指定多個信箱，並發佈到遠端的即時資訊看板。以下分別是某一課輔平台針對近 200 對的課輔連線使用時候的 CPU、記憶體、網路流量使用情況。

A.CPU 使用情況 :

(a) 規格：Intel 雙核心處理器，時脈頻率 2.4GHz

(b) 使用率：如下圖四呈現，在上課之巔峰期 (18:00~20:00)，最高使用率約為 42.75%，顯示負荷能力非常足夠。

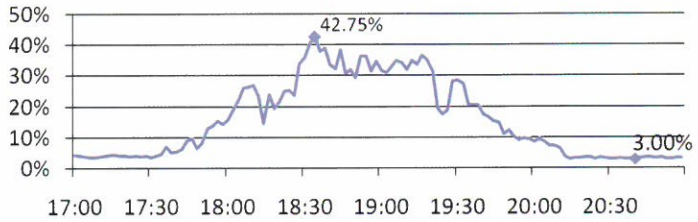

圖四 平台之 CPU 使用率

B. 記憶體使用情況 :

(a) 規格：2G*2 DDR Ⅱ 800MHz

(b) 使用率：如下圖五呈現，在上課之巔峰期 (18:00~20:00)，使用率至少還剩餘約有 72.61%，顯示負荷能力非常足夠。

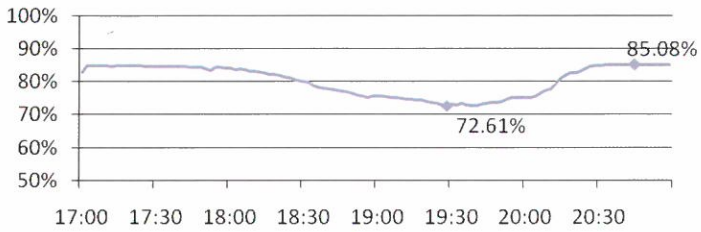

圖五 平台之記憶體使用剩餘百分比

C. 網路流量使用情況：

(a) 規格：輔仁大學對外網路頻寬超過 1Gbps

(b) 使用率：如下圖六呈現，在上課之巔峰期 (18:00~20:00)，使用率對於輔仁大學的對外頻寬仍顯相對非常小，表示頻寬非常足夠。

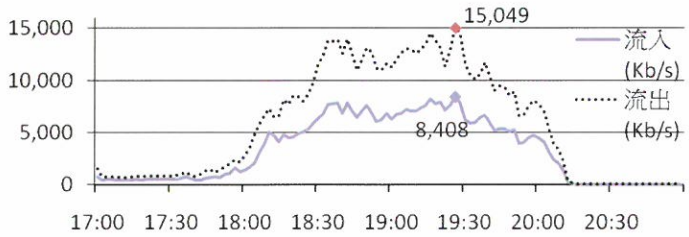

圖六 平台之網路流量

(3) 建置網路課輔平台錄影檔案管理

每天晚上下課後，依據圖七流程定時做備份，將錄影檔案除了系統化群組整理在 FTP 主機提供各夥伴學校批次大量下載之外，也同時另存一份在另一台的 NAS 主機當作備份。另外也提供從計畫網站登入後查詢下載個別錄影檔功能。因為錄影檔案內容關係到個人隱私，所以另訂立「教學錄影檔案管理、使用規範」，置於 http://www.dsg.fju.edu.tw/dsg/file/l3_7.doc。

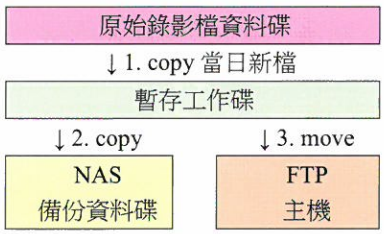

圖七 錄影檔自動備份機置

(4) 建置網路課輔平台操作諮詢

A. 提供專線電話諮詢與 E_mail 提問，記錄整理 130 則於系統維運的週報當中。

B. 製作 Q&A：(可參考 http://www.dsg.fju.edu.tw/dsg/ques.html) 共計九個分類，87 篇。

C. 整理文件下載專區：(可參考 http://www.dsg.fju.edu.tw/dsg/load.html) 共計 48 篇文件與辦法、5 份手冊。

D. 建置障礙提報系統：

為了能有效讓多方同時管控與掌握問題進度，開發障礙回報系統，引導提報問題單位能依據問題分類描述狀況，並配合相關夥伴學校、區輔導中心，以及本單位共同協助了解問題與提供解決辦法。以利作問題追蹤與未來問題的經驗參考，於 100.1.17 ~ 100.6.16 間，計有 55 則問題與 139 個回應處理。

(5) 建置通訊設備器材管理

建置設備管理系統，提供各單位填報需求數量，並方便盤點。

(6) 架設網路課輔平台

因為每台主機所容許的授權數量有限，以 J 系統而言，一台主機的最多授權數量為 400 個同時連線數，所以必須將同時大量連線的配置分散在不同主機。

(7) 架設服務網站與資料維護

本案的使用者眾多，相關服務與資源須有統一服務平台。而在當中，首重 : 視訊帳號 (視訊會議討論室) 的開設，以及如何配對眾多的教與學兩端成員。我們分別說明如下：

A. 建置視訊帳號開設系統 :

我們於網站上提供帳號需求登記申請，收集各單位所需的視訊帳號數量，其中，關鍵的資料輸入欄位有：申請數、密碼、類型 (一對一、一對多)、開課日期、上課時段選擇。待系統管理者審核決定數量之後，便可逕行自動依據申請單位代號開設完成所需數量連續號碼的視訊帳號。

B. 建置學童配對系統 :

該單位申請取得視訊帳號之後，即可將該些帳號透過我們設計的系統，進行教與學兩端成員的配對，也就是哪一對成員配置到那一個視訊帳號，之後便可依據該視訊帳號是否正在執行，判斷該對成員是否正在進行線上課輔，並可依據該帳號錄影檔案檢視該配對組的上課情況。而此配對功能在未來將更進一步研擬為更自動化的與帳號申請一起進行。

3. 結果與討論

1. 計畫成員反應

問卷整理－計畫在每期程結束時，都會針對計畫參與成員進行滿意度問卷調查。以下列舉 992 期末時 (100 年 6 月)，分別對於參與計畫之大學學伴、大學師長、中小學師長，針對 1. 電腦教室與網路 2. 教學平台與設備，滿意度的問卷結果：

(1) 大學學伴對電腦教室與網路的看法，如下圖八所呈現，滿意度偏低，顯見各夥伴大學所使用的電腦教室之穩定度與效能上應更加強處理維護。

(2) 大學學伴對教學平台與設備的看法，如下圖九所呈現，滿意度還算尚可，顯見電腦與網路的問題比較多。

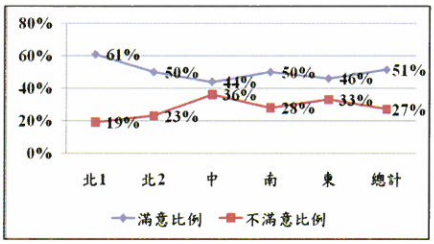

圖八 大學伴對電腦教室與網路的看法

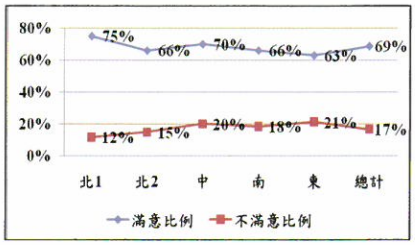

圖九 大學伴對教學平台與設備的看法

(3) 大學師長對電腦教室與網路的看法，如下圖十所呈現，滿意度還算不錯

(4) 大學師長對教學平台與設備的看法，如下圖十一所呈現，滿意度還算尚可

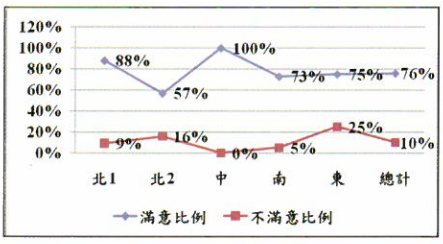

圖十 大學師長對電腦教室與網路的看法

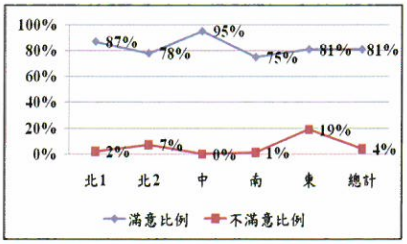

圖十一 大學師長對教學平台與設備的看法

(5) 中小學師長對電腦教室與網路的看法，如圖十二呈現，滿意度算是好的。

(6) 中小學師長對教學平台與設備的看法，如圖十三呈現，滿意度算是好的。

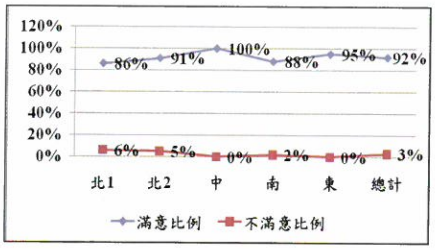

圖十二 中小學師長對電腦教室與網路的看法

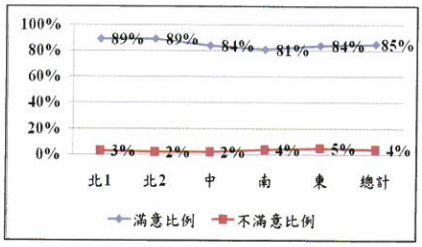

圖十三 中小學師長對教學平台與設備的看法

從以上結果看來，比較需進一步掌控的是各個在地電腦教室環境的維護與管理。呼應了我們經營過程中所看到的，機制與模式的建立，最終仍要有人 (人力與能力) 去執行，無法全盤由系統維運單位建立最後成績，而是要各單位同心合力才能完成。我們在最後的建議部分提出建議辦法。

2. 教學錄影檔重要典藏

本計畫在 99.4.29~100.6.30 期間，共協助分類整理了共計 116,849 個教學錄影檔案 (情境畫面如下圖十四，完整呈現實際的教學過程，可事後檢視檢討之用)。這些都是重要的教學紀錄，可以作為未來再研究了解關於遠距課輔之重要典藏，本計畫也同時建立了錄影檔案的存取機制。

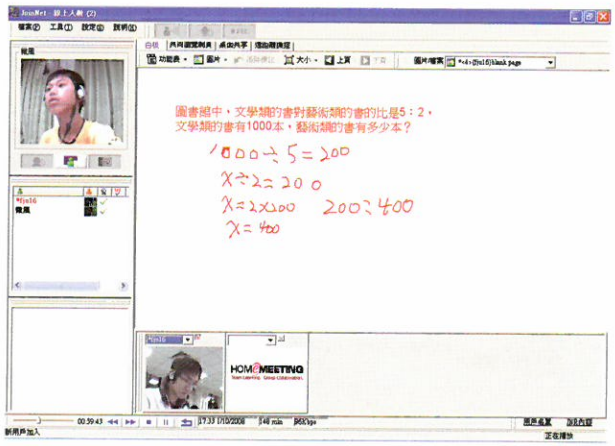

圖十四 錄影檔呈現實際的教學過程

3. 課輔時數陪伴共讀

本計畫在 99.4.29~100.6.30 期間，累計的線上課輔總時數為 91,095 小時，這背後意味著本計畫造就了多少個大小學伴在此系統架構環境下共同成長的過程。計畫執行以來已逾五年，當年第一批參與網路課輔的小學學童，升國中後，繼續參加計畫。在這一、兩年中，已陸續參加高中甄試、基測，順利升學。99 學年度，桃園縣復興鄉張○惠，高中基測因原住民身份加分後，總分 486，遠遠超過基測的滿分 412；台北縣瑞芳鎮九份山區學童兩位甄試入基隆女中，一位基隆高中。100 學年度，復興鄉山區學童一位經甄試入武陵高中、一位桃園高中；台東縣成功鎮兩位甄選入台東女中等，分別創下各偏鄉中學歷年升學最佳紀錄。檢討成效，網路遠距課輔，藉助資訊技術，引進大量外界課後輔導人力，幫助學童提升學習效果外，最關鍵處，在長期的陪伴。他們感受到外界的關心、開啟學童新視野、改變學習態度，點燃鬥志，主動積極讀書，終於破繭而出。

4. 建置課輔日誌系統做全方面管理

課輔日誌是計畫中，彙集所有資訊的集中地，運用得法，可以作為管理與績效評估的利器。在 99.4.29~100.6.30. 期間，計有 56,116 則日誌內容。依權責的不同，分別有各自版面陳述。圖十五，為大學課輔老師，每次上完課，要下線時，填寫的日誌；紀錄當天上進度、教學內容、與學童互動的感想，輔導老師並會針對內容回覆，並作適當的指導與鼓勵或糾正。圖十六，則為學童端現地帶班老師就每一位學童當天的上課表現、教室整體運作、網路或設備妥適否與個人感想，所作的紀錄。

圖十五 課輔日誌紀錄 - 大學課輔老師端畫面

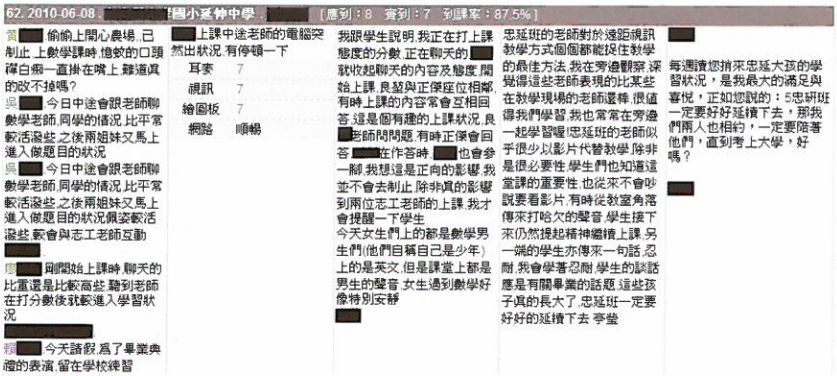

圖十六 課輔日誌紀錄 - 學童端現地帶班老師畫面

5. 建置線上教育訓練系統平台

本計畫除了透過線上課輔以解決傳統教學之交通安全與時間問題之外，同時也對於團隊的訓練，增加了線上教材製作與線上自學管理機制，如此也對於計畫經費的節省有很大的幫助，從管理機制當中，設計讓各區存放錄製的教材，並設計讓同學自行選擇時間上網學習 (圖十七為大學生登入訓練課程首頁的畫面)。並在學習之後，依循系統的要求留下回饋與心得，以作為確實依照規定線上研讀教學紀錄之依據。(圖十八為系統彙整的心得回饋結果)

	課程名稱	類型	對象	預估時間	開放日期	課程大綱	完成	最後修訂
1.	8 . 數位學伴輔導團隊如何連結社區資源與教學端及學習端共同建檔完善之課業輔導模制 --以魚池禮拜堂爲例	隨邊文件	所有人員	40m	2011-10-12 2011-10-31 開始學習	一、課輔運作交互關係及輔導模制建檔模式說明。 二、實施策略與方法--以南投縣魚池禮拜堂中小學學伴爲例 三、實施成效分析及說明 四、未來規劃與願景	118	中區 禮依岑 2011-10-13 11:08
2.	7 . 線上教學示範--數學科	隨邊文件	所有人員	50m	2011-10-04 2011-10-31 開始學習	課程名稱:線上教學示範--數學科 主講者:黃怡婷 課程大綱: 由優秀的數學課輔老師黃怡婷 分享自己的課輔經驗,了解自己的專長並發揮所學教導孩子,與孩子做更長遠的。	171	總計畫 蔣依玲 2011-10-04 09:49
3.	12 . 線上教學示範--英語科	隨邊文件	所有人員	50m	2011-10-03 2011-10-31 開始學習	課程名稱:線上教學示範--英語科 主講者:洪若珊 課程大綱: 由優秀的數學課輔老師洪若珊 分享自己的課輔經驗,了解自己的專長並發揮所學教導孩子,與孩子做更長遠的	71	總計畫 蔣依玲 2011-10-25 14:59
4.	9 . 國中小數位課輔資源之整合	隨邊文件	所有人員	52m	2011-10-02 2011-10-31 開始學習	由南區義守大學高慧芬副教授所錄製「數位課輔資源之整合」，希望能夠提供大學伴們在準備教學上有所幫助	86	南區 張芳榆 2011-10-19 16:38

圖十七 大學生登入訓練課程首頁的畫面

	單位	瀏覽人	類別	起訖時間	持續時間	預估差距	1. 由優秀的數學課輔老師洪若珊 分享自己的課輔經驗,了解自己的專長並發揮所學教導孩子. 與孩子做更長遠的 【 線上教學示範--英語科 】	2. 意見、心得感想:(可不填)
1.	輔仁大學		大學學伴	2011-10-12 20:13~20:58	45	-5		第一次參與遠距教學的活動，還蠻擔心自己是否能承擔、是否能帶給孩子好的教材，但在無意間想到自己最主要是想陪伴在孩子旁，和他們聊聊、替他們解決課業難題及生活中所遇到的問題，畢竟大家的經驗都是從無累積到有，自己盡力教孩子最重要。參予這活動不只可累積經驗，也能在和孩子的互動過程中培養耐性，及解決問題的方法。我真的非常高興自己參加遠距教學活動，讓大學生活更多采!!
2.	國立中央大學		大學學伴	2011-10-12 21:35~22:29	54	4		原來上課前需要做先暖身，可以拉近與孩子的距離，發現他有些分心時可以加入他有興趣的話題，也可以跟她一起訂定目標，多讓他發言而不是一味的填鴨，朗讀題目也可以了解題意，假如有不懂題意的地方，可以馬上做觀念上的澄清，多跟生活上結合可以讓他更深刻題幹，我欠缺的是毅力...繼續加油!

圖十八 系統彙整的線上教育訓練心得回饋結果

6. 協助人文成長與進步

98年底，每學期結束前，針對一千多名大學生參與計畫後，個人感受及受影響部分，進行問卷調查。結果顯示在「人際互動」、「同理心」、「耐心」、「尊重與關懷」等四個向度，有明顯進步 [22]。輔仁大學聶達安神父主持之教育部品德教育調查研究計畫，以本案參與之大學生為研究對象，並將成果提報到「行政院國家教育研究中心」。

4. 結論與建議

國內大學校院，具處理瞬間大量網路流量經驗者，匯集於擔任區網中心的大學。區網中心的運作，有高效率的交換機及路由器負責，與網路課輔平台、人員管理性質迥異。數位學伴計畫案，必須管理全國一千多名學童與其課輔老師，將近兩千人，同一瞬間一起上線時的龐大影音流量。壓力沉重如斯者，只此一案。在無前例可茲遵循下，一切都靠系統維運同仁由零開始逐項建置、自行摸索累積經驗，即時判斷因應突發狀況。五年來的管理成效，讓計畫推動順利、快速發展，累積數千名學童因而獲益；

幕後的系統維運運作是成功的。

負責計畫整體軟硬體設備運作、品質管理的任務成員，經由嚴苛的資訊技術挑戰、火線上即時解決問題的壓力，已焠鍊成實戰經驗豐富的資訊工程師，可以作為各界徵詢瞬間龐大網路流量管控技能之諮詢顧問。

總結執行計畫的想法，這是一個讓大學充分發揮「大學社會責任」的方案。藉由資訊科技搭建出來的弱勢關懷平台 [23]，讓偏鄉教育服務，以網路無遠弗屆的擴展開來，基於即時及安全的優勢，發展成日常常態型的服務模式，而非只能在寒暑假才得以進行。

網路遠距教學的軟硬體設備及環境、團隊營運都已依實際運作的經驗，撰寫成標準作業流程 (SOP)[24]，提供外界明確參考。教育部準備好了嗎？準備永續經營的政策了嗎？在以往有許多屬於實驗性質的計畫，伴隨著的是各中 / 小學的配合壓力，教育部是否有決心，準備整合各項偏鄉教育計畫的優缺點擬定深耕政策，如此應可節省資源並發揮更好的效能。

最後提出幾點建議如下，作為未來推行與研究改進之參考：

1. 提升各夥伴學校資訊設備維護能力
   各夥伴學校應有能力或嘗試尋求就近資源以解決自己校內電腦設備與網路環境的問題，如此才能有效的在每一次課輔上課時間達到課輔的效果，不至於因為設備問題而延誤進度。目前中小學沒有資訊人力 (師資或是技術人員) 或是單位 (例如：電算中心) 可以協助，建議解決辦法：
   (1) 無資訊人力之中小學：建議教育部以國防替代役編制支援。
   (2) 無資訊單位支援之中小學 (包含某些參與計畫的大學)：建議教育部應對此計畫參加的各校發文，鼓勵甚至要求該學校的資訊單位應該要配合計畫人員在資訊設備或是環境上的協助。
2. 主動了解夥伴學校的生態，有助於問題解決。例如：校內網路雍塞，可能不是網路出現問題，而是學校網路頻寬本就不充足，碰到課輔時段又有人執行大量下載的動作，可以建議該校建立網路使用規範以利解決。
3. 督促各校作例行維護檢查是必要的，不論是系統環境或是硬體設備，皆需要例行維護，才能熟悉知道哪些設備的特性，在問題發生時後做最有時效的處理。
4. 中小學端的網路設備 (耳麥、視訊) 最好能固定安裝在電腦上面，以減少插拔過程，

否則可能在下次使用時插錯孔位，甚至因經常性的插拔造成接觸不良或線路鬆脫，增加設備使用之不穩定情況。如此便會降低上課的效率。

5. 可考慮結合企業力量，發揮企業服務的價值。政府可以公開徵詢企業參與配合，不論是支援書籍、教材、甚或是電腦設備、網路服務，讓社會大眾共同經營此份理念。

5. 誌　謝

本論文承蒙教育部「數位學伴線上課業輔導服務計畫」的補助，謹致最誠摯的謝意。並以此文向所有參與此計畫的各界大小朋友們，與輔仁大學呂慈涵老師率領的「輔大偏鄉教育關懷團隊」全心全力投入，致上最高敬意。大家的愛心關懷與努力是人生教育課程中最好的教材，也是激發系統維運更進步的主要動力。

參考文獻

1. 教育部 , 教育部攜手計畫，http://asap.moe.gov.tw/ , last accessed:2011/10/29
2. 博幼基金會 , 課輔方案，http://www.boyo.org.tw/index.htm, last accessed: 2011/10/29
3. 永齡教育慈善基金會，永齡希望小學課輔計畫 , http://www.yonglin.org.tw/index.htm, last accessed: 2011/10/29
4. 教育部，教育部發展原住民族教育五年中程個案計畫，http://www.edu.tw/files/list/B0039/ 附件 -12 發展原住民族教育五年中程個案 .pdf
5. 行政院經濟建設委員會，挑戰 2008：國家發展重點計畫（2002-2007），2002.5.31 核定，2005.1.31 修訂，http://www.cepd.gov.tw/m1.aspx?sNo=0001539&ex=3, last accessed: 2011/10/29
6. 數位台灣計劃網站，http://www.etaiwan.nat.gov.tw/index.php , last accessed: 2011/10/29
7. 教育部 , 教育部創造偏鄉數位機會，http://itaiwan.moe.gov.tw/, last accessed: 2011/10/29
8. 行政院經濟建設委員會，新世紀第三期國家建設計畫 -- 民國 98 至 101 年四年計畫 , http://www.cepd.gov.tw/m1.aspx?sNo=0011413, last accessed: 2011/10/29
9. 行政院經濟建設委員會，中華民國 100 年國家建設計畫 (核定版)，2010 年 12 月 30 日行政院第 3228 次會議通過，http://www.ey.gov.tw/public/Attachment/1179483771.pdf, last accessed: 2011/10/29

10. 教育部 , 教育部 98 年偏鄉中小學網路課業輔導服務計畫—總計畫，教育部發文文號 : 臺電字第 098008846 號，2009/1/1~ 2010/1/31
11. 教育部，教育部 97-98 年偏鄉中小學網路課業輔導服務計畫—北區輔導中心，教育部發文文號 : 臺電字第 0970203229 號、臺電字第 09800178709 號，2008/9/4~ 2009/11/4
12. 教育部數位學伴線上課業輔導服務計畫網站，http://www.dsg.fju.edu.tw/, last accessed: 2011/10/29
13. 教育部，教育部 99 年數位學伴線上課業輔導服務計畫—總計畫暨北一區輔導中心，教育部發文文號 : 臺電字第 0990067780 號，2010/3/30~ 2011/7/29
14. 教育部，教育部 100 年數位學伴線上課業輔導服務計畫—總計畫暨北一區輔導中心，教育部發文文號 : 臺電字第 1000151681 號，2011/8/3~ 2012/8/2
15. 教育部，教育部 99 年數位學伴線上課業輔導服務計畫—系統維運，教育部發文文號 : 臺電字第 0990097636 號，2010/4/29~2011/8/28
16. 教育部，教育部 100 年數位學伴線上課業輔導服務計畫—系統維運，教育部發文文號 臺電字第 1000170458 號，2011/8/29~2012/7/31
17. 周原，五年視訊陪伴 - 輔大學生帶弱勢兒變狀元，天下雜誌第 473 期, 第 170-171 頁, 2011/6/1
18. 趙涵捷，談偏鄉中小學網路課業輔導計畫之緣起與發展，97-98 偏鄉中小學網路課業輔導服務計畫各分區輔導中心暨夥伴大學團隊九十七學年度第一學期擴大工作會議手冊，第 5 頁，2009/1/16。
19. 楊志田，距離不是問題 – 偏鄉中小學網路遠距課業輔導服務 - 以輔仁大學資訊中心教學組的執行經驗探討為例，TANet 2009 台灣網際網路研討會論文集，第 G114-G119 頁，2009/10/29
20. 太御科技，JoinNet 跟 Co-Life 有何差異， http://blog.joinnet.tw/index.php?op=ViewArticle&articleId=618&blogId=1, last accessed: 2011/10/29
21. 施富川，施富川的 e-Learning 布拉格，http://fcshih.blogspot.com/, last accessed: 2011/10/29
22. 呂慈涵，從偏鄉中小學網路課業輔導服務計畫談對大專課輔教師與課輔學童品德教育之影響，http://charaedu.fju.edu.tw/efgu.htm, 2009/10/12
23. 林宏彥、楊志田，系統 & 維運—以資訊技術搭建弱勢關懷平台，教育部 99 年數位學伴線上課業輔導服務計畫「數位 i 關懷 深耕 e 畝田」成果展，2011/6/29
24. 呂慈涵、林宏彥，偏鄉中小學遠距課業輔導執行模式與策略 -- 輔仁大學遠距課輔實施經驗為例，2008 電腦與網路科技在教育上的應用研討會，國立新竹教育大學，2008/10/30~2008/10/31

Received October 31,2011
Accepted January 6,2012

Using Network to assist tutoring after School's learning is no limit- The MOE's Project of Online Tutoring After School For Distance Learning Companion As An Example

Hong-Yen Lin and Chih-Tien Yang

Information Technology Center, Fu Jen Catholic University
Taipei, Taiwan 24205, R.O.C.

Abstract

With the quick improvement of Computer and Network technology, the learning opportunity had become multi-dimensional. The long distance online network learning education can solve the problem that traditional face to face education might have such as lower learning efficiency, traffic time waste and safety. In this article, with the experience of the system operation and maintenance on the MOE's project of online tutoring after school for distance learning companion, we build a highly efficient management model for Hugh amount of learning pairs that simultaneously held long distant online network class, and analyze the problem occurred in it to find a solutions. We also will propose the suggestion for improving this model.

The project of Online Tutoring after School's learning for lower developing area has three cores: counseling area, teaching area, digital technical, and all of it is Indispensable. Although the digital technical is the basement of this learning model, also the key for the success of teaching area, digital technical. We believe our model is feasible and effective. We still keep on developing it, also very happy to share the experience with you. It is our greatest hope that many college students and children can improve themselves under this learning model.

Key words: Distance Learning Companion, system operation and maintenance,Online Tutoring after School's learning for lower developing area

應用人工蜂群演算法調整陣列天線之最佳位置

余相寬　李坤洲

國立成功大學系統及船舶機電工程學系

摘　要

通訊科技的發展改變了人類的生活品質，而通訊陣列是實現無線通訊的基本媒介工具。本研究採用人工蜂群演算法，調整陣列元素之位置，且須符合主波瓣束寬之限制條件，來使陣列波束函數旁波瓣級之極小化，達成陣列問題最佳化之目的。首先，介紹陣列天線之相關知識和陣列波束函數方程，以及如何在限制條件內做最佳化處理。模擬結果顯示，應用人工蜂群演算法能有效率的達成最佳化目標，收斂至全域解所需花費時間較少，能有效處理線性和非線性最佳化問題，並能應用於其他研究領域，非常適合用於工程領域之最佳化問題。

關鍵詞：陣列天線、人工蜂群演算法、最佳化。

1. 前　言

本研究之目的主要是設計一個陣列天線 (antenna array)[1]。事實上，陣列天線求解方式可以分成解析解和數值解兩種，然而當陣列逐漸擴大時，解析方法已無法滿足其需求，因此在陣列設計上多半採用數值方法求解。現透過一種主要是在解決組合問題的最佳化方法，稱為人工蜂群演算法 (Artificial Bee Colony Algorithm)，來處理研究問題之位置和振幅，以證明天線之性能。若欲提升天線之性能，其首要課題為抑制旁波瓣級 (side-lobe level) 之能量，大體來說，旁波瓣 (side-lobe) 的數量越多，資料會越容易遭到外洩，所以必須對旁波瓣之數量有所控制。然而主波瓣 (main-beam) 之輻射方向也是一大關心課題，若其束寬 (beam-width) 越窄，表示聚束效果好，越能得到好的指向性。另外陣列元素 (array elements) 之位置擺放和排列方式，會決定波束函數的輻

[701] 台南市大學路 1 號成功大學自強校區系統及船舶機電工程學系

射效能之好壞，且其往往會受限於陣列或擺放地形等因素，所以擺放陣列元素之位置時會顯得更加困難，但一般習慣上都是採用半波長。陣列天線為通訊的基本媒介工具，且以往也有多位學者致力於此方面的研究。1968 年 R. K. Arora [2] 對線性天線陣列作出僅調整位置的對稱陣列研究；1988 年 P. Jarske [3] 針對對稱陣列的線性陣列天線作出調整權重與位置的研究；1996 年 V. Murino [4] 針對非對稱的線性陣列天線調整位置找出全域最佳解。近年來也有學者使用基因演算法 [5]、蟻群演算法 [6] 和粒子群演算法 [7] 來處理陣列天線問題。

2. 陣列波束函數

假設陣列為線性陣列，且為 N 個點元素所組成，並沿著 X 軸放置，如圖 (一)，其波束函數方程 (Beam Pattern Function) 可表為式 (1):

$$F(\theta)=\sum_{n=1}^{N} A_n \cdot e^{jkx_n u} \tag{1}$$

其中 X_n 為第 n 個元素位置，$k=\frac{2\pi}{\lambda}$ (λ 為波長)，A_n 表激發能量 (exciting source) 的振幅，$u=\sin\theta-\sin\theta_0$ (θ 為方向角，θ_0 為主波瓣峰值方向) [8][9]。

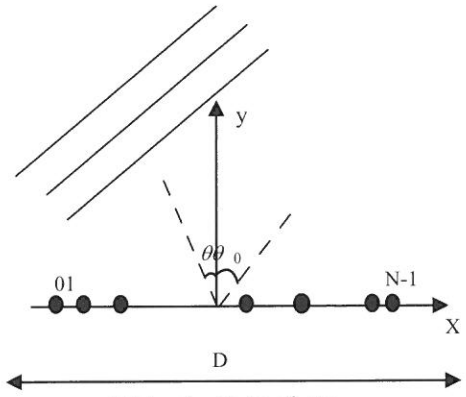

圖(一) 線性陣列

若我們要把波束函數繪製成 θ 函數，主波瓣通常發生在 $\theta = 0^\circ$ 的時候，且寬度並不會和主波瓣峰值方向產生相依之情形。若將陣列波束函數用分貝 (decibels) 來表示，則利用 20 log $\left|F(\theta)/M\right|$，其中 M 為所有振幅的總和，化成分貝後可以有效的利用波束函數之特性，將有助於做最佳化處理。其因波束函數為偶對稱於 ，即 $F(\theta)=F(-\theta)$，所以我們觀察範圍可以從 $0 \le \theta \le 90^\circ$。若只需觀察一次，可以先畫出波瓣圖 (pattern)，再用人工規則尋找旁波瓣，萬一需要觀察很多次，那麼最好用程式尋找。本研究找尋旁波瓣的方式為對每個輻射值兩邊兩邊比較，若某處大於它的兩邊的值，即為旁波瓣峰值，最後從大到小排序後，第一大的就是主波瓣，而第二大的則是旁波瓣級。束寬即主波瓣在波瓣圖裡的寬度。習慣上用 $\frac{1}{\sqrt{2}}$ 倍的主波瓣峰值發生處來當束寬的邊界，本研究尋找束寬之方式為以 0 為基準，減去各個輻射值加上 3dB 後，取最短距離者，即為所要之束寬。

3. 人工蜂群演算法

人工蜂群演算法是 2005 年由 D. Karaboga[10] 所提出，並在近幾年內也有做出各項改進 [11][12]。在人工蜂群演算法的模型中，主要包含三個基本構成要素，分別為引路蜂 (employed bees)、跟隨蜂 (onlooker bees) 和偵查蜂 (scout bees)，在每次循環中引路蜂和跟隨蜂的個數相等，偵查蜂個數設為 1。引路蜂和跟隨蜂負責開採過程，而偵查蜂執行探索過程，所以說人工蜂演群算法結合全局和局部搜索方法使蜜蜂在食物源的探索和開採兩方面達到了平衡。人工蜂群演算法在求解最佳化問題時，食物源的位置被抽象成解空間中的點，蜜蜂採蜜的過程也就是搜索最佳解的過程。現考慮全局優化問題P，P的多個可行解的一個結合稱為一個種群，種群中每個元素稱為一個食物源，每個食物源的優劣程度取決於待求解之最佳化問題之適應值 (Fitness)。設解的個數 SN 等於引路蜂和跟隨蜂的個數，我們用 d 維向量來表示每個解 $X_i(x_{i1}, x_{i2} \dots x_{id})^T$，然後蜜蜂對所有食物源進行循環搜索，循環次數為 C($C = 1,2,\dots MCN$)。引路蜂首先對相應的食物源 (解) 進行一次鄰域搜索，如果被搜索到的食物源 (解) 的花蜜質量 (適應度) 優於前解，則用新的位置替代舊的食物源位置，否則保留舊的。當所有引路蜂完成搜索後，引路蜂會把食物源花蜜質量信息傳給跟隨蜂，跟隨蜂根據得到的信息按照概率選擇食物源，花蜜越多的食物源被選中的機率越大，且跟隨蜂選中食物源後，也進行

一次鄰域搜索，並保留較好的解，經過最大循環次數後最終找到最優解。

$$v_{ij} = x_{ij} + r_{ij}(x_{ij} - x_{kj}) \tag{2}$$

引路蜂和跟隨蜂依據式 (2) 進行食物源位置更新，其中 k∈(1,2,…SN)，j∈(1,2,…d)，這兩個數都是隨機選取的，但是 k 不能等於 i(k 是 i 鄰域的一個解)，r_{ij}∈[-1,1] 是一個隨機數，控制 x_{ij} 鄰域的生成範圍，隨著搜索次數增加會越接近最佳解，鄰域範圍會逐漸變小。跟隨蜂要選擇到哪個食物源採蜜是依據引領蜂所帶回來之食物源的收益率 (適應值) 大小，選擇收益率的方式採取局部競爭機制 [13]，主要思想是隨機在群體中選擇 k 個個體進行比較，如果當前個體收益率好於另一個體的收益率，則給予該個體一分，對每個個體重複這一過程，得分最高者，即為跟隨蜂所要探索的對象，這樣的選擇方式在一定的程度上避免了提早收斂或停滯現象產生，其中 k 一般取 2。

以下整理出人工蜂群演算法的流程：

步驟一：初始化種群解 x_i (i = 1,2,…, SN)，並計算每個解 的適應值。

步驟二：引路蜂根據式 (2) 做鄰域搜索產生新解 ，並計算其適應值。

步驟三：如果 v_i 的適應值優於 x_i，則用 替換 ，並將 v_i 作為當前最優解，否則保留 x_i 不變。

步驟四：進行局部競爭機制，選擇出最高分的適應值。

步驟五：跟隨蜂根據所選擇的食物源依照式 (2) 進行鄰域搜索產生新解 v_i，並計算其適應值。

步驟六：如果 的適應值優於 x_i，則用 v_i 替換 ，否則保留 x_i 不變。

步驟七：紀錄到目前為止最好的解。

步驟八：判斷是否滿足終止條件，如滿足則輸出最佳解，否則返回步驟二。

4. 模擬與結論

考慮 25 個非均勻陣列元素排列在 X 軸上。 設定為 θ_0，中心元素被固定在 X 等於 0 的位置，作左右對稱，而最外層的元素是固定在 X=±25λ，元素位置都位於 x=q·$\frac{\lambda}{2}$，其中 q 是整數且 | q |≤49。並限制元素隨機擺放，但只能落在$\frac{\lambda}{2}$的整數倍位置，且同一個位置只能擺放 1 個元素，換句話說，不可多個元素放在同一地點。假設陣列

波束函數為正常的線性陣列且 θ 設定在 0 度到 90 度之間，尋找元素的最佳位置，盡可能使旁波瓣越小越好。主波瓣的寬度必須限制在小於或等於 4.6 度。

第一個例子是只調整陣列元素的位置。即陣列元素位置之振幅均設為 1，因此每個種群維度為 11，經由以上之限制條件後，最佳化結果適應值為 10.40，即旁波瓣級為 -10.40 分貝，其最佳化位置分別 1.0,1.5,3.0,4.0,5.0,6.0,6.5,7.5,9.5,10.0,19.5，束寬為 1.4 ° (degree)。本研究結果明顯優於 [3] 之旁波瓣級為 -10.14 分貝，束寬為 1.6 ° (degree) 之結果，圖 (二) 為最佳化後之陣列場型圖。

第二個例子是調整陣列元素之位置和振幅。本研究方法為利用例子一之最佳化位置，將振幅從原本為 1 進行最佳化調整，經人工蜂群演算法後其旁波瓣級 -12.76 分貝，其最佳化振幅分別為 1.47,1.99,1.48,1.29,1.13,1.07,0.91,1.02,0.64,0.06,0.32,0.16,0.16，模擬結果大幅降低旁波瓣級之位準，且結果明顯優於 [4] 之結果，圖 (三) 為最佳化後之陣列場型圖。

第三個例子則是對非對稱陣列進行探討，且僅對陣列位置元素進行調整，振幅均設為 1，因此問題維度為 23，經人工蜂群演算法最佳化後，旁波瓣級為 -12.48 分貝，其最佳化位置分別為 0.5,1.5,2.5,3.0,3.5,4.5,5.0,5.5,6.0,6.5,7.0,7.5,8.0,8.5,9.5,11.5,12.5,13.0,14.0,18.0,21.5,27.0,39.5，束寬為 1.6 ° (degree)，研究結果明顯優於 [5] 之旁波瓣級為 -12.07 分貝，束寬為 1.6 ° (degree) 之結果，圖 (四) 為最佳化後之陣列場型圖。

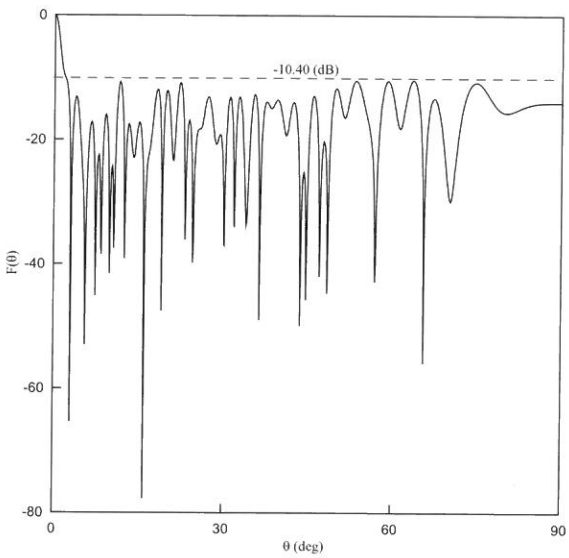

圖 (二) 例子一陣列場型圖

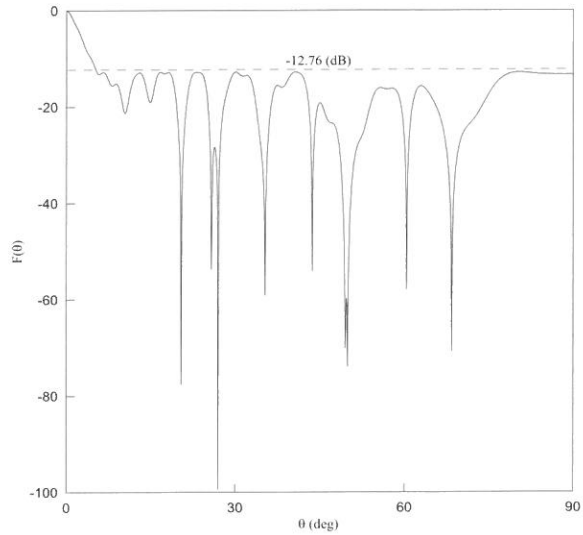

圖 (三) 例子二陣列場型圖

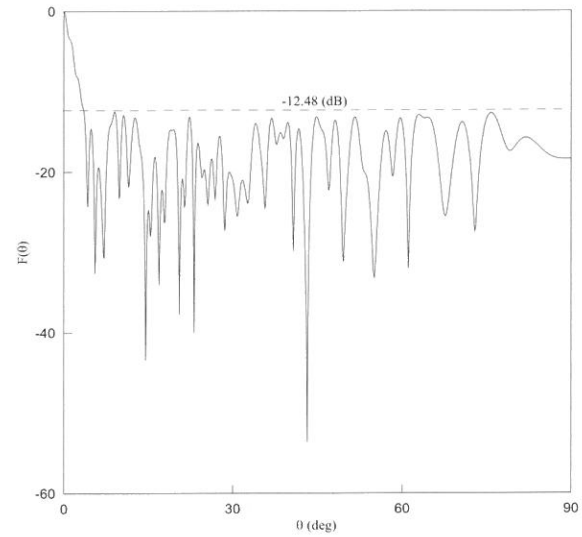

圖 (四) 例子三陣列場型圖

本研究採用人工蜂群演算法實現線性陣列之旁波瓣極小化及合乎主波瓣束寬之限制條件，結果證明人工蜂群演算法有效率並且容易達到最佳化目標。在整個模擬過程中發現，僅調整位置而固定權重之情況下 (例子一和例子三) ，其束寬範圍差異量極小，但若在限制束寬的條件不同之下進行最佳化設計，所得結果差異很大，由此可知束寬

與旁波瓣級位準之間息息相關，所以在設計天線陣列場型圖時，條件限制範圍必須依實際狀況而定。而在調整位置與權重之情況下 (例子二)，較容易達到我們所要之解，藉由束寬之限制條件，可大幅減少旁波瓣之數量和降低旁波瓣級位準，且此法更能夠應用在現實工程問題之中。

參考文獻

1. 張振晏，“應用最佳化演算法於通訊陣列之分析與設計”，博士論文，國立成功大學系統與船舶機電工程研究所，(2009)。
2. R. K. Arora and N. C. V. Krishnamacharyulu, “Synthesis of unequally spaced arrays using dynamic programming,” *IEEE Transactions on Antennas and Propagation*, vol. AP-16, no. 5, pp. 593-595, 1968.
3. P. Jarske, T. Saramaki, S. K. Mitra et al., “On properties and design of nonuniformly spaced linear arrays,” *IEEE Transactions on Acoustics, Speech and Signal Processing*, vol. 36, no. 3, pp. 372-380, 1988.
4. V. Murino, A. Trucco, and C. S. Regazzoni, “Synthesis of unequally spaced arrays by simulated annealing,” *IEEE Transactions on Signal Processing*, vol. 44, no. 1, pp. 119-123, 1996.
5. M. A. Panduro, “Design of coherently radiating structures in a linear array geometry using genetic algorithms,” *AEU-International Journal of Electronics and Communications*, vol. 61, no. 8, pp. 515-520, 2007.
6. E. Rajo-Iglesias and O. Quevedo-Teruel, “Linear array synthesis using an ant-colony-optimization-based algorithm,” *IEEE Antennas and Propagatuon Magazine*, vol. 49, no. 2, pp. 70-79, 2007.
7. P. J. Bevelacqua and C. A. Balanis, “Minimum sidelobe levels for linear arrays,” *IEEE Transactions on Antennas and Propagation*, vol. 55, no.12, pp. 3442-3449, 2007.
8. R. C. Hansen, *Phased Array Antennas*, 2nd ed., New Jersey: Wiley, 2009.
9. C. A. Balanis, *Antenna theory*: *analysis and design*, 3rd ed., Hoboken, N. J.: Wiley, 2005.
10. D. Karaboga, “An Idea Based On Honey Bee Swarm For Numerical Optimization,” *Technical Report-TR06, Erciyes University, Engineering Faculty, Computer Engineering Department*, 2005.
11. D. Karaboga and B. Basturk “A powerful and efficient algorithm for numerical function optimization: artificial bee colony(ABC) algorithm,” *Journal of Global Optimization*, vol. 39, no. 3, pp. 459-471, 2007.
12. D. Karaboga and B. Basturk, “On the performance of artificial bee colony (ABC) algorithm,” *Applied Soft Computing*, vol. 8, no. 1, pp. 687-697, 2008.
13. 暴勵，“人工蜂群演算法的混合策略研究”，碩士論文，太原科技大學，(2010)。

Received September 20,2011
Revised December 28,2011
Accepted January 9,2012

Application of Artificial Bee Colony Algorithm to Adjust the Optimization Position of Antenna Array

Siang-Kuan Yu and Kun-Chou Lee

Department of Systems and Naval Mechatronic Engineering
National Cheng Kung University

Abstract

The development of communications technology has done a lot in improving the quality of human life, and array communications is the basic medium for wireless technology. In this study, the Artificial Bee Colony Algorithm is applied to adjustment of optimum position for antenna arrays. Optimization is implemented by minimizing the side-lobe level under the constraint of desired main-beam width. Initially, fundamentals of antenna arrays and functions of radiation patterns are introduced. Next, detailed procedures for achieving the optimization are given under constraints. Simulation results show that optimization of radiation patterns based on Artificial Bee Colony Algorithm is very efficient. It spends less time to achieve global convergence, and is thus suitable to treat linear and nonlinear problems in engineering. In addition, the proposed scheme can also be extended to treat optimization problems in many other fields of engineering.

Key words: antenna array, Artificial Bee Colony Algorithm, optimization

Department of Systems and Naval Mechatronic Engineering National Cheng Kung University, Tainan, 701, Taiwan.

Grounded-inductor employing differential-voltage current conveyors

Yung-Chang Yin

Department of Electrical Engineering
Fu Jen Catholic University, Taiwan, R.O.C.

Abstract

The simulation of grounded inductor using two differential-voltage current conveyors (DVCCs), a grounded capacitor and two grounded resistors is presented. Proper selection of the values of the passive elements can yield very large as well as very small of simulated inductances. The grounded inductor simulated can be used in the LCR passive filters. Thus, their advantages include low component sensitivities and the ability to utilize the extensive knowledge of LCR filter design. In addition, these filters are suitable for integration. Finally, a simple biquad filter is experimentally demonstrated. The experimental result of a RLC passive bandpass filter confirming the theory is included.

Key words: differential-voltage current conveyor, inductor simulators, analog circuit design, active filters

1. INTRODUCTION

Active tuned filters are widely used in signal processing. Several circuits configurations for simulating inductors using current conveyors or four-terminal active current conveyors as active elements have been reported in the literatures [1]~[14]. Recently, the differential voltage current conveyor (DVCC) was constructed by Pal [15] and then was developed and realized in CMOS technology by Elwan and Soliman[16]. The DVCC has become very popular because of its high signal bandwidth, great linearity and large dynamic range, so it has been applied in the areas of oscillator design, active filters, and cancellation of parasitic elements [15]~[22]. For example: Elwan and Soliman employed two DVCCs and two capacitors to synthesize current-mode bandpass and lowpass filters [16]. Ibrahim, Minaei and Kuntman used three DVCCs and six passive elements to construct current-mode Kerwin uelsman ewcomb biquad[20]. Yin employs two DVCCs and some passive components to construct bandpass, lowpass, notch, allpass and highpass filters [21]. Yin used a DVCC and some passive elements to realize lowpass, bandpass and highpass filters [22]. However, the DVCC-based inductance-simulation circuit has never been presented.

In the area of active filter design, inductor simulation has attracted considerable interest, because the advantage of designing active filters by simulating the inductor of a passive LCR realization of the filter include low component sensitivities and the ability to utilize the extensive knowledge of LCR filter design. On the other hand, the grounded inductor is also frequently required for the design of analogue IC building blocks. It is, therefore, attractive to use DVCC-based circuits for simulating grounded-inductor. In this paper, a grounded inductance simulator using two DVCCs, a grounded capacitor and two grounded resistors was constructed. This inductance simulator can be used to RLC passive filters and enjoy the advantages of the RLC filters. Meanwhile, the use of the grounded capacitor simplifies the etching process for monolithic or hybrid fabrication. Therefore, these filters are suitable for monolithic implementation. Finally, a RLC passive filter using the proposed simulated inductor is experimentally verified.

2. CIRCUIT DESCRIPTION

The circuit symbol for a DVCC is shown in Fig.1. The port relations of a DVCC can be characterized as $V_x = V_{y1} - V_{y2}$, $I_Z+ = I_x$, $I_Z- = -I_x$ and $I_{y1} = I_{y2} = 0$. The '+' and '-' signs of the current iz denote the non-inverting and inverting, respectively. The proposed simulation of grounded inductor circuit is shown in Fig. 2. Using the standard notations of ideal DVCC, it is easy to show the input impedance of the circuit of Fig. 2 can be expressed as

$$Z_{in} = \frac{Z_1 Z_2}{Z_3} \quad \text{.....(1)}$$

where Z_1, Z_2 and Z_3 are the impedances. If the impedances are chosen as $Z_1 = R_1$, $Z_2 = R_2$, and $Z_3 = \frac{1}{sC}$ shown in Fig.3. This is equivalent to an inductor with inductance L_{eq} given by $L_{eq} = R_1 R_2 C$ .....(2)

From (2), it can be seen that by properly selecting values of the resistors R_1, R_2 and the capacitor C, very large as well as very small values of inductance can be easily obtained. Clearly, the grounded inductance simulator is constructed.

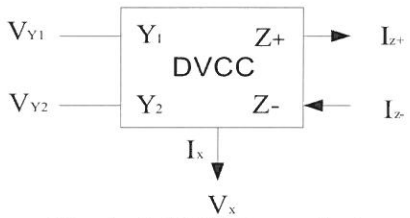

Fig.1. A DVCC symbol

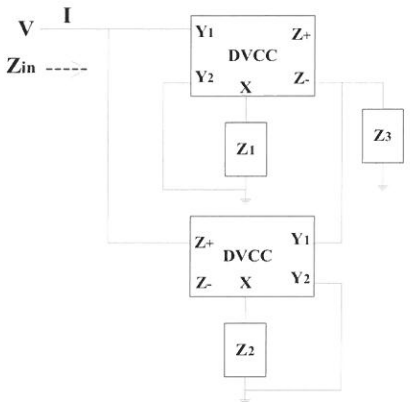

Fig.2 The proposed ground impedance simulator.

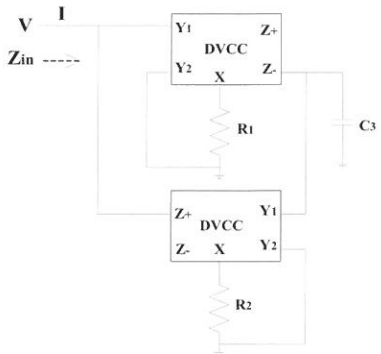

Fig.3. Grounded inductance simulator

3. EXPERIMENTAL RESULTS

The DVCC is implemented by three ICAD844s, three IC op-amps and five resistors. The proposed grounded inductor simulated was experimentally tested using $R_1 = R_2 = 1K\Omega$, $C = 1\,\mu F$ and AD844s, so this is equivalent to an inductor with $L_{eq} = 1H$. Then, this proposed grounded inductor simulated was used to replace the inductor of the RLC passive bandpass filter shown in the figure 4(a). The transfer function of the active filter has a biquadratic bandpass characteristic with

$$\frac{v_{out}}{v_{in}} = \frac{(\frac{1}{CR})s}{s^2 + s(\frac{1}{CR}) + \frac{1}{L_{eq}C}} \quad \text{.....(3)}$$

the central frequency: $\omega_o = (\frac{1}{L_{eq}C})^{1/2}$

the quality factor: $\vartheta = R(\frac{C}{L_{eq}})^{1/2}$

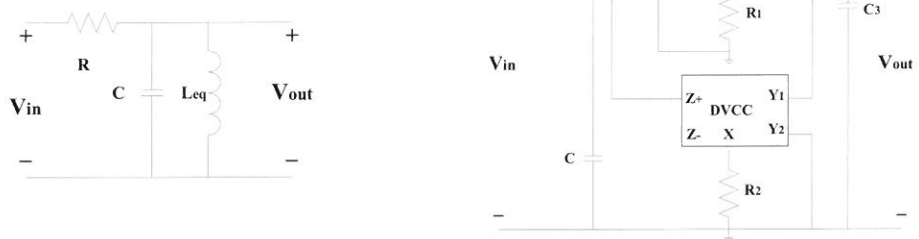

(a) The prototype passive RLC bandpass filter

(b) Bandpass filter circuit used to test the inductor realized using circuit of Fig. 3

Fig.4 (a) The prototype passive RLC bandpass filter
(b) Bandpass filter circuit used to test the inductor realized using circuit of Fig. 3

From the figure 4 (b), a biquadratic bandpass filter was constructed with $R = 10^3\ \Omega$, $C = 1\ \mu F$ and $L_{eq} = 1H$. The resonance frequency was monitored and measured and the corresponding inductance value was calculated and compared with the theoretical value calculated using equation (2). The experimental results for the gain and phase responses shown in the figure 5 (a) and (b) show a good agreement between theoretical calculations and practical measurements. The theoretical analysis correlated with the measured results with few errors which due to the errors of the use of passive elements.

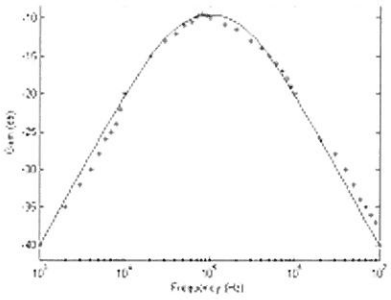

(a)The gain response curve of the banspass filter using simulated inductor.

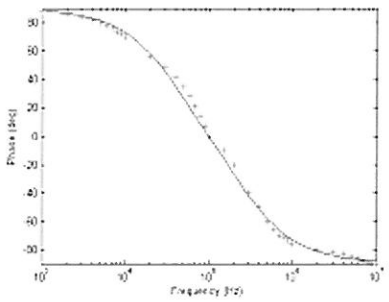

(b)The phase response curve of the banspass filter using simulated inductor.

Fig.5 (a): The gain response curve of the banspass filter using simulated inductor.
(b): The phase response curve of the banspass filter using simulated inductor.
*: Experimental result for banspass gain
+: Experimental result for bandpass phase
-: Ideal curve

4. CONCLUSION

The realization of grounded inductor using two DVCCs, a grounded capacitor and two grounded resistors has been proposed. A proper selection of the values of the resistors and capacitor, of the figure 2, can yield very large as well as very small of simulated inductances.

The advantages of designing active filters by simulating the inductors of a passive LCR realization of the filter include low component sensitivities and the ability to utilize the extensive knowledge of LCR filter design. Meanwhile, these filters are suitable for monolithic implementation. Finally, the experimental grounded inductors results of a LCR bandpass passive filter confirmed the theoretical analysis.

Reference

1. Wilson. B, "Recent Developments in Current Conveyors and Current-Mode Circuits" , IEE Proc-G, vol. 137, no. 2, pp.63-77, 1990.
2. Rober G.W. and Sedra A.S., "All Current-Mode Frequency Selective Circuits" , Electron. Lett., Vol.25, pp.759-761, 1989.
3. Toumazou C. and Lidgey E.J., "Universal active filter using current conveyous" , Electron. Lett.,vol. 22, pp.662-664, 1986.
4. Sun Y. and Fidler J.K., "Versatile active biquad based on second-generation current conveyors" , Int. J Electron., vol. 76, pp91-98 , 1994.
5. Singh V.K.and Senani R., "New multifunction active configuration employing current conveyors" , Electron. Lett., vol. 26, pp.1814-1816, 1990.
6. Robert G.W. and Sedra A.S., "A general class of current amplifier-based biquadratic filter circuits" , IEEE Transactions on Circuits and Systems., vol. 39, pp.257-263 , 1992.
7. Chang C.M., "Universal active current filters using single second-generation current conveyors" , Electron. Lett., vol. 27, no.18, pp.1614-1617 , 1991

8. Chang C.M. and Chen P.C., "Universal active current filter with three inputs and one output using current conveyors" , Int. J Electron., vol. 71, no.5, pp.817-819 , 1991.
9. Senani R., "New current-mode biquad filter" , Int. J Electron., vol. 73, no. 4, pp.735-742 , 1992.
10. Yin Y.C., "Current-Mode Biquad Using Two CFCCIIps" , Fu Jen Studies., vol. 3, no. 4, pp.367-370 , 2003.
11. Yin Y.C., Liou Y.C. "Realization of Current-Mode Highpass Lowpass and Bandpass Biquad Filters using Single CFCCIIp" , Fu Jen Studies, No.38, pp.89-99, 2004.
12. Yin Y.C., "Realization of Current-Mode Notch and Allpass Filters using Single CFCCII" , Fu Jen Studies, No.39, pp.11-22, 2005.
13. Gues E.O. and Anday F., "Realization of current-mode universal filter using CFCCIIps " , Electron. Lett., vol. 32, pp.1081-1082 , 1996.
14. Chang C.M.and Tu S.H., "Universal current-mode filters employing CFCCIIps" , Int. J Electron., vol. 85, no.6, pp.749-754, 1998.
15. PAL, K.: 'Modified current conveyors and their applications' , Microelectronics Journal, vol.20, no.4, pp.37-40, 1989.
16. Elwan H.O. and Soliman A.M., "Novel CMOS differential voltage current conveyor and its applications" , IEE Proceeding-Circuits Devices System, No.144, pp.195-200, 1997.
17. BIALOKOW, M., and NEWCOMB, R. W.: 'Generation of all finite linear circuits using the integrated DVCCS' , IEEE Trans., CT-18, pp.733-736, 1971.
18. BIALOKOW, M., SIENKO, W., and NEWCOMB, R. W.: 'Active synthesis using the DVCCS/DVCVS' , Int. J. Circuit Theory & Appl., vol.2, pp.23-38, 1974.
19. NANDI. R.: 'New Ideal Active Inductance and Frequency-Dependent Negative Resistance using D.V.C.C.S./D.V.C.V.S.: Applications in Sinusoidal-Oscillator Realization', Electron. Lett., vol.14, pp. 551-553, 1978.
20. Muhammed A. Ibrahim, Shahram Minaei and Hakan Kuntman, "A 22.5 MHz current-mode KHN-biquad differential voltage current conveyor and grounded passive elements" , International Journal of Electronics and Communications, pp.311-318, 2004.
21. Yin Y.C., "Realization of Current-Mode Filters Using Two Differential Voltage Current Conveyors" , 2010 Intelligent Living Technology Conference, pp.103-107, 2010
22. Yin Y.C. "Current-Mode Multifunction Filters using Single Differential Voltage Current Conveyor" , 2010 Workshop on Consumer Electronics Conference, pp.703-707, 2010

Received October 25,2011
Revised January 12,2012
Accepted January 18,2012

使用差動電流傳輸器合成接地電感模擬電路

鄞永昌

輔仁大學　電機工程學系

摘　要

本文提出使用兩個差動電壓電流傳輸器一個接地電容和二個接地電阻合成接地電感模擬電路。此合成接地電感模擬電路，只要選擇適當的電阻值與電容值，就可以得到非常大或非常小的模擬接地電感值。電感模擬電路的好處是，可以用來取代現有被動濾波器的電感值，使其可以被製作成積體電路，同時被動濾波器既有的好處，在被轉換成主動濾波器後，這些好處仍可繼續存在。除此之外，由於所設計之模擬接地電感之電容亦是接地，所以此電路有益於合成積體電路。最後，以既有的二階被動帶通濾波器，應用電感模擬電路取代其電感值，以驗證本文之理論預測。

關鍵字：差動電壓電流傳輸器，電感模擬器，類比電路設計，主動濾波器。

Novel Realization Filter employing Single Differential Voltage Current Conveyor

Yung-Chang Yin

Department of Electrical Engineering
Fu-Jen Catholic University, Taiwan, R. O. C.

Abstract

A new configuration for single differential-voltage current conveyor (DVCC) first-order and second-order filters is presented. It can synthesize current-mode lowpass, highpass, notch and all-pass functions with a single DVCC connected to two/four/six passive elements. The passive and active sensitivities of the proposed current-mode filters have been derived in order to determine the domain suitable for filtering applications. Finally, the experimental results of notch and all-pass filters are included to certify the theoretical prediction.

Key words: differential-voltage current conveyor, sensitivity, active filters, analogy circuit design, continuous-time filters.

1. INTRODUCTION

The advantages of the current-mode active element have been demonstrated to provide wider bandwidth and better accuracy compared with conventional operational amplifiers. Many current-mode active filters have been therefore attracted in the signal proceeding applications. For example, current conveyors (CCIIs), first introduced by noted experts, B.Smith and A.S.Sedra in 1970, have attracted considerable attention, and their various circuit applications have been explored [1][2]. Later, the four-terminal active current conveyor (CFCCII) has been used widely to synthesize multifunction filters and simulation inductance[3]~[13]. Recently, the DVCC was constructed by Pal [14] and then was developed and realized in CMOS technology by Elwan and Soliman[15]. The DVCC has many advantages such as large signal bandwidth, great linearity, wide dynamic range, high input impedance and arithmetic operation capability, so it is beneficial to develop various analogue signal processing circuits, such as low-pass, high-pass, band-pass, notch and all-pass filters and oscillators [14]~[21]. First, Elwan and Soliman employed two DVCCs and two capacitors to synthesize current-mode bandpass and lowpass filters [15]. However, the functions of notch, highpass and allpass of the proposed circuit can not be constructed. This is the drawback of [15]. Second, Ibrahim, Minaei and Kuntman used three DVCCs and six passive elements to construct current-mode Kerwin uelsman ewcomb biquad [19]. This proposed circuit can simultaneously realize lowpass, highpass, and bandpass filters, but the functions of notch and allpass can not be found directly. Third, Yin employed two DVCCs and some passive components to construct bandpass, lowpass, notch, allpass and highpass filters [20], however, the single-DVCC filter circuit was not constructed.

Minimizing the number of DVCCs has the advantage of low cost and power dissipation. In 2010, Yin proposed a current-mode filter circuit with only one DVCC and some passive elements [21]. The single-DVCC circuit can synthesize lowpass, bandpass and highpass filters, but it can not implement notch and all-pass filtering functions. In order to overcome the drawbacks of [21], a novel network for realizing a current-mode notch or all-pass filter using a DVCC as active element is presented. The new single-DVCC circuit provides a systematic method for first-order and biquadratic current-mode filters. Not only notch and allpass filters but also lowpass and highpass ones can be also obtained from the same single-

DVCC circuit configuration. Meanwhile, the active and passive sensitivities are derived to evaluate the performance of the circuit. Furthermore, the active sensitivities are zero. It means that the resultant current-mode filters will be insensitive to the current tracking error of a DVCC. Finally, the experimental results of the notch and all-pass filters are given to confirm the afore mentioned theoretical analysis.

2. PROPOSED CIRCUIT

The electrical symbol of the DVCC is shown in the figure 1 and its port relations are characterized by the following: $V_x = V_{y1} - V_{y2}$, $I_{Z^+} = I_x$, $I_{Z^-} = -I_x$ and $I_{y1} = I_{y2} = 0$. The proposed filter circuit based on and employing only one DVCC and some passive elements is shown in the figure 2. By applying routine circuit analysis, the transfer function of the figure 2 can be derived as $\frac{I_o}{I_{in}} = \frac{Y_2Y_3 - Y_1Y_4}{Y_2Y_3 + Y_1Y_2}$ .....(1)

where Y is the admittance.

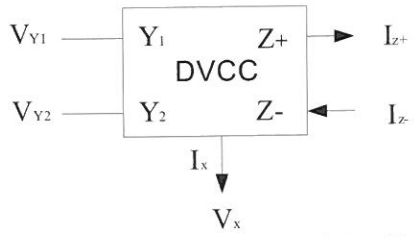

Fig 1 The electrical symbol of the DVCC

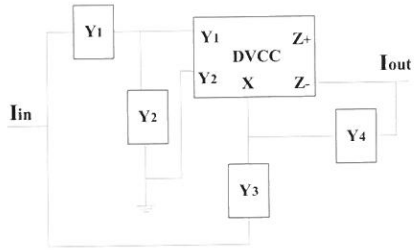

Fig 2 The proposed circuit using only one DVCC

In equation (1), the notch, all-pass, low-pass and high-pass filters can be synthesized from the same configuration. They are summarized as follow:

(1) If the admittances are chosen as $Y_1 = G_1$, $Y_2 = sC_2 + G_2$, $Y_3 = sC_3 + G_3$ and $Y_4 = sC_4$, then the transfer function will be

$$\frac{I_o}{I_{in}} = \frac{s^2C_2C_3 + s(C_2G_3 + C_3G_2 - C_4G_1) + G_2G_3}{s^2C_2C_3 + s(C_2G_3 + C_3G_2 + C_2G_1) + G_2G_3 + G_1G_2} \quad .....(2)$$

Hence, if $C_2G_3 + C_3G_2 = C_4G_1$, a second-order notch filter, shown in the figure 3, can be realized. The natural frequency ω_o and quality factor ϑ of the proposed filter are

$$\omega_o = \sqrt{\frac{G_1G_2 + G_2G_3}{C_3C_2}} \quad \text{and} \quad \vartheta = \frac{\sqrt{C_2C_3(G_2G_3 + G_1G_2)}}{C_2G_3 + C_3G_2 + C_2G_1}$$

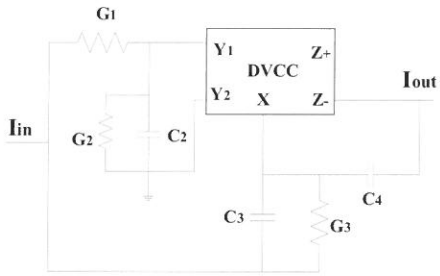

Fig 3 Second-order notch filter

(2) If the admittances are chosen as $Y_2 = Y_4 = G$, $Y_3 = G_3$ and $Y_1 = sC_1$, and $Y_2 = Y_4 = G$, $Y_3 = sC_3$ and $Y_1 = G_1$,the first-order all-pass filter, shown in the figure 4(a) and (b), are given by the following equations, respectively:

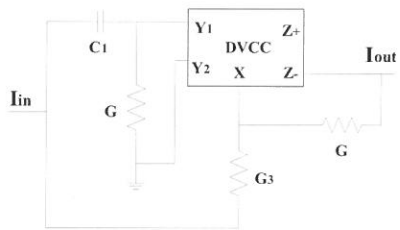

Fig 4(a) All-pass filter
(phase from 0^0 to -180^0)

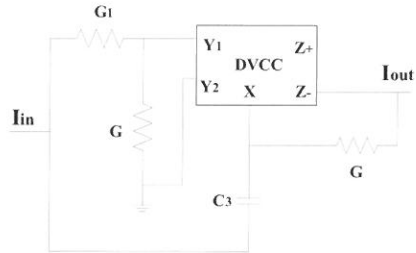

Fig 4(b) All-pass filter
(phase from 180^0 to 0^0)

$$\frac{I_o}{I_{in}} = \frac{-s + (\frac{G_3}{C_1})}{s + (\frac{G_3}{C_1})} \quad \text{.....(3)}$$

$$\frac{I_o}{I_{in}} = \frac{s - (\frac{G_1}{C_3})}{s + (\frac{G_1}{C_3})} \quad \text{.....(4)}$$

Thus, the circuits yield a phase from 0° to -180° and from 180° to 0° without constant loss in an all-pass characteristic, respectively.

(3) If the admittances of the equation (1) are chosen as $Y_2 = Y_4 = 0$, $Y_1 = sC_1$, and $Y_3 = G_3$, and $Y_2 = Y_4 = 0$, $Y_1 = G_1$, and $Y_3 = sC_3$, the lowpass and highpass filters, shown in The figure 5 and figure 6, are given by the following equations, respectively:

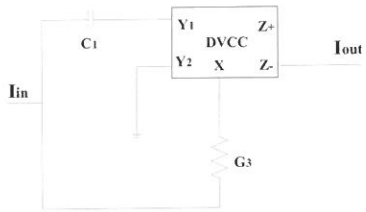

Fig 5 First-order lowpass filter

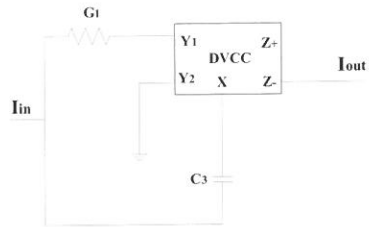

Fig 6 First-order highpass filter

$$\frac{I_o}{I_{in}} = \frac{(\frac{G_3}{C_1})}{s+(\frac{G_3}{C_1})} \quad .....(5)$$

$$\frac{I_o}{I_{in}} = \frac{s}{s+(\frac{G_1}{C_3})} \quad .....(6)$$

Thus, the circuits yield the lowpass and highpass filters characteristic, respectively. From the above description, the notch, all-pass, lowpass and highpass filters used only one DVCC and six/four/two passive elements are presented. The comparison between this paper and the recent one [21] [Yin (2010)] is shown in the table 1.

Filter / Paper	lowpass	highpass	bandpass	notch	allpass
Yin (2010)	V	V	V	X	X
Yin (present)	V	V	X	V	V

Table1. Comparison of the filter function

Taking into consideration the non-ideal DVCC, namely $i_{z+} = \beta i_x$ and $v_x = \alpha v_{y1}$, where $\beta = 1 - \varepsilon_1$ and ε_1 ($\varepsilon_1 << 1$) denotes the current tracking error of a DVCC, and where $\alpha = 1 - \varepsilon_2$ and ε_2 ($\varepsilon_2 << 1$) denotes the voltage tracking error. The transfer function of the proposed network shown in Fig. 2 can be obtained from the characteristics of a DVCC and by the routine circuit analysis:

$$\frac{I_o}{I_{in}} = \frac{\beta[(1-\alpha)Y_1Y_3 + Y_2Y_3 - \alpha Y_1Y_4]}{(1-\alpha)Y_1Y_3 + Y_1Y_2 + Y_2Y_3} \quad .....(7)$$

By relating a sensitivity parameter F to the element of variation Xi

$$S_{X_i}^{F} = \frac{X_i}{F}\frac{dF}{dX_i}$$

The passive sensitivities of the proposed lowpass, highpass and notch filters are described below:

(1): notch filter $S_{G_2}^{\omega_0} = \frac{1}{2}$, $S_{C_2}^{\omega_0} = S_{C_3}^{\omega_0} = -\frac{1}{2}$, $S_{G_1}^{\omega_0} = \frac{G_1G_2}{2\Delta_1}$, $S_{G_3}^{\omega_0} = \frac{G_2G_3}{2\Delta_1}$,

$$S_{C_2}^{\vartheta} = \frac{G_2[(G_1+G_3)(G_2C_3 - G_1C_2 - G_3C_2)]}{2\Delta_1\Delta_2},$$

$$S_{C_3}^{\vartheta} = \frac{G_2[(G_1+G_3)(C_2G_3 + C_2G_1 - C_3G_2)]}{2\Delta_1\Delta_2},$$

$$S_{G_1}^{\vartheta} = S_{G_3}^{\vartheta} = \frac{G_1G_2(G_2C_3 - G_3C_2 - G_1C_2)}{2\Delta_1\Delta_2},$$

$$S_{G_2}^{\vartheta} = \frac{G_2(G_1+G_3)(C_2G_3 + C_2G_1 - C_3G_2)}{2\Delta_1\Delta_2}$$

Where $\Delta_1 = G_1G_2 + G_2G_3$ and $\Delta_2 = C_2G_3 + C_3G_2 + C_2G_1$

(2): lowpass filter $S_{G_3}^{\omega_0} = 1$, $S_{C_1}^{\omega_0} = -1$

(3): highpass filter $S_{G_1}^{\omega_0} = 1$, $S_{C_3}^{\omega_0} = -1$

All of above are small. On the other hand, the active sensitivities of the proposed circuits are given by $S_{\alpha}^{\omega_0} = S_{\beta}^{\omega_0} = S_{\alpha}^{\vartheta} = S_{\beta}^{\vartheta} = 0$ Clearly, the filter will be insensitive to the voltage and current tracking errors of a DVCC.

3. EXPERIMENTAL RESULTS

To verify the theoretical prediction of the proposed circuit, notch and all-pass filter prototypes have been realized with discrete components to explain the reliability of the circuits given before. The experimental and simulation network in Fig. 3 were built with $G_1 = G_2 = G_3 = 10^{-3}\,\Omega^{-1}$, $C_2 = C_3 = 1\mu F$ and $C_4 = 2\mu F$. The figure 4(a) and figure 4(b) were built with $G_3 = G_2 = G_4 = 10^{-3}\,\Omega^{-1}$, $C_1 = 1\mu F$ and $G_1 = G_2 = G_4 = 10^{-3}\,\Omega^{-1}$, $C_3 = 1\mu F$, respectively. The DVCC is implemented by three ICAD844s, three IC op-amps and five resistors. The Matlab has carried out simulating the ideal curves of the filters. The figure 7 shows the experimental results for the notch and all-pass filters. The theoretical analysis correlated with the measured results with few errors which were due to the errors of the use of active and passive elements. However, the measured frequency response of the filter is in good agreement with the theory.

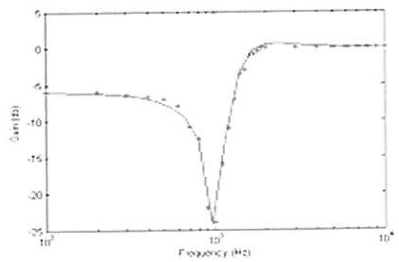

Fig 7 (a) Notch filter gain response

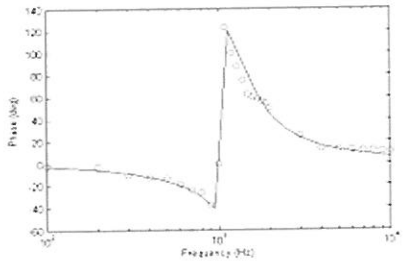

Fig 7 (b) Notch filter phase response

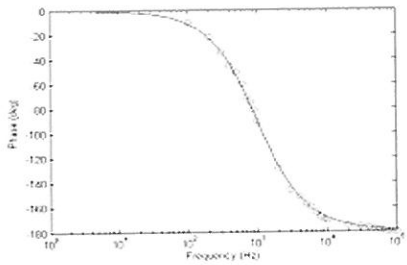

Fig 7(c) All-pass filter phase response for Fig 4(a)

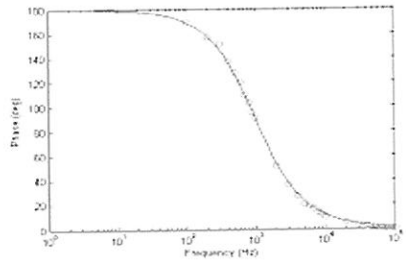

Fig 7(d) All-pass filter phase response for Fig 4(b)

Fig 7 (a): Notch filter gain response
(b): Notch filter phase response
(c): All-pass filter phase response for Fig 4(a)
(d): All-pass filter phase response for Fig 4(b)
o and * : experimental result
- : ideal curve

4. CONCLUSION

A novel network for realizing a current-mode lowpass , highpass , notch or all-pass filter using single DVCC as active elements together with two/four/six passive elements is presented. Most of these circuits utilize very small number of components. The active and passive sensitivities of these single DVCC filters are calculated to evaluate the performance of the circuits. The proposed filters enjoy the advantages as following: (i) low passive sensitivities of the parameters ω_o and ϑ ; (ii) insensitive to the voltage and current tracking errors of a DVCC; (iii) the least number of active element (only one DVCC). Finally, the notch and allpass filtering circuits with a single DVCC have been experimentally demonstrated to confirm the theoretical analysis. The results will be useful in analogue signal processing applications.

Reference

1. Wilson. B, "Recent Developments in Current Conveyors and Current-Mode Circuits" , IEE Proc-G, vol. 137, no. 2, pp.63-77, 1990.
2. Rober G.W. and Sedra A.S., "All Current-Mode Frequency Selective Circuits" , Electron. Lett., Vol.25, pp.759-761, 1989.
3. Toumazou C.and Lidgey E.J., "Universal active filter using current conveyous" , Electron. Lett.,vol. 22, pp.662-664, 1986.
4. Sun Y.and Fidler J.K., "Versatile active biquad based on second-generation current conveyors" , Int. J Electron., vol. 76, pp91-98 , 1994.

5. Gues E.O.and Anday F., "Realization of current-mode universal filter using CFCCIIps ", Electron. Lett., vol. 32, pp.1081-1082 , 1996.
6. Chang C.M. and Tu S.H., "Universal current-mode filters employing CFCCIIps" , Int. J Electron., vol. 85, no.6, pp.749-754 , 1998.
7. Yin Y.C., "Current-Mode Biquad Using Two CFCCIIps" , Fu Jen Studies, No.37, pp.64-74, 2003.
8. Yin Y.C., Y.C. Liou "Realization of Current-Mode Highpass Lowpass and Bandpass Biquad Filters using Single CFCCIIp" , Fu Jen Studies, No.38, pp.89-99, 2004.
9. Yin Y.C., "Realization of Current-Mode Notch and Allpass Filters using Single CFCCII" , Fu Jen Studies, No.39, pp.11-22, 2005.
10. Yin Y.C., "Active simulation of grounded inductor using CFCCIIs" , Fu Jen Studies, No.40, pp.71-79, 2006.
11. Yin Y.C., "Floating Inductance using Four-terminal Active Current Conveyors" , Fu Jen Studies, No.41, pp.47-56, 2007.
12. Yin Y.C., "Floating Inductance using CFCCIIs and Earthed Passive Elements" , 2008 Workshop on Consumer Electronics, pp.755-758, 2008
13. Yin Y.C., "Realization of current-mode universal filter using Four-terminal Active Current Conveyors" , 2009 Workshop on Consumer Electronics, pp.275-278, 2009
14. PAL, K.: 'Modified current conveyors and their applications' , Microelectronics Journal, Vol.20, No.4, pp.37-40, 1989.
15. Elwan H.O.and Soliman A.M., "Novel CMOS differential voltage current conveyor and its applications" , IEE Proceding-Circuits Devices System, No.144, pp.195-200, 1997.
16. BIALOKOW, M., and NEWCOMB, R. W.: 'Generation of all finite linear circuits using the integrated DVCCS' , IEEE Trans., CT-18, pp.733-736, 1971.
17. BIALOKOW, M., SIENKO, W., and NEWCOMB, R. W.: 'Active synthesis using the DVCCS/DVCVS' , Int. J. Circuit Theory & Appl., No.2, pp.23-38, 1974.
18. NANDI. R.: ' New Ideal Active Inductance and Frequency-Dependent Negative Resistance using D.V.C.C.S./D.V.C.V.S.: Applications in Sinusoidal-Oscillator Realization' , Electron. Lett., No.14, pp. 551-553, 1978.
19. Muhammed A. Ibrahim, Shahram Minaei and Hakan Kuntman, "A 22.5 MHz current-mode KHN-biquad differential voltage current conveyor and grounded passive elements" , International Journal of Electronics and Communications, pp.311-318, 2004.
20. Yin Y.C. and Yin Yung-Chwan "Realization of Current-Mode Filters Using Two Differential Voltage Current Conveyors" , 2010 Intelligent Living Technology Conference, pp.103-107, 2010.
21. Yin Y.C. "Current-Mode Multifunction Filters using Single Differential Voltage Current Conveyor" , 2010 Workshop on Consumer Electronics Conference, pp.703-707, 2010.

Received October 25,2011
Revised January 12,2012
Accepted January 18,2012

使用單一差動電壓電流傳輸器合成嶄新結構濾波器

鄞永昌

輔仁大學　電機工程學系

摘　要

本文提出使用單一差動電壓電流傳輸器，合成新結構一階和二階濾波器電路。此新結構濾波器電路，僅使用單一差動電壓電流傳輸器與少數被動元件，即可合成出低通、高通、帶拒和全通四種濾波器。同時其主動與被動靈敏度也被推導出來，以決定其濾波功能的合適應用性。最後本文以帶拒和全通濾波器電路，實驗驗證本文之理論預測。

關鍵字：差動電壓電流傳輸器，靈敏度，主動濾波器，類比電路設計，連續性時間濾波器。

Finite Dimensional Nonlinear Filters of a Class of Filtering Systems

Wen-Lin Chiou[1]

Department of Mathematics Fu-Jen University
New Taipei City, Taiwan, R.O.C.

Abstract

Nonlinear filtering has been a hot topic not only for engineerings but also for mathematicians for many years. The idea of using estimation algebras to construct finite dimensional nonlinear filters was first proposed by Brockett and Mitter independently. It turns out that the concept of estimation algebra plays a crucial role in the investigation of finite dimensional nonlinear filters. In 1990, Yau established finite dimensional filters including both Kalman-Bucy filter and Bene filter as special cases In this paper, we established a simple algebraic necessary and sufficient condition for an estimation algebra in a more general class of filtering systems including Yau filtering systems to be finite dimensional. In particular we prove Mitter conjecture for the filtering systems we consider, and give partial solution to the Brockett problem on classification of finite dimensional estimation algebras.

Key words: Estimation algebras, Filtering systems, Finite dimensional recursive filters,Classification, Maximal rank.

1. Introduction

Ever since the technique of the Kalman-Bucy filters was popularized, there has been an intensive interest in finding new classes of finite dimensional recursive filters.

The Lie algebra related to the DMZ equation (cf. equation (2.1))is called estimation algebra. Among extending Kalman filtering to nonlinear filtering by applying the Wei-Norman theorem to this stochastic partial differential equation, one get a finite-dimensional

[1] Funded by the Colledge of Science and Engineering, Fu-Jen Univ. grant
e-mail address: chiou@math.fju.edu.tw

filter based on a finite set of ordinary differential equation and generalized Kolmlgorov equation. In 1983, Brockett[1] proposed the idea of classifying all finite dimensional estimation algebras in his famous lecture at International Congress of Mathematicians. Ever since estimation algebras play an fundamental tool to investigate nonlinear filters as well as stochastic controls. The recent works Mitter[10], Wong[14][15], Tam-Wong-Yau[12], Dong-Tam-Wong-Yau[9], Yau[16], Chiou-Yau[7], Chen-Leung-Yau[4] [5], Chiou[6], Yau-Rasoulian[17], Yau [18]. in which they used Lie algebraic method, introduced new concepts and classified new finite dimensional estimation algebras.

There were some interesting results in 1987 due to Wong [14] (cf. filtering system equations (2.1) below) under the assumptions that the observation $h(x)$ and drift term $f(x)$ are real analytic functions on $\mathbf{R}^n$, and f satisfies the following growth conditions: for any i, all the first, second and third order partial derivatives of f_i are bounded functions. Under all these conditions, Wong provides partial information towards the classification of finite dimensional estimation algebra. Namely he showed that if the estimation algebra is finite dimensional, then the degree of h in x is at most one and the estimation algebra has a basis consisting of one second degree differential operator, L_0 (cf. equation (2.4) below), first degree differential operators of the form

$$\sum_{i=1}^{n} \alpha_i \left(\frac{\partial}{\partial x_i} - f_i \right) + \sum_{i=1}^{n} \beta_i \frac{\partial \eta}{\partial x_i}$$

where α_i and β_i are constants and $\eta = -\frac{1}{2}\left(\sum_{i=1}^{n} \frac{\partial f_i}{\partial x_i} + \sum_{i=1}^{n} f_i^2 + \sum_{i=1}^{m} h_i^2 \right)$, and zero degree differential operators affine in x. In [12], Tam, Wong, and Yau have introduced the concept of an exact estimation algebra with maximal rank of filtering system (2.3). Let n be the dimension of the state space. It turns out that all nontrivial finite dimensional estimation algebras are automatically exact with maximal rank if $n = 1$. It follows from the works of Ocone [11], Tam-Wong-Yau [12], and Dong-Tam-Wong-Yau [9] that the finite dimensional estimation algebras are completely classified if $n = 1$. In fact, Dong, Tam, Wong, and Yau have classified all finite dimensional exact estimation algebras with maximal rank of arbitrary finite state space dimension for filtering system (2.3), in which the drift term f (cf. the following system equation (2.3))is a gradient field and the diffusion term $g(x(t))$ (cf. the following system equation (2.3)) is an orthogonal matrix. For arbitrary finite dimensional state space, under the condition that the drift term f is a liner vector field plus a gradient field and the diffusion term $g(x(t))$ is an orthogonal matrix. Yau[16]

have classified all finite dimensional estimation algebras with maximal rank. It follows from the works of Chiou-Yau [7] and Chen-Leung-Yau [4][5] that the finite dimensional estimation algebras with maximal rank of filtering system (2.3) are completely classified for $n = 1, 2$, and $n = 3, 4$. The method to get the classification is to prove that the drift term f of a finite dimensional estimation algebra with maximal rank of filtering system (2.3) is necessary a liner vector field plus a gradient field, and then use the results of Yau. In fact, in 1999, Yau[18] have classified all finite dimensional estimation algebras with maximal rank of arbitrary finite state space dimension for filtering system (2.3). In 1995, Chiou considered a special class of filtering systems (cf. 2.5), in which the diffusion term $g(x(t)) = G$ is an invertible matrix with constant entry. Under the assumption that the drift term f satisfies $G^{-1}f(x) = (\ell_1(\widetilde{x}), ..., \ell_n(\widetilde{x}))^t + \left(\frac{\partial\psi(\widetilde{x})}{\partial x_1}, ..., \frac{\partial\psi(\widetilde{x})}{\partial x_n}\right)^t$, where $\widetilde{x} = G^{-1}x$, $\ell_1, ..., \ell_n$ are linear and ψ is a C^∞ function, Chiou have classified all finite dimensional estimation algebras with maximal rank of filtering system (2.5), and also without the above assumption concerning the drift term, Chiou have classified all finite dimensional estimation algebras with maximal rank of filtering system (2.5) for $n = 1, 2$, and $n = 3, 4$.(in fact the classification can be achieved for arbitrary n).

In this paper, we consider a new class of filtering systems (3.1) (cf. the following filtering equations (3.1)), in which the diffusion term $g(x(t))$ satisfies $g(x(t))g(x(t))^t$ being a diagonal matrix with constant entry. We have two main theorems: Theorem C and Theorem D. Theorem C states that the Mitter conjecture, saying that the observation terms h_i's in the filtering system (2.0) are necessary affine if one has finite dimensional filters, is true under the filtering systems we consider. Theorem D provides a simple necessary and sufficient condition for an estimation algebra of filtering systems (3.1) to be finite dimensional under a suitable restriction in drift term f.

Although the key ideas behind the proof of the main theorems are similar to Tam-Wong-Yau[12]and Yau[16], the main results here are quite fundamental. Besides, the novelty in this paper is that the rank of the matrix $g(x(t))g(x(t))^t$ is less than or equals to the state space dimension.

2. Basic Concepts.

In this section, we will recall some basic concepts and results we needed for the next section. Consider a filtering problem based on the following signal observation model:

$$\begin{cases} dx(t) &= f(x(t))dt + g(x(t))dv(t) \qquad x(0) = x_0 \\ dy(t) &= h(x(t))dt + dw(t) \qquad\quad y(0) = 0 \end{cases} \tag{2.0}$$

in which x, v, y and w are respectively $\mathbf{R}^n$, $\mathbf{R}^p$, $\mathbf{R}^m$ and $\mathbf{R}^m$ valued processes, and v and w have components which are independent, standard Brownian processes. We further assume that $n = p$, f, h are C^∞ smooth vector-valued functions, and that g is an n by n C^∞ smooth matrix. We will refer to $x(t)$ as the state of the system at time t and to $y(t)$ as the observation at time t.

Let $\rho(t,x)$ denote the conditional density of the state given the observation $\{y(s) : 0 \leq s \leq t\}$. It is well known (see Davis [8], for example) that $\rho(t,x)$ is given by normalizing a function, $\sigma(t,x)$, which satisfies the following Duncan-Mortensen-Zakai equation (see Zakai [19], for example) :

$$d\sigma(t,x) = L_0\sigma(t,x)dt + \sum_{i=1}^{m} L_i\sigma(t,x)dy_i(t), \qquad \sigma(0,x) = \sigma_0, \tag{2.1}$$

where

$$L_0 = \frac{1}{2}\sum_{i,j=1}^{n} \frac{\partial^2}{\partial x_i \partial x_j}(gg^t)_{ij} - \sum_{i=1}^{n} \frac{\partial}{\partial x_i} f_i - \frac{1}{2}\sum_{i=1}^{m} h_i^2$$

and for $i = 1, \cdots, m$, L_i is the zero degree differential operator of multiplication by h_i. σ_0 is the probability density of the initial point x_0. In this paper, we will assume σ_0 is a C^∞ function. Equation (2.1) is a stochastic partial differential equation. In real applications, we are interested in constructing state estimators from observed sample paths with some property of robustness. Davis in [8] studied this problem and proposed some robust algorithms. In our case, his basic idea reduces to defining a new unnormalized density

$$\xi(t,x) = \exp\Big(-\sum_{i=1}^{m} h_i(x)y_i(t)\Big)\sigma(t,x).$$

It is easy to show that $\xi(t,x)$ satisfies the following time varying partial differential equation

$$\begin{cases} \frac{\partial \xi}{\partial t}(t,x) & = L_0\xi(t,x) + \sum_{i=1}^{m} y_i(t)[L_0, L_i]\xi(t,x) \\ & \quad + \frac{1}{2}\sum_{i,j=1}^{m} y_i(t)y_j(t)[[L_0, L_i], L_j]\xi(t,x) \\ \xi(0,x) & = \sigma_0 \end{cases} \tag{2.2}$$

where $[\cdot\,,\cdot]$ is the Lie bracket defined as:

Definition. If X and Y are differential operators, the Lie bracket of X and Y, $[X,Y]$, is defined by

$$[X,Y]\varphi = X(Y\varphi) - Y(X\varphi)$$

for any C^∞ function φ.

We further assume in system equations (2.0) that $g(x(t)) = o(x(t))$ is an orthogonal matrix as follows:

$$\begin{cases} dx(t) & = f(x(t))dt + o(x(t))dv(t) & x(0) = x_0 \\ dy(t) & = h(x(t))dt + dw(t) & y(0) = 0 \\ o(x(t)) & \text{is an orthogonal matrix} \end{cases} \tag{2.3}$$

The filtering sysrem (2.3) was considerd by Yau[16]. Here

$$\begin{aligned} L_0 &= \frac{1}{2}\sum_{i=1}^{n}\frac{\partial^2}{\partial x_i^2} - \sum_{i=1}^{n} f_i\frac{\partial}{\partial x_i} - \sum_{i=1}^{n}\frac{\partial f_i}{\partial x_i} - \frac{1}{2}\sum_{i=1}^{m} h_i^2 \\ &= \frac{1}{2}\left(\sum_{i=1}^{n} D_i^2 - \eta\right), \end{aligned} \tag{2.4}$$

where

$$D_i = \frac{\partial}{\partial x_i} - f_i$$

and

$$\eta = \sum_{i=1}^{n}\frac{\partial f_i}{\partial x_i} + \sum_{i=1}^{n} f_i^2 + \sum_{j=1}^{m} h_j^2.$$

If we assume in system equations (2.0) that $g(x(t)) = G$ is an invertible matrix with each entry constant as follows:

$$\begin{cases} dx(t) & = f(x(t))dt + Gdv(t) & x(0) = x_0 \\ dy(t) & = h(x(t))dt + dw(t) & y(0) = 0 \\ G & \text{is an invertible matrix with each entry constant} \end{cases} \tag{2.5}$$

We get another filtering system considerd by Chiou[6].

Definition. The estimation algebra E of a filtering system (2.0) is defined to be the Lie algebra generated by $\{L_0, L_1, \cdots, L_m\}$ or, $E = \langle L_0, L_1, \cdots, L_m\rangle_{L.A.}$. If, in addition, for filtering system (2.3) there exists a potential function φ such that $f_i = \frac{\partial\varphi}{\partial x_i}$ for all $1 \le i \le n$, then the estimation algebra of a filtering system (2.3) is called exact.

In Yau[16], the following Proposition 1 and Theorem 2 were proven

Proposition 1. $\frac{\partial f_j}{\partial x_i} - \frac{\partial f_i}{\partial x_j} = c_{ij}$ are constants for all i and j if and only if $(f_1, \cdots, f_n) = (\ell_1, \cdots, \ell_n) + (\frac{\partial\varphi}{\partial x_1}, \cdots, \frac{\partial\varphi}{\partial x_n})$, where $\ell_1, cdots, \ell_n$ are linear functions of $x_1, \cdots, x_n$.

The following classification theorem was proven by Dong, Tam, Wong and Yau[9].

Theorem 2. Let E be a finite dimensional exact estimation algebra with maximal rank of filtering system (2.3) with arbitrary finite state space dimension. Then it has a basis: $1, x_1, \cdots, x_n, D_1, \cdots, D_n$, and L_0.

The following classification theorem was proven by Yau [16].

Theorem 3. Suppose that the state space of filtering system (2.3) is of dimension n. Let E be a finite dimensional estimation algebra with maximal rank of filtering system (2.3) satisfying $\frac{\partial f_j}{\partial x_i} - \frac{\partial f_i}{\partial x_j} = c_{ij}$ where c_{ij} are constants for all $1 \leq i, j \leq n$. Then it has a basis: $1, x_1, \cdots, x_n, D_1, \cdots, D_n$, and L_0.

Note. If $c_{ij} = 0$, then by Proposition 1, E is exact.

Suppose that the state space of the filtering system (2.3) is of dimension n. The following theorem is proven by Yau[18].

Theorem 4. If E is a finite dimensionalestimation algebra with maximal rank of filtering system (2.3), then the drift term f must be linear vector field plus gradient vector field and E is a real vector space of dimension $2n+2$ with basis given by $1, x_1, \cdots, x_n, D_1, \cdots, D_n$ and L_0, for arbitrary n.

The following Theorem 5 and Theorem 6 were proven by Chiou[6].

Theorem 5. Suppose the state space of a filtering system (2.5) is of dimension n and E is a finite dimensional estimation with maximal rank having property

$$G^{-1}f(x) = (\ell_1(\widetilde{x}), ..., \ell_n(\widetilde{x}))^t + \left(\frac{\partial \psi}{\partial \widetilde{x}_1}, ..., \frac{\partial \psi}{\partial \widetilde{x}_n}\right)^t,$$

where ψ is C^∞ smooth and $\ell_1, ..., \ell_n$ are polynomials of degree at most one in $\widetilde{x}$, here $\widetilde{x} = G^{-1}\ x$. Then E has a basis: 1, x_1, ..., x_n, $\frac{\partial}{\partial x_1} - f_1$, ..., $\frac{\partial}{\partial x_n} - f_n$.

Theorem 6. Suppose that the state space of a filtering system (2.5) is of dimension n, $n \leq 3$. If E is a finite dimensional estimation algebra with maximal rank, then

$$G^{-1}f(x) = (\ell_1(\widetilde{x}), ..., \ell_n(\widetilde{x}))^t + \left(\frac{\partial \psi}{\partial \widetilde{x}_1}, ..., \frac{\partial \psi}{\partial \widetilde{x}_n}\right)^t,$$

where $\widetilde{x} = G^{-1}x$ and ψ is C^∞ smooth. Therefore E is a real vector space of dimension $2n+2$ with basis given by 1, x_1, ..., x_n, $\frac{\partial}{\partial x_1} - f_1$, ..., $\frac{\partial}{\partial x_n} - f_n$, and L_0.

Note. In fact, Theorem 6 is true for arbitrary finite state space dimension.

The following Proposition 7, Theorems 8, 9, Corollary 11 and Lemma 12 will be used in section 3.

Proposition 7. (Chiou-Yau[7]) Let $\widetilde{x} = Rx$, where R is an invertible matrix , then

(1) $\widetilde{f}(\widetilde{x}) = Rf(x)$;

(2) $\widetilde{L}_0 = L_0$

where $\widetilde{L}_0 = \frac{1}{2}\sum_{i=1}^{n} \frac{\partial^2}{\partial \widetilde{x}_i^2} - \sum_{i=1}^{n} \frac{\partial}{\partial \widetilde{x}_i}\widetilde{f}_i(\widetilde{x}) - \frac{1}{2}\sum_{i=1}^{m} \widetilde{h}_i^2(\widetilde{x})$, with $\widetilde{h}(\widetilde{x}) = h(x)$;

(3) $\widetilde{E}$ is isomorphic to E as Lie algebra where $\widetilde{E}$ is the Lie algebra generated by $\widetilde{L}_0$, $\widetilde{h}_1, \ldots, \widetilde{h}_m$.

The following Theorem 8 is an extention of Theorem A2 in Yau-Rasoulian[17]. Their proofs are just the same.

Theorem 8. Let $E_\ell = \sum_{i=1}^{\ell} x_i \frac{\partial}{\partial x_i}$ be an Euler operator. Suppose that m is a nonzero constant and ξ is a C^∞ function on R^s such that $E_\ell(\xi) + m\xi$ is a polynomial of degree k in $x_1, x_2, \cdots, x_s$ variables. If $k + m > 0$ then ξ is a polynomial of degree k in $x_1, x_2, \cdots, x_s$ variables.

Theorem 9. (Yau-Rasoulian[17]) Let $E_\ell = \sum_{i=1}^{\ell} x_i \frac{\partial}{\partial x_i}$ be an Euler operator. Suppose that ξ be a C^∞ function on R^s such that $E_\ell(\xi)$ is a polynomial of degree k in $x_1, x_2, \cdots, x_s$ variables. Then $\xi = P_k(x_1, \cdots, x_s) + a(x_{\ell+1}, \cdots, x_s)$, where $P_k(x_1, \cdots, x_s)$ is a polynomial of degree k in $x_1, x_2, \cdots, x_s$ variables, and $a(\cdot)$ is a C^∞ function on $R^{s-\ell}$.

Theorem 10. (Yau[16]) Let $F(x_1, \cdots, x_s)$ be a C^∞ function on $\mathbf{R}^s$. Suppose that there exists a path $c : \mathbf{R} \to \mathbf{R}^s$ and $\delta > 0$ such that $\lim_{t\to\infty} \|c(t)\| = \infty$ and $\lim_{t\to\infty} \sup_{B_\delta(c(t))} F = -\infty$, where $B_\delta(c(t)) = \{x \in \mathbf{R}^s : \|x - c(t)\| < \delta\}$. Then there are no C^∞ functions $f_1, f_2, \cdots, f_s$ on $\mathbf{R}^s$ satisfying the equation

$$\sum_{i=1}^{s} \frac{\partial f_i}{\partial x_i} + \sum_{i=1}^{s} f_i^2 = F.$$

Corollary 11. (Yau[16]) Let $F(x_1, \cdots, x_s)$ be a polynomial on $\mathbf{R}^s$. Suppose that there exists a polynomial path $c : \mathbf{R} \to \mathbf{R}^s$ such that $\lim_{t\to\infty} \|c(t)\| = \infty$ and $\lim_{t\to\infty} F \circ c(t) = -\infty$. Then there is no C^∞ functions $f_1, f_2, \cdots, f_s$ on $\mathbf{R}^s$ satisfying the equation

$$\sum_{i=1}^{s} \frac{\partial f_i}{\partial x_i} + \sum_{i=1}^{s} f_i^2 = F.$$

Lemma 12. (i) $[D_i, g\frac{\partial}{\partial x_j}] = \frac{\partial g}{\partial x_i}\frac{\partial}{\partial x_j} + g\frac{\partial f_i}{\partial x_j}$ (ii)$[hD_i, g\frac{\partial}{\partial x_j}] = h\frac{\partial g}{\partial x_i}\frac{\partial}{\partial x_j} + hg\frac{\partial f_i}{\partial x_j} - g\frac{\partial h}{\partial x_j}D_i$
(iii) $[D_i^2, \frac{\partial}{\partial x_j}] = 2\frac{\partial f_i}{\partial x_j}D_i + \frac{\partial^2 f_i}{\partial x_i x_j}$

Proof. The computation is direct.

§3. Estimation Algebras of A New Class of Filtering Systems.

In this section, we consider the following special filtering system, namely, in filtering system (2.0) we further assume that $g(x(t))g(x(t))^t = G$ is an n by n diagonal matrix with constant entries:

$$\begin{cases} dx(t) &= f(x(t))dt + g(x(t))dv(t) \qquad x(0) = x_0 \\ dy(t) &= h(x(t))dt + dw(t) \qquad y(0) = 0 \\ gg^t & \text{is a diagonal matrix with constant entries} \end{cases} \tag{3.1}$$

we first notice that if $rank(gg^t) = s, 1 \le s \le n$, then we may assume $d_i \neq 0, i = 1, \cdots, s$ and $d_{s+1} = \cdots = d_n = 0$ by interchanging the indice of x_i if necessary, then

$$\begin{aligned} L_0 &= \frac{1}{2}\sum_{i=1}^{s} d_i\frac{\partial^2}{\partial x_i^2} - \sum_{i=1}^{n} f_i\frac{\partial}{\partial x_i} - \sum_{i=1}^{n}\frac{\partial f_i}{\partial x_i} - \frac{1}{2}\sum_{i=1}^{m} h_i^2 \\ &= \frac{1}{2}\sum_{i=1}^{s}\frac{\partial^2}{\partial(\frac{x_i}{\sqrt{d_i}})^2} - \sum_{i=1}^{s}\frac{f_i}{\sqrt{d_i}}\frac{\partial}{\partial\frac{x_i}{\sqrt{d_i}}} - \sum_{i=1}^{s}\frac{\partial\frac{f_i}{\sqrt{d_i}}}{\partial\frac{x_i}{\sqrt{d_i}}} - \sum_{i=s+1}^{n} f_i\frac{\partial}{\partial x_i} - \sum_{i=s+1}^{n}\frac{\partial f_i}{\partial x_i} - \frac{1}{2}\sum_{i=1}^{m} h_i^2, \end{aligned}$$

In view of (2.4), we have

$$L_0 = \frac{1}{2}\sum_{i=1}^{s}(\frac{\partial}{\partial\frac{x_i}{\sqrt{d_i}}} - \frac{f_i}{\sqrt{d_i}})^2 - \frac{1}{2}\left(\sum_{i=1}^{s}\frac{\partial\frac{f_i}{\sqrt{d_i}}}{\partial\frac{x_i}{\sqrt{d_i}}} + \sum_{i=1}^{s}(\frac{f_i}{\sqrt{d_i}})^2 + \sum_{i=1}^{m} h_i^2\right) - \sum_{i=s+1}^{n} f_i\frac{\partial}{\partial x_i} - \sum_{i=s+1}^{n}\frac{\partial f_i}{\partial x_i}.$$

so if for $i = 1, \cdots, s, j = s+1, \cdots, n$, we put $\widetilde{x}_i = \frac{x_i}{\sqrt{d_i}}, \widetilde{x}_j = x_j$, and $\widetilde{f}_i(\widetilde{x}) = \frac{f_i(x)}{\sqrt{d_i}}, \widetilde{f}_j(\widetilde{x}) = f_j(x)$, then $\frac{\partial}{\partial\widetilde{x}_i} = \sum_{k=1}^{n}\frac{\partial}{\partial x_k}\frac{\partial x_k}{\partial\widetilde{x}_i} = \sqrt{d_i}\frac{\partial}{\partial x_i} = \frac{\partial}{\partial\frac{x_i}{\sqrt{d_i}}}$, and hence $\frac{\partial}{\partial\frac{x_i}{\sqrt{d_i}}} - \frac{f_i(x)}{\sqrt{d_i}} = \frac{\partial}{\partial\widetilde{x}_i} - \widetilde{f}_i(\widetilde{x})$ and $\frac{\partial f_l(x)}{\partial x_l} = \frac{\partial\widetilde{f}_l(\widetilde{x})}{\partial\widetilde{x}_l}$ for all $l = 1, \cdots, n$. Consequently, we have the following:

Lemma A. Let $\widetilde{x}_i = \frac{x_i}{\sqrt{d_i}}, i = 1, \cdots, s, \widetilde{x}_j = x_j, j = s+1, \cdots, n$. Then

(1) $\widetilde{f}_i(\widetilde{x}) = \frac{f_i(x)}{\sqrt{d_i}}$ for all $i = 1, \cdots, s$ and $\widetilde{f}_j(\widetilde{x}) = f_j(x)$ for all $j = s+1, \cdots, n$;

(2) $\widetilde{L}_0 = L_0$

where $\widetilde{L}_0 = \frac{1}{2}\sum_{i=1}^{s}(\frac{\partial}{\partial\widetilde{x}_i} - \widetilde{f}_i(\widetilde{x}))^2 - \frac{1}{2}(\sum_{i=1}^{s}(\frac{\partial\widetilde{f}_i(\widetilde{x})}{\partial x_i} - \sum_{i=1}^{s}\widetilde{f}_i(\widetilde{x})^2 + \sum_{i=1}^{m} h_i^2(\widetilde{x}))$
$- \sum_{i=s+1}^{n}\widetilde{f}_i\frac{\partial}{\partial\widetilde{x}_i} - \sum_{i=s+1}^{n}\frac{\partial\widetilde{f}_i(\widetilde{x})}{\partial\widetilde{x}_i}$, with $\widetilde{h}(\widetilde{x}) = h(x)$;

(3) $\widetilde{E}$ is isomorphic to E as Lie algebra where $\widetilde{E}$ is the Lie algebra generated by $\widetilde{L}_0$, $\widetilde{h}_1, \cdots, \widetilde{h}_m$.

So whenever we consider the estimation algebra E, we only need to consider the estimation algebra $\widetilde{E}$. If we drop the tilde notation. Define

$$D_i = \frac{\partial}{\partial x_i} - f_i, \ i = 1, \cdots, s, \tag{3.2}$$

and

$$\eta = \sum_{i=1}^{s} \frac{\partial f_i(x)}{\partial x_i} + \sum_{i=1}^{s} f_i(x)^2 + \sum_{i=1}^{m} h_i^2(x), \tag{3.3}$$

then

$$L_0 = \frac{1}{2}\Big(\sum_{i=1}^{s} D_i^2 - \eta\Big) - \sum_{i=s+1}^{n} f_i \frac{\partial}{\partial x_i} - \sum_{i=s+1}^{n} \frac{\partial f_i(x)}{\partial x_i} \tag{3.4}$$

Let U^k denote the linear space consisting of all differential operators of order $\leq k$ with real C^∞ functions as coefficients. We have a similar result as in Ocone[11]

Theorem B. Let E be a finite dimensional estimation algebra of filtering system (3.1). If a C^∞ smooth function ξ is in E, then ξ is a polynomial of degree ≤ 2 in $x_1, \cdots, x_s$ variables with coefficients in C^∞- functions of $x_{s+1}, \cdots, x_n$.

Proof. By Lemma A we may assume that

$$L_0 = \frac{1}{2}\sum_{i=1}^{s}(\frac{\partial}{\partial x_i} - f_i))^2 - \frac{1}{2}(\sum_{i=1}^{s}(\frac{\partial f_i}{\partial x_i} + \sum_{i=1}^{s} f_i^2 + \sum_{i=1}^{m} h_i^2) - \sum_{i=s+1}^{n} f_i \frac{\partial}{\partial x_i} - \sum_{i=s+1}^{n} \frac{\partial f_i(x)}{\partial x_i}$$

First we claim that

$$Ad_{L_0}^k \xi = \sum_{i_1, \cdots, i_k = 1}^{s} \frac{\partial^k \xi}{\partial x_{i_1} \cdots \partial x_{i_k}} \frac{\partial^k}{\partial x_{i_1} \cdots \partial x_{i_k}} \bmod U^{k-1}.$$

Write $L_0 = \frac{1}{2}\sum_{i=1}^{s} \frac{\partial^2}{\partial x_i^2} \bmod U^1$. For $k = 1$,

$$\begin{aligned}
(Ad_{L_0}\xi)(\cdot) &= \big[\frac{1}{2}\sum_{i=1}^{s} \frac{\partial^2}{\partial x_1^2} \bmod U^1, \xi\big](\cdot) \\
&= \Big(\frac{1}{2}\sum_{i=1}^{s} \frac{\partial^2}{\partial x_i^2} \bmod U^1\Big)\big(\xi(\cdot)\big) \\
&\quad - \xi\frac{1}{2}\sum_{i=1}^{s} \frac{\partial^2}{\partial x_i} \bmod U^1(\cdot) \\
&= \frac{\partial \xi}{\partial x_i}\frac{\partial}{\partial x_i} \bmod U^0(\cdot).
\end{aligned}$$

Suppose that it is true for $k-1$, i.e.,

$$Ad^k_{L_0}\xi = \sum_{i_1,\cdots,i_{k-1}=1}^{s} \frac{\partial^{k-1}\xi}{\partial x_{i_1}\cdots\partial x_{i_{k-1}}} \frac{\partial^{k-1}}{\partial x_{i_1}\cdots\partial x_{i_{k-1}}} \mod U^{k-2}.$$

Then

$$\begin{aligned}
(Ad^k_{L_0}\xi)(\cdot) &= (Ad_{L_0}Ad^{k-1}_{L_0}\xi)(\cdot) \\
&= [\frac{1}{2}\sum_{i_k=1}^{s}\frac{\partial^2}{\partial x_{i_k}^2} \mod U^1,\ \sum_{i_1,\cdots,i_{k-1}}^{s} \frac{\partial^{k-1}\xi}{\partial x_{i_1},\cdots,\partial x_{i_{k-1}}} \frac{\partial^{k-1}}{\partial x_{i_1}\cdots\partial x_{i_{k-1}}} \mod U^{k-2}](\cdot) \\
&= \Big(\frac{1}{2}\sum_{i=1}^{s}\frac{\partial^2}{\partial x_{i_k}^2} \mod U^1\Big)\Big(\sum_{i_1\cdots i_{k-1}=1}^{s} \frac{\partial^{k-1}\xi}{\partial x_{i_1}\cdots\partial x_{i_{k-1}}} \frac{\partial^{k-1}}{\partial x_{i_1}\cdots\partial x_{i_{k-1}}} \mod U^{k-2}\Big)(\cdot) \\
&- \Big(\sum_{i_1,\cdots,i_{k-1}=1}^{s} \frac{\partial^{k-1}\xi}{\partial x_{i_1}\cdots\partial x_{i_{k-1}}} \frac{\partial^{k-1}}{\partial x_{i_1}\cdots\partial x_{i_{k-1}}} \mod U^{k-2}\Big)\Big(\frac{1}{2}\sum_{i_k=1}^{s}\frac{\partial^2}{\partial x_{i_k}^2} \mod U^1(\cdot)\Big) \\
&= \sum_{i_1,\cdots,i_k=1}^{s} \frac{\partial^k\xi}{\partial x_{i_1}\cdots x_{i_k}} \frac{\partial^k}{\partial x_{i_1}\cdots\partial x_{i_k}} \mod U^{k-1}(\cdot).
\end{aligned}$$

Since E is finite dimensional, there exists a integer ℓ such that

$$\frac{\partial^\ell\xi}{\partial x_{i_1}\cdots\partial x_{i_\ell}} = 0,$$

for all $1 \le i_1,\cdots,i_\ell \le s$, hence ξ is a polynomial in $x_1,\cdots,x_s$. Let $p_0 = \xi$, $p_k = [[L_0,p_{k-1}],p_{k-1}]$, $k \ge 1$. We have

$$\begin{aligned}
p_k &= [[L_0,p_{k-1}],p_{k-1}] \\
&= [\sum_{i=1}^{s}\frac{\partial p_{k-1}}{\partial x_i}D_i + \frac{1}{2}\frac{\partial^2 p_{k-1}}{\partial x_i}, p_{k-1} - \sum_{i=s+1}^{n} f_i\frac{\partial p_{k-1}}{\partial x_i}] \\
&= \sum_{i=1}^{s}\Big(\frac{\partial p_{k-1}}{\partial x_i}\Big)^2,
\end{aligned}$$

for $k = 1,2,3\cdots$, $p_k(x)$'s are polynomials in $x_1,\cdots,x_s$ and as a polynomial of $x_1,\cdots,x_s$, $\deg p_k = 2(\deg p_k - 1)$. If ξ were of degree > 2 in in $x_1,\cdots,x_s$, then $\lim_{k\to\infty}\deg p_k = \infty$, i.e., $\{p_k\}_{k=1}^{\infty}$ has infinitely many distinct polynomials in $x_1,\cdots,x_s$. This is contradictory to the assumption that E is finite dimensional. *Q.E.D.*

The following Theorem C states that Mitter conjecture is true under the filtering systems we consider

Theorem C. Consider a filtering system of (3.1) with the drift term $f = (f_1, \cdots, f_n)$, satisfying (i) $f_i(x) = l_i(x) + d_i \frac{\partial \phi(\frac{x_1}{\sqrt{d_1}}, \cdots, \frac{x_s}{\sqrt{d_s}})}{\partial x_i}$, where ϕ_i are C^∞- functions on $\mathbf{R}^s$ and $l_i \in C^\infty(R^n)$ are linear in $x_1, \cdots, x_s$ variables with coefficients in C^∞-functions of $x_{s+1}, \cdots, x_n$ for all $i = 1, \cdots, s$, and (ii) $f_{s+1}(x), \cdots, f_n(x) \in C^\infty(R^n)$ are linear in $x_1, \cdots, x_s$ variables with coefficients in C^∞- functions of $x_{s+1}, \cdots, x_n$. If the estimation algebra E is finite-dimensional and the observation terms $h_1, \cdots, h_m$ are C^∞- functions on $\mathbf{R}^s$, then they are polynomials of degree at most one on $\mathbf{R}^s$

Proof of theorem C. Using the notations in lemma A, we have for $1 \leq i \leq s$

$$\widetilde{f}_i(\widetilde{x}) = \widetilde{l}_i(\widetilde{x}) + \frac{\partial \phi(\widetilde{x}_1, \cdots, \widetilde{x}_s)}{\partial \widetilde{x}_i} \tag{3.5}$$

where $\widetilde{l}_i(\widetilde{x}) = \frac{l_i(\sqrt{d_1}\widetilde{x}_1, \cdots, \sqrt{d_s}\widetilde{x}_s, \widetilde{x}_{s+1}, \cdots, \widetilde{x}_n)}{\sqrt{d_i}}$. Therefore

$$\frac{\partial \widetilde{f}_j(\widetilde{x})}{\partial \widetilde{x}_i} - \frac{\partial \widetilde{f}_i(\widetilde{x})}{\partial \widetilde{x}_j} = \widetilde{d}_{ij}(\widetilde{x}_{s+1}, \cdots, \widetilde{x}_n) \in C^\infty(R^{n-s}), \text{ for all } 1 \leq i, j \leq s. \tag{3.6}$$

Remark. : $\widetilde{f}_{s+1}(\widetilde{x}_1, \cdots, \widetilde{x}_n), \cdots, \widetilde{f}_n(x_1, \cdots, x_n) \in C^\infty(R^n)$ are linear in $\widetilde{x}_1, \cdots, \widetilde{x}_s$, and $\widetilde{l}_i \in C^\infty(R^n)$ are linear in $\widetilde{x}_1, \cdots, \widetilde{x}_s$ for $i = 1, \cdots, s$.

Now by lemma A (with the notations of equation (3.2), (3.3) and (3.4)), we may assume that $L_0 = \frac{1}{2}\left(\sum_{i=1}^s D_i^2 - \eta\right) - \sum_{i=s+1}^n f_i \frac{\partial}{\partial x_i} - \sum_{i=s+1}^n \frac{\partial f_i(x)}{\partial x_i}$, in which the drift term f satisfies the equation (3.6) and the remark stated as above if x_i 's are instead of $\widetilde{x}_i$'s. Since E is finite dimensional, by Theorem B and the assumption of h_i's, each h_i is a polynomial of $x_1, \cdots, x_s$ with degree at most two. We may assume h_1 is of degree two of $x_1, \cdots, x_s$. By a translation after an orthonormal transformation (cf. Proposition 9 in section two) , we may assume that $h_1(x)$ is of the form

$$\widetilde{h}_1(\widetilde{x}) = \sum_{i=1}^{\ell} c_i \widetilde{x}_i^2 + \sum_{i=\ell+1}^{s} c_i \widetilde{x}_i + c_0$$

where $c_1, \cdots, c_\ell$ are nonzero constants, and $\ell \leq s$ (If $\ell = s$, the second summation vanishes.) Notice that the drift term $\widetilde{f}$ satisfies equation (3.5) and the remark stated as above. Consequently $\widetilde{f}_i, i = 1, \cdots, s$, satisfy the equation (3.6). Without causing any confusion, from now on, we drop the tilde notation.

Let $X_0 = h_1$, and define X_i for $i \geq 1$ recursively by $X_i = \big[[L_0, X_{i-1}], X_0\big]$. Observe that if two smooth functions P_1 and P_2 are polynomials in $x_1, \cdots, x_s$, we have

$$\begin{aligned}
[[L_0, P_1], P_2] &= \left[\left[\frac{1}{2}\left(\sum_{i=1}^{s} D_i^2 - \eta\right) - \sum_{i=s+1}^{n} f_i \frac{\partial}{\partial x_i} - \sum_{i=s+1}^{n} \frac{\partial f_i(x)}{\partial x_i}, P_1\right], P_2\right] \\
&= \left[\sum_{i=1}^{\ell} \frac{\partial P_1}{\partial x_i} D_i + \frac{1}{2}\frac{\partial^2 P_1}{\partial x_i^2} - \sum_{i=s+1}^{n} f_i \frac{\partial P_1}{\partial x_i}, P_2\right] \\
&= \sum_{i=1}^{\ell} \frac{\partial P_1}{\partial x_i}\frac{\partial P_2}{\partial x_i}
\end{aligned} \tag{3.7}$$

so

$$\begin{aligned}
X_1 &= [[L_0, X_0], X_0] \\
&= \sum_{i=1}^{\ell}\left(\frac{\partial X_0}{\partial x_i}\right)^2 = 4\sum_{i=1}^{\ell} c_i x_i^2 + \sum_{i=\ell+1}^{n} c_i^2 \\
X_2 &= [[L, X_1], X_0] = \sum_{i=1}^{\ell} \frac{\partial X_1}{\partial x_i}\frac{\partial X_0}{\partial x_i} \\
&= 4^2 \sum_{i=1}^{\ell} c_i^3 x_i^2 \\
X_3 &= [[L_0, X_2], X_0] = \sum_{i=1}^{\ell} \frac{\partial X_2}{\partial x_i}\frac{\partial X_0}{\partial x_i} \\
&= 4^3 \sum_{i=1}^{\ell} c_i^4 x_i^2 \\
&\vdots \\
X_j &= 4^j \sum_{i=1}^{\ell} c_i^{j+1} x_i^2.
\end{aligned}$$

By the invertibility of the Vandermonde matrix, it follows after some relabelling, if necessary, that

$$p := \frac{1}{2}\sum_{i=1}^{\ell} x_i^2$$

is an element in E. Observe

$$\begin{aligned}
Y_1 :&= [L_0, p] \\
&= \frac{1}{2}\Big[\sum_{i=1}^{s} D_i^2 - \eta, \frac{1}{2}\sum_{i=1}^{\ell} x_i^2\Big] - \Big[\sum_{i=s+1}^{n} f_i \frac{\partial}{\partial x_i} + \sum_{i=s+1}^{n} \frac{\partial f_i}{\partial x_i}, \frac{1}{2}\sum_{i=1}^{\ell} x_i^2\Big] \\
&= \sum_{i=1}^{\ell} x_i D_i + \frac{\ell}{2} \\
Y_2 :&= [L_0, Y_1] \\
&= \frac{1}{2}\Big[\sum_{i=1}^{s} D_i^2 - \eta, \sum_{j=1}^{\ell} x_j D_j + \frac{\ell}{2}\Big] - \Big[\sum_{i=s+1}^{n} f_i \frac{\partial}{\partial x_i} + \sum_{i=s+1}^{n} \frac{\partial f_i}{\partial x_i}, \sum_{j=1}^{\ell} x_j D_j + \frac{\ell}{2}\Big] \\
&= \sum_{i=1}^{\ell} D_i^2 - \sum_{i=1}^{s}\sum_{j=1}^{\ell} x_j d_{ij} D_i + \frac{1}{2}\sum_{i=1}^{\ell} x_i \frac{\partial \eta}{\partial x_i} + \sum_{i=s+1}^{n}\Big(\sum_{j=1}^{l} x_j \frac{\partial f_i}{\partial x_j}\Big)\frac{\partial}{\partial x_i} \\
&\quad + \sum_{i=s+1}^{n}\sum_{j=1}^{\ell} f_i x_j \frac{\partial f_j}{\partial x_i} + \sum_{i=s+1}^{n}\Big(\sum_{j=1}^{\ell} x_j \frac{\partial}{\partial x_j}\Big(\frac{\partial f_i}{\partial x_i}\Big)\Big).
\end{aligned}$$

Let $\alpha_i = \sum_{j=1}^{\ell} x_j d_{ij}(x_{s+1}, \cdots, x_n)$ and $E_\ell = \sum_{i=1}^{\ell} x_i \frac{\partial}{\partial x_i}$. First notice that $E_\ell(\beta^{(k)}) = k\beta^{(k)}$, if $\beta^{(k)}$ is a homogeneous polynomial of degree k in $x_1, \cdots, x_\ell$ So if we express a polynomial β in $x_1, \cdots, x_\ell$ being of the form $\beta = \beta^{(p)} + \beta^{(p-1)} \cdots + \beta^{(0)}$, because $\alpha_i, i = 1, \cdots, s$ are homogeneous polynomial of degree 1 in $x_1, \cdots, x_\ell$ and $f_j, j = s+1, \cdots, n$ are at most linear in $x_1, \cdots, x_s$ and hence in $x_1, \cdots, x_\ell$ we have $E_\ell(f_j) = f_j^{(1)}, E_\ell(\frac{\partial f_j}{\partial x_j}) = \Big(\frac{\partial f_j}{\partial x_j}\Big)^{(1)} = \frac{\partial f_j^{(1)}}{\partial x_j}, j = s+1, \cdots, n$ and $E_\ell(\alpha_i) = \alpha_i, i = 1, \cdots, s$. Then

$$\begin{aligned}
Y_2 &= \sum_{i=1}^{\ell} D_i^2 - \sum_{i=1}^{s} \alpha_i D_i + \frac{1}{2}E_\ell(\eta) + \sum_{i=s+1}^{n} f_i^{(1)} \frac{\partial}{\partial x_i} + \sum_{i=s+1}^{n}\sum_{j=1}^{l} f_i x_j \frac{\partial f_j}{\partial x_i} + \sum_{i=s+1}^{n} \frac{\partial f_i^{(1)}}{\partial x_i} \\
Y_3 &= [Y_2, Y_1] \\
&= \Big[\sum_{i=1}^{\ell} D_i^2 - \sum_{i=1}^{s} \alpha_i D_i + \frac{1}{2}E_\ell(\eta), \sum_{j=1}^{\ell} x_j D_j + \frac{\ell}{2}\Big] \\
&\quad + \Big[\sum_{i=s+1}^{n} f_i^{(1)} \frac{\partial}{\partial x_i} + \sum_{i=s+1}^{n} \frac{\partial f_i^{(1)}}{\partial x_i} + \sum_{i=s+1}^{n}\sum_{j=1}^{l} f_i x_j \frac{\partial f_j}{\partial x_i}, \sum_{k=1}^{\ell} x_k D_k + \frac{\ell}{2}\Big]
\end{aligned}$$

$$= 2\sum_{i=1}^{\ell} D_i^2 - 2\sum_{i=1}^{\ell} \alpha_i D_i + \sum_{i=\ell+1}^{s} \alpha_i D_i + \sum_{i=1}^{s} \alpha_i^2 - \frac{1}{2}E_\ell^2(\eta)$$
$$- \sum_{i=s+1}^{n} f_i^{(1)} \frac{\partial}{\partial x_i} - \sum_{i=s+1}^{n}\sum_{j=1}^{\ell} f_i^{(1)} x_j \frac{\partial f_j}{\partial x_i} - \sum_{i=s+1}^{n} E_\ell(\sum_{j=1}^{l} f_i x_j \frac{\partial f_j}{\partial x_i}) - \sum_{i=s+1}^{n} \frac{\partial f_i^{(1)}}{\partial x_i}$$

$$Y_4 = [Y_3, Y_1]$$
$$= 4\sum_{i=1}^{\ell} D_i^2 - 4\sum_{i=1}^{\ell} \alpha_i D_i - \sum_{i=\ell+1}^{s} \alpha_i D_i - \frac{1}{2}E_\ell^3(\eta) - 3\sum_{i=l+1}^{s} \alpha_i^2 + \sum_{i=s+1}^{n} f_i^{(1)} \frac{\partial}{\partial x_i}$$
$$+ \sum_{i=s+1}^{n}\sum_{j=1}^{\ell} f_i^{(1)} x_j \frac{\partial f_j}{\partial x_i} + \sum_{i=s+1}^{n} E_\ell(\sum_{j=1}^{l} f_i^{(1)} x_j \frac{\partial f_j}{\partial x_i}) + \sum_{i=s+1}^{n} E_\ell^2(\sum_{j=1}^{l} f_i x_j \frac{\partial f_j}{\partial x_i}) + \sum_{i=s+1}^{n} \frac{\partial f_i^{(1)}}{\partial x_i},$$

Notice that α_i^2 are quadratic of $x_1, \cdots, x_\ell$ variables with coefficients in C^∞-functions of $x_{s+1}, \cdots, x_n$ for all $i = 1, \cdots, s$,and $\sum_{j=1}^{\ell} f_i x_j \frac{\partial f_j}{\partial x_i}$ and $\sum_{j=1}^{\ell} f_i^{(1)} x_j \frac{\partial f_j}{\partial x_i}, i = s+1, \cdots, n$ are polynomials of degree ≤ 2 in $x_1, \cdots, x_s$ variables with coefficients in C^∞-functions of $x_{s+1}, \cdots, x_n$, so are $\sum_{i=s+1}^{n} E_\ell(\sum_{j=1}^{\ell} f_i x_j \frac{\partial f_j}{\partial x_i})$, $\sum_{i=s+1}^{n} E_\ell(\sum_{j=1}^{\ell} f_i^{(1)} x_j \frac{\partial f_j}{\partial x_i})$ and $\sum_{i=s+1}^{n} E_\ell^2(\sum_{j=1}^{\ell} f_i x_j \frac{\partial f_j}{\partial x_i})$. Then

$$Y_3 - 2Y_2 = 3\sum_{i=\ell+1}^{s} \alpha_i D_i - \frac{1}{2}E_\ell^2(\eta) - E_\ell(\eta) - 3\sum_{i=s+1}^{n} f_i^{(1)} \frac{\partial}{\partial x_i}$$
$$+ a\ polynomial\ of\ degree\ at\ most\ two\ in\ x_1, \cdots, x_s$$
$$Y_4 - 2Y_3 = -3\sum_{i=\ell+1}^{s} \alpha_i D_i + \frac{1}{2}E_\ell^3(\eta) + E_\ell^2(\eta) + 3\sum_{i=s+1}^{n} f_i^{(1)} \frac{\partial}{\partial x_i}$$
$$+ a\ polynomial\ of\ degree\ at\ most\ two\ in\ x_1, \cdots, x_s$$

and

$$Y_3 - 2Y_2 + Y_4 - 2Y_3$$
$$= \frac{1}{2}E_\ell[E_\ell^2 + E_\ell(\eta) - 2\eta] + a\ polynomial\ of\ degree\ at\ most\ two\ in\ x_1, \cdots, x_s$$

By theorem B, $E_\ell[E_\ell^2 + E_\ell(\eta) - 2\eta]$ is a polynomial of degree at most two in $x_1, \cdots, x_s (\ell \leq s \leq n)$. Since $E_\ell[E_\ell^2 + E_\ell(\eta) - 2\eta] = E_\ell(E_\ell + 2)(E_\ell - 1)\eta$, by theorem 8 and theorem 9, η is a polynomial of degree two in $x_1, \cdots, x_s$ variables with coefficients in C^∞-functions of $x_{s+1}, \cdots, x_n$.

Recall that

$$\sum_{i=1}^{s}\frac{\partial f_i}{\partial x_i}+\sum_{i=1}^{s}f_i^2=-\sum_{j=1}^{m}h_j^2+\eta. \tag{3.8}$$

Let $\psi\in C_0^\infty$ be any C^∞ function with compact support. Multiplying equation (3.8) with ψ^2 and integrating the equation over $\mathbf{R}^s$,

$$\int_{\mathbf{R}^s}\Big(\eta-\sum_{j=1}^{m}h_j^2\Big)\psi^2=\int_{\mathbf{R}^s}\psi^2\Big(\sum_{i=1}^{s}f_i^2\Big)+\int_{\mathbf{R}^s}\psi^2\sum_{i=1}^{s}\frac{\partial f_i}{\partial x_i}, \tag{3.9}$$

Integrating by parts on $\int_{\mathbf{R}^n}\psi^2\frac{\partial f_i}{\partial x_i}$ and using the notation $d\widetilde{x}_i=dx_1\cdots dx_{i-1}dx_{i+1}\cdots dx_n$,

$$\begin{aligned}\int_{\mathbf{R}^s}\psi^2\frac{\partial f_i}{\partial x_i}dx&=\int_{\mathbf{R}^{s-1}}\int_{\mathbf{R}}\psi^2\frac{\partial f_i}{\partial x_i}dx_i d\widetilde{x}_i \\ &=-\int_{\mathbf{R}^{s-1}}\int_{\mathbf{R}}2\psi\frac{\partial\psi}{\partial x_i}f_i dx_i d\widetilde{x}_i \\ &=-2\int_{\mathbf{R}^s}\frac{\partial\psi}{\partial x_i}(\psi f_i)dx.\end{aligned} \tag{3.10}$$

From the fact

$$\Big(\frac{\partial\psi}{\partial x_i}\Big)^2+(\psi f_i)^2\geq 2\frac{\partial\psi}{\partial x_i}\psi f_i,$$

we have

$$-\int_{\mathbf{R}^s}\Big(\frac{\partial\psi}{\partial x_i}\Big)^2-\int_{\mathbf{R}^s}\psi^2 f_i\leq -2\int_{\mathbf{R}^s}\frac{\partial\psi}{\partial x_i}\psi f_i. \tag{3.11}$$

In view of (3.9), (3.10) and (3.11) we have

$$\begin{aligned}\int_{\mathbf{R}^s}\Big(\eta-\sum_{j=1}^{m}h_j^2\Big)\psi&=-2\int_{\mathbf{R}^s}\sum_{i=1}^{s}\frac{\partial\psi}{\partial x_i}(\psi f_i)+\int_{\mathbf{R}^s}\psi^2\sum_{i=1}^{s}f_i^2 \\ &\geq-\int_{\mathbf{R}^s}\sum_{i=1}^{s}\Big(\frac{\partial\psi}{\partial x_i}\Big)^2,\end{aligned}$$

or

$$\int_{\mathbf{R}^s}\sum_{i=1}^{s}\Big(\frac{\partial\psi}{\partial x_i}\Big)^2-\int_{\mathbf{R}^s}\Big[\sum_{j=1}^{m}h_j^2-\eta\Big]\psi^2\geq 0. \tag{3.12}$$

which is true for all $\psi\in C_0^\infty$. Take any nonzero C^∞ function θ with compact support. Define ψ to be θ followed by a translation in $x_1,\cdots,x_\ell$ variables directions. Observe that $\int_{\mathbf{R}^s}|\nabla\psi|^2$ is independent of the translation selected. On the other hand, since η is quadratic in $x_1,\cdots,x_\ell$ variables and h_1^2 is of degree four in $x_1,\cdots,x_\ell$, $\sum_{j=1}^{m}h_j^2-\eta$ becomes

very positive when one of the $x_1, \cdots, x_\ell$ tends to infinity while the other variables remain fixed. We can choose translation in directions $x_1, \cdots, x_\ell$ in such a way that

$$\int_{\mathbf{R}^s} \left(\sum_{j=1}^{m} h_j^2 - \eta \right) \psi^2$$

is arbitrarily large while $\int_{\mathbf{R}^s} |\nabla \psi|^2$ is bounded. This of course contradicts the inequality (3.12). *Q.E.D.*

Definition. The estimation algebra E of a filtering problem (3.1) is said to be the estimation algebra with maximal rank provided that (i) all the observation terms are linear in x, and (ii) $x_i + c_i$ is in E for all $1 \leq i \leq n$,where c_i are constants.

Definition. The estimation algebra E of a filtering problem (3.1) is said to be the estimation algebra with sufficient rank provided that (i) all the observation terms are linear in x, and (ii) $x_i + c_i$ is in E for all $1 \leq i \leq s$,where c_i is a constant.

If we further restrict the assumption of $f_1, \cdots, f_n$, we have the following:

Theorem D. Consider a filtering system of (3.1) with the drift term $f = (f_1, \cdots, f_n)$ satisfying (a)$f_i(x) = l_i(x) + d_i \frac{\partial \phi(\frac{x_1}{\sqrt{d_1}}, \cdots, \frac{x_s}{\sqrt{d_s}})}{\partial x_i}$, where $l_i(x) \in C^\infty(R^n)$ are linear in x and ϕ_i are C^∞ functions on R^s for all $i = 1, \cdots, s$, and (b) $f_{s+1}(x), \cdots, f_n(x) \in C^\infty(R^n)$ are linear in x.

(i) If η is a polynomial of degree at most two in x and $h_1, \cdots, h_m$ are linear in x, then E is finite-dimensional and has a basis consisting of $E_0 = L_0$, differential operators E_i of the form

$$\sum_{j=1}^{s} \alpha_{ij} D_j + \sum_{j=s+1}^{n} \alpha_{ij} \frac{\partial}{\partial x_j} + \beta_i,$$

for $1 \leq i \leq p$ (for some p), where α_{ij}'s are constants and β_i's are affine in x, zero degree differential operators $E_{p+1}, \cdots, E_q$ (for some $q > p$) where E_k's are affine in x for $p + 1 \leq k \leq q$ (if q=1, then $p = 0$), and 1 (if $1 \in E$). Moreover the quadratic part of $\eta - \sum_{j=1}^{m} h_j^2$ is positive semi-definite.

(ii) Conversely, if E is finite dimensional and if the observation terms $h_1(x_1, \cdots, x_s), \cdots, h_m(x_1, \cdots, x_s)$ are C^∞ smooth functions of R^s, then $h_1, \cdots, h_m$ are affine in $x_1, \cdots, x_s$. Furthermore, if E has maximal rank then η is a polynomial of degree at most two in $x_1, \cdots, x_n$.

Proof. (i) Let F be the real vector space spanned by $\sum_{i=1}^{s}\alpha_i D_i+\sum_{i=s+1}^{n}\alpha_i\frac{\partial}{\partial x_i}+\beta$ where α_i's are constants and $\beta\in C^\infty(R^n)$ is affine in x. Clearly the dimension of F is $1+2n$. If $\sum_{i=1}^{s}\alpha_i D_i+\sum_{i=s+1}^{n}\alpha_i\frac{\partial}{\partial x_i}+\beta$ is an element in F, then by using the computation in Yau [16] and by Lemma 12, we have

$$\begin{aligned}
&\Big[L_0,\ \sum_{i=1}^{s}\alpha_i D_i+\sum_{i=s+1}^{n}\alpha_i\frac{\partial}{\partial x_i}+\beta\Big]\\
&=\frac{1}{2}\Big[\sum_{j=1}^{s}D_j^2+\eta,\ \sum_{i=1}^{s}\alpha_i D_i+\sum_{i=s+1}^{n}\alpha_i\frac{\partial}{\partial x_i}+\beta\Big]\\
&\quad+\Big[\sum_{j=s+1}^{n}f_j\frac{\partial}{\partial x_j}+\sum_{j=s+1}^{n}\frac{\partial f_j}{\partial x_j},\ \sum_{i=1}^{s}\alpha_i D_i+\sum_{i=s+1}^{n}\alpha_i\frac{\partial}{\partial x_i}+\beta\Big]\\
&=\sum_{i,j=1}^{s}\alpha_i d_{ij}D_j+\frac{1}{2}\sum_{i=1}^{s}\alpha_i\frac{\partial\eta}{\partial x_i}\\
&\quad+\sum_{j=1}^{s}\sum_{i=s+1}^{n}\alpha_i\Big(\frac{\partial f_j}{\partial x_i}D_j+\frac{1}{2}\frac{\partial^2 f_j}{\partial x_i\partial x_j}\Big)+\sum_{i=1}^{s}\beta_i D_i+\frac{1}{2}\sum_{i=s+1}^{n}\alpha_i\frac{\partial\eta}{\partial x_i}\\
&\quad-\sum_{i=1}^{s}\sum_{j=s+1}^{n}\alpha_i\Big(\frac{\partial f_j}{\partial x_i}\frac{\partial}{\partial x_j}+f_j\frac{\partial f_i}{\partial x_j}+\frac{\partial^2 f_j}{\partial x_i\partial x_j}\Big)\\
&\quad-\sum_{i=s+1}^{n}\sum_{j=s+1}^{n}\alpha_i\Big(\frac{\partial f_j}{\partial x_i}\frac{\partial}{\partial x_j}+\frac{\partial^2 f_j}{\partial x_i\partial x_j}\Big)+\sum_{j=s+1}^{n}f_j\beta_j\\
&=\sum_{j=1}^{s}\Big(\sum_{i=1}^{s}\alpha_i d_{ij}+\sum_{i=s+1}^{n}\alpha_i\frac{\partial f_j}{\partial x_i}+\beta_j\Big)D_j-\sum_{j=s+1}^{n}\Big(\sum_{i=1}^{n}\alpha_i\frac{\partial f_j}{\partial x_i}\Big)\frac{\partial}{\partial x_j}\\
&\quad+\frac{1}{2}\sum_{i=1}^{n}\alpha_i\frac{\partial\eta}{\partial x_i}-\sum_{i=1}^{s}\sum_{j=s+1}^{n}\alpha_i f_j\frac{\partial f_i}{\partial x_j}+\sum_{j=s+1}^{n}f_j\beta_j\in F
\end{aligned}\tag{3.13}$$

where $\beta=\sum_{i=1}^{n}\beta_i x_i+\beta_0$, $\beta_0,\cdots,\beta_n$ are constants. If $\sum_{i=1}^{s}\alpha_i' D_i+\sum_{i=s+1}^{n}\alpha_i'\frac{\partial}{\partial x_i}+\beta'$ is another element in F, then

$$\begin{aligned}
&\Big[\sum_{i=1}^{s}\alpha_i D_i+\sum_{i=s+1}^{n}\alpha_i\frac{\partial}{\partial x_i}+\beta,\sum_{j=1}^{s}\alpha_j' D_j+\sum_{j=s+1}^{n}\alpha_j'\frac{\partial}{\partial x_j}+\beta'\Big]\\
&=\sum_{i,j=1}^{s}\alpha_i\alpha_j' d_{ji}-\sum_{j=1}^{s}\sum_{i=s+1}^{n}\alpha_i\alpha_j'\frac{\partial f_j}{\partial x_i}-\sum_{j=1}^{s}\alpha_j'\frac{\partial\beta}{\partial x_j}\\
&\quad+\sum_{i=1}^{s}\sum_{j=s+1}^{n}\alpha_i\alpha_j'\frac{\partial f_i}{\partial x_j}-\sum_{j=s+1}^{n}\alpha_j'\frac{\partial\beta}{\partial x_j}+\sum_{i=1}^{n}\alpha_i\frac{\partial\beta'}{\partial x_i}\\
&=constant.
\end{aligned}\tag{3.14}$$

By (3.13) and (3.14), we know that the Lie algebra $\bar{F}$ generated by L_0 and F is exactly the vector space spanned by L_0 and F. In particular $\bar{F}$ has dimension $2n+2$. Since by assumptions that $h_1, \cdots, h_m$ are in F we have $E \subseteq \bar{F}$. Next whether or not 1 belongs to E depends on the following possible conditions: First if there exists a $h_i = \sum_{k=1}^{n} h_{ik}x_k + e_i$ with $h_{ik} \neq 0$ for some $1 \leq k \leq s$, where h_{ik} and e_i are constants. Then it follows from (3.7) that $\Big[[L_0, h_i], h_i\Big] = \sum_{k=1}^{s} h_{ik}^2$ is a nonzero constant in E, and hence 1 is in E. Second if no such h_i stated as above exist, observe that in (3.13) if we put $\alpha_i = 0, i = 1, \cdots, n, \beta = h_k = \sum_{j=s+1}^{n} h_{kj}x_j, k = 1, \cdots, m$, we get $(\sum_{j=s+1}^{n} f_j h_{kj})$'s are in E, which are polynomial of degree at most one in x. If at least one of them is a nonzero constant or a linear function of the form in the first case, we have $1 \in E$, otherwise $1 \notin E$.

From all above notes, we have that E is finite-dimensional with basis as claimed .

To prove state (ii) in theorem D, we notice that the first result follows from theorem C. Furthermore if E has maximal rank, there are constants c_j's such that $x_j + c_j$ is in E for $j = 1, \cdots, n$. The following computations follow from (3.13):

$$[L_0, x_j + c_j] = D_j, 1 \leq j \leq s \tag{3.15}$$

$$[L_0, x_j + c_j] = f_j, \ j \geq s+1 \tag{3.16}$$

$$[D_i, x_j + c_j] = \delta_{ij}, 1 \leq i \leq s, 1 \leq j \leq n \tag{3.17}$$

$$[L_0, D_j] = \sum_{i=1}^{s} d_{ji}D_i + \frac{1}{2}\frac{\partial \eta}{\partial x_j} + \sum_{i=s+1}^{n} f_i \frac{\partial f_j}{\partial x_i}, 1 \leq j \leq s. \tag{3.18}$$

(3.15),(3.16), (3.18) and the assumptions of theorem D imply that $\frac{\partial \eta}{\partial x_j}$ is in E for all $1 \leq j \leq s$. Hence, by theorem C $\frac{\partial \eta}{\partial x_i}$, for all $1 \leq i \leq n$, are polynomials of degree at most two in $x_1, \cdots, x_s$ with coefficients in C^∞ functions of $x_{s+1}, \cdots, x_n$. If $\frac{\partial \eta}{\partial x_i}$ is a polynomial of degree exactly two in $x_1, \cdots, x_s$ for some i, we shall prove that this is impossible. Without loss of generality, we may assume that the degree of $\frac{\partial \eta}{\partial x_1}$ is exactly two. So

$$\eta = x_1 q + r$$

where $q = \sum_{1 \leq i < j \leq n} a_{ij}(x_{s+1}, \cdots, x_n)x_i x_j + \sum_{j=1}^{n} a_j(x_{s+1}, \cdots, x_n)x_j + a(x_{s+1}, \cdots, x_n)$ is a polynomial with degree two in $x_1, \cdots, x_s$, and r is independent of x_1.

Depending on the degree of q in x_1, we have three possible cases.

(1) Degree 2 Case. $\eta - \sum_{j=1}^{m} h_j^2$ can be arbitrarily negative by taking a polynomial path $x_1 = -(sign\ a_{11}(x_{s+1}, \cdots, x_n))\ t, x_2 = x_3 = \cdots = x_s = 0$ as t tends to infinity.

(2) Degree 1 Case. We may assume $a_{12}(x_{s+1}, \cdots, x_n) \neq 0$ and then $\eta - \sum_{j=1}^{m} h_j^2 = a_{12}(x_{s+1}, \cdots, x_n)x_1^2 x_2 - b^2 x_1^2 + \beta x_1 + r$ where b is a constant and β, r are independent of x_1. $\eta - \sum_{j=1}^{m} h_j^2$ can be arbitrarily negative by taking a polynomial path $x_1 = t, x_2 = -a_{12}(x_{s+1}, \cdots, x_n), x_3 = \cdots = x_s = 0$ as t tends to infinity.

(3) Degree 0 Case. If $\sum_{j=1}^{m} h_j^2$ is dependent on x_1, then $\sum_{j=1}^{m} h_j^2 = -b^2 x_1^2 + \beta x_1 + r$ where b is a constant and β, r are independent of x_1 and hence $\eta - \sum_{j=1}^{m} h_j^2$ can be arbitrarily negative by taking a polynomial path $x_1 = t, x_2 = \cdots = x_s = 0$ as t tends to infinity. If $\sum_{j=1}^{m} h_j^2$ is independent of x_1, then we may assume $a_{22}(x_{s+1}, \cdots, x_n) \neq 0$ because of $deg\ \eta = 3$ in $x_l, \cdots, x_s$, and hence $\eta - \sum_{j=1}^{m} h_j^2 = a_{22}(x_{s+1}, \cdots, x_n)x_1 x_2^2 - c^2 x_2^2 + \beta x_2 + r$ where c is a constant and β, r are independent of x_2. Again $\eta - \sum_{j=1}^{m} h_j^2$ can be arbitrarily negative by taking a polynomial path $x_2 = t, x_1 = -a_{22}(x_{s+1}, \cdots, x_n), x_3 = \cdots = x_s = 0$ as t tends to infinity.

In all three cases, there is a contradiction to the Corollary 9. We have proved that $\frac{\partial \eta}{\partial x_i}$ is a polynomial of degree at most one for all $1 \leq i \leq s$. Hence η is a polynomial of degree at most two in $x_1, \cdots, x_s$. with coefficients in C^∞ functions of $x_{s+1}, \cdots, x_n$ for all $1 \leq i \leq s$, consequently, η is a polynormial of degree at most two in $x_1, \cdots, x_s$ with coefficients in C^∞ functions of $x_{s+1}, \cdots, x_n$.

We shall prove that in fact η is a polynomial of degree two in $x_1, \cdots, x_n$. Now write $\eta = \sum_{1 \leq i < j \leq n} a_{ij}(x_{s+1}, \cdots, x_n)x_i x_j + \sum_{j=1}^{n} a_j(x_{s+1}, \cdots, x_n)x_j + a(x_{s+1}, \cdots, x_n), l_i(x) = \sum_{k=1}^{n} b_{ik}x_k + c_i$ for $i = 1, \cdots s,$, and notice that $f_i(x) = l_i(x) + d_i \frac{\partial \phi(\frac{x_1}{\sqrt{d_1}}, \cdots, \frac{x_s}{\sqrt{d_s}})}{\partial x_i}$. Plug them

into equation (3.3), we have

$$\begin{aligned}
&\sum_{1\le i<j\le s} a_{ij}(x_{s+1},\cdots,x_n)x_ix_j + \sum_{j=1}^{s} a_j(x_{s+1},\cdots,x_n)x_j + a(x_{s+1},\cdots,x_n)\\
&= \sum_{i=1}^{s}[\frac{\partial l_i(x)}{\partial x_i} + \frac{\partial\phi(\frac{x_1}{\sqrt{d_1}},\cdots,\frac{x_s}{\sqrt{d_s}})}{\partial x_i}]\\
&\quad + \sum_{i=1}^{s}[l_i(x)^2 + 2l_i(x)\frac{\partial\phi(\frac{x_1}{\sqrt{d_1}},\cdots,\frac{x_s}{\sqrt{d_s}})}{\partial x_i} + (\frac{\partial\phi(\frac{x_1}{\sqrt{d_1}},\cdots,\frac{x_s}{\sqrt{d_s}})}{\partial x_i})^2] + \sum_{i=1}^{m} h_i^2(x)\\
&= [\sum_{i=1}^{s} l_i^2(x) + \sum_{i=1}^{m} h_i^2(x)] + \sum_{i=1}^{s}[2(\sum_{k=1}^{s} b_{ik}x_k + c_i)\frac{\partial\phi(\frac{x_1}{\sqrt{d_1}},\cdots,\frac{x_s}{\sqrt{d_s}})}{\partial x_i} + (\frac{\partial\phi(\frac{x_1}{\sqrt{d_1}},\cdots,\frac{x_s}{\sqrt{d_s}})}{\partial x_i})^2]\\
&\quad + \sum_{i=1}^{s} 2\sum_{k=s+1}^{n} b_{ik}x_k\frac{\partial\phi(\frac{x_1}{\sqrt{d_1}},\cdots,\frac{x_s}{\sqrt{d_s}})}{\partial x_i} \qquad (3.19)
\end{aligned}$$

Notice that $[\sum_{i=1}^{s} l_i^2(x) + \sum_{i=1}^{m} h_i^2(x)]$ is a polynomial of degree two in x, $\sum_{i=1}^{s}[2(b_ix_i + c_i)\phi(\frac{x_1}{\sqrt{d_1}},\cdots,\frac{x_s}{\sqrt{d_s}}) + \phi^2(\frac{x_1}{\sqrt{d_1}},\cdots,\frac{x_s}{\sqrt{d_s}})]$ is a C^∞ function of $x_1,\cdots,x_s$, and $\sum_{i=s+1}^{n} 2(b_ix_i + c_i)\phi(\frac{x_1}{\sqrt{d_1}},\cdots,\frac{x_s}{\sqrt{d_s}})$ is linear in $x_{s+1},\cdots,x_n$ with coefficients in C^∞- functions of $x_1,\cdots,x_s$. By comparing the coefficients of the terms in the first and the third expressions of the equations (3.19), we have that $a_{ij}(x_{s+1},\cdots,x_n) = a_{ij}, a_j(x_{s+1},\cdots,x_n) = a_j$ are all constants and η is a polynomial of degree two in x. *Q.E.D.*

If we further restrict the sufficient condition of $f_1,\cdots,f_s$ in theorem D and replace the assumption E being of maximal rank by being of sufficient rank in state (ii) in theorem D, we get a result similar to state (ii) in theorem D.

Theorem E. Let E be a finite dimensional estimation algebra of (3.1) with the drift term $f = (f_1,\cdots,f_n)$ satisfying (a)$f_i(x_1,\cdots,x_s) = l_i(x_1,\cdots,x_s) + d_i\frac{\partial\phi(\frac{x_1}{\sqrt{d_1}},\cdots,\frac{x_s}{\sqrt{d_s}})}{\partial x_i}$, where ϕ_i are C^∞ functions on R^s and $l_i(x_1,\cdots,x_s)$ are linear functions of $x_1,\cdots,x_s$ for all $i = 1,\cdots,s$, and (b) $f_{s+1}(x),\cdots,f_n(x)$ are linear functions of x. If E has sufficient rank then η is a polynomial of degree at most two in $x_1,\cdots,x_n$.

Proof. Notice that under the assumption of f, (3.18) is reduced to

$$[L_0, D_j] = \sum_{i=1}^{s} d_{ji}D_i + \frac{1}{2}\frac{\partial\eta}{\partial x_j}, 1 \le j \le s. \qquad (3.20)$$

(3.15) and (3.20) imply that $\frac{\partial\eta}{\partial x_j}$ are in E for all $1 \le j \le s$. Again, we get that η is a polynomial of degree two . *Q.E.D.*

The following theorem follows from the proof of theorem D.

Theorem F. Let E be an estimation algebra of filtering (3.1) with the drift term $f = (f_1, \cdots, f_n)$ satisfying (a)$f_i(x) = l_i(x) + d_i \frac{\partial \phi(\frac{x_1}{\sqrt{d_1}}, \cdots, \frac{x_s}{\sqrt{d_s}})}{\partial x_i}$, where ϕ_i are C^∞ functions on R^s and $l_i(x)$ are linear funtions on R^n for all $i = 1, \cdots, s$, and (b) $f_{s+1}(x), \cdots, f_n(x)$ are linear functions on R^n. If E is finite dimensional with maximal rank, then E is of dimension $n + s + 2$ with basis given by $1, x_1, \cdots, x_n$, $D_1, \cdots, D_s, L_0$.

The following theorem follows from the proof of theorem E.

Theorem G. Let E be an estimation algebra of filtering (3.1) with the drift term $f = (f_1, \cdots, f_n)$ satisfying (a) $f_i(x_1, \cdots, x_s) = l_i(x_1, \cdots, x_s) + d_i \frac{\partial \phi(\frac{x_1}{\sqrt{d_1}}, \cdots, \frac{x_s}{\sqrt{d_s}})}{\partial x_i}$, where ϕ_i are C^∞ functions on R^s and $l_i(x_1, \cdots, x_s)$ are linear function on R^s for all $i = 1, \cdots, s$, and (b) $f_{s+1}(x), \cdots, f_n(x)$ are linear functions on R^n. If E is finite dimensional with sufficient rank, then E as a vector space is isomorphic to a vector space with a basis given by $1, x_1, \cdots, x_p$ (some $p \geq s$), $D_1, \cdots, D_s, L_0$.

From the proof of theorem D and theorem E we have the following result.

Theorem H. The estimation algebras discussed in theorem D, theorem F and theorem G are solvable.

Proof. Suppose E is the estimation algebra of theorem D or theorem F or theorem G.

Let $E = E^{(0)}$, $E^{(n)} = [E^{(n-1)}, E^{(n-1)}]$. It is easy to see $E^{(3)} = 0$, so E is solvable.

Acknowledgement. I am grateful to my student C.-W. Liao for some help in algebraic computation of lemma A.

References

1. R. W. Brockett and J. M. C. Clark, The geometry of the conditional density , in : Analysis and Optimization of Stochastic Systems, O. L. R. Jacobs, et. al. (Ed.), Academic Press, New York, 1979, pp. 299–309.
2. R. W. Brockett, Nonlinear systems and nonlinear estimation theory, in: Mathematics of Filtering and Identification Applications, M. Hazewinkel and J.S. Williems (Ed.), Reidel, Dordrecht, The Netherlands, 1981, pp. 441–477.
3. R.W. Brockett, Nonlinear Control Theory and Dierential Geometry, Proceedings of the International Congress of Mathematicians, 1983, pp. 1357–1368.
4. J. Chen, C.-W. Leung and S. S.-T. Yau, Finite dimensional Filters with nonlinear drift VI: Classification of finite dimensional estimation algebras of maximal rank with state space dimension 3, SIAM J. Control and Optimization 29 (1991) 866–877.
5. J. Chen, C.-W. Leung and S. S.-T. Yau, Finite dimensional Filters with nonlinear drift VIII, Classification of finite dimensional estimation algebras of maximal rank with state space dimension 4, SIAM J. Control and Optimization 35 (1997) 1132– 1141.
6. W. -L. Chiou, A note on estimation algebras on nonlinear filtering theory, Systems and Control Letters 28 (1996) 55–63.
7. W.-L. Chiou and S. S.-T. Yau, Finite dimensioonal filters with nonlinear drift II: Brockett's problem on classification of finite-dimensional estimation algebras, SIAM J. Control and Optimization 32 (1994) 297–310.
8. M. H. A. Davis, On a Multiplicative functional transformation arising in nonlinear filtering theory, Z. Wahrsch. Verw. Gebiete 54 (1980) 125–139.
9. R. T. Dong, L. F. Tam, W. S. Wong and S. S.-T.Yau, Structure and classification theorems of finite dimensional exact estimation algebras, SIAM J. Control and Optimization 29 (1991) 866–877.
10. S. K. Mitter, On the analogy between mathematical problems of nonlinear filtering and quantum physics, Richerche di Automatica 10(2) (1979) 163–216.
11. D. L. Ocone, Finite dimensional estimation algebras in nonlinear filtering theory, in: The Mathematics of Filtering and Identification Applications, M. Hazewinkeland J.S. Williems (Ed.), Reidel, Dordrecht, The Netherlands, 1981, pp. 629–636

12. L. F. Tam, W. S. Wong and S. S.-T. Yau, On a necessary and and sucient condition for finite dimensionality of estimation algebras, SIAM J. Control and Optimization 28 (1990) 173–185.
13. J. Wei and E. Norman, On global representations of the solutions of linear dierential equations as product of exponentials, Proc. Amer. Math. Sock. 15 (1964) 327–334.
14. W. S. Wong, New classes of finite dimensional nonlinear filters, Systems Control 3 (1983) 155–164.
15. W. S. Wong, Theorem on the structure of finite dimensional estimation algebras, Systems Control Lett. 19 (1987) 117–124.
16. S. S.-T. Yau, Finite dimensional filters with nonlinear drift I: A class of filters including both Kalman-Bucy filters and Benes filters, Journal of Mathematical Systems, Estimation, and Control 4 (1994) 181–203.
17. S. S. -T. Yau and A. Rasoulian, Classification of 4-Dimensional Estimation Algebras, IEEE Transactions on Automatic Control 44 (1998) 2312–2318.
18. S. S.-T. Yau, Finite dimensional filters with nonlinear drift XIV: Clasification of Finite-Dimensional Estimation Algebras of maximal Rank with Arbitrary State Space Dimension and Mitter Conjecture, 1999. (preprint)
19. M. Zakai, On the optimal filtering of diusion processes, Z. Wahrsch. Verw. Gibe. 11(1969) 230–243.

Received October 25,2011
Revised December 29,2011
Accepted January 2,2012

一組濾波系統的有限維非線性濾波

邱文齡

輔仁大學數學系

摘　要

非線性濾波多年來不僅在工程學也在數學是一個熱門的題材。Brockett 與 Mitter 個別獨立提出使用估計代數構造有限維非線性濾波的想法，結果顯現出估計代數的概念在探討了解有限維非線性濾波扮演重要的角色。 1990 年，Yau 構造出一個包含 Kalman-Bucy 濾波與 Bene 濾波的有限維遞濾波。在本論文中，我們考慮一個包含 Yau 濾波的濾波系統， 對於其有限維估計代數提出一個簡單的代數的充分必要條件並證明之。特別是，我們證明了在這個有限維遞濾波，Mitter 的猜想是對的，並給予由 Brockett 提出有限維估計代數的分類的問題部分解答。

關鍵字：估計代數，過濾系統，有限維遞迴濾波，分類，最大秩。

* E-mail 049805@mail.fju.edu.tw

An Efficient Coverage Algorithm with Sleep Scheduling and Range Adjustment for Wireless Sensor Networks

Chun-Hsien Lu and Kei-Chen Tung

Dept. of Computer Science and Information Engineering
Fu Jen Catholic University

Abstract

The network coverage for wireless sensor networks is an important issue because the information may not be considered useful when the total coverage drops below a certain required level. One way to maintain good coverage and extend the system lifetime is to schedule some sensor nodes to sleep between active cycles, as well as dynamically adjust the sensing ranges of active sensors. In this paper, we propose an algorithm to determine if a sensor node should sleep based on its residual energy and the size of the overlap area between the sensor and its neighbors. For those sensors that remain active, we use our algorithm to compute the sensing range of each active sensor such that the total coverage is maintained above a user-specified requirement for as long as possible. Simulation results show that our proposed scheme achieves a better performance in providing the user-required coverage and extending the system lifetime 20 percent longer than the Coverage-Aware method, and 3 percent longer than the Random-Sleep method, respectively.

Key words: wireless sensor network, sleep scheduling, network coverage, dynamic sensing range adjustment

* E-mail address:jonlu@csie.fju.edu.tw

1. Introduction

Due to the fast development of embedded system and wireless communication technologies in recent years, wireless sensor network (WSN) has become one of the most important research areas. A Sensor network is a network system composed of multiple small and inexpensive devices deployed in a region to provide monitoring and communication capabilities for commercial and military applications including fire detection, asset tracking, habitat monitoring, and security surveillance [1-6]. In general, a wireless sensor network consists of a base station and many sensor nodes operating on small-sized batteries as shown in figure 1. When a sensor node detects an event within its coverage area, it would generate a report and send it in a data packet to the base station. The base station is responsible for collecting data from all the sensor nodes for further processing and decision making. A WSN may contain hundreds or even thousands of sensor nodes and it is desirable to operate these nodes as energy efficiently as possible. A sufficient number of sensor nodes must be deployed in order to provide a satisfactory performance.

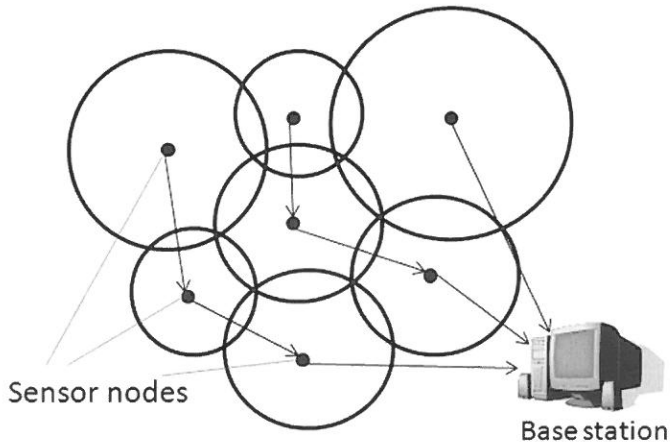

Fig. 1. An example of wireless sensor network.

Some sensor nodes will stop functioning due to electronic breakdown or energy exhaustion after the network system has operated for a period of time. Dead sensors can result in holes in coverage or packet routing, which may lead to serious network degradation [7-10]. The system cannot perform its desirable function satisfactorily since the base station will

not be able to collect sufficient information when the coverage is too low. One way to prevent this situation is to try to make the energy consumptions of different sensor nodes as even as possible by asking sensors with more residual energy to cover larger areas. In addition, sensor nodes in some system such as IEEE 802.15.4 ZigBee [11] can switch between active state and sleep state. A node that enters the sleep state will stay in an energy-saving mode by not participating in most activities. In this paper, we propose a mechanism to try to maintain the coverage level of a WSN above the user requirement for as long as possible. We first determine the set of the sensors in areas of high density that should enter the sleep state to conserve battery energy. For those sensor nodes that remain active, we would dynamically adjust their sensing ranges such that the total coverage can be maintained at or above the user requirement.

The rest of this paper is organized as follows: Section two lists the related work. We describe our sleep scheduling and sensing range adjustment algorithm in section three, while section four shows the experimental results and the performance comparisons. The conclusion is given in section five.

2. Related Work

Various mechanisms have been proposed to maintain a good coverage level for WSN. One approach is to use mobile sensors that are frequently trying to move to new target locations based on the virtual force interactions between sensors [12-15]. Each sensor is assumed to generate attractive or repulsive force on the other sensors. There will be a repulsive force to separate any two sensors if they are too close and an attractive force if they are far away. The idea is to constantly keep the sensors spread out in a balanced way. Each sensor then calculates its sensing range according to its relative residual energy and position to the other sensors in the neighborhood, where a sensor with relatively higher amount of energy should cover a larger area. The major disadvantages of this type of approaches are its heavy computation and constant moving, which could require significant amount of energy [16]. Another set of approaches try to mover sensors to predefined regular positions such that they will be spread out perfectly evenly. ISOGRID [17] and CLP [18] both suggest the movement of sensors to the vertices of a hexagon such that the system forms a perfect cellular structure. This approach requires a minimum number of active sensors to occupy all the

hexagon vertex positions, which may not be a problem at an early stage of system operation. However, there may not be enough active sensors to maintain a perfect structure as sensors gradually die out after the system has operated for a period of time.

Another class of mechanism is to do sleep scheduling [19-23], which is usually applied to networks of high density where sensors can alternate between the active and sleep modes from time to time to conserve energy. The active nodes in a neighborhood can cooperate with one another to maintain a good coverage. In the Random Sleep scheme [19], each sensor goes to sleep randomly with a probability set by the user. In the Distance-Based Sleep scheme [19], the sleep probability is based on the distance between the sensor and the base station, where a sensor node that is farther away will be put into the sleep state with higher probability. The Balanced-Energy Sleep scheme [20] tries to determine the sleep probability such that the maximal number of sensor nodes would consume energy at the same rate independent of the distance to the base station. In the Coverage-Aware Sleep Scheduling scheme [21], each sensor computes the total overlap area between itself and its active neighbors during each scheduling cycle. It then goes to sleep in the next cycle with a probability proportional to the size of the overlap area. The drawback of this method is that the computation may be too time-consuming to fit into the small computational power of a sensor when there are a large number of neighbors.

3. Distributed Sleep-Scheduling and Range Adjustment Algorithm

We hereby propose a mechanism called Distributed Sleep-scheduling and Range Adjustment (DSRA) that periodically determines the set of active nodes and sleep nodes for each cycle. Our system consists of a base station and many sensors nodes that do not move. We assume that every sensor node knows its own location by GPS or any other locationing mechanism. Every sensor node can adjust its own sensing range R_s ranging from 0 to R_{max}. A sensor is assumed to transmit its packets to the base station using multihop transmissions along the path of minimum number of hops if such path exists. The sensor is considered disconnected from the base station if there is no path between them. The sensors are assumed to be randomly deployed initially. A sensor node in sleep does nothing except waking up periodically to exchange control information with other neighboring nodes. The user is

allowed to specify a coverage requirement C ranging from 0 to 100%, and our goal is to prolong the time period that the system coverage stays above this requirement for as long as possible. The DSRA algorithm consists of the three following stages:

A. Information Exchange

At the beginning of each cycle, every active node broadcasts Hello messages to find neighbor nodes within its transmission range. The Hello message contains the following information: node coordinate, node id, residual energy, sensing range, type, state and S-value. Each active sensor node stores the received Hello messages in the *neighborhood information table* shown in table 1. Assuming its own location as the origin, each sensor can then identify the quadrant each of its neighbors resides in based on their coordinates.

Table 1. Neighborhood Information Table.

Node ID	Coordinate	S-Value	Type	...	Quadrant	State
Node 1	(X_1,Y_1)	8.775	Interior	...	I	Active
Node 2	(X_2,Y_2)	10.615	Interior	...	II	Sleep
...	...	...	...	...	...	
Node n	(X_g,Y_g)	9.124	Boundary	...	IV	Active

Figure 2 shows an example where node p finds its neighbors a, b, c, d, and e, and the quadrant each resides in. A sensor node that has at least one active neighbor in each of the four quadrants is called an interior node; otherwise, it is called a boundary node. We do not allow a boundary node to sleep by setting its S-value to zero because its sleep may result in undesirably large coverage holes. An interior node, g, will calculate its S-value using the following formula:

$$S\text{-}value = \frac{\alpha}{g's\ energy} + \beta \times (\text{total overlap areas in all four quadrants}), \quad (1)$$

where α and β are two weight parameters. The formula takes into consideration both the sensor' s own residual energy and the sum of the overlap areas between the sensor itself and the neighbors in all the quadrants. A sensor with large amount of energy should stay active, while a sensor with large coverage overlap between itself and its neighbors is a good

candidate to sleep. The active sensor nodes will wait for some amount of time to account for network delay, and enters the next stage.

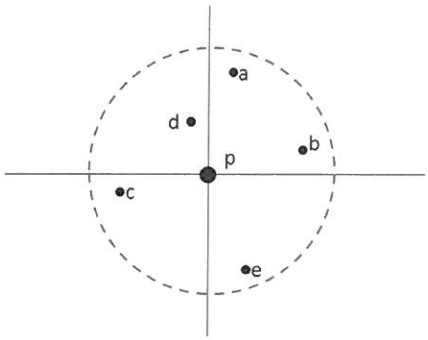

Fig. 2. Neighbors around an active sensor.

B. Sleep Scheduling

After the calculation of the S-value, each active node will again broadcast its S-value to its neighbors for comparison. If a sensor node has the maximum S-value among its neighbors, it will broadcast its decision to sleep to its neighbors and switches to sleep. Otherwise, the sensor remains active and enters the next stage of sensing range adjustment.

C. Sensing Range Adjustment

After the sleep scheduling phase, every active sensor node is fully aware of the identities of all its active neighbors. The sensing range calculation is different for boundary node and interior node. A boundary node should adopt a larger sensing range to maintain good coverage. For each quadrant without any neighbor, a boundary node measures its distance to the physical network boundary. Let d be the maximum of these distances. Let $y = min$ (R_{max} , d). The actual sensing range to use will be $C * y$, where C is the coverage requirement the user specifies. The sensor will then notify all the neighbors of its sensing range. The interior nodes will wait until all the boundary nodes to finish their calculations and broadcast their sensing ranges. An interior node p first computes a temporary sensing range for each quadrant, and chooses the maximum of the four values as its final sensing range to use. The computation is as follows: If there is no boundary node in a quadrant, the sensing range for that quadrant will be set to ($D/\sqrt{2}$), where D is the distance between the node and its nearest

neighbor in that quadrant. Otherwise, let b be a boundary node in that quadrant and R_b be its sensing range. Let D_{pb} be the distance between the node p and b, and R_p be p's current sensing range, respectively. If R_b is greater than $(R_p + D_{pb})$, this means that node p's sensing area can be fully covered by node b. Therefore, node p will go to sleep and notify all the neighbors of its decision. Otherwise, the sensing range of p will be set to $(D_b - R_b) / \sqrt{2}$. After node p has calculated the sensing ranges for all the four quadrants, let R denote the maximum of these values. The new sensing range of node p will be equal to $f \times C \times R$, where f is the ratio of p's residual energy over the average residual energy of p's neighborhood.

4. Simulation Results

4.1 Simulation Environment

We built a simulator in MATLAB platform to evaluate the performance of our scheme. We randomly deployed 100 sensor nodes in a square area of size 200m×200m. The initial energy of each sensor is 80J. Each packet is 512K bytes long. We use the following formulas to calculate the energy consumption [24]:

-Transmission energy consumption: $E_t = H + \theta \times packet_{size} \times R_c^2$

-Reception energy consumption : 0.25 J per packet

-Sensing energy consumption : $E_s = e_c + \gamma \times R_s^2$

where γ and θ are both adjustment parameters. H and e_c denote the fixed costs of transmission and sensing, respectively. R_s and R_c represent the current communication range (maximum of 100m) and sensing range (maximum of 50m), respectively.

4.2 Simulation Results

In our simulation, we compared our method with two other methods: the Random Sleep (RS) [19] and Coverage-Aware (CA) [21] schemes on the metrics of coverage percentage, residual energy, the number of active nodes, and the total number of packet received by the base station. The RS scheme randomly selects sensors to sleep with a user-given probability, while the CA scheme puts sensor nodes to sleep in order to maximally reduce the overlap sensing area while trying to maintain 100% coverage. Both these two schemes use fixed

sensing range, which is set to 20m in our experiment. The sleep probability in the RS scheme is set to 0.2 because that value produces the best experimental results. Figure 3 shows the comparison of the coverage percentages where all three schemes try to maintain a 100 % coverage. We can see that the CA scheme does maintain full coverage in the early stage, but its lifetime is shorter than the others. Our DSRA can provide almost 100% coverage with a 20% longer lifetime than CA because we try to make each sensor consume energy at about the same rate. The RS scheme also has a comparable lifetime to ours, but its coverage percentage is lower than the others because the sensors to sleep are chosen randomly. Figure 4 plots the number of active nodes in these three schemes. We can see that our DSRA scheme uses fewer active nodes to maintain the system coverage such that more nodes can preserve energy by switching to sleep and the system can operate longer.

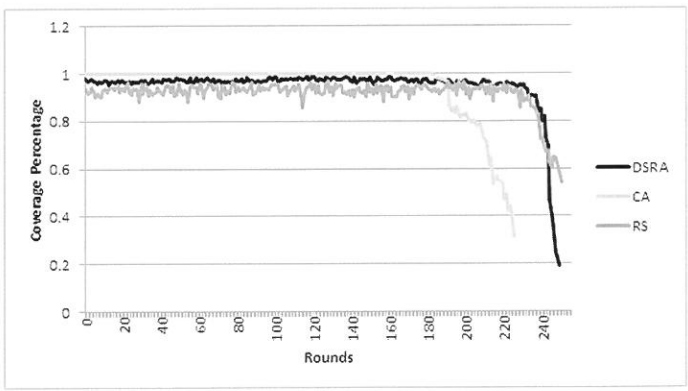

Fig. 3. Comparison of the coverage percentages.

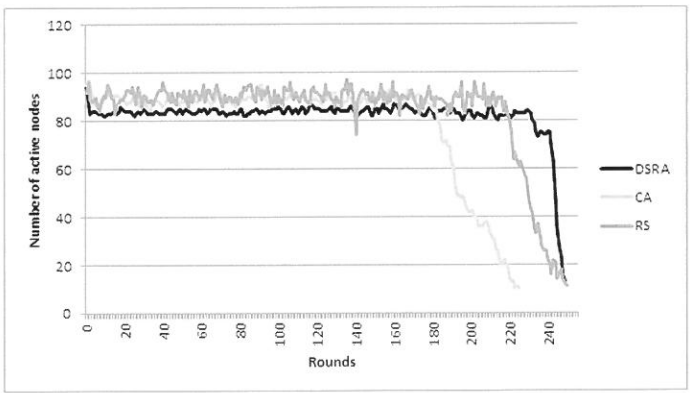

Fig. 4. Number of active nodes.

Figure 5 displays the accumulative number of packets successfully received by the base station. Both CA and our DSRA can receive almost all the packets since the coverage are about the same. However, the curve for CA flattens out after 200 rounds because most sensors are disconnected from the base station, while our DSRA still keeps receiving packets. Figure 6 shows the residual energy in the system. CA consumes its energy faster than the others because it uses a larger sensing range and has fewer nodes in sleep. Although our DSRA uses fewer active nodes to operate in the network, it adjusts the sensing range of each active node effectively to provide a good coverage. Both the DSRA and RS consume energy at about the same rate.

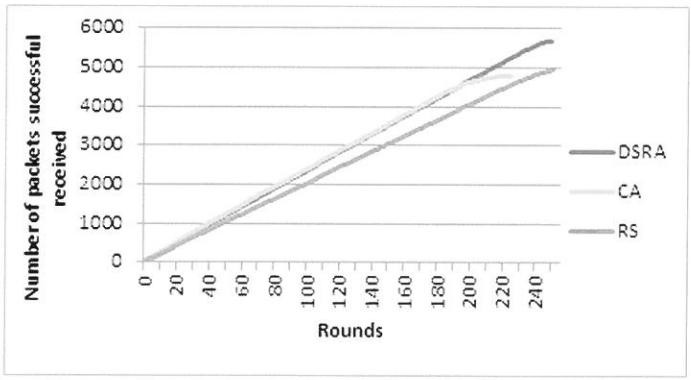

Fig. 5. Accumulative number of data packets successfully received by the base station.

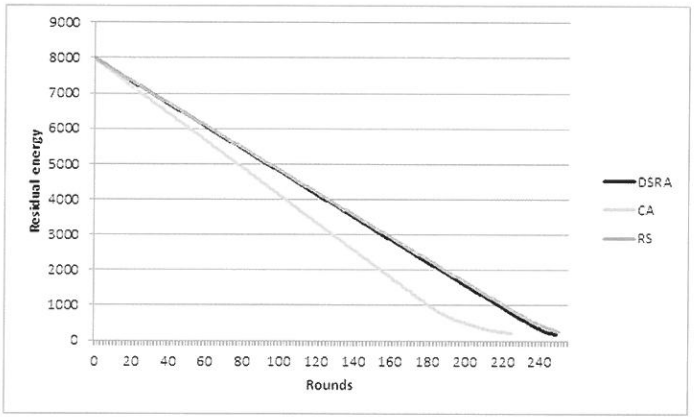

Fig. 6. Comparison of residual energy.

Our DSRA allows the user to specify a minimum coverage requirement C while the others do not. Figure 7 plots the actual coverage achieved given different values of C. For the

case of $C = 1$, the coverage percentage achieved is in the range of 0.95 to 0.99 that is a little bit below full coverage, while the system operates at a coverage above what the user specifies for all the other cases. In general, our DSRA can maintain the system coverage that satisfies the user requirement for as long as possible.

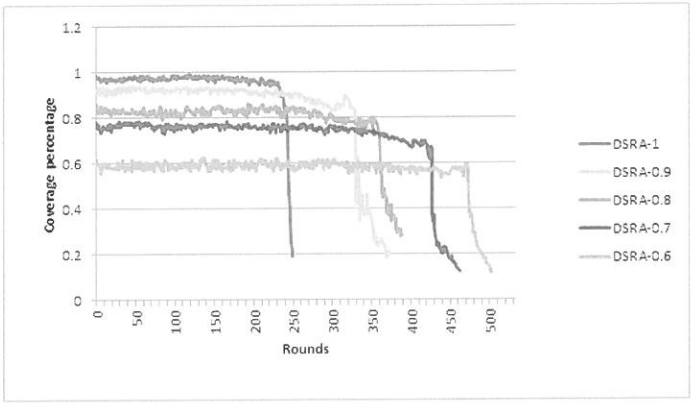

Fig. 7. Coverage percentages under different user requirements.

Figure 8 shows the number of the active nodes given various values of C. It seems that the value of C does not affect the number of nodes in sleep. Figure 9 shows that the total number of packets received by the base station closely depends on the coverage percentage. When C = 1, the number of packets received by the base station is the largest initially, but the total number of packets is fewer than the others because the system lifetime is shorter. Figure 10 shows that the energy is consumed faster when the coverage requirement is higher.

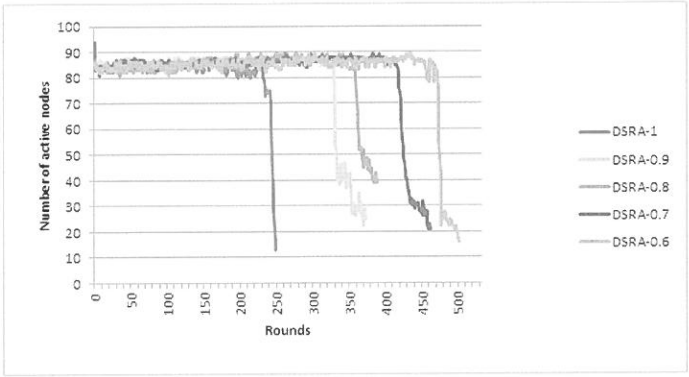

Fig. 8. Number of active nodes under different user requirements.

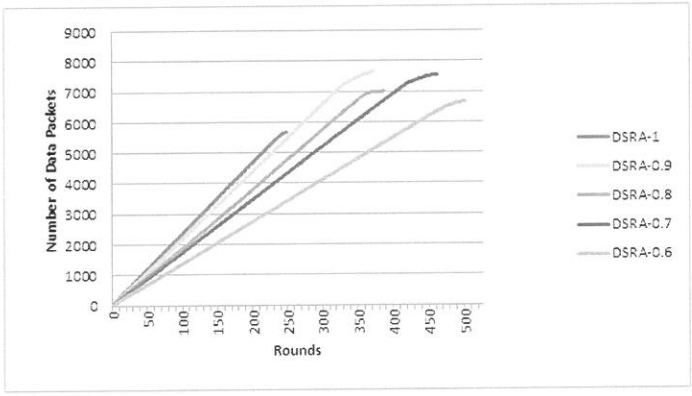

Fig. 9. Number of packets received under different user requirements.

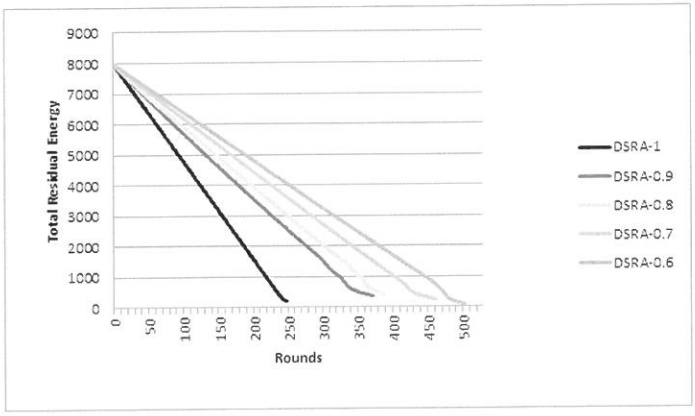

Fig. 10. Total residual energy under different user requirements.

5. Conclusion

Wireless sensor network has been widely used in many important applications, and it is essential to keep a minimum coverage for the network to function properly. We proposed an efficient DSRA method to generate a total coverage at the desirable level the user requires. Some of the sensors in an area of high density will be selected to sleep to conserve energy. Each of the active sensors then sets its sensing range such that the total coverage by all the

active sensors is maintained at the required level. The network is reconfigured periodically such that the sensors consume their energy at roughly the same rate. The simulation results showed that the DSRA scheme could achieve the required coverage for a long period of time, and the system lifetime can be extended about 20% and 3% longer than the CA and RS schemes, respectively.

References

1. Akyildiz, I. et al., "A Survey on Sensor Networks," IEEE Communications Magazine, Vol. 40, No. 8, pp. 102-114, 2002.
2. Tian, D. and Georganas, N.D., "A Coverage-preserving Node Scheduling Scheme for Large Wireless Sensor Networks," ADM International Workshop on Wireless Sensor Networks & Applications, 2002.
3. Brooks, R.R., Ramanathan, P., and Sayeed, A.M., "Distributed Target Classification and Tracking in Sensor Networks," Proceedings of IEEE, Vol. 91, No. 8, pp. 1163-1171, 2003.
4. Li, X., et al., "Coverage in Wireless Ad-hoc Sensor Networks," IEEE Transactions on Computers, Vol. 52, No. 6, pp. 753-763, 2003.
5. Huang, C.F. and Tseng, Y.C., "The Coverage Problem in a Wireless Sensor Network," 2nd ACM International Conference on Wireless Sensor Networks and Applications, San Diego, CA, USA, 2003.
6. Ye, F., Zhong, G., Cheng, J., Lu, S., and Zhang, L., "PEAS: A Robust Energy Conserving Protocol for Long-lived Sensor Networks," 23rd International Conference on Distributed Computing Systems, 2003.
7. Jiang, J. and Dou, W., "A Coverage-preserving Density Control Algorithm for Wireless Sensor Networks.," LNCS on Ad-Hoc, Mobile, and Wireless Networks, Vol. 3158, Springer, 2004.
8. Li, L., Sun, L., Ma, J., and Chen, C., "A Receiver-based Opportunistic Forwarding Protocol for Mobile Sensor Networks," 28th International Conference on Distributed Computing Systems Workshops, 2008.
9. Zabin, F., et al, "REEP: Data-Centric Energy-Efficient and Reliable Routing Protocol for Wireless Sensor Networks," IET Communications, Vol. 2, Issue 8, 2008.
10. Wang, Y.H., Yu, C.Y., Chen, W.T., and Wang, C.X., "An Average Energy Based Routing

Protocol for Mobile Sink in Wireless Sensor Networks," First IEEE International Conference on Ubi-Media Computing, 2008.
11. IEEE Standards, http://www.ieee.org.
12. Zou, Y. and Chakrabarty, K., "Sensor Deployment and Target Localization Based on Virtual Forces," IEEE INFOCOM, 2003.
13. Younghwan, Y. and Agrawal, D.P., "Mobile Sensor Relocation to Prolong the Lifetime of Wireless Sensor Networks, " IEEE Vehicular Technology Conference, 2008.
14. Li, S., Xu, C., Pan, W., and Pan, Y., "Sensor Deployment Optimization for Detecting Maneuvering Targets," 8th International Conference on Information Fusion, 2005.
15. Lin, C.H., and Lu, C.H., "Efficient Relocation and Range Adjustment to Maintain Coverage in Wireless Sensor Networks," 5th Workshop on Wireless, Ad Hoc and Sensor Networks, Taiwan, 2009.
16. Wang, G., Cao, G., Porta, T.L., and Zhang, W., "Sensor Relocation in Mobile Sensor Networks," IEEE INFOCOM, 2005.
17. Lam, M.L., and Liu, Y.H., "ISOGRID: an Efficient Algorithm for Coverage Enhancement in Mobile Sensor Networks," IEEE/RSJ International Conference on Intelligent Robots and Systems, 2006.
18. Wang, P.C., Hou, T.W., and Yan, R.H., "Maintaining Coverage by Progressive Crystal-Lattice Permutation in Mobile Wireless Sensor Networks," International Conference on Systems and Networks Communications, 2006.
19. Deng, J., Han, Y.S., Heinzelman, W.B., and Varshney, P.K., "Scheduling Sleeping Nodes in High Density Cluster-based Sensor Networks," MONET Special Issue on Energy Constraints and Lifetime Performance in Wireless Sensor Networks, 2004.
20. Deng, J., Han, Y.S., Heinzelman, W.B., and Varshney, P.K., "Balanced-energy Sleep Scheduling Scheme for High Density Cluster-based Sensor Networks," 4th Workshop on Applications and Services in Wireless Networks, Boston, MA, 2004.
21. Shen, F., Liu, C., and Zhang, J., "A Distributed Coverage-aware Sleep Scheduling Algorithm for Wireless Sensor Networks," 6th International Conference on Information Technology, 2009.
22. Lu, G., Sadagopan, N., Krishnamachari, B., and Goel, A., "Delay Efficient Sleep Scheduling in Wireless Sensor Networks," IEEE INFOCOM, Miami, FL, 2005.
23. Balakrishnan, M., Johnson, E., and Huang H., "TEAN-Sleep for Distributed Sensor Networks: Introduction and α-Metrics Analysis," IEEE Military Communications Conference, 2007.

Received October 31,2011
Revised January 3,2012
Accepted February 14,2012

在無線感測網路中利用睡眠排程及半徑調整以維護涵蓋率之演算法

呂俊賢　湯凱程

輔仁大學資訊工程系

摘　要

無線感測網路中的網路涵蓋率是個很重要的參數，因為當整體涵蓋率低於某個數字時，所收集到的資料可能會沒有效用。一個維護良好的涵蓋以及延長系統壽命的方法是去動態調整感測半徑，並且對活動的感測器節點做睡眠排程安排。在本篇論文中，我們提出一個演算法，根據節點的剩餘電量以及和其他鄰居間重疊的感測區域大小，來對感測器節點做睡眠排程。對於那些維持運作沒有排入睡眠的節點，我們再透過演算法去調整它們的感測半徑，使得整體涵蓋率可以維持在使用者給定的要求之上愈久愈好。實驗結果顯示我們提出的機制，在滿足使用者給定需求以及延長生命週期上，都有更良好的表現。我們的方法所能提供的生命週期，和 Coverage-Aware 以及 Random-Sleep 等兩種方法相比，個別延長了 20% 及 3% 左右。

* E-mail address:jonlu@csie.fju.edu.tw

過氧化體增生活化接受器 γ 與 δ 致效劑減少 C-反應蛋白接受器在 H9c2 心肌原細胞中的表現

陳朝鎰、崔文慧、梁耀仁*

輔仁大學理工學院生命科學系所

摘　要

心血管疾病是世界上最嚴重的健康問題之一，其中粥狀動脈硬化是一個常見的疾病，發炎反應造成內皮細胞的功能異常是導致粥狀動脈硬化的一個關鍵的步驟，近期 C- 反應蛋白 (C-Reactive Protein, CRP) 被認為在心血管疾病中扮演一個重要的角色，做為一個臨床上非專一性發炎指標物的 CRP，主要是由肝臟分泌，存在於血清當中，並會經由心血管系統循環至全身，而內皮細胞及心臟細胞將會直接的接觸到並受到影響。過氧化體增生活化接受器 (Peroxisome proliferations-activated receptor, PPAR) 對於高等生物來說扮演一個相當重要的角色，與細胞的生長、分化和代謝有關。目前發現 PPAR 家族中有三種次分型（subtypes），PPAR α 與 PPAR γ 分別是高血脂和第二型糖尿病的治療用藥的目標，在臨床上 PPAR γ 的活化被認為與胰島素的感受性有關，也發現具有抑制細胞激素釋放的能力，這結果顯示 PPAR γ 的致效劑 (agonist) 除了具有治療糖尿病的能力外，也具有抗發炎的效果，近期發現 PPAR δ 的活化也具有抑制發炎的能力，雖然 PPARs 被認為有益於心血管疾病患者，但是確切的機制尚未清楚，有證據指出這可能是抗發炎所帶來的效果，因此 PPARs 致效劑的抗發炎能力可能對於心血管疾病是一個良好的治療物。

本實驗將 H9c2 細胞分別做不同的處理：未處理；處理 15 μg CRP 培養 18 個小時；前處理 10 μM PPAR γ 致效劑 (troglitazone) 或 1 μM PPAR δ (L-165,041) 致效劑，再加入 15 μg CRP 培養 18 個小時。實驗主要研究 CRP 下游的訊號分子改變以及 PPARs 致效劑能否有效的抑制 CRP 所帶來的影響。實驗結果顯示 CRP 會刺激 H9c2 細胞分泌 MCP-1，並受到 PPARs 致效劑的抑制。目前認為 Fc γ 受器是 CRP 的主要受器之一，在 H9c2 的實驗中證實 CRP 會刺激 CD64 的 mRNA 表現量增加，並受到 PPARs 致效劑的抑制。在實驗的過程中 PPAR δ 致效劑所使用的濃度只有 PPAR γ 致效劑的十分之一，但所帶來的效果卻是差不多的，或許 PPAR δ 對於 PPAR γ 來說是一個更好的治療心血管疾病的一個標的。

關鍵字： C-Reactive Protein、PPARs、Fc γ Receptor。

* Correspondence: 梁耀仁，輔仁大學理工學院生命科學系所，新北市新莊區中正路 510 號
E-mail: 071558@mail.fju.edu.tw

1. 前　言

C- 反應蛋白 (C-Reactive Protein, CRP) 由 Tillet 及 Francis 在 1930 年所發現的，當時是在研究受到肺炎鏈球菌 (Streptococcus pneumonia) 感染的病人，在早期或急性的病人血清裡發現一種蛋白質，因為在有鈣離子的狀況下可以沉澱出肺炎鏈球菌細胞壁裡的 “C” polysaccharide，所以剛開始認為 CRP 是抗體，後來則發現 CRP 是非特異性的反應蛋白而不是抗體。CRP 可以活化典型的補體系統、刺激吞噬作用以及結合到 Fc γ R (immunoglobulin receptor)，藉由與 Fc γ R 結合導致許多發炎激素的產生 [1]。人類在急性發炎的刺激下，CRP 在血清裡的濃度可迅速且明顯的上升，最多可達到原本的千倍或甚至更多，而絕大部分的 CRP 是由肝臟所製造的，並且透過心血管系統循環至全身，肝臟分泌 CRP 絕大部分是透過 IL-6 (interleukin-6) 去調控 CRP 的轉錄，並且可以透過另一個分子 IL-1 β (interleukin-1 β) 增強 CRP 的表現量 [2]，IL-6 和 IL-1 β 可以透過活化 STAT3 (signal transducer and activator of transcription 3)、C/EBP (CCAAT-enhancer-binding protein) 家族、NF- κ B (Rel protein) 去調節許多在急性發炎時期蛋白質的表現量。除了肝臟之外可以合成 CRP 的還有神經元 (neurons)、粥狀動脈硬化斑 (atherosclerotic plaques)、單核球 (monocyte)、淋巴球 (lymphpcytes) [3]。當 CRP 在急性發炎反應時期表現量增加時，會誘導一部分血清中的蛋白質增加，會最先受到影響的便是血管的內皮細胞以及心肌細胞。發炎反應是導致粥狀動脈硬化的一個關鍵步驟，前人的研究指出 CRP 會結合到氧化的低密度脂蛋白上的 phosphocholine，進而使得內皮細胞的黏附因子表現量增加，會誘導免疫細胞附著在血管壁上，並增加巨噬細胞吞噬低密度脂蛋白 [4]，進而形成巨噬泡沫細胞 (macrophage foam cell)，並且釋放出一些與發炎相關的細胞激素及氧化壓力 [5]，產生發炎反應，之後泡沫細胞集中在脂肪條紋 (fatty streaks)，這是粥狀動脈硬化 (atherosclerosis) 過程中早期的病徵，目前研究也指出，CRP 在血管內皮細胞上會透過 CD32 活化下游 NF- κ B 及 MCP-1，因此 CRP 在形成粥狀動脈硬化上扮演一個重要的角色。目前的研究顯示，CRP 對於心血管疾病來說是一個獨立的風險因子，CRP 的上升可以被用當作是心血管疾病的線索，可以用來評估是否是得到心血管疾病的高危險群 [6]。但現今對於 CRP 接受器的研究不甚清楚，目前認為 CRP 在白血球上的接受器為 Fc γ R，但在心肌細胞上，則沒有確認其是否具有專一的接受器。所有的 Fc γ Rs 屬於 immunoglobulin superfamily，它們是 Fc receptor 當中最重要的 [7]，可以誘導免疫細胞進行吞噬作用，因為 Fc γ Rs 的分子結構有些不同，造成 Fc γ Rs 對於抗體的親和力也不同 [8]，所以可將 Fc γ Rs 分成 Fc γ RI (CD64)、Fc γ RII (CD32) 與 Fc γ RIII (CD16)。

(Peroxisome proliferations-activated receptor, PPAR) 是一類的核受器，包含三種 subtypes：PPARα 是高三酸甘油血脂的臨床用藥目標，目前與抗發炎的相關性較少，相較於 PPARα，PPARγ 主要研究是在胰島素抗性的相關研究上，其致效劑 Troglitazone 已經是在治療第二型糖尿病上的臨床用藥，除了在治療糖尿病的相關研究上 [9]，在癌症的實驗上，發現也具有抗腫瘤活性，也會透過 p53 的路徑誘導細胞進行細胞凋亡 [10]，PPARγ 的致效劑也被發現可以透過減少 NF-κB 的活性，進而抑制發炎反應，最新發現的 PPARδ 在一些研究也顯現出具有抗發炎的能力，但作用機制路徑尚未清楚，目前在老鼠實驗模式上已經對於 PPAR-δ 扮演的角色有所了解，尤其在組織生長、修復、發炎和代謝 [11]，當 PPARδ 被活化也具有抑制發炎的能力，在內皮細胞上可以抑制 VCAM-1 (vascular cell adhesion molecule-1) 的表現 [12]。由於 PPARs 的抗發炎能力可能對於心血管疾病是一個良好的治療目標。前人的研究主要在探討 CRP 在內皮細胞上的作用，對於也屬於循環系統的心臟細胞的探討較少，因此實驗除了要探討 CRP 對於心臟細胞的影響外，也要探討 PPARs 致效劑對 CRP 在心臟細胞作用的影響。

2. 材料與方法

H9c2 細胞培養：

將一個單位的 DMEM (GIBCOTM) 粉末配在 800mL 滅菌的 ddH_2O，加入 1.5 g 的 $NaHCO_3$，pH 值以 HCl 或 NaOH 調成 7.4，之後再以滅菌 ddH_2O 補至 1 L，再到 Laminar Flow 以 0.22 μm 的過濾膜過濾後分裝，加入 10% FBS (Fetal Bovine Serum，Qualified ； GIBCO®)、1% PSA (Antibiotic-Antimycotic ； GIBCO™)，並取 3mL 培養液以 3 cm 的培養皿在培養箱培養一星期，確定有無汙染，並將培養液保存在 4℃。細胞培養在 37℃、5% CO_2 細胞培養箱 (CO_2 Air-Jacketed incubator ; NUAIRE) 中。

細胞核醣核酸的抽取 (RNA extraction)：

採用 Chomczynski 和 Sacchi(1987) [13] 的文獻中所提出的 single-step method of RNA isolation 的方法加以修飾。首先將適量的 TRIZOL-Reagent (Invitrogen) 加入細胞培養皿中，以 cell lifter 將細胞刮下，倒入離心管中，加入氯仿 chloroform (0.2mL cholorform/mL TRIzol® Reagent)，混合均勻後，靜置於室溫中十分鐘。之後將離心管

以 14000rpm，4℃，離心 10 分鐘。離心完後，取上清液至另一離心管中，再加入異丙醇 isopropanol (0.5 mL isopropanol/mL TRIzol® Reagent)，混合均勻後，靜置於 -20℃中一小時，再以 14000rpm，4℃，離心 15 分鐘。倒掉上清液，加入 70% 酒精 Ethanol (1mL 70% ethanol/mL TRIzol® Reagent) 與 pellet 沖洗混合後，再以 14000rpm，4℃，離心 10 分鐘。去上清液後，加入 27ul 的 DEPC 水充分溶解 pellet。之後取出 5ul 溶液稀釋一百倍後，利用分光光度計，來測量其 OD260 及 OD280 的吸光值，以判定 RNA 的濃度。

反轉錄 - 聚合連鎖反應 (Reverse transcription-polymerase transcripition)：

實驗中利用 MMLV RT 1st-Strand cDNA Synthesus Kit (EPICENTRE) 進行 RT-PCR，取 1 μg 全量 RNA 於 0.5ml 的微量離心管中，利用 RNase-free 水補足體積至 10.5 μl，加入 2 μl 的 Oligo (dT) primer，在 65℃下加熱兩分鐘後立刻置於冰中，接著加入 7.5 μl 的反應緩衝液於微量離心管中，混合均勻後，於 37℃中培養一小時以合成 cDNA，接著 85℃反應五分鐘後立刻置於冰上一分鐘以中止反應，最後存於 -20℃冰箱備用。於 50 μl 的聚合連鎖反應溶液中含有 2 μl 的反轉錄產物，10X PCR Buffer (200mM Tris-HCl，pH8.0，500mM KCl)；50mM $MgCl_2$；10mM dNTP Mix；Taq DNA polymerase (5U/ μl) (Invitrogen)； 10 μM 的各對引子 (如表一所示)；補水至 50 μl。混合均勻後，加熱至 94℃兩分鐘，再使用溫度循環控制器 (Biometra T1 Thermocycler) 進行聚合連鎖反應，反應條件如表二所示。PCR 反應產物以 2% 瓊酯膠片電泳分析，經 EtBr (Ethidium bromide) 染色後分析比較。

表一，所使用之引子

Gene	Primers	Base pair
CD16	F：5'GAA GCA TCG CTT CTT GGG AG 3' R：5'ACC AAG TTT GAG TGG CAG GAA T 3'	192 bp
CD32	F：5'GGT GCC ATA GCT GGA GGA ACA AAC 3' R：5'GGA GGC ACA TCA CTA GGG AGA AAG 3'	264 bp
CD64	F：5'GTC CCC AGT CAT CAG CTC CTG 3' R：5'CGC TTC TAA CTT GCT GAA AGG AA 3'	188 bp
GAPDH	F：5'AGA CAG CCG CAT CTT CTT GT 3' R：5'TTC CCA TTC TCA GCC TTG AC 3'	223 bp

表二，反轉錄聚合連鎖反應條件

Gene	Denaturing	Amplification	Extension
CD16 CD32 CD64	95℃ ：3 分鐘	95℃ ：30 秒 56℃ ：30 秒 72℃ ：3 分鐘	72℃ ：10 分鐘
		36 個循環	

酵素免疫分析 (Enzyme-Linked ImmunoSorbent Assay) ：

利用 MCP-1 ELISA development kit (PEROTECH INC.) 來測定 medium 中的 MCP-1 含量。使用 Kit 中的 Capture Antibody (利用 PBS 稀釋至 0.5 μg/ml) 每個 well 加入 100 μl 在 96 孔盤中，培養過夜。之後將 96 孔盤中的液體移除，在每個 well 加入 300 μl的 wash buffer (0.05%Tween-20 in PBS) 洗四次後，再加入300 μl的 block buffer (1% BSA in PBS)。靜置於室溫一個小時後，將液體移除，在每個 well 加入 300 μl 的 wash buffer (0.05% Tween-20 in PBS) 洗四次後，在每個 well 加入 100 μl 的代測樣品或者標準液 (2ng/ml to zero)，靜置於室溫最少兩小時。之後將液體移除，在每個 well 加入 300 μl 的 wash buffer (0.05% Tween-20 in PBS) 洗四次後，每個 well 加入 100 μl 的 Detection antibody (稀釋至 0.5 μg/ml)，靜置於室溫兩小時。之後將液體移除，在每個 well 加入 300 μl 的 wash buffer (0.05% Tween-20 in PBS) 洗四次， 之後每個 well 加入 100 μl 的 Avidin-HRP Conjugate 稀釋液 [5.5 μl Avidin-HRP Conjugate 加入 diluent buffer (0.05% Tween-20，0.1% BSA in PBS) 補到 11ml] ，靜置於室溫 30 分鐘，將液體移除，在每個 well 加入 300 μl 的 wash buffer (0.05% Tween-20 in PBS) 洗四次，利用 ABTS Liquid Substrate (sigma) 呈色，測其 405nm 的吸光值。

同步定量聚合連鎖反應 (Real-time quantitative PCR)

實驗以 Smart Quant Green Master Mix with dUTP and ROX (Protech Technology Enterprise Co.) 進行反應產物標誌，以 StepOne™ Real-Time PCR System (Applied Biosystems Inc.；ABI) 偵測結果。20 μl 的混合液中內含 10 μl 的 Smart Quant Green Master Mix、0.4 μl 的 $MgCl_2$ (25mM)、2 μl 的 Forward and Reverse Promers (1 μM)、2.5 μl 的 cDNA (50ng) 和 3.1 μl 的 Nuclease-Free Water。反應條件如下圖所示。實驗所得數據為各個基因的 CT 值。

一、反應條件

Step1	Step2	Step3
95℃ ： 10 分鐘	95℃ ： 15 秒 60℃ ： 60 秒	95℃ ： 15 秒 60℃ ： 60 秒 95℃ ： 15 秒
	循環 40 次	

二、比較 CT 值的方法 (Applied Biosystems ； ABI)

Step1	Normalization to endogenous control ：
	Ct Target gene - Ct endogenous control = ΔCt
Step2	Normalization to cali brator sample ：
	ΔCt Sample – ΔCt Calibrator = ΔΔCt
Step3	use the formula ：
	$2^{-\Delta\Delta Ct}$

統計分析 (Statistical analysis)

所有實驗為具再現性的獨立實驗。Western blot 各時間的成像底片以 Dolphin-1D Gel Analysis Software (WEALTEC) 量化結果，量化結果與 housekeeping gene (β-actin) 相除標準化，每個組別再與對照組 (control) 相除 (令其對照組為 1)。實驗數據以平均值 ± S.E.M (mean ± standard error of mean) 表示。利用 Turkey HSD 比較各實驗組 (兩組以上) 與對照組的差異性。當 P 值小於 0.05 代表在統計上有顯著差異。

* $P < 0.05$ ； ** $P < 0.01$

# $P < 0.05$ ； ## $P < 0.01$

3. 結　果

H9c2 有表現 CD16、CD32 和 CD64

首先為了確定 H9c2 細胞有表現 CD16、CD32 和 CD64 三種受器的基因，因此利用 RT-PCR 的技術分析，結果顯示出沒有做過任何處理的 H9c2 都有表現出個別想要確定的受器基因。圖一， 因為 Fc 受器主要存在於白血球上，因此取大鼠血液中的白血

球檢體當作陽性控制組，最後結果顯示 H9c2 經 RT-PCR 和電泳結果與陽性控制組相同，DNA 產物送基因定序確認目標產物。因此證實 H9c2 有表現 CD16、CD32 和 CD64 三種受器的基因。

在 H9c2 上，CRP 會誘導與發炎相關的細胞激素增加，並且受到 PPAR δ 和 PPAR γ 致效劑抑制

前人研究與我們先前發表的實驗得知，CRP 會對於內皮細胞有所影響，而 PPARs 致效劑對於 CRP 所帶來的效果也有抑制性，但在 H9c2 上會不會改變細胞激素的分泌量還不確定，也不清楚 PPARs 致效劑有無作用，因此細胞經由前處理 10 μM PPAR γ 和 1 μM PPAR δ 的致效劑 30 分鐘後，加入 CRP 培養 18 個小時，其後將培養液收集起來，並進行 ELISA 實驗。圖二，H9c2 受到 CRP 的刺激，使得 MCP-1 (monocyte chemoattractant protein-1) 分泌量增加，但受到 PPAR γ (Troglitazone) 與 δ 致效劑 (L-165,041) 的抑制。從目前結果初步看來，較低濃度的 PPAR δ 致效劑的效果似乎就能達到與 PPAR γ 致效劑相同的效果。

在 H9c2 中，CRP 會刺激 CD64 的 mRNA 表現量上升，並受到 Troglitazone 與 L-165,041 的抑制，而 CD16 與 CD32 並無顯著影響

CRP 的受器為 Fc γ 受器家族，但目前認為 CRP 的主要受器為 CD32，而且在內皮細胞上也證實 CRP 會刺激 CD32 的表現量上升，透過 CD32 的路徑使得下游的 NF-κB 活化與 VCAM-1 (vascular cell adhesion molecule-1) 表現量增加 [13]，但是在同樣為心血管循環系統的心臟細胞方面則尚未確定，而 PPARs 致效劑對於 CD32 的影響也不清楚，因此實驗將 H9c2 細胞分別前處理 PPAR γ (Troglitazone) 與 δ 致效劑 (L-165,041) 致效劑 30 分鐘，再分別加入 CRP 培養 18 個小時。圖三、四、五，結果顯示 CD16、CD32 的 mRNA 表現量在各個組別中沒有顯著的差異性，但是 CD64 的表現量卻受到 CRP 的刺激而上升，並且受到 Troglitazone、L-165,041 的抑制，目前推測 CRP 較為可能的路徑為 CD64。

4. 討　論

粥狀動脈硬化形成的一個關鍵步驟就是內皮細胞的功能不全，形成過程中包括

發炎反應與許多細胞激素的參與，前人的研究中，在單核球上利用 PPARα 致效劑 (WY14643) 與 PPARγ 致效劑 (troglitazone) 抑制 CRP 所誘導的 interleukin 分泌 [15]，而在人類的內皮細胞的實驗則是利用 PPARγ (troglitazone) 和 PPARδ (L-165,041) 致效劑有效的抑制 CRP 所誘導的 MCP-1、IL-6、VCAM-1 (vascular cell adhesion molecule-1)、IL-8 表現量上升 [16]，除此之外 CRP 也會誘導人類的內皮細胞進行細胞凋亡 (apoptosis)。我們的實驗證實，在心臟細胞方面，H9c2 也會受到 CRP 的刺激，會活化下游受器的向上調節，並且產生細胞激素的分泌增加 (MCP-1)。

前人在人類內皮細胞上的研究，確定 CRP 訊號傳導是透過 Fcγ 受器家族，CRP 會透過 Fcγ 受器 CD32 促進單核球與內皮細胞的黏附作用 [17]，並且也會刺激 CD32 表現量上升，並透過 NF-κB 的路徑誘導 MCP-1 的表現 [14]，這顯示出 Fcγ 受器對於 CRP 在內皮細胞上的訊號傳導扮演一個重要的角色，但在我們的實驗中發現，H9c2 上的 CD32 mRNA 沒有受到 CRP 的刺激造成表現量有受到顯著的影響。目前有研究指出 CD16 的訊號傳導牽涉到 Src kinase [18]，並且也有研究指出利用 MSUM (monosodium urate monohydrate) 誘導嗜中性球 (neutrophils) 釋放前發炎因子，是透過 CD16、c-Src 路徑 [19]。在我們的實驗結果 (圖三、四、五)，CD16、CD32 的 mRNA 沒有受到 CRP、troglitazone、L-165,041 的影響，但是 CD64 的 mRNA 受到 CPR 的刺激表現量上升，並且受到 troglitazone、L-164,041 的抑制，因此推測在 H9c2 上，可能是透過 Fcγ 受器家族的 CD64 這條路徑。

此外，在實驗中所使用的 PPARγ 致效劑為 troglitazone，有研究指出 H9c2 並沒有表現 PPARγ，但是有表現 PPARα、PPARδ [20]，但在我們的研究中卻看到加入 troglitazone 對於 H9c2 是有效用的，推測可能是因為 troglitazone 除了是 PPARγ 的配體 (ligand) 外也是 PPARα 的配體，目前 PPARα 在巨噬細胞上也被發現具有抗發炎的能力，可以減少 LPS 與 INF-γ (interferon-gamma) 刺激小鼠的巨噬細胞釋放發炎因子 [21]，因此在實驗上加入 troglitazone 可能因為如此才會有抑制細胞激素跟發炎相關蛋白質的效果。前人研究大鼠腦部的星狀細胞 (astrocytes)，提出 PPARγ 會增加 PPARδ 的表現，但是 PPARα 會抑制 PPARδ 的表現 [22]，因此推測在 H9c2 中，可能透過 trogliazone - PPARα 的路徑抑制 PPARδ 的表現。在 H9c2 上沒有表現 PPARγ，但是有表現出 PPARα 和 PPARδ，由本實驗可推論 PPARα 和 PPARδ 在 H9c2 上扮演的角色可能比 PPARγ 還要來的重要。因此，進一步 PPARα 致效劑在心肌原細胞上的實驗是需要的。

我們的實驗證實 CRP 會誘導 H9c2 分泌 MCP-1，並且刺激 CRP 接受器 CD64 的表現。而 CRP 的影響不論是刺激 MCP-1 的分泌，或是自身接受器的向上調節表現，都

會受到 PPAR γ 與 δ 致效劑的抑制。而對於瞭解 CRP 接受器在心肌細胞上的變化，將有助於開發 PPAR γ 與 PPAR δ 致效劑在發炎性的心血管疾病上之應用。

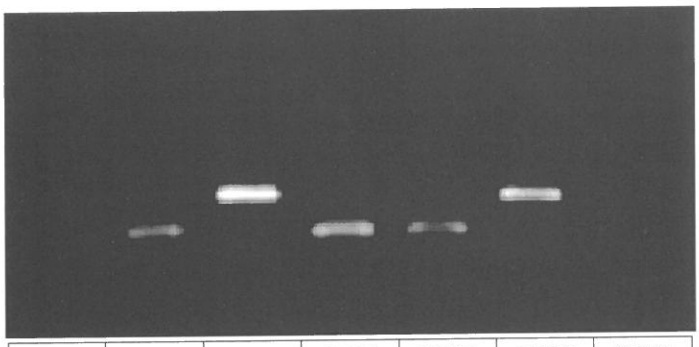

Marker	CD16	CD32	CD64	CD16	CD32	CD64
	Rat WBC			H9c2		

圖一、H9c2 有表現 CD16、CD32 和 CD64

Rat WBC（大鼠白血球）：取 Rat 的新鮮血液離心後，將 buffy coat 取出，加入適量的 TRIZOL-Reagent 進行 RNA 的抽取 。H9c2：以適量的 TRIZOL-Reagent 加入細胞培養皿中，以 cell lifter 將細胞刮下，收集到 eppendorf 裡進行 RNA 的抽取。各自取 1 μg 的 RNA 進行反轉錄，將 RNA 反轉錄成 cDNA，在以 cDNA 進行 PCR，最後將 PCR 產物進行電泳並呈現結果。結果顯示，Rat 血液組的 PCR 產物有 CD16（192 bp）、CD32（264 bp）、CD64（188 bp），H9c2 也呈現相同的結果，相互對照下証實 H9c2 有表現 CD16、CD32 和 CD64。

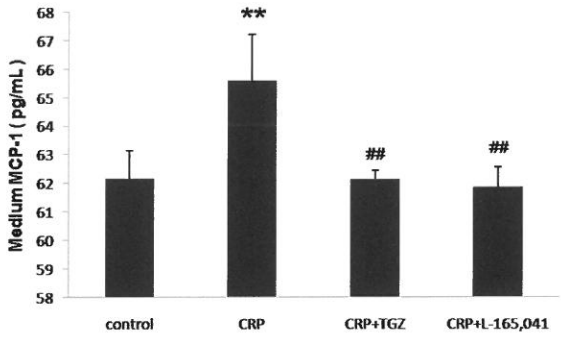

圖二、H9c2 受到 CRP 的刺激使得 MCP-1 表現量上升，並受到 PPARs 致效劑的抑制

H9c2 經由前處理 10 μ M TGZ (troglitazone ; PPAR γ 致效劑) 與 1 μ M L-165,041 (PPARδ 致效劑) 培養 30 分鐘後，再加入 15 μ g/mL CRP 進行 18 個小時的誘導，之後將培養液取出進行 ELISA 測量 MCP-1 的含量。結果顯示 CRP 誘導 H9c2 分泌 MCP-1 的量增加，但受到 TGZ、L-165,041 的抑制。(n=6)

當與 control 組相互比較時， **p<0.01。

當與 CRP 組相互比較時，## p<0.01。

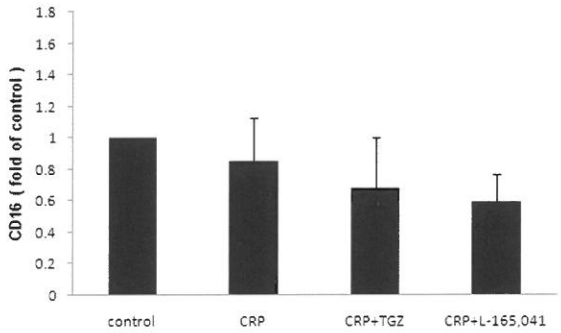

圖三、在 H9c2 中，CRP 的受器之一 CD16，其 mRNA 表現量沒有受到顯著的影響

H9c2 經由前處理 10 μ M TGZ (troglitazone ; PPAR γ 致效劑) 與 1 μ M L-165,041 (PPARδ 致效劑) 培養 30 分鐘後，再加入 15 μ g/mL CRP 進行 18 個小時的誘導，之後將細胞收集起來進行 reverse transcription 與 real-time PCR。結果顯示，CD16 的 mRNA 表現量並沒有受到 CRP、TGZ 和 L-165,041 的刺激有顯著的改變。(n=5)

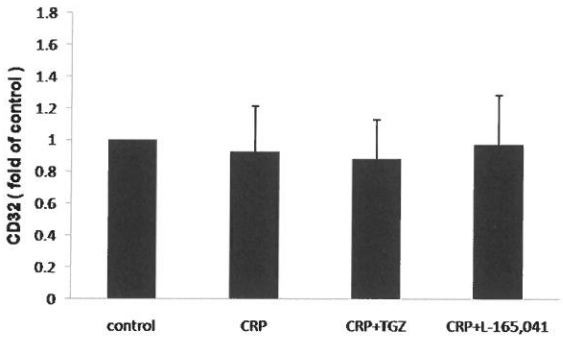

圖四、在 H9c2 中，CRP 的受器之一 CD32，其 mRNA 表現量沒有受到顯著的影響

H9c2 經由前處理 10μM TGZ (troglitazone；PPARγ 致效劑) 與 1μM L-165,041 (PPARδ 致效劑) 培養 30 分鐘後，再加入 15μg/mL CRP 進行 18 個小時的誘導，之後將細胞收集起來進行 reverse transcription 與 real-time PCR。結果顯示，CD32 的 mRNA 表現量並沒有受到 CRP、TGZ 和 L-165,041 的刺激有顯著的改變。(n=7)

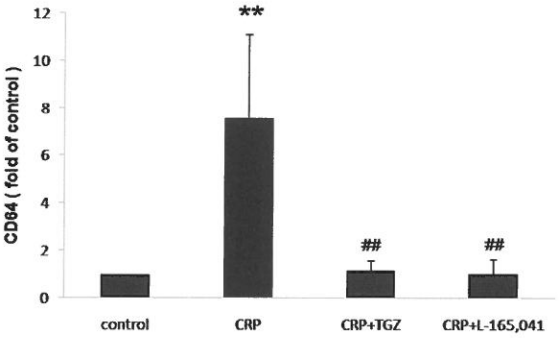

圖五、在 H9c2 中，CRP 刺激 CD64 的 mRNA 表現量上升，並受到 TGZ 與 L-165,041 的影響

H9c2 經由前處理 10μM TGZ (troglitazone；PPARγ 致效劑) 與 1μM L-165,041 (PPARδ 致效劑) 培養 30 分鐘後，再加入 15μg/mL CRP 進行 18 個小時的誘導，之後將細胞收集起來進行 reverse transcription 與 real-time PCR。結果顯示，CD64 的 mRNA 表現量受到 CRP 的刺激表現量上升，並且受到 TGZ 和 L-165,041 的抑制。(n=5)

當與 control 組相互比較時，*$p<0.05$，**$p<0.01$。

當與 CRP 組相互比較時，#$p<0.05$，##$p<0.01$。

參考文獻

1. Pepys MB, Hirschfield GM. C-reactive protein: a critical update. J Clin Invest. 111:1805-12, (2003)
2. Cha-Molstad H, Agrawal A, Zhang D, Samols D, Kushner I. The Rel family member P50 mediates cytokine-induced C-reactive protein expression by a novel mechanism. J Immunol. 165:4592-7, (2000)
3. Jialal I, Devaraj S, Venugopal SK. C-reactive protein: risk marker or mediator in atherothrombosis? Hypertension. 44:6-11, (2004)
4. Paul A, Ko KW, Li L, Yechoor V, McCrory MA, Szalai AJ, Chan L. C-reactive protein accelerates the progression of atherosclerosis in apolipoprotein E-deficient mice. Circulation. 109:647-55, (2004)
5. Libby P. Inflammation in atherosclerosis. Nature. 420:868-74, (2002)
6. Danesh J, Wheeler JG, Hirschfield GM, Eda S, Eiriksdottir G, Rumley A, Lowe GD, Pepys MB, Gudnason V. C-reactive protein and other circulating markers of inflammation in the prediction of coronary heart disease. N Engl J Med. 350:1387-97, (2004)
7. Fridman WH. Fc receptors and immunoglobulin binding factors. FASEB J. 5:2684-90, (1991)
8. Indik ZK, Park JG, Hunter S, Schreiber AD. The molecular dissection of Fc gamma receptor mediated phagocytosis. Blood. 86:4389-99, (1995)
9. Lehmann JM, Moore LB, Smith-Oliver TA, Wilkison WO, Willson TM, Kliewer SA. An antidiabetic thiazolidinedione is a high affinity ligand for peroxisome proliferator-activated receptor gamma (PPAR gamma). J Biol Chem. 270:12953-6, (1995)
10. Okura T, Nakamura M, Takata Y, Watanabe S, Kitami Y, Hiwada K. Troglitazone induces apoptosis via the p53 and Gadd45 pathway in vascular smooth muscle cells. Eur J Pharmacol. 407:227-35, (2000)
11. Peters JM, Lee SS, Li W, Ward JM, Gavrilova O, Everett C, Reitman ML, Hudson LD, Gonzalez FJ. Growth, adipose, brain, and skin alterations resulting from targeted disruption of the mouse peroxisome proliferator-activated receptor beta(delta). Mol Cell Biol. 20:5119-28, (2000)
12. Fan Y, Wang Y, Tang Z, Zhang H, Qin X, Zhu Y, Guan Y, Wang X, Staels B, Chien S, Wang N. Suppression of pro-inflammatory adhesion molecules by PPAR-delta in human

vascular endothelial cells. Arterioscler Thromb Vasc Biol. 28:315-21, (2008)
13. Chomczynski P, Sacchi N. Single-step method of RNA isolation by acid guanidinium thiocyanate-phenol-chloroform extraction. Anal Biochem. 162:156-9, (1987)
14. Liang YJ, Shyu KG, Wang BW, Lai LP. C-reactive protein activates the nuclear factor-kappaB pathway and induces vascular cell adhesion molecule-1 expression through CD32 in human umbilical vein endothelial cells and aortic endothelial cells. J Mol Cell Cardiol. 40:412-20, (2006)
15. Xie L, Chang L, Guan Y, Wang X. C-reactive protein augments interleukin-8 secretion in human peripheral blood monocytes. J Cardiovasc Pharmacol. 46:690-6, (2005)
16. Liang YJ, Liu YC, Chen CY, Lai LP, Shyu KG, Juang SJ, Wang BW, Leu JG. Comparison of PPARdelta and PPARgamma in inhibiting the pro-inflammatory effects of C-reactive protein in endothelial cells. Int J Cardiol. 143:361-7, (2009)
17. Devaraj S, Davis B, Simon SI, Jialal I. CRP promotes monocyte-endothelial cell adhesion via Fcgamma receptors in human aortic endothelial cells under static and shear flow conditions. Am J Physiol Heart Circ Physiol. 291:H1170-6, (2005)
18. Korade-Mirnics Z, Corey SJ. Src kinase-mediated signaling in leukocytes. J Leukoc Biol. 68:603-13, (2000)
19. Ryckman C, Gilbert C, de Médicis R, Lussier A, Vandal K, Tessier PA. Monosodium urate monohydrate crystals induce the release of the proinflammatory protein S100A8/A9 from neutrophils. J Leukoc Biol. 76:433-40, (2004)
20. Pesant M, Sueur S, Dutartre P, Tallandier M, Grimaldi PA, Rochette L, Connat JL. Peroxisome proliferator-activated receptor delta (PPARdelta) activation protects H9c2 cardiomyoblasts from oxidative stress-induced apoptosis. Cardiovasc Res. 69:440-9, (2006)
21. Crisafulli C, Cuzzocrea S. The role of endogenous and exogenous ligands for the peroxisome proliferator-activated receptor alpha (PPAR-alpha) in the regulation of inflammation in macrophages. Shock. 32:62-73, (2009)
22. Aleshin S, Grabeklis S, Hanck T, Sergeeva M, Reiser G. PPAR{gamma}positively and PPAR{alpha} negatively control COX-2 expression in rat brain astrocytes through a convergence on PPAR{beta}/{delta} via mutual control of PPAR expression levels. Mol Pharmacol. 76;414-24, (2009)

Received October 31,2011
Revised January 3,2012
Accepted January 16,2012

Peroxisome proliferations-activated receptor γ and δ agonists attenuated the C-reactive protein receptor expression in H9c2 cardiomyoblasts

Chao-Yi Chen, Wen-Huei Tsui and Yao-Jen Liang *

Department and Institute of Life Science, Fu-Jen Catholic University, Taipei, Taiwan.

Abstract

Cardiovascular disease is one of the serious health problems in the world, in which atherosclerosis is a common cardiovascular disease. Inflammation causes endothelial cell dysfunction which is a key step of atherogenesis. Recently, C-reactive protein (CRP) was considered to play an important role in cardiovascular disease. CRP used to serve as clinical nonspecific inflammation marker. It is mainly secreted by the liver and circulates in serum through out the body. Endothelial cells and cardiomyocytes are directly exposed and affected by CRP. PPARs play a very important role in growth, differentiation and metabolism in cells of higher organisms. There are three kinds of PPAR subtype which have already been found: PPAR α, PPAR γ and PPAR δ. PPAR α and PPAR γ are therapeutic target for hyperlipidemia and type II diabetes, respectively. Clinically, activation of PPAR γ was considered to increase insulin sensitivity, and inhibit inflammatory cytokines. These previous studies show that PPAR γ agonist can be used for diabetes and anti-inflammatory treatment. PPARs have been showed to be beneficial for patients with cardiovascular disease, despite the exact mechanisms are not yet fully understood. Currently, activation of PPAR δ shows the anti-inflammation ability. Therefore, PPARs may be a good therapeutic target for inflammatory cardiovascular disease.

We used H9c2 in the experiment. The cells were treated in different groups : untreated; 15 μg CRP alone for 18 hours; 15 μg CRP for 18 hours with pre-treated 1 μM PPAR δ (L-165,041) or 10 μM PPAR γ (troglitazone) agonists for 30 minutes. This research focused on CRP induced signal molecular changes and mechanism of PPARs agonists. Our results showed that CRP induced inflammation-related protein (MCP-1) up-regulation in H9c2. PPARs agonists inhibited CRP-stimulated MCP-1 secretion in H9c2. FC γ receptor is one of main receptor for CRP at present. CRP stimulated that CD64 mRNA expression increased and inhibited by PPARs agonist in H9c2. In our experiment, the potency of PPAR δ (L-165041) and troglitazone are the same in anti-inflammatory effects, but PPAR δ agonist concentration is only one in ten for PPAR γ agonist. This study clearly provide a potential application for the use of PPAR δ agonists in inflammatory cardiovascular diseases.

Key words: C-Reactive Protein、PPARs、Fc γ Receptor

* Correspondence: Yao-Jen Liang, Department and Institute of Life Science, Fu-Jen Catholic University School
E-mail: 071558@mail.fju.edu.tw

The Synthesis and Chemistry of 8-Chlorobicyclo[5.1.0]oct-1(8)-ene

Gon-Ann Lee* , Hsin-Yi Lee, Chaur-Sheng Shiau and Jay Chen

Department of Chemistry, Fu Jen Catholic University, Hsinchuang, New Taipei 24205, Taiwan, R.O.C.

Abstract

8-Chlorobicyclo[5.1.0]oct-1(8)ene **(7)**, a 2-chlorinated bicyclic 1,3-fused cyclopropene, was synthesized from 1-bromo-8,8-dichlorobicyclo[5.1.0]octane by treating with MeLi. Compound **7** in THF / H_2O (1:1) solution would undergo ring-opening reactions to produce carbenes, and ene reaction to afford ene dimers. Carbene **18** reacted with water via conjugate addition and ipso addition to give compound **12** and **15**. Carbene **17** underwent oxidization with oxygen to result enone **13**. The ene dimerization adducts also rearranged to vinyl carbene and transformed into enone and diene products.

Key words: bicyclic 1,3-fused cyclopropenes、carbene insertion、ene dimerization.

* E-mail address: 016850@mail.fju.edu.tw

1. Introduction

Cyclopropene as the smallest ring cycloalkene, which contains 52.2 kcal/mol high strain energy (27.5 kcal/mol ring strain energy and 24.7 kcal/mol olefinic strain energy).[1] In order to release the high strain energy, cyclopropene will undergo several specific reactions, such as ring-opening reactions to yield vinyl carbenes and ene dimerizations to give 3-cyclopropylcyclopropenes.[2] These unique properties of cyclopropene have attracted considerable attention of both theoretical and experimental chemists.[3-5]

The chemistry of 1,3-fused bicyclic cyclopropenes are complicated and have been studied for many years. Billups had reported that 7-chlorobicyclo[4.1.0]-hept-1(7)-ene **(1)** rearranges to vinyl carbene **2** and subsequent intramolecular C-H insertion to deliver compound **3** under neat condition.[6] Banwell's group also found that under solution condition, the intermediate vinyl carbene **4** is then protonated and followed by the conjugate addition of chloride ion or hydroxide to result compound **5** and **6** (Scheme 1).[7] The 8-chlorobicyclo[5.1.0] oct-1(8)ene **(7)** also has the same transformation under solution condition to afford compound **8**,[7] otherwise, for the neat condition, our group has found that compound **7** could generate two regioselective ene dimers through the ene reaction [8] (Scheme 2).

Scheme 1

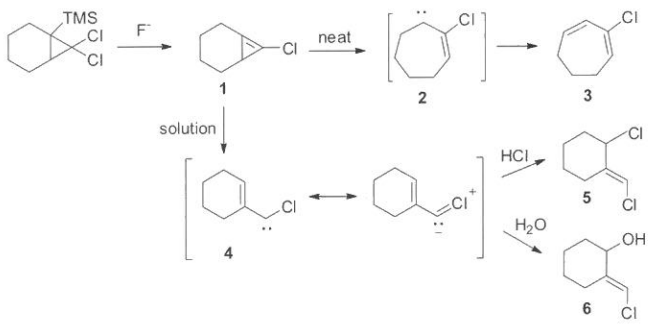

Scheme 2

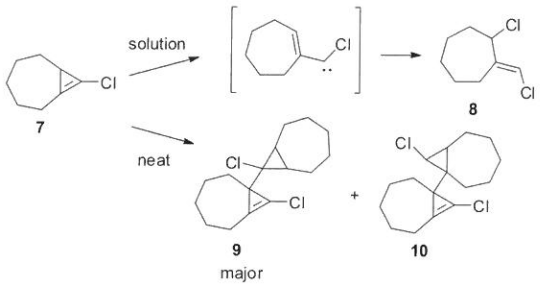

For the chemistry of the more stable bicyclo[6.1.0] 1,3-fused cyclopropenes, our group had found out that 9-chlorobicyclo[6.1.0]non-1(9)-ene dissolved in the THF/H_2O (5:1) solution, the carbene intermediates would undergo 1,3-addition, 1,1-additon and oxidization with oxygen.[9] These results were different from the Banwell's study, only afforded the conjugate addition products (Scheme 3). The interest results inspired us to study the chemistry of the less stable bicyclo[5.1.0] 1,3-fused cyclopropene 7 under solution condition, in this paper, we wish to describe the reactions of 7 with oxygen and water.

Scheme 3

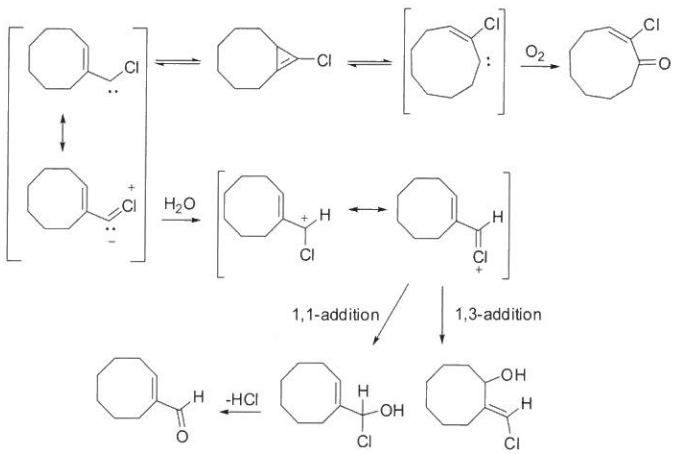

2. Results and Discussion

We previously reported an easier synthesis of the 2-substituted bicyclic 1,3-fused cyclopropenes,[10] 8-substituted bicyclo[5.1.0]oct-1(8)-ene, using1-bromo-8,8-dichloro-bicyclo[5.1.0]octane, which was generated from cycloheptene. The cycloalkene reacted by bromination, dehydrobromination and dichlorocarbene addition to give 1-bromo-8,8-dichlorobicyclo[5.1.0]octane. Treatment of cyclopropane **11** with 1.2 equiv. of methyllithium in diethyl ether at –78 ℃ generated bicyclic 1,3-fused cyclopropene **7** (Scheme 4).

Scheme 4

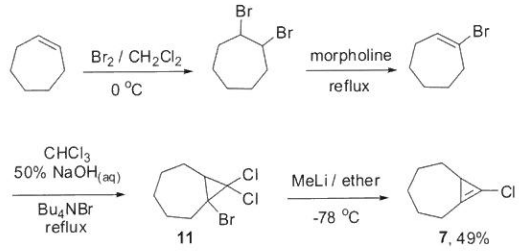

After compound 7 had been synthesized in 49% yield, it was dissolved in the solution of THF / H_2O (1:1) and kept at room temperature for 7 days, the adduct was purified by column chromatography, six compounds afforded, **12, 13, 9**, and **14** were isolated in yields of 31.2%, 2.5%, 46.2%, 8.8%, and trace amount of compound **15** and **16** (Scheme 5).

Scheme 5

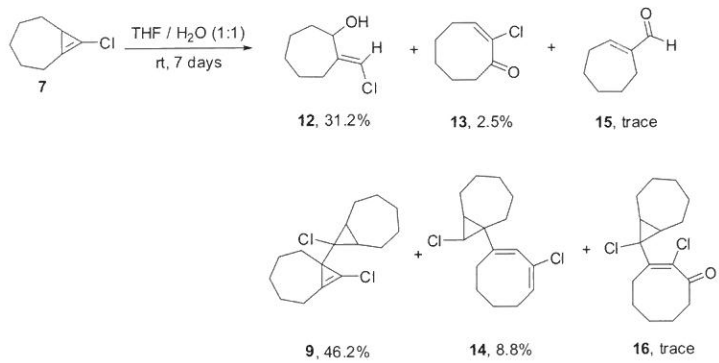

From these results, we demonstrated that compound **7** could undergo ring-opening reaction to generate vinyl alkylcarbene **17** and vinyl chlorocarbene **18,** carbene **18** is more stable than **17** due to the resonance effect of chlorine atom, therefore, most of the ring-opening reaction products are formed from carbene **18.** Protonation of carbene **18** gives the carbocation which can be stabilized by the neighboring chlorine atom. The carbocation reacted with water to give the conjugate addition adduct **12** and the ipso addition adduct immediate followed by repulsion of hydrogen chloride to form compound **15**. From the yield of these two adducts, it is proved that the conjugate addition with water is more favorable than the ipso addition. In the presence of oxygen, the small amount of carbene **17** was oxidized to form enone **1**3 (Scheme 6).

Scheme 6

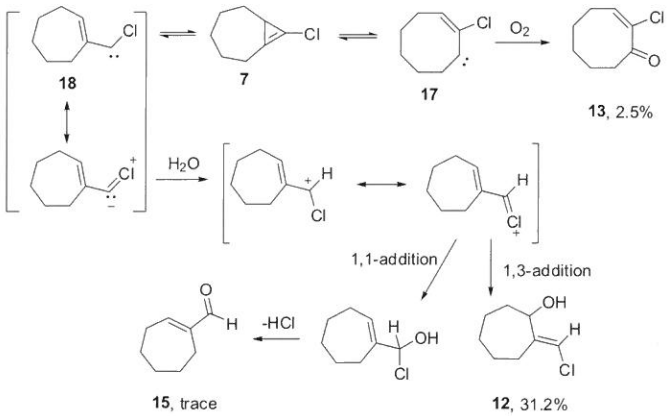

The unstable cyclopropne **7** also underwent ene reaction to give two regioselective isomers, the major dimer **9** converted into enone **16** via cyclopropene-vinylcarbene rearrangement followed by oxidization with oxygen. The minor dimer **10** underwent the intramolecular carbene insertion to generate cyclic allene which then isomerized to form diene **14** (Scheme 7). The ene reaction results were briefly reported from our previous work in 1995.[8]

Scheme 7

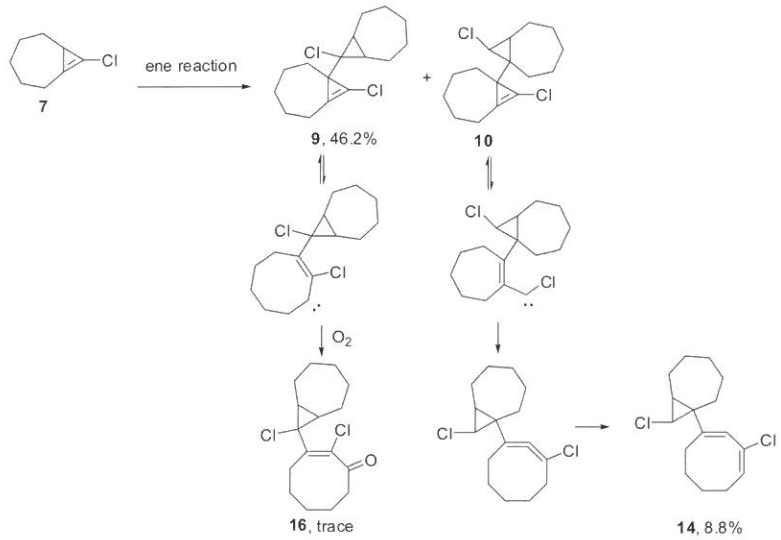

In summary, the unstable 1,3-fused bicyclic cyclopropene **7** would undergo ring-opening and ene reaction to release the high strain energy. Carbene **18** reacted with water to give conjugate and ipso addition products, and carbene **17** was oxidized with oxygen to result enone. The ene dimer adducts also converted into carbenes and afforded carbonyl and diene compounds.

3. Experimental Section

The synthesis of 8-chlorobicyclo[5.1.0]oct-1(8)-ene (7).

Compound **11** (1.0 g, 3.9 mmol) in 5 mL of dry ether was cooled to -78 °C, and 5 mL of 1.5 M methyllithium in ether was added. The mixture was stirred for 10 min at -78 °C. The reaction was quenched with water (1 mL) and allowed to warm to room temperature. The ethereal solution was dried, concentrated, and chromatographed to give **7** (49%).

Compound 7: ^{1}H NMR ($CDCl_3$) δ 2.48-2.41 (m, lH), 2.25-2.16 (m, lH), 2.03-1.76 (m, 6H),

1.57-1.43 (m, lH), 1.35-1.18 (m, 2H); ^{13}C NMR (75 MHz, $CDCl_3$) δ 116.75 (C), 111.04 (C), 33.40 (CH_2), 29.58 (CH_2), 29.40 (CH_2), 28.55 (CH), 26.93 (CH_2), 24.50 (CH_2).

The chemistry of compound 7 in H_2O/THF solution

Compound 7 (0.6 g, 4.3 mmole), was dissolved in 5 mL THF and 5 mL distilled water was added. After 7 days, the mixture was extracted with ether (50 mL). The ethereal solution was dried, concentrated, and chromatographed to give compound **9** (0.55g, 46.2%), **12** (0.21 g, 31.2%), **13** (0.016g, 2.5%), **14** (0.11g, 8.8%), trace **15** and **16**.

Compound **9**: IR (neat, cm^{-1}) 2915, 2855, 1695, 1440; ^{1}H NMR (300 MHz, $CDCl_3$) δ 2.85-2.59 (m, lH), 2.45-2.28 (m, lH), 2.27-1.90 (m, 20H); ^{13}C NMR (75 MHz, $CDCl_3$) δ 119.27 (C), 109.45 (C), 67.14 (C), 44.70 (C), 32.96 (CH_2), 32.70 (CH_2), 29.19 (CH_2), 29.08 (CH_2), 29.04 (CH_2), 28.90 (CH_2), 28.22 (CH), 28.16(CH), 26.6 (CH_2), 26.4 (CH_2), 26.0 (CH_2), 23.4 (CH_2); MS *m/z* 284 (M^+, 4%), 247 (42%), 193 (100%); HRMS calcd for $C_{16}H_{22}Cl_2$ *m/z* 284.1098, found 284.1094.

Compound **12**: IR (neat, cm^{-1}) 3400, 2940, 2880, 1625, 1450, 1350, 1295, 1055, 1015, 810, 775; ^{1}H NMR (300 MHz, $CDCl_3$) δ 6.06 (s,1H), 4.21-4.16 (m,1H), 3.15 (s, 1H), 2.35-2.32 (m,1H), 2.26-2.23 (m, 1H), 2.01-1.97 (m, 1H), 1.72-1.33 (m, 6H), 1.18-1.15 (m, lH) ^{13}C NMR (75 MHz, $CDCl_3$) δ 145.78 (C), 115.91 (CH), 73.90 (CH), 36.42 (CH_2), 29.60 (CH_2), 26.44 (CH_2),26.34 (CH_2), 23.34 (CH_2); HRMS calcd for $C_8H_{13}OCl$ *m/z* 160.0655, found 160.0653.

Compound **13**: IR (neat, cm^{-1}) 2915, 2855, 1665, 1430, 1245, 1085, 1010, 875, 845, 790; ^{1}H NMR (300 MHz, $CDCl_3$) δ 6.73-6.67 (t,1H, J = 7.9Hz), 2.80-2.75 (m, 2H), 2.57-2.50 (m, 2H), 1.86-1.77 (m, 2H), 1.67-1.52 (m, 4H); ^{13}C NMR (75 MHz, $CDCl_3$) δ 197.96 (C), 137.61 (CH), 132.95 (C), 41.84 (CH_2), 28.45 (CH_2), 24.54 (CH_2), 23.24 (CH_2), 22.88 (CH_2); HRMS calcd for $C_8H_{11}OCl$ *m/z* 158.0498, found 158.0492.

Compound **14**: IR (neat, cm^{-1}) 2890, 2830,1595,1425,1245,990,840; ^{1}H NMR (300 MHz, $CDCl_3$) δ 6.00 (s, lH), 5.54 (t, J = 7.9Hz, lH), 3.10 (d , J = 7.1 Hz, lH),2.42-1.22 (m, 19H); ^{13}C NMR (75 MHz, $CDCl_3$) δ 139.60 (C), 136.65 (C), 130.31 (CH), 124.48 (CH), 46.70 (CH), 36.87 (CH_2), 34.90 (CH), 32.18 (CH_2), 28.67 (CH_2), 28.35 (CH_2), 28.07 (CH), 27.66 (CH_2), 25.58 (CH_2), 25.17 (CH_2), 24.18 (CH_2), 21.67 (CH_2); HRMS calcd for $C_{16}H_{22}Cl_2$ *m/z* 284.1098, found 284.1092.

Compound **15**: IR (ATR, cm^{-1}) 1679, 1641; ^{1}H NMR (300 MHz, $CDCl_3$) δ 9.34 (s, 1H), 6.87

(t, J = 6.4 Hz, 1H), 2.49-2.41 (m, 4H), 1.84-1.76 (m, 2H), 1.64-1.58 (m, 2H), 1.54-1.46 (m, 2H); HRMS calcd for $C_8H_{12}O$ *m/z* 124.0888, found 124.0896.

Compound **16**: IR (neat, cm^{-1}) 2940, 2865,1690,1440, 1260, 1080, 1020, 860, 800; ^1H NMR (300 MHz, $CDCl_3$) δ 2.70-2.65 (m, lH), 2.56-2.52 (m, lH), 2.17-1.30 (m, 20H); ^{13}C NMR (75 MHz, $CDCl_3$) δ 202.34 (C), 142.41 (C), 128.66 (C), 58.24 (C), 42.50 (CH_2), 32.60 (CH_2), 32.26 (CH_2), 29.95 (CH), 28.82 (CH_2), 26.94 (CH_2), 26.31 (CH_2), 24.27 (CH_2), 22.80 (CH_2); HRMS calcd for $C_{16}H_{22}C1_2O$ *m/z* 300.1048, found 300.1049.

References

1. Wiberg, K. B. "Structures, Energies and Spectra of Cyclopropanes" *in The Chemistry of the Cyclopropyl Group*; Rappoport, Z., Ed. Wiley: New York, Chapt. 1 (1987).
2. Dowd, D.; Gold, A. "The Thermal Dimerization of Cyclopropene" *Tetrahedron Lett.* 85-86 (1969).
3. Halton, B; Banwell M. B. "Cyclopropenes" *in The Chemistry of the Cyclopropyl Group*; Rappoport, Z., Ed. Wiley: New York, Chapt. 21 (1987).
4. Liebman, J. F.; Greenberg, A. "A Survey of Strained Organic Molecules" *Chem. Rev.* 76, 311-365 (1976).
5. Billups, W. E.; Haley, M. M.; Lee, G.-A. "Bicyclo[n.1.0]alkenes" *Chem. Rev.* 89, 1147-1159 (1989).
6. Billups, W. E.; Lee, G.-A.; Amey, B. E., Jr.; Whitmire, K. H. "1,3-Bridged cyclopropenes" *J. Am. Chem. Soc.* 113, 7980-7984 (1991).
7. Banwell, M. G.; Corbett, M.; Gulbis, J.; Mackay, M. F.; Reum, M. E. "Generation and Solution-phase Behaviour of Some 2-Halogeno-I ,3-ring-fused Cyclopropenes" *J. Chem. Soc.*, Perkin Trans. 1, 945-963 (1993).
8. Lee, G.-A.; Shiau, C.-S.; Chen, J. "Regioselectivity of the Ene Reaction: Dimerization of 8-Chlorobicyclo[5.1.0]oct-1(8)-ene" *J. Org. Chem.* 60, 3565-3567 (1995).
9. Lee, G.-A.; Chen, J.; Chen, C.-S.; Shiau, C.-S.; Cherg, C.-H. "The Synthesis and Chemistry of 9-Chlorobicyclo[6.1.0]non-1(9)-ene" *J. Chin. Chem. Soc.* 43, 297-300 (1996).
10. Lee, G.-A.; Chen, P-K.; Chen, M-Y. "The Synthesis and Chemistry of 8-Substituted Bicyclo[5.1.0]oct-1(8)-ene" *J. Chin. Chem. Soc.* 45, 381-385 (1998).

Received October 31,2011
Revised January 3,2012
Accepted January 5,2012

8- 氯雙環 [5.1.0] 辛 -1(8)- 烯的合成與化性研究

李國安*、李欣怡、蕭朝盛、陳杰

輔仁大學 新北市新莊區中正路 510 號

摘　要

8- 氯雙環 [5.1.0] 辛 -1(8)- 烯 (7) 可經由 1- 溴 -8,8- 二氯雙環 [5.1.0] 辛烷與甲基鋰進行脫除反應而得，環丙烯 **7** 在四氫呋喃與水的條件下會進行開環反應得到碳烯以及因反應得到雙子化產物。碳烯 **18** 與水進行共軛加成及 1,1 加成反應得到化合物 **12** 和 **15**。碳烯 **17** 則會與氧氣進行反應得到化合物 **13**。此外化合物 **7** 也會進行因反應接著開環進一步轉變成烯酮與雙烯的產物。

關鍵字： 1,3 融合雙環環丙烯、碳烯插入、因反應。

Development of the Data Preprocessing Approach for Proteomic Data

Jen-Ing G. Hwang* , Hao-Hang Ling

Department of Computer Science and Information Engineering
Fu Jen Catholic University, Taipei, Taiwan

Bao-Ling Adam

Department of Surgery, Georgia Health Sciences University
Augusta, Georgia, USA

Abstract

With the fast development of mass spectrometry technology, application of proteomics to the classification and the diagnosis of cancer has become an important research field. However, the classification of proteomic data is usually hindered by the excessively high dimension and the presentation of noise. This leads us to the study of the data preprocessing and develop a novel four-step procedure for proteomic data. The objectives of our approach are to reduce the data dimensions and remove the noise in the data under the premise by keeping the important features. In particular, an algorithm called Maximum Envelope Peak Search (MEP search) is developed for peak detection. MEP search is a simple and low cost computational method to determine the peaks from a proteomic spectra data. The MEP search, as well as other data preprocessing steps, is implemented and demonstrated in comparison with a manual peak selection method using a proteomic data set. The results have shown that our method is comparable with the manual selection method. This indicates that our approach provides an advantage of fully automated data preprocessing and may have potential being used for analysis of other high-throughput spectral data sets.

Key words: Mass spectrometry, proteomics, baseline subtraction, normalization, peak alignment, peak detection.

* Corresponding author: Email: jihwang@csie.fju.edu.tw

1. Introduction

In recent years, rapid development in the application of mass spectrometry in proteomics studies prompts to the need of new strategies for the data analysis. Surface Enhanced Laser Desorption/Ionization Time-of-Flight Mass Spectrometry (SELDI TOF MS) is a high throughput technology for the detection of many protein simultaneously. It only needs very small amount of sample, such as body fluids or lysate from organisms or tissues, for the assay and it virtually takes only few minutes to read a single sample. However, the mass spectrometer generates excessively high dimensional spectra data which demands for a more effective and efficient way to analyze the data. The major challenge for analyzing spectral data is how to reduce both the noise and dimensionality before we can select the relevant features for further analysis, such as classification or clustering analysis.

A typical approach to analyzing mass spectrometry (MS) data consists of data preprocessing, clustering or classification. In this paper we focus on the development of algorithms for preprocessing MS data. Some common issues for data preprocessing include alignment [1], denoising [2], baseline subtraction [3, 4], normalization [3], and peak detection [5]. To date, no standard method has been established for the MS data preprocessing, including the steps and the order in which they might be executed. This leads us to develop a preprocessing procedure for MS data.

The reminder of this paper is organized as follows: in next section, a brief description of the MS dataset and its past usage are given. The proposed algorithm that performs baseline subtraction, normalization, peak detection, and peak alignment is explained in section 3. The computational experiments to verify the approach of data preprocessing are reported in section 4. Finally, some concluding remarks are presented in section 5.

2. Datasets and Previous Works

The database used for our research is provided by the researchers at Eastern Virginia Medical School (EVMS), and the data was generated using the technology of SELDI TOF MS. This technology is similar to the Matrix-Assisted Laser Desorption/Ionization-Time-of-Flight Mass Spectrometry (MALDI TOF MS) technology with the ability to pre-select

specific group of proteins onto a chemically activated surface. Its sensitivity and the ability to detect many proteins in one assay in a short period of time provide the potential for discovering biomarkers for diseases, especially for cancer [6].

The database contains 326 patients in four groups: Normal, BPH (Benign prostate hyperplasia), CAB (Early stage of prostate cancer) and CCD (Late stage of prostate cancer). There were repeated assay for each patient's sample to make 652 records in the database. Every record displays as a two dimensional spectrum. The X-axis is the value of mass per charge which is denoted by m/z and its unit is Dalton. The Y-axis is the intensity which represents the quantity of received ions at every time unit. There are approximately 48,000 (x, y) data points in each spectrum, and we refer to this data set as raw data. A manually preprocessed data set is also available from EVMS. Spectra in the set were preprocessed with the manual peak selection and stored as vectors of dimension 779. We applied our four-step procedure to the raw data set and obtained a new data set which was defined as automatically processed data set. Both automatically and manually processed data sets were used in the classification algorithm of decision tree to measure their performance.

This prostate cancer dataset was first studied by Adam et al. [7], and was also investigated by several other authors [5, 8-12]. Most of them were concerned about the problem of classifying different groups of patients using the manually processed data [7-9] or the raw data set [10-12], and few of them discussed the problem of data preprocessing [5, 11]. Although those authors who used the raw data set [10, 12] for classifications also handled the problems of data reduction and noise removal, they transformed the original data set in the X-Y (m/z – intensity) space into some other feature spaces and lost the ability for further data analysis, such as biomarker discovery. The authors [5, 11] indeed provided the data preprocessing approaches that were available for the study of biomarker discovery, however, Yasui et al. [11] investigated the effect of their approach in the cases of binary classifications, and Yasui et al. [5] considered 3-way classification only. In this study, we perform 2-, 3- and 4-way classifications on both automatic and manual data sets in computational experiments and compared their results to show the validity of the four-step procedure. As to the related works of data preprocessing for mass spectra, there is a great deal of effort that has been made on this problem, such as [3, 5, 6, 11, 13-15]. However, it seems to lack for providing a systematic approach in detail for the entire procedure of data preprocessing.

3. Methods

To assist data analysis of high-dimensional complex proteomic data, we developed a four-step procedure for data preprocessing. These four steps are baseline subtraction, normalization, peak detection/selection, and peak alignment. We will describe how to implement each step in this section. In particular, the MEP search used for peak detection and selection is introduced and explained in detail.

3.1 Baseline Subtraction

The baseline is an offset of the intensities in the y-value, which happens mainly at small x-value of m/z ratios, and baseline subtraction is used to eliminate the excess baseline for each sample. After the process of baseline subtraction, the resulting spectrum is hovering slightly above zero value of intensity and maintaining the peaks in their true intensities. The baseline adjustment method we applied is based on the approach of Wong [1] and used the percentage of spectra range as a parameter to define a window size. The sensitivity of baseline subtraction depends on the window size; a smaller window size which causes a higher sensitivity removes more baselines in the adjustment. The parameter setting for our procedure was 10% of spectral range.

3.2 Normalization

The purpose of intensity normalization is to identify and eliminate any systematic effects between mass spectra. The normalization approach we developed is very simple and can be calculated using the following three steps:

1. For a certain sample, compute its total intensities, or called total area under the curve (AUC):

$$total\ intensities = AUC = \Sigma_i\ intensity\ (x_i) \tag{1}$$

where the intensity (x_i) represents the intensity at the ith value of *m/z*.

2. For each x_i, evaluate the relative ratio between its original intensity and its AUC of the spectrum:

$$intensity\ percentage\ (x_i) = intensity\ (x_i) / AUC \tag{2}$$

Thus, the calculation is to find the percentage of the total intensities at x_i.

3. For each x_i in the spectrum, calculate its normalized intensity by the following equation:

$$\begin{aligned} &\textit{normalized intensity } (x_i) \\ &= \textit{intensity percentage}(x_i) * \textit{average AUC over all spectra} \end{aligned} \tag{3}$$

Thus, each spectrum has same value of AUC after the normalization.

3.3 MEP Search

As we have mentioned earlier, one of the changeling problem in the data preprocessing is noise appearing in the mass spectra. This particularly increases the difficulty for peak detection and selection. The noise data may produce spurious peaks and must be treated with care. To overcome this problem, the MEP search is developed in our procedure. The algorithm was originally used to find the direction of sound [16] and was performed by a moving N-point maximum envelope peak (MEP) search. The size of the sliding window, N, is a parameter used to smooth out the spurious peaks. The algorithm of MEP search is described as follows:

1. Start at some point, k, in the X-axis.
2. Search the next N-1 points in the window.
3. Compare the y-value of intensity corresponding to each of these N points and store the point with the local maximum intensity in the window. Note that a point corresponding to a maximum is stored only once.
4. Move to the next point and repeat step 1 through step 3 until all points have been visited.

To explain the method of MEP search, an illustrative example is given and shown in Fig.1, the MEP search is performed with N =4 in this case:

(1)Set the parameter of window size 4, and start at point 1.
(2)Perform a moving 4-point MEP search, find the point with the local maximal intensity during this window search and store the point and its corresponding intensity.
(3)Slide the window one point to the right and repeat (2) until all of 27 windows are examined (the last three windows are short of size 4.).

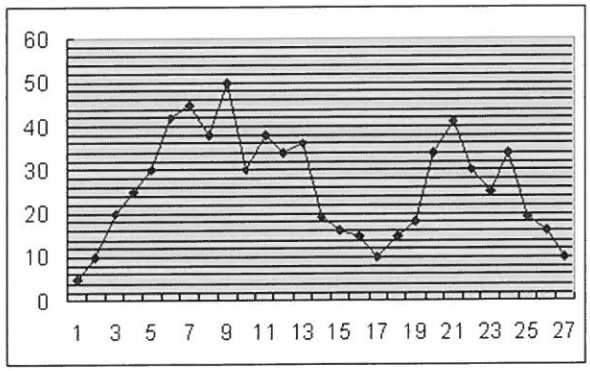

Fig. 1. An illustrative example for MEP search

A portion of the resulting *4*-point MEP search is shown in Table 1. Note that a point is corresponding to a local maximum in the several searches of consequent sliding windows, we only store the point and its intensity (not shown in the table) for the first time. For instance, point 7 is not stored again in the window starting at point 5.

Table 1. Applying *4*-point MEP in the illustrative example shown in Fig. 1

Start Point	Search Points				Maximum Point	Data Disposition
1	1	2	3	4	4	Store
2	2	3	4	5	5	Store
3	3	4	5	6	6	Store
4	4	5	6	7	7	Store
5	5	6	7	8	7	No store
…	…	…	…	…	…	…
12	12	13	14	15	13	Store
…	…	…	…	…	…	…
24	24	25	26	27	24	No store
25	25	26	27		25	Store
26	26	27			26	Store
27	27				27	Store

The step after the MEP search is to smooth out the mass spectrometry by using the linear interpolation. Thus, we only keep the original information at the point corresponding to a local maximum. For those points not stored during the process of MEP search, their intensities are interpolated using the left and right nearest neighbor points to estimate. The calculation is shown as follows.

$$intensity\ (x_i) = (intensity\ (x_R) - intensity\ (x_L)) / (x_R - x_L) + intensity\ (x_L) \quad (4)$$

where intensity (x_i) represents the intensity at x_i, and x_L and x_R are the left and right nearest neighbors of x_i. Fig. 2 shows the results after *4*-point MEP search with the linear interpolations of Eq. (4).

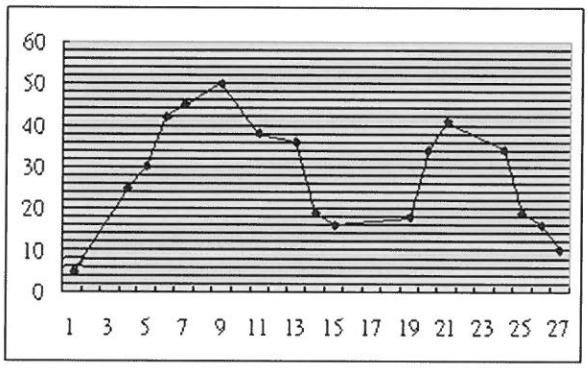

Fig. 2. The result after performing 4-point MEP search

The number of peaks detected by the MEP search is related to the parameter of the window size *N*, a larger value of *N* would reduce the number of obtained peaks and minimizes the detection of spurious peaks. However, this also increases the possibility to miss the detection of true peaks. Thus, the sensitivity of peak detection is depended on the window size and its value of setting is very important. In our implementation, we have chosen either a constant or an adaptive window size during the MEP search. The reason to consider an adaptive window size is based on the feature of the mass spectrometry, peaks on large m/z ratios are wide and peaks on small m/z ratios are narrow. Therefore, a larger window size should be applied on large m/z ratios, and a smaller window size would be suitable for small m/z ratios. Eq. (5) is the formula we used to determine an adaptive window size.

$$N(i) = (Nmax - Nmin) * i / dimensions + Nmin. \quad (5)$$

where $N(i)$ is the window size for the ith point along the X-axis, *Nmin* and *Nmax* are the window sizes for the starting and ending points of the sample, and dimension is the total points in the X-axis of the sample. In other words, the parameter of window size is determined by a pair of values for each spectrometry, *Nmin* and *Nmax*, one with the smallest window size in the spectrometry at the starting point and the other is the largest one at the ending point.

3.4 Peak Alignment

The step of peak alignment for proteomic data also plays an important role during the data preprocessing. There is always a difference in the samples due to machine drift that does not reflect any real sample variations, peak alignment is therefore required to detect and adjust these variations between samples. The procedure of our peak alignment is stated as follows:

1. For each class of patients, average their mass spectra as a reference spectrum.
2. Perform MEP search on each reference spectrum to generate a list of peaks as the common peaks for the related class.
3. Collect the peaks over all reference spectra to produce a set of the overall common peaks.
4. Align each sample with the overall common peaks using a sliding widow.

To provide a consistent approach for both training and testing processes in classifications, we do not use the individual reference spectrum of each class in the alignment, since we do not know the class labels in advance for testing samples. The sliding window size is defined as mass values $\pm$ r %, where r is mainly affected by the instrument resolution or calibration. For example, the variance for SELDI may be $\pm$0.1% - $\pm$0.2% [1, 5, 11].

The setting parameter of the window size must be handled with care. A larger window size would be reliable to contain all the peaks reflected to the same point of m/z ratio. However, it may also have the possibility to include spuriously associated peaks.

4. Experimental Results

The purpose of our study is to provide a data preprocessing procedure for proteomic data. To validate the effect of our approach, we utilized the four-step procedure to the prostate cancer data set to generate a low dimensional data set. We then applied the classification algorithm of decision tree to this new processed data set and evaluated its classification accuracies using 2-, 3-, and 4-way experiments.

The accuracies of six categories of binary classifications, and 3-, 4-way classifications with different parameter settings of window sizes in MEP search are shown in Table 2. The numbers listed on row 2 are the dimensions of the new generated data sets. As we have mentioned in section 3.3, the number of peaks (dimensions) detected by the MEP search is related to the window size of N, a larger value of N would generate fewer number of peaks generally. This also can be verified from the results of Table 2. The computational results were verified for 10 times by ten-fold cross validation. In each ten-fold cross-validation, the data is divided randomly into ten parts, each part is held out in turn and the learning scheme trained on the remaining nine-tenths, then its test accuracy rate is calculated in the holdout set. Thus the procedure is executed ten times on different training subsets. Finally, the ten accuracy estimates are averaged to yield an overall accuracy estimate. In our computational tests, all of the experiments were run 10 times of ten-fold cross-validation. As can be seen in Table 2, the classification accuracies were not much different among various parameter settings of window size. We therefore chose the generated data set with the lowest number of dimension 740 for the further experiment testing.

The chosen data set which we called an automatically processed data set was compared with the manually preprocessed data set from EVMS. We performed the classification algorithm of decision tree on both automatically and manually processed data sets to measure their performance. The computational results using 10 times of ten-fold cross validations were shown in Table 3. The results have shown that our method is comparable with the manual selection method. This indicated that our approach provides an advantage of fully automated for data preprocessing.

Table 2. Accuracies of 2-, 3-, 4- way experiments with different window sizes

% of m/z ratio (= window size *N*)	0.001	0.002	0.005	0.01	0.02	0.04
Dimensions after preprocess procedure	2574	2176	1749	1462	1082	740
NO vs. BPH	100%	100%	100%	100%	100%	100%
NO vs. CAB	84.5%	80.8%	82.0%	83.5%	83.3%	86.1%
NO vs. CCD	90.8%	90.8%	91.3%	91.3%	91.5%	90.0%
BPH vs. CAB	100%	100%	100%	100%	100%	100%
BPH vs. CCD	100%	100%	100%	100%	100%	100%
CAB vs. CCD	70.5%	75.0%	74.0%	70.8%	72.0%	70.5%
3-way (NO/BPH/PCA)	91.4%	91.9%	92.4%	92.6%	91.6%	90.8%
4-way (NO/BPH/CAB/CCD)	78.4%	80.4%	79.5%	78.8%	76.0%	76.1%

Table 3. The comparison of classification accuracies between the manually and automatically processed data sets; the manually preprocessed data set is provided from EVMS, spectra in the set were preprocessed with the manual peak selection and stored as vectors of dimension 779 ; our four-step procedure to the raw data set is defined as automatically processed data set

Classification	Manually processed data set (779 dimensions)	Automatically processed data set (740 dimensions)
NO vs. BPH	95.2%±4.2%	100%±0%
NO vs. CAB	93.0%±4.3%	86.1%±7.5%
NO vs. CCD	89.0%±5.6%	90.0%±5.1%
BPH vs. CAB	93.5%±4.9%	100%±0%
BPH vs. CCD	87.9%±5.8%	100%±0%
CAB vs. CCD	85.7%±7.1%	70.5%±8.2%
3-way (NO/BPH/PCA)	86.1%±4.8%	90.8%±3.3%
4-way (NO/BPH/CAB/CCD)	75.9%±4.7%	76.1%±5.0%

5. Conclusion

This study focuses on the development of a preprocess strategy to analyze a prostate cancer database generated by SELDI system. The major obstacle of cancer classification and discovering biomarker from proteomic data is the excessively high dimension and the disturbance by the noise. Therefore we have developed a four-step preprocessing approach and used it to analyze the prostate cancer database. The first step is baseline subtraction which subtracts the amount of intensity caused mostly by chemical noise from matrix molecules. The second step is intensity normalization which is essential to remove any sources of systematic variation between samples, such as varying amounts of protein or degradation over time in the sample, or even variation in the instrument detector sensitivity. The third step is peak detection for which we use an MEP search algorithm to identify and select peaks in each spectrum. The last step is peak alignment which corrects miss-aligned peaks across spectra. From the experimental results, the effectiveness of our proposed method has been proven. The results indicatecl that the problem of data noise could be handled efficiently and the number of dimension was able to be reduced dramatically without losing important features.

Besides the results shown in Section 4, we also performed some other numerical experiments in our study, such as an individual testing for every single step of the four-step procedure. According to the results we had, although the performance of baseline subtraction was not satisfactory in some certain cases, it seemed that the step was still required and indeed improved the results of the classifications in most cases. In the experiments of other three steps, the benefits from these processes were quite obvious.

Regarding the performance of the entire procedure of data preprocessing, the results shown in Section 4 were quite successful. In particular, the step of the MEP search for peak detection and selection was very crucial to data reduction. In our numerical results (not shown in this paper), we found that we could reduce the number of peaks down to 500 and the classification accuracies were still satisfied and comparable to the data set with 700 peaks. This result indicated that the MEP search seemed to be an appropriate approach for peak detection and selection.

Finally, the experimental results have also shown that the proposed approach is comparable with a manual data processing method. This indicates that our approach provides a systematic procedure for data preprocessing and has an advantage of fully automatic. This

also designates that the approach may have potential being used for other type of spectral data sets, such as gas chromatographic data.

References

1. Jason W. H. Wong, Gerard Cagney and Hugh M. Cartwright, "SpecAlign—Processing and Alignment of Mass Spectra Datasets" , Bioinformatics, Vol. 21 no. 9, 2088 – 2090, 2005.
2. H. Shin, M. Mutlu, John M. Koomen and Mia K. Markey, "Parametric Power Spectral Density Analysis of Noise from Instrumentation in MALDI TOF Mass Spectrometry" , Cancer Inform., 3, 317–328, 2007.
3. Anne C. Sauve and Terence P. Speed, "Normalization, Baseline Correction and Alignment of High-Throughput Mass Spectrometry Data" , Procedings Gensips 2004.
4. H. Shin, and M. Markey, "A Machine Learning Perspective on the Development of Clinical Decision Support Systems Utilizing Mass Spectra of Blood Samples" , J. Biomed. Inform., 39, 227–248, 2006.
5. Y. Yasui, D. McLerran, B. Adam, M. Winget, M. Thornquist, and Z. Feng, "An Automated Peak Identification/Calibration Procedure for High-Dimensional Protein Measures From Mass Spectrometers" , Journal of Biomedical and Biotechnology, 242-248, 2003.
6. Eric T. Fung and Cynthia Enderwick, "ProteinChip Clinical Proteomics: Computational Challenges and Solutions" , Biotechniques, Suppl:34-8, 40-1, 2002.
7. B. Adam, Y. Qu, J. Davis, M. Ward, M. Clements, L. Cazares, OJ. Semmes, P. Schellhammer, Y. Yasui, Z. Feng, and G. Wright Jr. "Serum Protein Fingerprinting Coupled with a Pattern-Matching Algorithm Distinguishes Prostate Cancer from Benign Prostate Hyperplasia and Healthy Men" , Cancer Research, 62:3609-3614, 2002.
8. R. Lilien, H. Farid, and B. Donald. "Probabilistic Disease Classification of Expression-Dependent Proteomic Data from Mass Spectrometry of Human Serum" , Journal of Computational Biology, 2003.

9. C. C. Huang, C. W. Huang, T. J. Chen, J. C. Yue, G. Hwang, Y. C. Chang, B. Adam. "Comparison of Classification Algorithms for Prostate Cancer Detection Using Mass Spectrometry Data". In Proceedings of 2005 International Conference on Intelligent Technologies and Applied Statistics, Taipei, Taiwan, June 2005.
10. Y. Qu, B. Adam, M. Thornquist, J. Potter, M. Thompson, Y. Yasui, J. Davis, P. Schelhammer, L. Cazares, M. Clements, G. Wright, Jr., and Z. Feng. "Data Reduction using a Discrete Wavelet Transform in Discriminant Analysis of Very High Dimensionality Data", Biometrics, 59, 143-151, 2003.
11. Y. Yasui, M. Pepe, M. Thompson, B. Adam, G. Wright, Jr., Y. Qu, J. Potter, M. Winget, M. Thornquist, and Z. Feng, "A Data-Analytic Strategy for Protien Biomarker Discovery: Profiling of High-Dimension Proteomic Data for Cancer Detection", Biostatics, 4, 449-463, 2003.
12. G. J. Hwang, C. Huang, T. Chen, J. C. Yue, Y. I. Chang, B. Adam, "Integrating Discrete Wavelet Transform and Neural Networks for Prostate Cancer Detection Using Proteomic Data", BIOINFO2005, Busan, Korea, 2005.
13. Andreas F. Ruckstuhl, Matthew P. Jacobson, Robert W. Field, James A. Dodd, "Baseline Subtraction Using Robust Local Regression Estimation", Journal of Quantitative Spectroscopy & Radiative Transfer, 68, 179 – 193, 2001.
14. B. Carrillo, R. E. Kearney, C. Yanofsky, K. Lekpor, A. Bell, D. Boismenu, "Surface Analysis of Peptide Mass Spectra to Improve Time and Mass Localization", Annual International Conference of the IEEE EMBS San Francisco, CA, USA. September 1-5, 2004.
15. Neal Jeffries, "Algorithms for Alignment of Mass Spectrometry Proteomic Data", Bioinformatics, Vol. 21 no. 14 2005, pages 3066–3073
16. Judd, M.D., "A Simple, Low-Computation Peak Detection Algorithm for the Angle-of-Arrival Spectrum for Signal Subspace Methods", IEEE, Vol 28, Issue 4, 1158 – 1163, Oct. 1992.

Received October 31,2011
Revised January 6,2012
Accepted March 27,2012

蛋白質體資料之前置處理

黃貞瑛、凌浩航

輔仁大學資訊工程系

蔡寶陵

喬治亞醫療保健大學外科醫學系

摘　要

近年來由於質譜相關技術的快速成長，使得蛋白質體學在生物醫學方面對於癌症之診斷、檢驗等逐漸受到重視。但是質譜資料在分類工作中，往往受到資料的高維度所困擾。另外，資料庫中存在的雜訊干擾，也是必須解決的問題之一。

本文因此針對質譜技術之“表面加強雷射脫附游離 – 飛行時間”所取得的攝護腺癌症蛋白質體資料庫做前置處理方面的研究，主要目的在於過濾雜訊以及降低維度，並且盡量避免資料失真。研究方法經過四個步驟的前置處理：去除基線、正規化、過濾雜訊挑選刻度、對齊刻度，各個步驟都是針對資料的特性所設計，並對資料產生過程中可能造成的誤差予以調整。而其中過濾雜訊並挑選刻度的步驟，使用的演算法為改進的最大包絡線搜尋法 (MEP Search)，其為一有效且低運算量的處理方式。本文並對所提出之前置處理資料，予以數值驗證，將處理後資料以分類演算法檢驗其資訊保存效果。在驗證結果中，證實本研究方法在有效降低維度的情況下，仍可保持良好的分類效果。總言之，本研究提供一系統化及自動化的前置處理方法，確實保存資料的重要資訊，並能有效的過濾訊號並降低維度。

關鍵字：質譜圖、蛋白質體學、去除基線、正規化、質譜峰偵測、質譜峰對齊。

多標籤子序列分群方法[1]

吳玉舒　徐嘉連[2]

輔仁大學 資訊工程學系

摘　要

序列分群的問題是基本的研究，然而大多演算僅可應用於單一標籤的序列上。我們提出一個演算法，可應用於多標籤序列和不等長序列。在我們的方法中，我們使用特徵擷取的技術將序列對應到特徵空間中，接著利用量化 (quantization) 的技術和直方圖的概念，將序列在特徵空間上的分佈情形以量化向量表示，最後將依據序列標籤的性質 (單一標籤 or 多標籤)，對量化向量作不同的分群方法。在單一標籤等長序列上利用 Rand index 驗證，準確度可達 88%，此外我們將量化的概念加入 Rand index 提出一個驗證方法，在多標籤不等長序列上準確度可達 84%。藉由 minimum bounding rectangle (MBR) 演算法的概念，可將原來的執行時間降為六分之一，而準確度仍達 84%。

關鍵詞：序列分群、多標籤、子序列。

第 1 章　前言

序列分群的研究在過去的幾年皆有不少的相關文獻，而在經濟學、醫學和音樂搜尋上也有許多應用，在音樂上面，將其音調對應到特徵空間中，再利用子序列分群去找出相似的音樂，下面的篇幅針對於背景和相關研究作簡單的介紹。

[1] 本論文，為輔仁大學（計畫編號：410031044042）與國科會（國科會計畫編號： NSC-100-2221-E-030-021）之補助研究。
[2] 論文通訊作者，電子郵件：alien@csie.fju.edu.tw

第 1 節 背景

序列分群主要分成兩個部分，一個為分群的演算法，其在過程中會漸漸的將相似的序列分在同一群，另一個為相似度的計算方式，其藉由計算序列間的距離去量化序列間相似程度，常見的距離公式有歐式距離和 dynamic time warping 距離等。

在序列相似的部分可分為全域相似和部分相似，全域相似是指整條序列間的相似，可能是整條序列的趨勢，而部分相似是指序列內片段子序列間的相似。Figure 1 為全域相似的範例，有 4 條 sequences $S^{(i)}$，將其 mapping 到特徵空間中可看出趨勢相似序列將會有群聚的現象，我們將其分成兩群，分別為 $C_1=\{S^{(1)},S^{(2)}\}$ 和 $C_2=\{S^{(3)},S^{(4)}\}$。而 Figure 2 為部分相似的例子，$S^{(1)}$) 的中間片段相似於 $S^{(2)}$) 中間片段，且 $S^{(1)}$) 的後面片段相似於 $S^{(3)}$) 後面片段，我們將其分群為 $C\_1=\{S^{(1)},S^{(2)}\}$ 和 $C\_2=\{S^{(1)},S^{(3)}\}$。

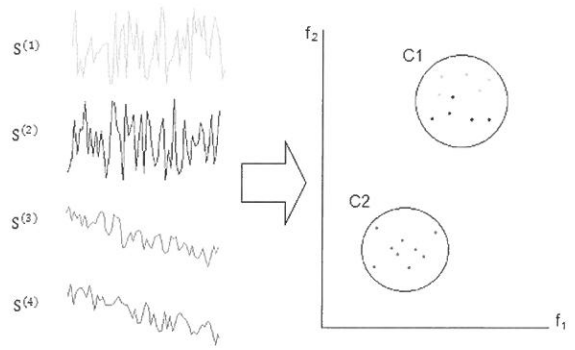

Figure 1 : 序列全域相似示意圖

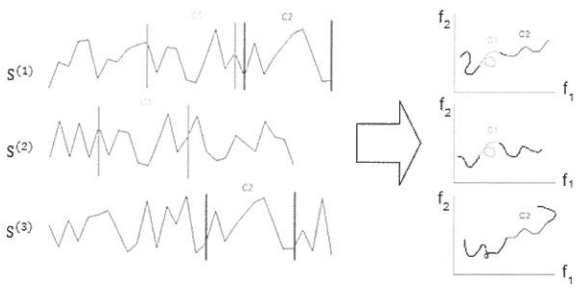

Figure 2 : 序列部分相似示意圖

在序列資料本身，有兩個重要的屬性，一個為序列的長度，另一個為標籤的性質，前者可分為長度一致的等長情況和長度不同的不等長情況，而後者可分為單一標籤和多標籤。單一標籤的序列僅屬於一個標籤，而多標籤的序列可能屬於一個標籤，也可能屬於多個標籤。

在序列分群的研究中，部分相似伴隨著多標籤，因為一條序列內的不同子序列，可能分別會跟不同序列的子序列相似，所以序列在部分相似的情況下為多標籤較合理，同樣的全域相似則為單一標籤。我們將序列分群依長度和相似情況分成四種情況如 Table 1，基於實際上的合理性，在我們的研究中只探討等長序列的全域相似和不等長序列的部分相似。部分相似並不需序列長度一致，因為其相似是以序列內的子序列為主，然而全域相似是序列的趨勢等，其相似以序列間的相似為主，故序列長度一致較為合理。

Table 1 : Four cases in sequence clustering.

	Equal - length	Variable - length
Whole similarity (single - label)	○	△
Partial similarity (multi - label)	△	○

第 2 節 相關研究

子序列分群方法是否有實質上的意義曾受到爭議，在 Keogh E 和 Lin J [1] 的研究中，提到子序列分群有個嚴重的問題，在做子序列分群的過程中，會先利用 sliding window 的方式將序列切割成子序列，所以如果序列本身是比較平滑的，或者改變較緩慢的，那麼此部分切出來的子序列就會非常相似，故在分群的過程中容易找到那些改變緩慢的子序列，但其並不是真正有意義之子序列。然而在 Chen JR [5] 的研究中，其認為 Keogh 對子序列分群有意義的定義在本質上有瑕疵，此外透過序列間的 temporal 和 formal 兩種形式的相似，可讓子序列分群變得有意義。

在序列分群的相關研究中如 Lai C-P [3]，提出了一個二階層的序列分群方法，其認為不論是全域分群或子序列分群皆有其優劣，故在其方法第一階層針對於全域分群，而第二階層則針對於子序列分群，其透過 Symbolic Aggregate ApproXimation (SAX) 方法將序列以符號的方式呈現作降維，利用一個密度基礎的分群方法 Cluster affinity search technique (CAST) 作第一階層分群，再利用第一階層的 N 群結果分別作 N 次

CAST 的第二階層分群，藉此滿足不同的需求。

而在過去的幾年中，從序列中找出重覆率高的序列片段 (找主題)，是持續受到關注的問題，在 Li Y 和 Lin J [4] 的研究中，提出了一個可找出任意長度主題的方法，將序列透過 SAX 轉換成符號，利用 sliding window 的技巧將符號切成片段符號，再利用文法基礎的推論方法 Sequitur 找出重覆率高的片段符號，在其實驗中，根據不同的資料集可找出長度不一致的主題。其方法優點在於可找出不等長的主題以及 linear-time 的高運算效率，但 SAX 轉換本質上還是有些限制，像是在轉換過程中會將序列的噪音平滑掉，此外有時會將不一樣的序列轉換成相同的字串符號。

在多標籤的相關研究中如 Lukashevich [2]，其作音樂的自動化類型分類系統，在其系統中藉由分割時間片段和特徵領域可將多標籤分類的問題轉換成多個單一標籤分類的問題，其將音樂分成多個片段音樂，分別擷取每個片段音樂的音色、節奏和旋律特徵，利用 Principal Component Analysis 降維，最後藉由 Gaussian Mixture Models 去作機器學習，在其實驗中，利用 F-measure 驗證方式，其音樂類型分類系統準確度可達 0.61。

第 2 章　問題

在此部分，我們先介紹子序列分群的相關定義，接著再對問題作描述。

Definition 1. *Sequence S*: 序列是一個有次序的實數集合，$S = < r_1, r_2, ..., r_m >$ 且 $|S|=m$。

Definition 2. *Subsequence* T: T 是 S 的子序列，$T=< t_1, t_2, ..., t_w >$ 且 $|T|= w$，其中 $t_i = r_{i+k}$，$0 \le k \le m - w$。

Definition 3. *Distance*: 給定兩個長度相同且長度為 n 的序列，第 i 個序列 $S^{(i)}$ 與第 k 個序列 $S^{(k)}$ 的距離定義如公式 (1):

$$dist(S^{(i)}, S^{(k)}) = \left(\sum_{j=1}^{n} (r^{(i)}_j - r^{(k)}_j)^2 \right)^{1/2} \tag{1}$$

在本研究中，我們要處理序列分群的問題，在單一標籤和等長序列的情況中，給定 n 個序列和一個分群個數 K，我們將 n 個序列分成 K 群，使得每群之中序列間的 intra-distance 最小，而群與群間序列的 inter-distance 最大。在多標籤和不等長序列的情況中，給定 n 個序列和 M 個標籤，我們將給予每個序列至少一個標籤，最多 M 個標籤。

第 3 章　方法

我們的架構圖參考 Figure 3，包括特徵擷取模組 (feature extraction module)、量化模組 (quantization module) 和分群模組 (clustering)。在特徵擷取模組中，將每一個序列 $S^{(i)}$ 經由 sliding window 將序列切成多個子序列，並將分別對每個子序列利用 discrete cosine transform (DCT) mapping 將子序列對應到特徵空間中的特徵向量，接著可用 MBR 方法將相近的特徵向量以方框形式呈現。在量化模組中，將特徵向量或方框 MBRs 作量化，量化後將會以一個類似直方圖的向量 $H^{(i)}$ 表示。而在分群模組中，依照標籤的性質 (單一標籤 or 多標籤) 分成兩個部分，在 Single-label (whole similarity) 的部分利用 Hierarchical clustering 的 Single-linkage 將 $H^{(i)}$ 作分群，而在 Multi-label (partial similarity) 的部分則藉由門檻值當作對 $H^{(i)}$ 作分群的依據。第一節到第三節描述 feature extraction 模組內的三個主要程序，而第四節描述 quantization 模組，而第五節則描述分群模組，最後一節介紹驗證的方法。

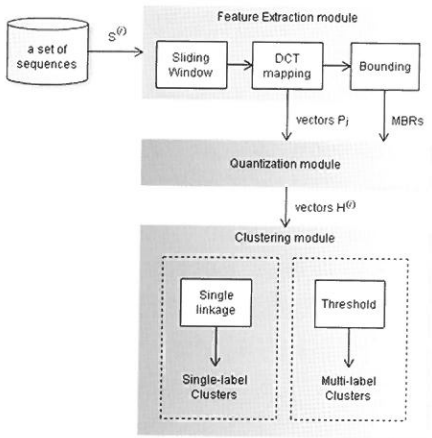

Figure 3：系統架構圖

第 1 節 sliding window

儘管序列長度並不一致，利用 sliding window 可將任意長度之序列切割成多個固定長度子序列，藉此得到序列局部訊息。若任意序列長度為 m，視窗大小為 w，位移長度為 x，則可切成 y 個長度為 w 之子序列，其中 $y = \lceil \frac{m-w}{x} \rceil + 1, m \geq w$，$y$ 會隨著不同 S 的長度而改變，x 是 sliding offset，由參數序列之重覆率 (overlap) 決定。舉例來說，Figure 4 為 w =19, m =22, x =1 之 sliding window 概念圖，在我們的研究中，x 皆為 1。

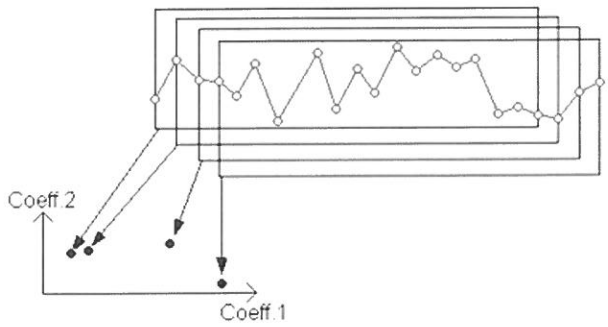

Figure 4 : Sliding window 概念圖 [6].

第 2 節 DCT mapping

經過 sliding window 程序，會得到很多的子序列，若直接對子序列做運算，當資料量較大時，會花費大量時間。利用 Faloutsos 提到的 Discrete Cosine Transform (DCT) [7] 將各個子序列對應到特徵空間中作運算可減少計算時間，在特徵空間中每個子序列為一個特徵向量 P_j。

Definition 4. *feature vector of subsequence* P: P 是子序列 T 經過 DCT mapping 後的特徵向量，而 P_j 為序列經由 sliding window 後，第 j 個子序列 mapping 後的向量。

一般來說，非隨機的序列對應到 DCT 空間中的向量，其前面維度的數值通常較高，意即前幾維佔了高比例的總平均能量，也就是說此向量的數值由第一維至最後一維有逐漸變小的趨勢，此特性稱為 Energy Concentration，利用此特性將趨近於零的後面維度當成零作計算，即可達到減少計算量提升效率的效果。此外相似的兩個序列經過 DCT 轉換到特徵空間中的兩個點，此兩點也會相近，參考 Figure 5。任兩序列 $S^{(1)}$, $S^{(2)}$ 之距離 $d_1 = \text{dist}(S^{(1)}, S^{(2)})$，而序列 $S^{(1)}$, $S^{(2)}$ 經由 DCT mapping 後分別為 $P^{(1)}$ 和 $P^{(2)}$，其距離 $d_2 = \text{dist}(P^{(1)}, P^{(2)})$，根據 Faloutsos C 定義的 lower-bounding lemma [7]，$d_1 \geq d_2$。

子序列在 DCT mapping 之後需要決定欲取的 DCT 係數，當 window length 固定為 w 時，若取的 DCT 係數為 c（$c \leq w$），代表的是保留前 c 維的 DCT 係數，而第 $c+1$ 維到第 w 維的係數以 0 取代。故在 w 固定的情況下，c 越大則失真越小，而在 c 固定的情況下，w 越大則失真越大。

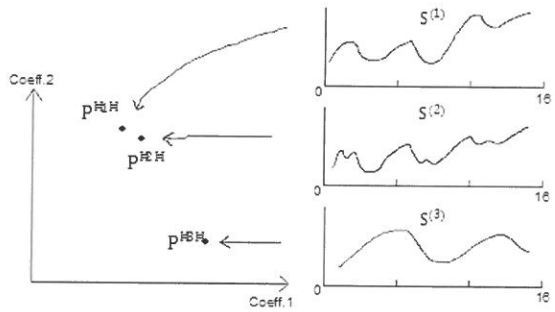

Figure 5 : DCT mapping.

第 3 節 MBR

當序列轉換到特徵空間後，分群演算法所耗的時間將隨著特徵向量的多寡所影響，利用 Hsu JL 和 Yang HX 提出的 minimum bounding rectangle，簡稱 MBR [6]，此方法概念主要是將相近的特徵點以方框的方式去表示，在適當的參數設定下，準確度下降 4%，但執行時間約減少為原來的六分之一，詳細的實驗請參考第四章第三節。

Definition 5. *MBR*: 在 n 維歐式空間中，一個 MBR M 由兩個端點表示，分別為 L (low point) and H (high point) [13]: M = (L,H), where L = ($l_1,l_2,...,l_n$), H =($h_1,h_2,\cdots,h_n$), $l_i \le h_i$ for $1 \le i \le n$。如 Figure 6。

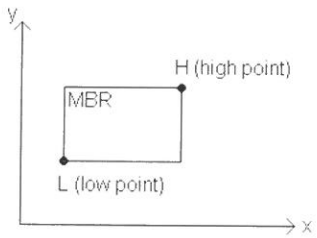

Figure 6 : A MBR [6].

對於每條序列，我們利用 MBR 演算法將 y 個 P_j 轉換成 r 個 M，r 恆小於 y，在此演算法中有四個參數，分別為起始距離 (*sd*)、結束距離 (*ed*)、low distance (*ld*) 和增加值 (*IR*) 參數，首先利用定義四的距離公式計算序列中相鄰且未被框起來的特徵向量間，開始時可計算出集合大小為 y-1 的距離集合 D，其中 *sd* 為 D 集合中的最小值，*ed* 為 D 集合中的最大值，*ld* 起始值為 -1，*ld* 和 *sd* 是判斷是否框起來的依據，而 *IR* 為每回合 *sd* 所增加的數值，當 $ld < d_j \le sd$，即將其框成一個方框 M 表示，作完一個回合後將 *ld*

的值改為 *sd*，而 *sd* 的值加上 *IR*，而 *ed* 不改變，持續相同的步驟直到 $sd \leq ed$。

以 Figure 7 為例，S = { P_1, P_2,..., P_{12} }，P_1 和 P_2 的距離為 1，分別計算相鄰 P_j 可得到 D = { d_1, d_2,...,d_{11}} = {1,1,2,1,1,1,2.236,1,2,1.732,1.414}，*sd* 為 1，*ld* 為 -1，而 *ed*。為 2.2236，在第一個回合中，因為 d_1 比 -1 大且小於等於 *sd*，所以 P_1 和 P_2 會被框在一起，形成一個方框 M_1={ P_1, P_2 }，d_2 比 -1 大且小於等於 *sd*，所以 P_3 會加入 M_1，且 M_1={ P_1, P_2, P_3 }，但 d_3 比 *sd* 還大，所以 P_4 並不會加入 M_1，同理 M_2={ P_4, P_5,P_6,P_7 }，M_3={ P_8,P_9}，此時第一回合結束，在下次的回合中重新計算未被框起來的 P_j 得到 D_1，而 *sd* 和 *ed* 僅與 D 有關而不受 D_n 所影響，當 P_j 與前後兩方框的距離皆在 *ld* 和 *sd* 之內時，則將 P_j 框在與前後 P 較短距離的方框內，最後完成的圖如 Figure 8。

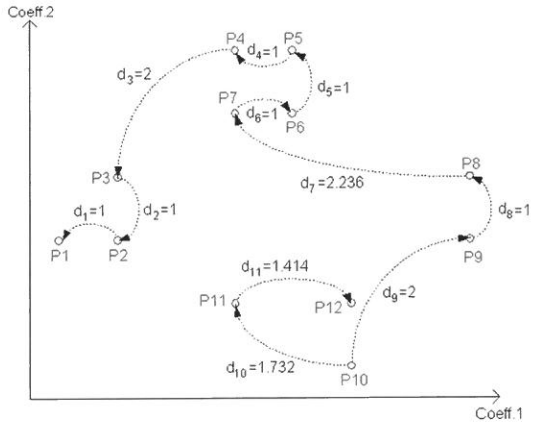

Figure 7 : Subsequences of a sequence in 2-dimensional feature space [6].

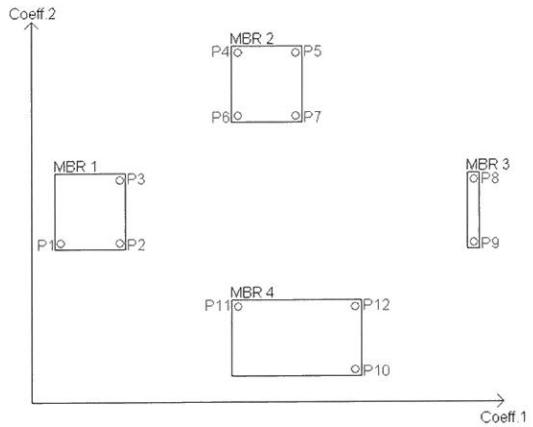

Figure 8 : MBRs of a sequence in 2-dimensional feature space [6].

在 MBR 演算法中的參數值 *IR*，其影響 M 的數量，當 *IR* 較小時，P 必須非常靠近才會被框在一起，而當此參數越大時則反之，所以當一樣多 P 的序列利用 MBR 去表示時，*IR* 越小 M 越多，*IR* 越大 M 越少，如 Figure 9 中的 *IR* 值 : (a) 0.2 (b) 0.5 (c) 0.8 (d) 1。此方法可有效減少計算量，降低執行時間。

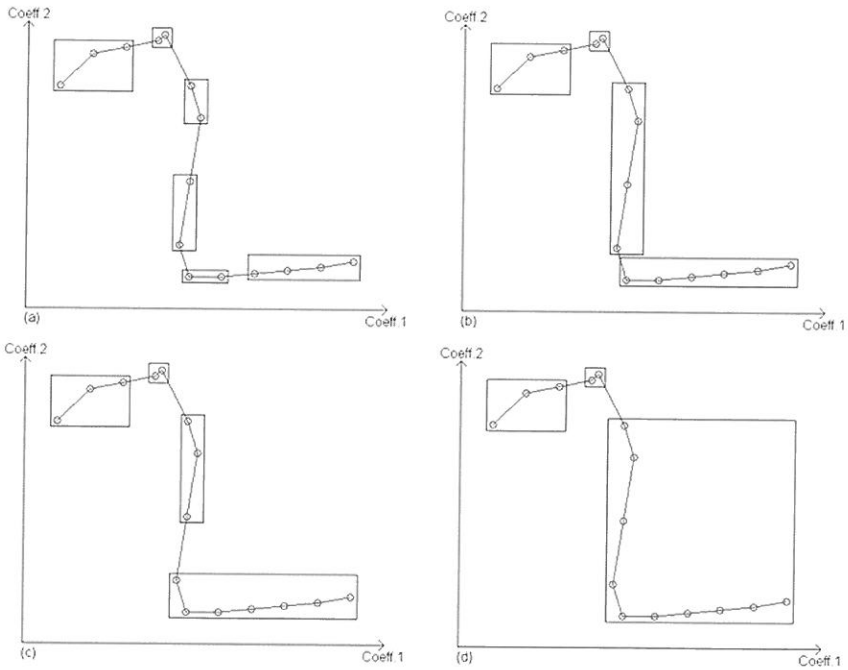

Figure 9 : The effect of threshold *IR* : (a) *IR* = 0.2 (b) *IR* = 0.5 (c) *IR* = 0.8 (d) *IR* = 1 [6].

第 4 節 quantization

序列切成子序列在特徵空間以多個特徵向量表示，雖然間隔的子序列會因為 sliding window 時 overlapping 的關係而顯得靠近，但序列的第一個和最後一個子序列向量通常會有段距離，也就是一條序列在特徵空間中的特徵向量並不會完全集中在單一區域，因此利用 *K*-means 將子序列作量化，再利用 histogram 的方式去表達序列，可減少計算量，並且有效獲得序列的特性。

對於 P_j 而言，我們將所有序列的子序列向量 $P_j^{(i)}$ 當作 *K*-means 的輸入的資料，用向量 P_j 取代點，利用歐式距離計算相似度，藉由 *K*-means 找出 *K* 個代表的 mean 向量，因此每個 $P_j^{(i)}$ 會有一個最靠近的 mean 向量，接著利用 mean 向量去表達該序列的子序列，可將序列轉成 $Y^{(i)}$ 的形式，最後再統計 $Y^{(i)}$ 中不同 mean 向量的個數，藉此得到該

序列 P_j 大致的分佈情況，並以 $H^{(i)}$ 表示。

以 Figure 10 來說明，其為二維 DCT 空間的例子，序列 $S^{(1)}$ 的特徵向量分別為 $P_1^{(1)}, P_2^{(1)}, ..., P_9^{(1)}$，利用 *K*-means (*K*=3) 將 *n* 條序列所有的 P 找出三個 mean 向量，其中 $P_1^{(1)}$ 最靠近第一個 mean 向量 C1，所以 $\{P_1^{(1)}, P_2^{(1)}, ..., P_9^{(1)}\}$ 將會轉成 $Y^{(1)}$ = [C1,C1,C1,C3,C3,C3,C2,C2,C1]，接著再藉由類似直方圖的轉換將 $Y^{(1)}$ 轉為三維向量 $H^{(1)}$，其有 4 個 P 最靠近 C1，2 個 P 最靠近 C2，3 個 P 最靠近 C3，所以 $H^{(1)}$ = [4,2,3]。

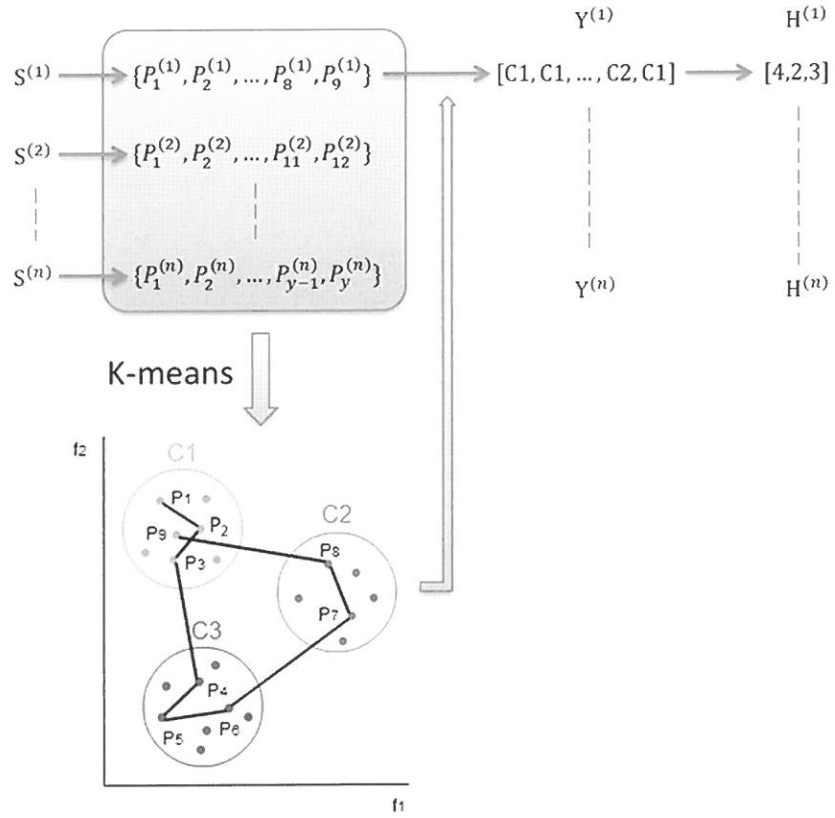

Figure 10 : Illustration of quantization module.

而對於MBR而言，在*K*-means找代表向量的過程中，我們將求出方框的代表向量，再利用全部的方框代表點去求出 *K* 個 mean 向量，在計算方框與 mean 向量的距離時，我們並不是直接利用方框代表向量與 mean 向量去作距離計算，而是利用方框端點與 mean 向量作精確的距離計算。

分別對每個維度去作算，而在每個維度中分成三種情況，若 mean 向量該維度數值在方框左右邊界之間，則該維度的距離為零，若 mean 向量該維度數值比左右邊界大，距離為右邊界與 mean 向量該維度的數值的差值，而 mean 向量該維度數值比左右邊界小，則距離為左邊界與 mean 向量該維度數值的差值，最後將每個維度距離平方相加再開根號，即為方框端點與 mean 向量距離計算的方式。

而在計算方框的代表向量過程中，我們並不是僅的利用兩端點的向量去求平均，而是根據該方框內所有子序列向量去求平均，將權重的概念加入，以減少 P 簡化成 M 的誤差。

第 5 節 Clustering

不論是特徵向量或者 MBRs，再經過量化後，每個序列皆以一個量化向量表式。在 multi-label 的情況中，我們藉由 threshold 參數，當作給予序列標籤的依據。以 Figure 10 為例，其 $H^{(1)}$=[4,2,3]，若 threshold 參數設為 4，在 $H^{(1)}$ 裡面只有第一維的數值大於等於 4，所以系統會給予 $S^{(1)}$ 一個第一維標籤，若 threshold 參數設為 3，則會給予 $S^{(1)}$ 第一維標籤和第三維標籤，依序將所有序列都設完暫時的標籤後，再將相同標籤的序列分到同群。

在 single-label 的情況中，我們藉由 hierarchical clustering 方法作分群，其為一種階層式的方群方式，可分為聚合 (agglomerative) 或分割 (divisive) 兩類，我們的方法使用 hierarchical agglomerative clustering，透過計算序列或二個以上的序列構成的群集間的距離，將最短距離的序列或群集逐漸合併，最後會建出一個樹狀結構的 dendrogram，而常見的 linkage method 有 single linkage、complete linkage 和 average linkage，而在我們的系統中使用 single linkage。我們也可以透過 $H^{(i)}$ 中最大值的索引當作給予序列標籤依據，然而在我們的方法中是採用 hierarchical agglomerative clustering 作更進階的分群。若使用最大值的索引方法，以 Figure 10 的例子來說明，$H^{(1)}$ 的最大值為 4，其索引為 1，所有最大值在索引為 1 的序列將會分在同一群。

第 6 節 驗證方式（validity）

此部分分成 Single-label 和 Multi-label 討論。Single-label 利用 Rand index 的認證方式，透過此方法可得到一個界於 0~1 的數值簡稱 R，而 Multi-label 採用新的驗證方式，其類似於 Rand index，但加入量化的概念，利用此方式可得到一個 R_multi 的數值，R 和 R_multi 皆代表著分群的品質。Rand index 僅適用於資料為單一標籤的序列，而新的驗證方式不論在單一標籤序列或者多標籤序列皆適用，此外若應用於單一標籤上，其數值會等同於 Rand index。驗證的方法主要是將分群的結果轉換成關聯矩陣，再去比較關聯矩陣的差異度來得知分群的好壞。

第 1 項 Single-label

Rand index 先將 n 條序列建出一個 n x n 的關聯矩陣 M，關聯矩陣內的值 $M_{i,j}$ 會根據第 i, j 筆資料的分群標籤所決定，若兩序列的分群標籤相同，則代表兩表續列為同一群，$M_{i,j}$ 的值為 1，反之則為 0。故在計算分群品質時對兩個 M 作運算，一個為實際關聯矩陣 Mact （actual class matrix），一個為預測關聯矩陣 *Mpre*（predicted cluster matrix），其算式如公式 (2)，R 的值介於 0 到 1 之間，越接近 0 代表分群的效果越差，反之越接近 1 則代表分群效果越佳。

$$\mathrm{R} = \frac{(A+B)}{(A+B+C+D)} \tag{2}$$

$$Msta_{i,j}(Mact_{i,j}\ ,\ Mpre_{i,j}) = ss\ ,\ \text{if}\ Mact_{i,j} = Mpre_{i,j} = 1$$

$$Msta_{i,j}(Mact_{i,j}\ ,\ Mpre_{i,j}) = sd\ ,\ \text{if}\ Mact_{i,j} = 1\ and\ Mpre_{i,j} = 0$$

$$Msta_{i,j}(Mact_{i,j}\ ,\ Mpre_{i,j}) = sd\ ,\ \text{if}\ Mact_{i,j} = 0\ and\ Mpre_{i,j} = 1$$

$$Msta_{i,j}(Mact_{i,j}\ ,\ Mpre_{i,j}) = dd\ ,\ \text{if}\ Mact_{i,j} = Mpre_{i,j} = 0$$

藉由一個統計矩陣 *Msta* (*Mact,Mpre*) 來運算，A 是 $Mact_{i,j}$ 和 $Mpre_{i,j}$ 皆為 1 的個數，B 是 $Mact_{i,j}$ 為 1 而 $Mpre_{i,j}$ 為 0 的個數，C 是 $Mact_{i,j}$ 為 0 而 $Mpre_{i,j}$ 為 1 的個數，而 D 則是 $Mact_{i,j}$ 和 $Mpre_{i,j}$ 皆為 0 的個數，在計算兩關聯矩陣之分群品質時，若直接對統計矩陣 *Msta* 作個數計算，同樣的 pair 會被運算到兩次，所以只運算其上三角矩陣。

Example:

假設有五條序列 $S^{(1)}, S^{(2)},..., S^{(5)}$ 分成兩群，分別 $C_1 = \{S^{(1)}, S^{(4)}\}$，$C_2 = \{S^{(2)}, S^{(3)}, S^{(5)}\}$，Mact 如 Table 2，預測的分群情況為 $C_1 = \{S^{(1)}, S^{(4)}, S^{(5)}\}$，$C_2 = \{S^{(2)}, S^{(3)}\}$，*Mpre* 如 Table 3。

Table 2 : Mact for single-label case.

$S^{(i)}$	$S^{(1)}$	$S^{(2)}$	$S^{(3)}$	$S^{(4)}$	$S^{(5)}$
$S^{(1)}$		0	0	1	0
$S^{(2)}$			1	0	1
$S^{(3)}$				0	1
$S^{(4)}$					0
$S^{(5)}$					

Table 3 : Mpre for single-label case.

$S^{(i)}$	$S^{(1)}$	$S^{(2)}$	$S^{(3)}$	$S^{(4)}$	$S^{(5)}$
$S^{(1)}$		0	0	1	1
$S^{(2)}$			1	0	0
$S^{(3)}$				0	0
$S^{(4)}$					1
$S^{(5)}$					

Table 4 : Msta for single-label case.

$S^{(i)}$	$S^{(1)}$	$S^{(2)}$	$S^{(3)}$	$S^{(4)}$	$S^{(5)}$
$S^{(1)}$		*dd*	*dd*	*ss*	*ds*
$S^{(2)}$			*ss*	*dd*	*sd*
$S^{(3)}$				*dd*	*sd*
$S^{(4)}$					*ds*
$S^{(5)}$					

$Msta_{1,4} = Msta_{2,3} = ss$

$Msta_{2,5} = Msta_{3,5} = sd$

$Msta_{1,5} = Msta_{4,5} = ds$

$Msta_{1,2} = Msta_{1,3} = Msta_{2,4} = Msta_{3,4} = dd$

$a = 2, b = 2, c = 2, d = 4$

$$\mathrm{R} = \frac{(2+4)}{(2+2+2+4)} = 0.6$$

第 2 項 Multi-label

此驗證方法精神如同 Single-label 的關聯矩陣差異度，差別在於序列的標籤不再僅有一個，加入量化的概念，讓驗證的方式更加完善。在 Single-label 的關聯矩陣中，$M_{i,j}$ 的值非一則零，而在 Multi-label 中，$M_{i,j}$ 的值則為分數，分子為第 *i* 筆和第 *j* 筆資料被分在同一群的集合個數，而分母為第 *i* 筆或第 *j* 筆資料出現的集合個數。

藉由統計矩陣 Msta 來計算分群品質 (R_multi)，其陣列內的值為一個四維向量，依序代表 *ss,sd,ds,dd* 的比例，其 $a + b + c + d = 1$。

$$\mathrm{R\_multi} = \frac{(A+B)}{(A+B+C+D)}$$

$$V = [A\ B\ C\ D] = \sum_{i=1}^{n-1} \sum_{j=i+1}^{n} v_{ij}, v_{ij} = [a\ b\ c\ d]$$

$$a = Mact_{i,j} * Mpre_{i,j}$$

$$c = (1 - Mact_{i,j}) * Mpre_{i,j}$$

$$d = (1 - Mact_{i,j}) * (1 - Mpre_{i,j})$$

Example:

假設有五條序列 $S^{(1)}$, $S^{(2)}$,..., $S^{(5)}$ 分成三群，分別 $C_1 = \{S^{(1)}, S^{(4)}\}$，$C_2 = \{S^{(2)}, S^{(4)}, S^{(5)}\}$， $C_3 = \{S^{(3)}, S^{(5)}\}$，Mact 如 Table 4。預測的分群情況為 $C_1 = \{S^{(1)}, S^{(4)}, S^{(5)}\}$， $C_2 = \{S^{(2)}, S^{(5)}\}$， $C_3 = \{S^{(3)}, S^{(4)}, S^{(5)}\}$，其 *Mpre* 如 Table 5，而 *Msta* 如 Table 6。

Table 4 : Mact for multi-label case.

$S^{(i)}$	$S^{(1)}$	$S^{(2)}$	$S^{(3)}$	$S^{(4)}$	$S^{(5)}$
$S^{(1)}$		0	0	1/2	0
$S^{(2)}$			0	1/2	1/2
$S^{(3)}$				0	1/2
$S^{(4)}$					1/3
$S^{(5)}$					

Table 5 : Mpre for multi-label case.

$S^{(i)}$	$S^{(1)}$	$S^{(2)}$	$S^{(3)}$	$S^{(4)}$	$S^{(5)}$
$S^{(1)}$		0	0	1/2	1/3
$S^{(2)}$			0	0	1/3
$S^{(3)}$				1/2	1/3
$S^{(4)}$					2/3
$S^{(5)}$					

Table 6 : Msta for multi-label case.

$S^{(i)}$	$S^{(1)}$	$S^{(2)}$	$S^{(3)}$	$S^{(4)}$	$S^{(5)}$
$S^{(1)}$		*dd*	*dd*	*ss*	*ds*
$S^{(2)}$			*ss*	*dd*	*sd*
$S^{(3)}$				*dd*	*sd*
$S^{(4)}$					*ds*
$S^{(5)}$					

$A = (0+0+1/4+0)+(0+0+1/6)+(0+1/6)+2/9 = 0.8$

$B = (0+0+1/4+0)+(0+1/2+1/3)+(0+1/3)+1/9 = 1.53$

$C = (0+0+1/4+1/3)+(0+0+1/6)+(1/2+1/6)+4/9 = 1.86$

$$D = (1+1+1/4+2/3)+(1+1/2+1/3)+(1/2+1/3)+2/9=5.81$$

$$\text{R\_multi} = \frac{(0.69 + 5.81)}{(0.69 + 1.64 + 1.86 + 5.81)} = 0.661$$

第 4 章　實驗

我們分成三個小節，第一節介紹實驗資料集，接來的小節討論參數設定，最後的小節則討論我們方法的實驗結果。

第 1 節 Data set

我們使用 Keogh E et. al. 所整理的 synthetic control chart time series data set [9] 當作單一標籤實驗的資料集，此資料集共有 6 類不同趨勢的序列，每類有 100 筆，包含 normal、cyclic、increasing trend、decreasing trend、upward shift 和 downward shift (Figure 11)，每筆序列長度皆為 60。

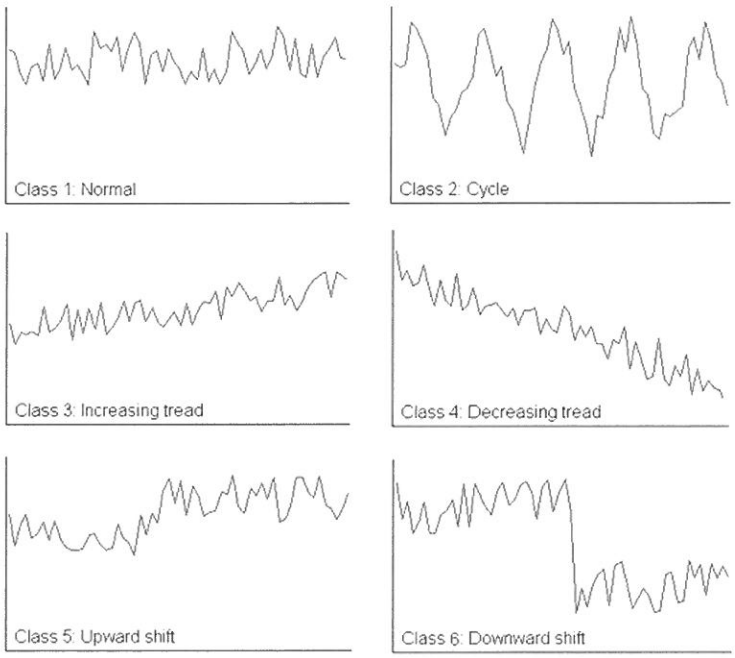

Figure 11 : Six classes of synthetic control dataset [9].

第 1 項 Locality

在我們的方法中，序列 $S^{(i)}$ 的特徵向量經由量化後，再藉由 histogram 以 $H^{(i)}$ 表示，由於 $H^{(i)}$ 只將序列在特徵空間中的分佈比例保留下來，並沒有儲存序列順序的相關訊息，所以藉由以下實驗展現其對 locality 破壞並無太大影響。

首先，我們先以一組序列為例，Figure 12 (K-means quantization，K=18) 為各類別序列經由 K-means 量化的表示圖，大致上 cyclic 和 normal 類以外的子序列，皆呈現出明顯的 locality，而 cyclic 類由於序列本身變化較大且頻繁，所以其 locality 稍微不明顯。

我們藉由公式 (4) 檢視序列的 locality，y 為該序列經 sliding window 所切成的子序列個數，而 Z 為 Y 中與後一個相同的的個數，也就是 P_j 與 P_{j+1} 最靠近的代表向量相同之個數，如果 $S^{(i)}$ 的特徵向量分佈只靠近特徵空間中的某代表向量，其 Z 值為 1，此條序列 L 即為 1，相反的若在特徵空間中其分佈非常散亂，其 Z 值就會高，而 L 則會趨近於 0。

Table 7 為序列的 Locality 詳細數值，第 2 到 7 欄為各類別序列的 Locality 平均值，第 8 欄為全部序列的 Locality 平均值，而最後一欄是 10 條隨機產生序列 Locality 平均值。

$$L = \frac{\sum_{f=1}^{y-1} Z_f}{y-1} \tag{4}$$

$$Z_f = \begin{cases} 1, \text{if } Y_i[f] = Y_i[f+1] \\ 0, \text{if } Y_i[f] \neq Y_i[f+1] \end{cases}$$

Table 7 : Locality value of different classes.

	Normal	Cyclic	Increasing trend	Decreasing trend	Upward shift	Downward shift	Average	Random
L	0.5617	0.6046	0.8163	0.8832	0.82	0.831	0.7528	0.5439

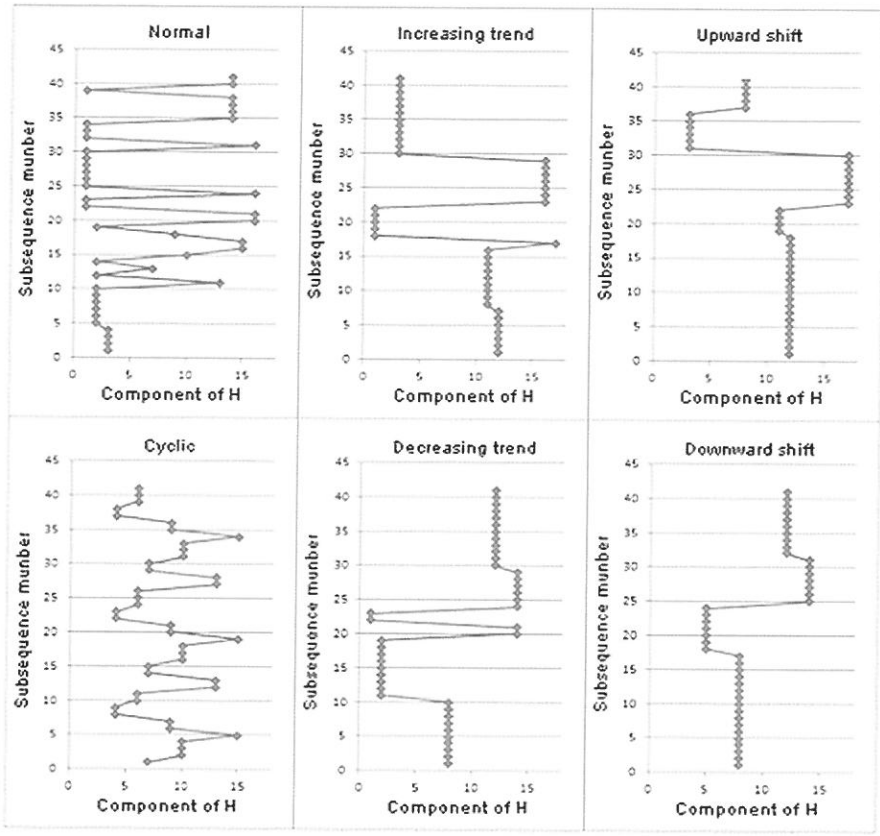

Figure 12 : Locality

第 2 項 Multi-label data generate

我們利用 synthetic control 的資料去生成多標籤序列，從 600 條序列中隨機取出 1~3 條序列利用頭尾相接的方式合成，序列 $S^{(i)}= r_1^{(i)}, \ r_2^{(i)},..., r_{60}^{(i)}$ 和 $S^{(k)} = r_1^{(k)}, r_2^{(k)},..., r_{60}^{(k)}$，兩個序列可合成為一個多標籤序列 $D = r_1^{(i)}, r_2^{(i)},..., r_{60}^{(i)}, r_1^{(k)}, r_2^{(k)},..., r_{60}^{(k)}$，所以生成出來的多標籤序列標籤種類為 1~3 種，而其長度為 60、120 或 180。

第 2 節 Factor

	default
Window length (w)	20
DCT coeff (d)	8
Quantization (k)	18

第 1 項 Window length (w)

我們想要觀察序列經過滑動視窗和 DCT mapping 後，取固定的 DCT 係數再將其反轉換和原序列的差異程度，藉此決定 window length 參數。我們僅取前 5 維的 DCT 係數，並利用 5 到 30 不同的 window length 觀察其轉換所需時間和經過轉換後失真的距離差距，如 Figure 13 為 6 類 100 條序列的實驗結果取平均。在時間上面，當 window length 越長，雖然有擺盪的情況出現，但可看出來有變短的趨勢。而在距離差距上，可以看出在 window length 較短時（5~10），其長度增加距離差距明顯上升，而在 window length 較長時（25~30），其長度增加距離差距僅緩緩上升。

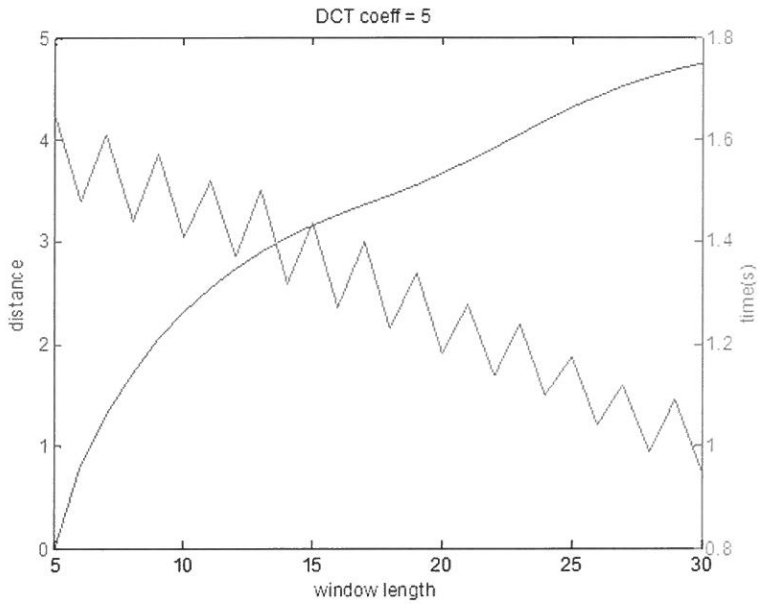

Figure 13 : 600 條序列轉換失真圖

然而我們可以簡單藉由時間和失真的交點去決定參數，但實際上當 y 軸的時間或距離變長變短時交點會跟著改變，利用正規化的方式可以將此問題解決，而下圖為 6 類各 100 條序列平均的距離差距，從 Figure 14 中可發現正常類序列距離差距明顯高於其他類序列，而週期類序列 window length 在小於 19 前，序列的距離差距是最小，但當 window length 大於 20 後，距離差距大幅上升，所以最後我們將 window length 係數取 20。

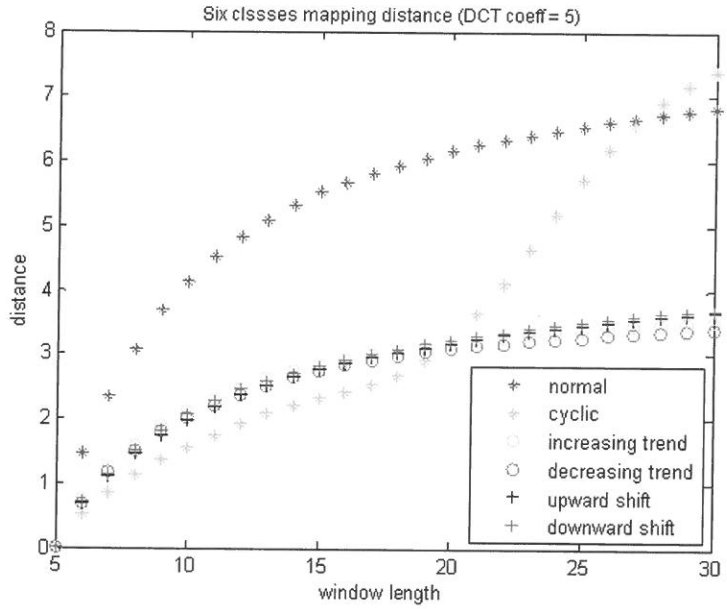

Figure 14 : 6 類序列 100 條平均轉換失真圖

第 2 項 DCT 係數 (*d*)

此外可以固定序列的 Energy Concentration 去找尋距離差距較少所對應的參數值，Energy Concentration 固定後 DCT 係數會隨著 window length 的長度而改變，當 window length 增加時距離差距漸漸增加，而其增加到某值時，距離差距會驟減，是因為 DCT 係數增加的關係，如 Figure 15 為 600 條序列 Energy Concentration 平均為 0.75 的例子，在距離差距上可看出其為鋸齒狀，可從圖中看出距離差距的低點在 window length 為 9、12、14、17 和 20 等，由於固定 Energy Concentration 的關係 window length 為 9 到 11 時的 DCT 係數一致為 4，而 window length 12 到 13 時比 9 到 11 時多一維 DCT 係數，此為其鋸齒狀的主因。而在時間上面，當 window length 越高，在 sliding window 的過程中切出來的子序列數量較少，所以時間有減少的趨勢。

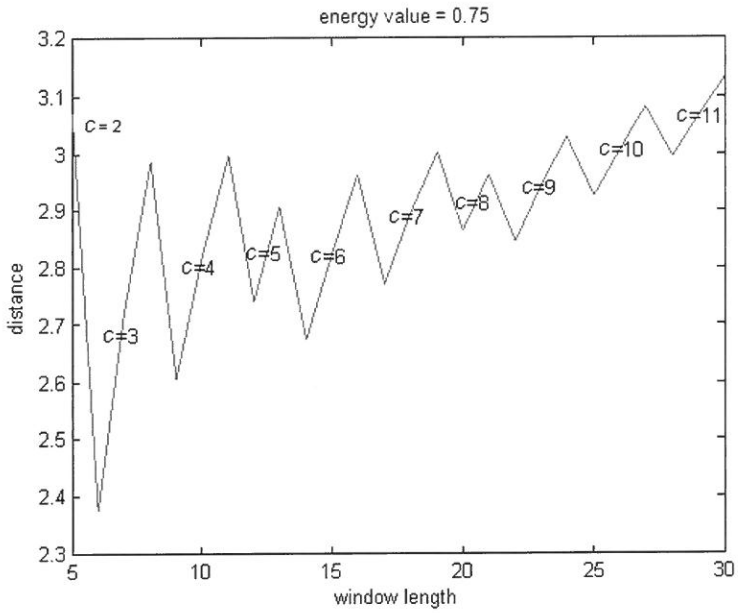

Figure 15 : 距離差距與視窗長度變化

第 3 項 量化參數 (K)

一般決定 K-means 之 K 值有 Mardia KV 提到的 Rule of thumb [10]、The Elbow Method、Goutte C et. al. 提到的 Information Criterion Approach [11] 和 Sugar CA and James GM 提到的 An Information Theoretic Approach [12] 等方式，我們採用 The Elbow Method 方法，利用 sum of square error 與 K 的關係曲線去取 K 值，Figure 16 為 600 條等長序列的關係曲線圖，利用求 saddle point 的方法求出 K 為 18，藉此方法找到適當的參數。

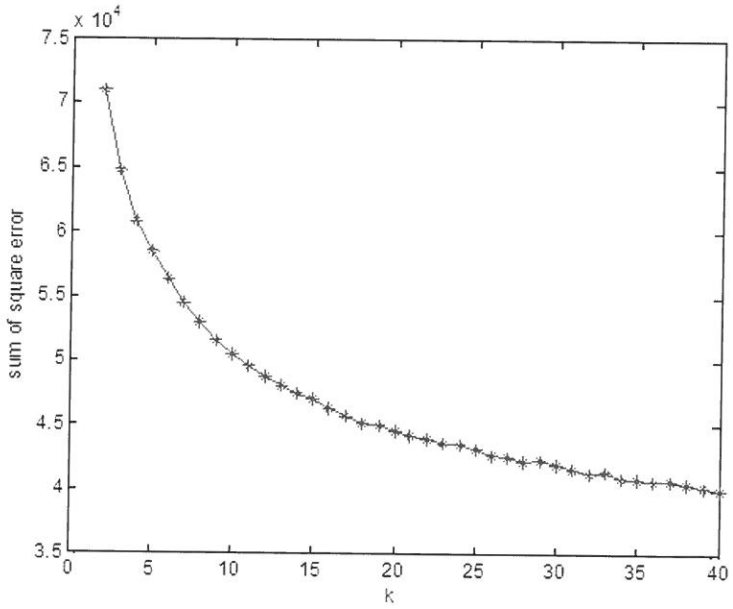

Figure 16 : 不同 k 值對應之 SSE

第 4 項 分群個數 (*h*)

在單一標籤的情況中，利用 hierarchical clustering 的方群方法作分群，而分群個數透過 dendrogram 內的 longest stem 去決定 ，一般作法會對先每個 link 作正規化並且計算 link 間的差距，藉由最大差距的 link 當成分群個數的參數值。

第 3 節 validity

第 1 項 單一標籤等長

在此將展示我們方法在等長序列的 single-label 實驗，前面的篇幅為序列在特徵空間中以點的形式表示，而後面的篇幅則利用 MBR 將特徵點以方框表示。在 single-label 的方法中有利用到 hierarchical clustering，所以簡單作了 3 個常見的 linkage method 比較，Table 8 為 10 次實驗的平均數據，可看出在我們的實驗中 Single linkage 有較高的準確度，而在時間上面並無明顯差異。然而我們在其他的實驗中發現當 K 和 h 兩參數低於 10 時，Single linkage 會比另外兩 linkage method 來的不準，而在 K 和 h 高於 20 時則相反。

Table 8 : Accuracy in R for single-label without MBR.

Method	R (%)	Elapsed time (sec.)
Average	84.02	572.0 3
Complete	83.95	572.0 2
Single	88.04	572.0 4

在 MBR 的情況中，我們在 hierarchical clustering 的部分沿用上面實驗較佳的 Single linkage，而 Table 9 為 10 次實驗的平均數據，可看出當 *IR* 變大時，在時間上明顯的下降，而在準度上面僅有微小的變差，然而在 *IR* 在 0.1 時比 0.01 時高了一些準確度，此原因可能為量化過程中 *K*-means 起始中心點不同所造成準度上的浮動所致。

Table 9 : Accuracy in R for single-label with MBR.

IR	R (%)	Elapsed time (sec.)
0.01	87.48	496.37
0.1	87.87	482.52
0.5	84.61	313.7 1
1	84.38	89.9 5

第 2 項 多標籤不等長

在此將展示我們方法在不等長序列的 multi-label 實驗，我們利用不同的 threshold 參數去驗證我們方法的準度，而總體上準度皆在 75% 以上，在適當的參數下可達 83.75% 的準度，然而準度隨著 threshold 參數的上升而變高，但當達到某值後開始下降，Table 10 為 10 次實驗的平均數據。

Table 10 : Accuracy in R_multi for multi-label without MBR.

threshold	5	10	15	20	25	30	35	40
R_multi (%)	82.26	83.75	82.24	79.89	78.33	77.35	76.75	76.69

而在 MBR 的部分實驗結果並不太大差異，差別主要在於原來眾多的特徵點以較少的方框去表示，所以在參數上必須使用較小的 threshold 參數，較特別的是 threshold

參數為 3 時的準度略高於 point case 的 83.75，可能是因為在 point case 中 threshold 參數間格較大，其最佳的準度在 10 附近而不剛好為 10，另外一個原因可能為 MBR 將 trivial match 適當地排除所致，Table 11 為 MBR 之 10 次實驗的平均數據。

Table 11 : Accuracy in R_multi for multi-label with MBR.

threshold	2	3	4	5	6	7	8	9
R_multi (%)	82.16	84.23	83.9	83.14	81.98	80.67	79.88	79.37

第 3 項 總結

最後我們利用一個簡單的表格來呈現我們方法利用 Rand index 在 Single-label 上以及我們提出的 R-multi 在 Multi-label 上的準度和時間如 Table 12，並與 Yang HX 的研究成果 Table 13 比較。

Table 12 : Overview of our method quality.

	R_multi (%)	Elapsed time (sec.)
Single-label and equal-length (point)	88.04	572.04
Single-label and equal-length (MBR)	87.87	482.52
multi-label and variable-length (point)	83.75	120.35
multi-label and variable-length (MBR)	84.23	88.67

Table 13 : Overview of Yang HX's method quality.

	R (%)
Single-label with equal-length (point)	86.67
Single-label with variable-length (point)	70.64
Single-label with variable-length (MBR)	67.86

第 5 章 結論

我們提出了一個序列分群的演算法，可應用於多標籤序列上，方法中利用 DCT mapping 將序列對應到特徵向量，透過 MBR 方法有效減少計算時間，藉由 *K*-means 作量化並用類似直方圖概念的向量呈現，最後使用 hierarchical clustering (single-label case) 或 threshold (multi-label case) 對其作分群。

分群結果驗證方面，我們將量化的概念加入到 Rand index 上面，提出一個驗證方式，可驗證多標籤和單一標籤序列的分群品質。在實驗的部分，我們對參數作討論，提供參數設定的方向，在分群品質上，single-label case 可達 88%，而 multi-label case 可達 84%。

參考資料

1. Keogh E, Lin J (2003) Clustering of time-series subsequences is meaningless: implications for previous and future research. In : Proceedings of 3rd IEEE International Conference on Data Mining:115 - 122. doi:10.1109/ICDM.2003.1250910
2. Lukashevich H, Abeßer J, Dittmar C, Grossmann H(2009)From multi-labeling to multi-domain-labeling: A novel two-dimensional approach to music genre classification. In: Proceedings of the 10th International Society for Music Information Retrieval, 2009. ISMIR.
3. Lai C-P, Chung P-C, Tseng VS (2010) A novel two-level clustering method for time series data analysis. Expert Systems with Applications 37 (9):6319-6326. doi:10.1016/j.eswa.2010.02.089
4. Li Y, Lin J (2010) Approximate variable-length time series motif discovery using grammar inference. In: Proceedings of the 10th International Workshop on Multimedia Data Mining, Washington, D.C., 2010. MDMKDD. ACM press, pp 1-9. doi:10.1145/1814245.1814255
5. Chen JR(2005) Making subsequence time series clustering meaningful. In: Proceedings of the 5th IEEE International Conference on Data Mining, 2005. ICDM. IEEE Computer Society, pp 114-121. doi:10.1109/ICDM.2005.91
6. Hsu JL, Yang HX(2009) A modified k-means algorithm for sequence clustering. In: Proceedings of the 9th International Conference on Hybrid Intelligent Systems, Shenyang 2009. HIS. IEEE, pp 287-292. doi:10.1109/HIS.2009.64
7. Faloutsos C (1996) Searching multimedia databases by content, vol 3. Kluwer Academic Publishers.
8. Ben-Dor A, Yakhini Z(1999) Clustering gene expression patterns. In: Proceedings of the 3rd Annual International Conference on Computational Molecular Biology, Lyon, France, 1999. vol 3-4. pp 33-42. doi:10.1145/299432.299448
9. Keogh E, Xi X, Wei L, Ratanamahatana CA (2006) The UCR time series classification/clustering homepage. http://www.cs.ucr.edu/~eamonn/time_series_data/.
10. Mardia KV, Kent JT, Bibby JM (1979) Multivariate analysis. Academic Press, New York.
11. Goutte C, Hansen LK, Liptrot MG, Rostrup E (2001) Feature-space clustering for fMRI meta-analysis. Human Brain Mapping 13 (3):165-183
12. Sugar CA, James GM (2003) Finding the number of clusters in a dataset. Journal of the American Statistical Association 98 (463):750-763
13. Roussopoulos N, Kelley S, Vincent Feder(1995) Nearest neighbor queries. In: Proceedings of the 1995 ACM International Conference on Management of Data, San Jose, California, United States, 1995. ACM press, pp 71-79. doi:10.1145/223784.223794

Received October 31,2011
Revised December 29,2011
Accepted January 6,2012

Multi-label subsequence clustering method [3]

Yu-Shu Wu and Jia-Lien Hsu [4]

Department of Computer Science and Information Engineering
Fu Jen Catholic University

Abstract

The problem of sequence clustering is one of fundamental research topics in data mining research. However, most algorithms are dedicated to the case of single-label sequence. We propose a sequence clustering algorithm which can be applied for finding multi labels with respect to variable-length sequences. In our research, we map sequences into feature space by applying feature extraction techniques. Then, the feature vectors represent the distribution of sequences in feature space by quantization techniques and histogram concept. We use hierarchical clustering algorithm to determine sequence labels. We also apply minimum bounding rectangle (MBR) techniques to approximate the distribution of feature vectors, and the elapsed time can be reduced accordingly.

According to our experiment, the accuracy can be up to 88% for single-label and equal-length case by Rand index validity. By applying MBR techniques, the elapsed time of improved approach can be reduced as much as 15% of original approach. In addition, we add the concept of quantization to Rand index propose a verification method, the accuracy up to 84% for single-label and variable-length sequence.

Key words: sequence clustering, multi-label, subsequence

---

[3] This paper was supported by Fu Jen Catholic University (Project No. 410031044042), and National Science Council (NSC-100-2221-E-030-021).

[4] Corresponding author. Email: alien@csie.fju.edu.tw

音樂物件之社群標籤[1]

黃建彰　徐嘉連[2]
輔仁大學 資訊工程學系

摘　要

音樂的自動分析在音樂資訊檢索 (MIR) 上有許多的相關研究，包含音樂標籤的自動分析、相似歌曲的推薦系統和音樂分群。我們提出了一個 Framework，可將音樂的自動標籤系統 (Auto tagging)、尋找相似度 (Similarity) 和分群 (Clustering) 等功能整合起來，方便使用者作不同的查詢。在我們的研究中，我們根據音樂不同的領域作各別的特徵擷取，接著利用高斯混和模型 (GMM) 將特徵向量作機器學習，建立出圖形架構的連結模型，透過 PageRank 的技術作 link analysis。此外我們提出了 Algebraic solution，其執行時間約為原始 PageRank 的 power method 時間降為五分之一，但針對自動化標籤系統的準確度依然為 75%。

關鍵詞：跨模態、圖形理論、連結分析、社群標籤。

第 1 章　簡介

在日新月異的現今，音樂已經成為現代人生活中不可或缺的元素之一，每個人都有各自所喜好的音樂性質，如何從音樂中找尋使用者的偏好已經成為多媒體領域中的重要任務。然而針對尋找偏好的多媒體推薦系統中，也有許多不同的功能。在 Music Information Retrieval (MIR) 研討會上，主要都是針對音樂不同的功能提出對應解決的

[1] 本論文，為輔仁大學（計畫編號：410031044042）與國科會（國科會計畫編號：NSC-100-2221-E-030-021）之補助研究
[2] 論文通訊作者，電子郵件：aliem@csie.fju.edu.tw

方式，像是提出自動化標籤系統，或者是尋找相似歌曲等功能。而在本論文中，提出一個系統將這些功能整合在一起，使用同一種操作原則解決大部分音樂推薦系統的問題。首先透過音樂物件我們可以擷取出不同領域的特徵，包含我們常見的特徵域有音高、節奏、音色……等，每個不同領域的特徵都有該領域的比較方式，我們將音樂視為多種特徵域的多媒體物件，我們提出一個新的Graph架構，我們稱Power Graph (PG)，並建立出一個平台能夠整合不同領域的特徵，並使用一致性的方式解決音樂推薦的問題。不同於 Jia-Yu Pan 所使用的 Mixed Media Graph (MMG) [1] 來當作核心，也加入了歌手專輯等之間的連線關係，並可針對使用者提出的問題進行調整。透過 Graph 來處理不同領域的特徵，把音樂推薦的問題，改變為 Link analysis 的問題來討論，如同過去 Hsu & Li 的研究方法 [2]。

此外，也提出 Algebraic solution 做為新的 Link analysis 方法，來提升運算出 prestige 數值所需的時間，最後做出如推薦系統、分群、尋找相似歌手歌曲以及自動標籤等多項 MIR 功能。更詳細的細節將會在第二章後面加以說明。

第 1 節　相關研究

網路的快速發展讓越來越多的多媒體系統得以重視，近幾年在 International Society for Music Information Retrieval (ISMIR) 研討會上也針對音樂推薦檢索的問題提出許多篇論文 [3][4]，對於過去的 Graph 架構上只針對 Auto tagging 所設計，然而 Graph 是一個很有彈性的架構型態，因此我們將針對整個音樂架構進行改良，設計為一個可以針對使用者進行不同功能的框架概念，其目的在建立一個框架來管理或組織整個音樂資料，並且可以針對內容進行查詢或推薦。從近幾年來的 ISMIR 中提到許多關於框架部分的論文，像是 Theimer, W. [5] 針對音樂建立了一個新的框架設計來管理音樂相關的特徵，而在 Ewert, S. [6] 的論文中也建立一個多評估的框架，可以跨不同的領域的資料，並針對不同的內容給予和弦標籤。我們主要是使用 Jia-Yu Pan 在研究中 [1] 提到的 MMG 架構，把它改成是音樂與音樂之間的跨模組型態，其作法是將音樂物件和所有特徵層分開，而每一層之間彼此計算相似度，Hsu & Li 的研究中 [2] 也提到，音樂物件當成 Level-0，其次將不同的特徵稱為 Level-1 至 Level-n，而 target 層稱為 Level-k，此外，內容中也將音樂物件與特徵之間的 edge 稱為 OF-Link；特徵彼此之間的 edge 稱為 FF-Link。將 training data 建立 model 後，把 testing data 加入進去，之後透過 Link analysis 得到 target 層的數值，最後根據數值高低判斷 target 是否正確。如下圖 1 顯示，圖中的 FA 表示 Feature A 的 node，FB 表示 Feature B 的 node。

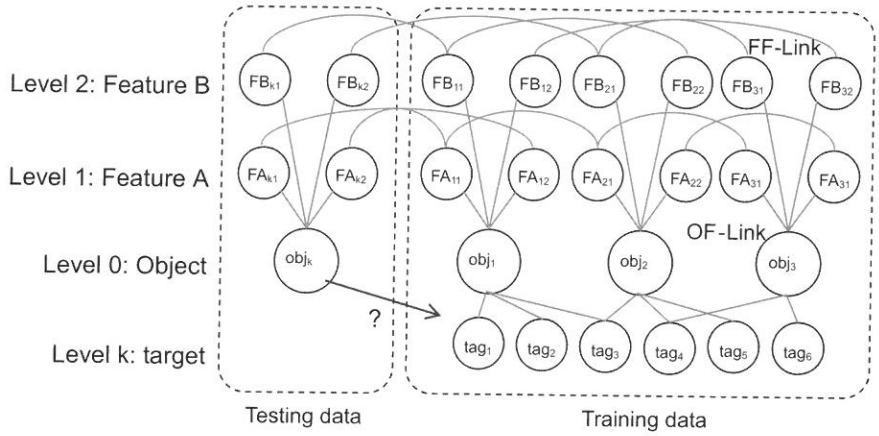

圖 1: MMG 結構圖

在多媒體領域中使用 graph 的方法時多會搭配使用 Link analysis 來運算，像是 Wei Chai 所使用的 Hidden Markov model（HMM）[7] 或是 Page Lawrence 提出的 PageRank [8]，HMM 原本是統計模型，主要是先將狀態依據馬可夫模型（Markov model）計算，找出穩定的狀態模型，再依據 output probabilities 改變輸出序列的機率結果；而 PageRank 是說一個 node 的價值決定於此 node 的 in-link 的價值的總和，用下圖 2 簡單說明 PageRank。以藍色的 node 來說明，此 node 的 prestige 是由 in-link node 綠色 node 以及黃色 node 所給予的，綠色 node 的 out-link degree 為 3，便把 90/3 得到 30 給予藍色 node；黃色 node 的 out-link degree 為 1，便把 70/1 得到 70 給予藍色 node，因此最後藍色 node 的 prestige 為 100。

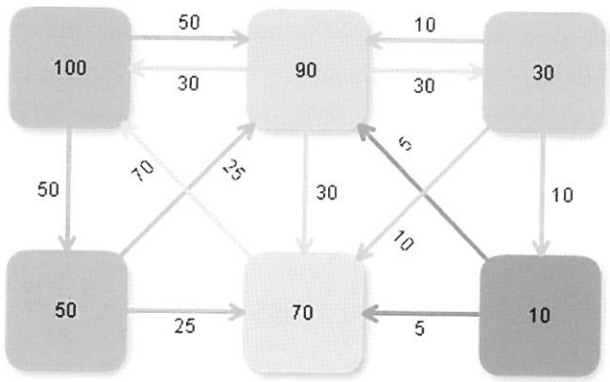

圖 2 : PageRank 的簡單流程計算

因此我們開始定義每個 node Q 都有一個 prestige pr (Q)，pr (Q) 的算法是透過 in-link node P 的 prestige (P)，根據 Degree deg (P) 分散給每一個 out-link node 後的值總加後取得的結果，因此公式為：

$$\mathrm{pr(Q)}=\sum\frac{\mathrm{pr(P)}}{\mathrm{deg(P)}} \tag{1}$$

經過多次的 i 次的 Power iteration 後，得到：

$$\mathrm{pr}_i(Q)=\sum\frac{\mathrm{pr}_{i-1}(P)}{\mathrm{deg}(P)} \tag{2}$$

在整個 Graph 的架構下 G = (N,E)，而且並未含有 isolated node 時，如果 (p,q) ∈ E，並建立出 $M_{p,q}$ = 1/deg (p) or 0 的 Adjacency 矩陣，我們將所有 node 的 prestige 合稱 $\overrightarrow{PR}$，則上述公式 (2) 變為：

$$\overrightarrow{PR_i}=\begin{bmatrix}\mathrm{pr}_i(1)\\ \mathrm{pr}_i(2)\\ \vdots\\ \mathrm{pr}_i(n)\end{bmatrix}=M\times\begin{bmatrix}\mathrm{pr}_{i-1}(1)\\ \mathrm{pr}_{i-1}(2)\\ \vdots\\ \mathrm{pr}_{i-1}(n)\end{bmatrix}=M\times\overrightarrow{PR_{i-1}} \tag{3}$$

如同馬可夫鏈矩陣一樣，當 i 很大的時候，直到 $\|PR - PR_{i-1}\| < \delta$，其中的 δ 當作門檻，最後可以得到一個遞迴式：

$$\overrightarrow{PR}=M\overrightarrow{PR} \tag{4}$$

一般 PageRank 的過程中，會發生兩種算不出結果的狀況，分別是 Dead ends 以及 Rank sinks。Dead ends 表示某一個 node 只有 in-link 沒有 out-link，對於這樣狀況會讓運算 Random Walk 最後的結果往此 node 陷入，因此稱為 Dead ends；而 Rank sinks 表示在整個 graph 架構中出現迴圈的狀況，導致計算出的 prestige 結果出現震盪狀況。

為了防止這兩個狀況發生，針對第一個問題，我們將針對整個 graph 檢查是否出現 out-link degree 為 0 的 node，而避免他發生。而針對第二狀況我們將加上 restart vector 的部分，將整個計算 PageRank 的 Power iteration 過程稱為 Random Walk with Restart (RWR).

$$\overrightarrow{PR}=(1-\alpha)M\overrightarrow{PR}+\alpha V \tag{5}$$

由公式 (5) 顯示的 α 表示有多少機率會 restart。而 V 表示 damping vector，一般在 PageRank 中為了防止掉入 sink 中，會將 V 設定為公式 (6) 的型態，這裡我們稱為 V_{average}。

$$V_{\text{average}} = \left[\frac{1}{N}\ \frac{1}{N}\ \cdots\ \frac{1}{N}\right] \tag{6}$$

而另外一種 V 是針對搜尋有關，此時會將 設定為公式 (7) 的型態，其中只有一個值是 1，代表 Restart 至 query 的 node 上。

$$V_{\text{query}} = [0\ \cdots 0\ 1\ 0 \cdots\ 0] \tag{7}$$

其中 Wang, C., et al 研究中 [9] 和 Tong, H., Faloutsos, C., & Pan, J.-Y. 研究中 [10] 針對 RWR 提出化簡以及加快執行結果，而 Bailloeul, T., Zhu, C., & Xu, Y. [3] 則是為了避免數量懸殊的 in-link 數，因此在連結到 tag 的部分使用 td-idf 的方式正規化。

第 2 章 方法

在這個章節我們先介紹我們的方法，接著第二章說明系統架構，再來針對 Graph 中裡面的模組加些說明。

第 1 節 Framework

本論文中，我們建立一個 framework 架構，此架構是由圖型概念進行，給一個 Graph 架構 G = (N,E)，N(G) 表示所有的歌曲歌手專輯，以及所有從歌曲歌手專輯中取得分析的特徵或是網路上獲得的特徵，每一個 node 有個 property 屬性；$(x,y) \in E$, $M_{x,y} = w$ and $x,y \in N$. 其中 M 為 Adjacency matrix，若 x 對 y 有關聯性，就將此 x 到 y 做線段連結，並給予一個權重 w，w. 若 w 是 0 或 1 時，special case 為 simple graph。透過 Graph 結構，進行多項 Music Information Retrieval (MIR) 問題，包括 Auto tagging、Similarity、Clustering 等。

第 2 節 系統架構

在整體的系統架構如下圖：

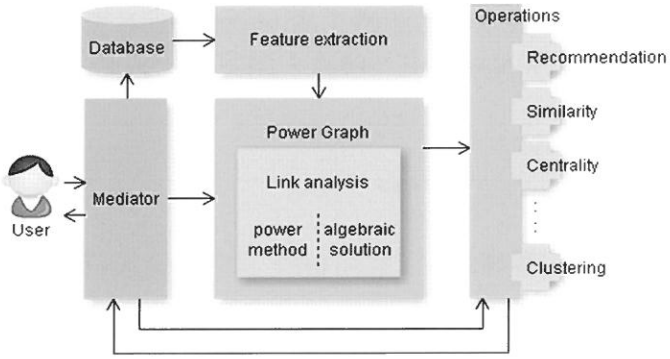

圖 3：系統流程架構圖

我們將整個系統架構定義成一個 Framework，依據使用者不同的功能需求進行不同的工作。Mediator 可以針對使用者的 Query 進行管理。Feature 是把資料庫中取得的資料進行特徵擷取，包含針對音訊部分的處理以及網路資源上的篩選。Power Graph 則是依據 Graph 的定義將整個 Graph 建立出來，並進行 Link analysis，在 Link analysis 部分我們使用兩種方式來進行，一種是一般的 power method；另外一種是我們提出的 algebraic solution。依據 Link analysis 進行的結果顯示出 prestige。將獲得的 prestige 進行不同的 Function 像是 Auto tagging、Similarity、Clustering 等，最後將結果透過 Mediator 顯示給使用者。以下針對特徵的擷取、如何建立 Power Graph、Link analysis 的過程和使用者進行的 Function 做更進一步的說明。

第 3 節 特徵擷取

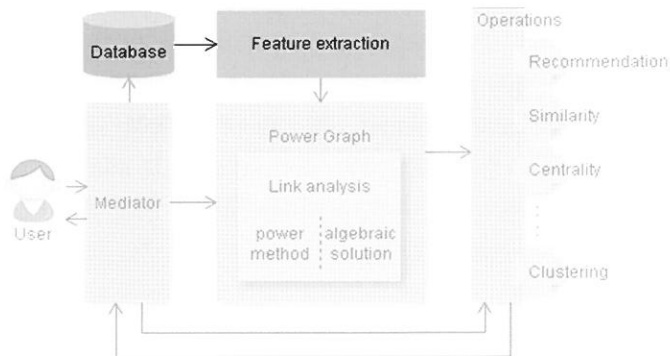

圖 4：特徵擷取之系統流程架構圖

首先將 Database 內提供的歌手、歌曲以及專輯等資料進行特徵擷取。特徵擷取部份，我們首先針對歌曲的部份說明，對一個歌曲來說，我們能從歌曲中取得到的特徵域越多，則音樂可分析的範圍就越大，歌曲主要的特徵有「聲音（Acoustic）」、「旋律（Rhythmic）」以及「結構（Structural）」三個大類別可以進行特徵擷取，圖 5 分別說明此類別包含的特徵域。此外，圖 5 也能顯示出歌手以及專輯在 Structural 中也能使用，像是從網路上取得的風格，甚至是專輯的發行日期、發行公司等標籤也能代表 Structural 部分。而像 tag 之類的資訊我們針對每首歌曲去 MusicBrainz [11] 中取得 Social tag，並將所有 tag 與歌手歌曲和專輯做連線。

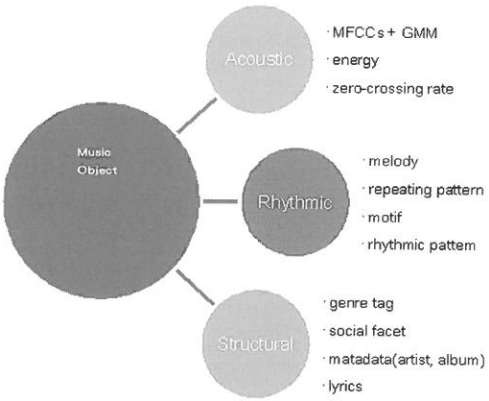

圖 5：音樂物件之特徵

其中在聲音上面較需要討論的是 (Mel frequency cepstral coefficient) MFCC 結合 Gaussian Mixture model (GMM) 的部份。而歌手和專輯則是針對 tag 以及歌曲之間做連線。

GMM 的部份，要從 MFCC 開始說明，一首歌曲經過 MFCC 轉換後會獲得到多個高維度的向量點，此時要比較兩首歌曲之間是否相似只用這些向量點似乎有點難，因此利用高斯模型來處理音訊部分資料，高斯模型可以將 MFCC 轉換後的點找出用多個高斯分布模型能表達這些點。因為高斯模型可視為常態分布下的機率模型，將一群資料以機率模型來表示來做到降維的作用。

以 30 秒的音樂物件來說，我們經過特徵擷取運算後得到 l 個 12 維的 MFCC 數值 x，$x = \{x_i | 1 \leq i \leq l\}$，經過高斯機率模型運算後得到 k 個高斯模型，各個高斯模型都算出一組平均數 μ_κ 以及共變異數 Σ_κ，我們使用函數 $p(x;\theta)$ 來表示各個高斯模型帶入 x 後計算出機率值的結果，其中 $\theta = \{\mu_\kappa, \Sigma_\kappa | 1 \leq i \leq l\}$ 當合併再一起討論 GMM 時，我們

給予每個高斯模型一個權重 ，因此我們用函數 $g(x;\theta)$ 來表是整個 GMM 帶入 x 後所得到的機率值。公式如 (8) ，其中 $\sum \beta_k = 1$ 。

$$g(x;\theta) \equiv \sum_{i=1}^{k} \beta_k \cdot p(x;\theta_k) \tag{8}$$

比較 GMM 是需要用多少個高斯模型來表示的方法時，在研究中我們使用 log-likelihood $L(x,\theta)$ ，計算方式為 x 經過 $g(x;\theta)$ 後算出的機率值 $g(x|\theta)$ 取 log，如公式 (9)， 即表示 帶入 $p(x_j|\theta_i)$ 後算出來的機率值，最後顯示當 K 為 6 的時候效果最好。

$$L(x,\theta) = \log\big(g(x|\theta)\big) = \log\left(\sum_{i=1}^{k}\sum_{j=1}^{l} \beta_i \cdot p\big(x_j|\theta_i\big)\right) \tag{9}$$

有了擷取出來的特徵後，接著討論相似度的計算方式，由於我們提出了很多特徵，在整個 framework 下可以將每個有關聯的特徵相連，也可以計算一些可以經由計算得到的相似度距離，如下表中，我們舉例幾點說明可以使用的相似度計算法。

- Acoustic:
  - GMM: Kullback-Leibler divergence
  - Vector: Euclidean distance
- Rhythmic:
  - String: Dynamic time warping
  - Vector: Euclidean distance
- Structural:
  - Keyword/Tag: Ontology-based similarity, WordNet

我們針對 GMM 使用的相似度 Kullback-Leibler (KL) divergence method 來說明，提到計算 Gaussian distribution 距離的方法不外乎是 KL divergence [12]，此方法是利用積分算出機率模型之間的相似度，再用 entropy 計算彼此之間的差異。最初公式是針對各個高斯分布之間計算距離，如公式 (10)。

$$D\big(p_1(x|\theta), p_2(x|\theta)\big) = \int p_1(x|\theta)\log\left(\frac{p_1(x|\theta)}{p_2(x|\theta)}\right) dx \tag{10}$$

接著因為我們無法將所有 x 都帶入計算，因此我們使用 Monte Carlo sampling 從

GMM p_1 中取得到的資料 x，但是 x 並非連續資料，所以公式 (10) 改為 (11)，其中 t 表示資料 x 的數量。

$$D(p_1(x|\theta), p_2(x|\theta)) \cong \frac{1}{t}\sum_{i=1}^{t} \log\left(\frac{p_1(x_t|\theta)}{p_2(x_t|\theta)}\right) \tag{11}$$

由於我們需要比較的是 GMM 與 GMM 之間的距離，在 [13] 中提到了一個 Monte carlo sampling，是 Gaussian mixture model 之間比較距離的方式，是根據 GMM 給予每個高斯分布不同權重值，挑選出不同的高斯模型產生出隨機的點，再透過這些點去記算兩個混合高斯模型的機率值。之後使用 KL divergence 來計算差異。

第 4 節 Power Graph

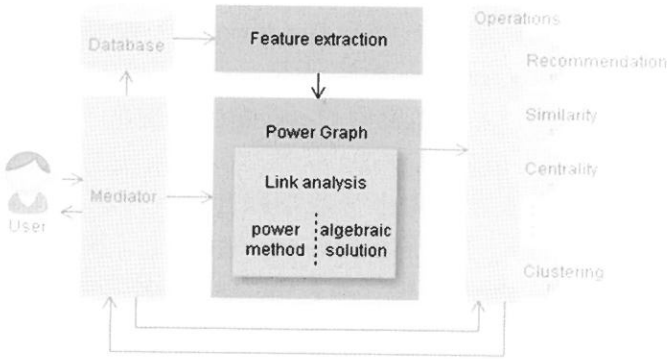

圖 6：針對 Link analysis 之系統流程架構圖

對於整個 General Graph G=(N,E)，其中 $N = N_1 \cup N_2 \cup ... \cup N_s$，每一個 N_i 表示音樂物件以及透過音樂物件所擷取出的特徵都視為 node。Edge 的產生有兩種，一種是當音樂物件擷取出特徵後，所產生的特徵與當初的音樂物件雙向的連線關係，並且給予權重 w，另外一種是特徵與特徵之間若可以計算相似度，則給予兩者特徵連線，連線依據特徵相似度計算得到結果視為權重 w，可能發生彼此不相等的權重狀況 (KL divergence 計算結果為非對稱性)。並建立出 $M_{p,q} = w\ (p,q) \in E$ 的 Adjacency 矩陣。圖 7 為 PG 的模擬連線狀況。

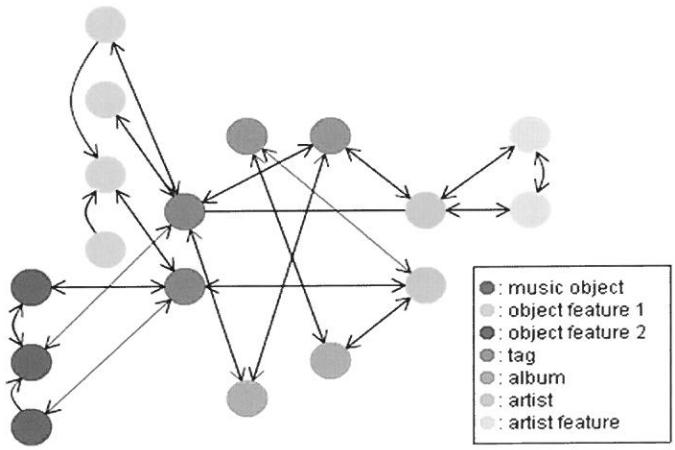

圖 7：PG 的模擬連線狀態

如圖 7 所示，每個 node 都有一個屬性 (property)，像是指歌手、歌曲之類的 metadata，或者是表示不同的 feature，根據 node 之間的相似度，給予不同的權重值。為了滿足運算 RWR 的條件，必須再針對 Graph 進行正規化，將每個 node 的 out-link 總和正規化為 1。

在 Link analysis 部分，主要使用上分成兩種方式，一種是傳統所使用的 Power method，經過多次 iteration 後，使得運算出的 prestige 與上一次 iteration 算出的 prestige 差距小於 δ，我們將最後的 prestige 當作最後 node 和 node 之間的相似狀況。

然而我們發現，當 graph 為 Undirected 時，又沒有 damping vector 的狀況下，計算出 prestige 的結果會完全與 degree 有關，我們根據 Graph 結構進行推導，提出另外一個 Algebraic solution。

我們假設整個 graph G = (N,E)，$|N| = s$，$n_i \in N$，$1 \le i \le s$，而 $a_{ij} = M(i,j) = w$，若沒有連線的連線，則 $a_{ij} = 0$。indeg 表示 n_i 的 in-link degree，公式推導如下，首先由公式 (3) 顯示透過 power method 計算出 prestige 的狀態。

$$\overrightarrow{PR_i} = M \times \overrightarrow{PR_{i-1}} \tag{12}$$

由於我們希望當 i 很大的時候，最後 PR 會收斂為相同的值，因此：

$$\overrightarrow{PR} = M\overrightarrow{PR} \tag{13}$$

$$\begin{bmatrix} n_1 \\ n_2 \\ \vdots \\ n_i \\ \vdots \\ n_s \end{bmatrix} = \begin{bmatrix} \frac{a_{11}}{indeg_1} & \frac{a_{12}}{indeg_2} & \cdots & \frac{a_{1i}}{indeg_i} & \cdots & \frac{a_{1s}}{indeg_s} \\ \frac{a_{21}}{indeg_1} & \frac{a_{22}}{indeg_2} & \cdots & \frac{a_{2i}}{indeg_i} & \cdots & \frac{a_{2s}}{indeg_s} \\ \vdots & \vdots & & \vdots & & \vdots \\ \frac{a_{i1}}{indeg_1} & \frac{a_{i1}}{indeg_2} & \cdots & \frac{a_{ii}}{indeg_i} & \cdots & \frac{a_{is}}{indeg_s} \\ \vdots & \vdots & & \vdots & & \vdots \\ \frac{a_{s1}}{indeg_1} & \frac{a_{s2}}{indeg_2} & \cdots & \frac{a_{si}}{indeg_i} & \cdots & \frac{a_{ss}}{indeg_s} \end{bmatrix} \times \begin{bmatrix} n_1 \\ n_2 \\ \vdots \\ n_i \\ \vdots \\ n_s \end{bmatrix} \tag{14}$$

$$n_i = \frac{a_{i1}}{indeg_1} \cdot n_1 + \frac{a_{i2}}{indeg_2} \cdot n_2 + \cdots + \frac{a_{ii}}{indeg_i} \cdot n_i + \cdots + \frac{a_{is}}{indeg_s} \cdot n_s \tag{15}$$

接著，我們假設：

$$n_i = \frac{indeg_i}{\sum indeg_i} \tag{16}$$

$$n_i = \frac{a_{i1}}{\sum indeg_i} + \frac{a_{i2}}{\sum indeg_i} + \cdots + \frac{a_{ii}}{\sum indeg_i} + \cdots + \frac{a_{ik}}{\sum indeg_i} \tag{17}$$

若 PG 架構下的 Adjacency Matrix 是個對稱矩陣，因此我們可以說 $a_{ij} = a_{ji}$，所以說式子 (17) 的部份會剛好成為 (16)，也剛好符合我們假設。

第 5 節 功能

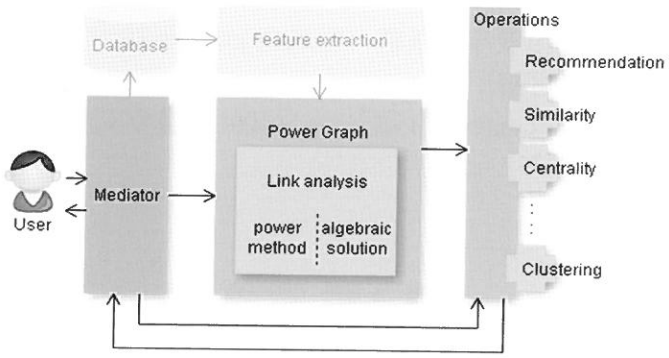

圖 8 : 針對 Function 之系統流程架構圖

使用者從 Mediator 給予 Operation 進入系統，系統依據使用者所選擇的條件進行運算。由於整個架構是由 Graph 構成，因此也可以進行許多 Graph 相關的運算功能，如 Diane J. Cook, Lawrence B. Holder [14] 提到的幾個方法，像是 Similarity, Centrality, Recommendation, Global efficiency, Homogeneity, Density, Girth, Clustering 等許多功能。以下針對 Similarity 做更細節的討論。

Similarity: 由於最後透過 prestige 數值可以知道 Query 與其他 node 之間的相似度，考量使用者輸入的需求是什麼，給予相似的歌手、歌曲或專輯，甚至可以給予相似的標籤。

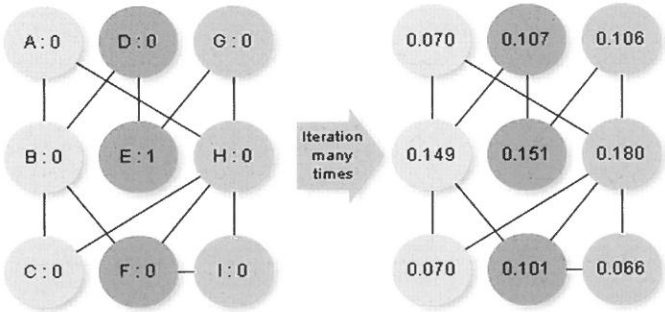

圖 9 : 透過 Link analysis 計算出 prestige 的結果

圖 9 是當 α=0.05，V_{query} 為 Damping vector 時所計算出 prestige 的結果，我們用此圖來說明，若左邊綠色 node 表示歌手，中間紫色 node 表示歌曲，右邊藍色表示標籤，假設使用者針對 E node 進行 Query，透過 Link analysis 計算得到結果顯示，H node 的數值最高，表示 E node 與 H node 相似，因此我們可以針對不同的屬性給予適合的答案，若使用者希望能夠找出歌手，我們一樣透過 prestige 找出左邊綠色中最大值的 B node，並回傳給使用者。同理，像是 Auto tagging 以及 Recommendation 等功能也使用 Similarity 的功能下實現，從 Graph 中找尋出 tag 之間的相似度或是查詢歌手專輯等功能。

第 3 章 實驗

在實驗部分我們使用 Million Song Dataset 作為資料集，並針對資料及提供的資訊建立模組，接著將針對方法中提到的 Factor 進行討論，最後是針對 Auto tagging 實驗的結果。

第 1 節 資料集

我們所選用的 dataset 是 Million songs dataset [15] 提供的 MillionSongSubset，其中包含 10000 個音樂檔案，其中每個音樂檔案含有許多結構資料，針對其中眾多的資料中我們挑選出我們所需要的特徵：

- Metadata: artist 、album、song
- Acoustic: MFCC、Pitch
- Rhythmic: 調性 (Key)、loudness、tempo
- Structural: artist tag、social tag

針對上述的特徵建立出 graph。程式使用 Matlab 2009b 撰寫。而電腦配備部份，是使用 Intel Core2 Quad CPU Q9400 2.66GHz 2.67GHz, 3.25GB RAM 的電腦，並在 windows XP 下執行運算。

若我們直接使用 10,000 首歌曲來建立 Graph 的話，整個 Graph 架構會超過記憶體範圍，因此我們改成隨機抽取 1,000 首歌曲並且使用 10-fold 的方式來進行運算。最後運算後所建立出來的 Graph 大小是 $G = (N,E)$, $N \cong 3\,000$, $E \cong 90000$

在原始資料集內的 MFCC 是 12 維資料，我們使用 MIRToolbox [16] 和 DCPR [17] 這兩個工具來把 MFCC 去計算 GMM 的結果。

Tempo 的數值偏差很大，我們也先正規化，以下面表格的方法降低 node 數

表格 1：Tempo 正規化與所被標記的名稱

Tempo	Markings
[0,20)	Larghissimo
[20,40)	Grave
[40,65)	Largo
[65,80)	Adagio
[80,100)	Andante
[100,110)	Moderato
[110,120)	Allegretto
[120,140)	Allegro
[140,150)	Vivace
[150,165)	Allegrissimo

[165,200)	Presto
[200,∞)	Prestissimo

第 2 節 因數

其中主要的影響因數有以下兩類：

K (component) 表示 GMM 所需要產生多少個高斯模型，本論文中將挑選出來的每一個歌曲以一半 training 另外一半 testing 所計算 Likelihood 的值。可以看出準度最好的時候是當 K 為 6。

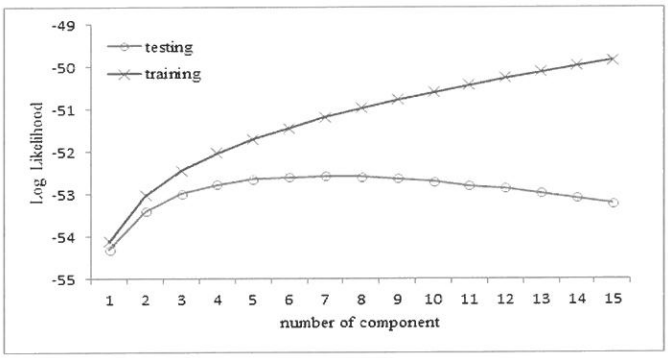

圖 10 : K's component 數量顯示狀況

α (restart probability) 表示有多少機率會進入 RWR 的狀況，分別以不同的 α 來看準度結果。我們準度測量是使用 MIREX 2010 的比較方式，是計算 Top-1 時的正確度取平均值。計算的方式是根據 PR rate 的方式計算後，根據內插法將全部 tag 分成所有的 recall 值，計算出所有的 precision。預計最接近第一個 tag 是正確的 precision 值為準確度。

表格 2 α 準度結果

α	0.05	0.1	0.15	0.2	0.25
Accuracy	75.36%	75.37%	75.38%	75.39%	75.40%

第 3 節 結果

測量準度的算法我們根據 MIREX 2010 年針對 tag 的測量標準來當測量依據。

Performers 部分，根據我們提出的兩種 Link analysis，根據這兩種方法，以下列出時間效率的表格。

表格 3 Link analysis 的準度與效率表

	Elapsed time (sec.)	Accuracy
Power method	12.62	75.42 %
Algebraic solution	2.41	75.36 %

結果明顯顯示當使用 Algebraic solution 時，時間消耗遠小於 RWR 所需時間，然而準確度卻是差不多的。

Accuracy 部分，我們使用 K=6，α=0.05 的條件下去執行全部的 1000 首歌曲的實驗，並依是否對稱 (Undirected) 與 Damping V 兩種不同的狀況顯示。

表格 4 對稱與否與 Damping V

	$V_{average}$	$V_{average}$
Undirected	75.36 %	75.42 %
Directed	75.32 %	75.38 %

第 4 節 Discussion

在討論的部份，我們要針對幾個項目多作說明，其一是在 TOP 1 的要求下為何準度卻還只有 75%，主要是因為我們針對的是 tagging，1,000 首歌曲整個結果呈現出來的 tag 數超過 7,000 多，而且有許多 tag 是只有單獨一個音樂物件連結，有非常明顯的長尾效應，而且每首歌曲的 tag 標記的數量少則 4,5 個，多則 15 到 20 個，以 TOP1 的名稱說明，其實差不多是 Recall 10% 的位置，此外，這些 tag 中並沒有經過篩選，也就是會發生” folk rock” 與” folk-rock” 視為不同 tag 的狀況，在未來的研究中將會針對此問題進行改良。

在 RWR 運算過程中，會因為 node 的 in-link 數量而有偏重的影響，我們嘗試過給每個 node 依據 in-link 數量給予處罰，將計算出來的 prestige 除上 in-link 數，不過這個動作將會造成 node 之間的差異變小，甚至可能發生找不出相似的 node。

第 4 章 Conclusions

在本篇論文中，我們提出了一個整合的系統，建立一個新的 Graph 架構，使用一制性的方法來解決多個不同的 MIR 功能，像是自動標籤、相似度以及分群，並使用跨模態的方式來達到不同的特徵領域之間比較，也提出了新的 Algebraic solution 降低執行 Link analysis 運算所需的時間。

在實驗部份，我們使用 Million song dataset 的 subset，並從中取出 1000 首歌曲，針對的是系統的自動標籤功能，我們決定了 restart 的機率，結果顯示準度有 75.42%。雖然說針對 Auto tagging 準度結果尚未比 MIREX 2010 所提出的結果準度高，但是我們提出的是一個 framework，此方法是整合所有的方法用同一個概念來解決問題，這也是我們所提出的貢獻。

參考資料

1. J.-Y. Pan, H.-J. Yang, C. Faloutsos, and P. Duygulu, "Automatic multimedia cross-modal correlation discovery," *in Proceedings of the tenth ACM International Conference on Knowledge Discovery and Data Mining* (SIGKDD 2004), 2004, pp. 653-658.
2. J.-L. Hsu and Y.-F. Li, "A cross-modal method of labeling music tags," *Multimedia Tools and Applications* (accepted in press), pp. 1-21, 2011.
3. T. Bailloeul, C. Zhu, and Y. Xu, "Automatic image tagging as a random walk with priors

on the canonical correlation subspace," in *Proceedings of the 1st ACM International Conference on Multimedia Information Retrieval (MIR 2008)*, 2008, no. 168, pp. 75-82.
4. R. Miotto, L. Barrington, and G. Lanckriet, "Improving auto-tagging by modeling semantic co-occurrences," in *Proceedings of the 11th International Society for Music Information Retrieval Conference (ISMIR 2010)*, 2010, pp. 297-302.
5. I. Vatolkin, W. Theimer, and M. Botteck, "Amuse (Advanced Music Explorer) - A Multitool Framework For Music Data Analysis," *in Processdings of the 11th International Society for Music Information Retrieval Conference (ISMIR 2010)*, 2010, no. Ismir, pp. 33-38.
6. V. Konz and S. Ewert, "A Multi-Perspective Evaluation Framework For Chord Recognition," *in Proceedings of the 11th International Society for Music Information Retrieval Conference (ISMIR 2010)*, 2010, pp. 9-14.
7. W. Chai and B. Vercoe, "Folk music classification using hidden Markov models," in *Proceedings of International Conference on Artificial Intelligence*, 2001.
8. L. Page, S. Brin, R. Motwani, and T. Winograd, *The PageRank Citation Ranking: Bringing Order to the Web*. Technical report, Stanford Digital Library Technologies Project, 1998, 1998, pp. 1-17.
9. C. Wang, F. Jing, L. Zhang, and H.-J. Zhang, "Image annotation refinement using random walk with restarts," in *Proceedings of the 14th annual ACM International Conference on Multimedia (MULTIMEDIA 2006)*, 2006, pp. 647-650.
10. H. Tong, C. Faloutsos, and J.-Y. Pan, "Random walk with restart: fast solutions and applications," *Knowledge and Information Systems*, vol. 14, no. 3, pp. 327-346, 2007.
11. "MusicBrainz," 2011. [Online]. Available: http://musicbrainz.org.
12. M. N. Do and M. Vetterli, "Wavelet-based texture retrieval using generalized Gaussian density and Kullback-Leibler distance.," *IEEE Transactions on Image Processing*, vol. 11, no. 2, pp. 146-58, Jan. 2002.
13. J. R. Hershey and P. A. Olsen, "Approximating the Kullback Leibler divergence between Gaussian mixture models," in *Proceedings of the IEEE International Conference on Acoustics Speech and Signal Processing (ICCASSP 2007)*, 2007, vol. 4, p. IV-317-IV-320.
14. D. J. Cook and L. B. Holder, *MINING GRAPH DATA* Wiley-Blackwell, 2007, p. 500.
15. T. Bertin-Mahieux, D. P. W. Ellis, B. Whitman, and P. Lamere, "The million song dataset," *Proceedings of the 12th International Society for Music Information Retrieval Conference (ISMIR 2011)*, pp. 591-596, 2011.
16. O. Lartillot, P. Toiviainen, and T. Eerola, "MIRtoolbox," 2011. [Online]. Available: https://www.jyu.fi/hum/laitokset/musiikki/en/research/coe/materials/mirtoolbox.
17. R. Jang, "DCPR Toolbox," 2011. [Online]. Available: http://neural.cs.nthu.edu.tw/jang/books/dcpr/.

Received October 31,2011
Accepted December 29,2011

Social Tagging for Music Objects [3]

Chien-Chang Huang and Jia-Lien Hsu [4]

Department of Computer Science and Information Engineering
Fu Jen Catholic University

Abstract

There are many related research about automatic analysis of music in the Music Information Retrieval (MIR) community, include identifying of music tag, recommendation of the similar song and music clustering. We propose a framework that integrated auto tagging, similarity, clustering and so on, it can make easier when user do different query. In our research, we retrieval music features based on different domain, then the feature vectors using Gaussian Mixture Model (GMM) for machine learning to construct the graph-based link model, and using Random Walk with Restart (RWR) for link analysis. We also propose the algebraic solution that can be quickly for link analysis. In the experiment of auto tagging, the execution time of algebraic solution is one-fifth of power method, however the accuracy with both of the algebraic solution and the power method are up to 75%.

Key words: cross-modal, graph, link analysis, social tagging

[3] This paper was supported by Fu Jen Catholic University (Project No.410031044042), and National Science Council (NSC-100-2221-E-030-021).
[4] Corresponding author. Email: alien@csie.fju.edu.tw

用離子束濺鍍系統鍍製含不同氧成分之氧化鋅鋁薄膜

徐進成[1,2*], 陳譽云[2], 李俊逸[1]

[1] 輔仁大學物理學系 [2] 輔仁大學應用科學與工程研究所

摘 要

本研究是在室溫下使用離子束共鍍的方式鍍製氧化鋅鋁 (AZO, ZnO:Al) 薄膜，並探討在不同氧分壓下其光學特性、結構特性與電性性質。在光學特性上，利用光譜儀量測 AZO 薄膜的光學穿透光譜，並計算其能隙。在結構特性上，使用 X-Ray 繞射儀（XRD）來研究樣品。電性性質上，則使用霍爾效應 (Hall effect) 量測 AZO 薄膜之電阻率、載子濃度與電子遷移率。當氧分壓為 1.3×10^{-4} Torr 時，有最低的電阻率 7.8×10^{-4} Ω・cm、最佳的晶向性，且有較大的載子濃度 1.72×10^{21} /cm3 以及電子遷移率 4.66 cm^2/V-s。

關鍵詞： AZO 透明導電膜、離子束共鍍 (ion-beam co-sputtering)、霍爾效應 (Hall effect)。

1. 前 言

隨著 3C 產業的蓬勃發展，人們對物質生活的要求也日趨以重，為了跟隨時代潮流的腳步，電子產品除了要具備輕薄短小外，更要符合人性化設計與便利性，然而如何降低其成本更是大家所關心的重要議題。像是近幾年發展火熱的液晶顯示器（Liquid Crystal Display, LCD）、掌上型電腦（Personal Digital Assistant, PDA）、電漿顯示器（Plasma Display Panel, PDP）和 3C 產品等，這樣的趨勢顯然已經在全球各地掀起一股研究的熱潮。

伴隨著這些電子產品的嶄露頭角，透明導電膜亦扮演著一個舉足輕重的角色，透明導電膜係指在可見光區域具高透光度（穿透率＞ 80%）及低電阻率（～ 10^{-3} Ω-cm）之導電薄膜，其中以 ITO (In_2O_3：Sn) 最被大家所廣泛應用。但由於 ITO 薄膜需求量大且銦為稀有金屬而價格昂貴，重要的是在熱穩定性上表現不佳。因此積極開發其他可與 ITO 之電性與光學性質相比擬之材料。因此，與 ITO 薄膜在光學性質和電性上能互相抗衡之氧化鋅鋁（ZnO:Al, AZO）薄膜逐漸受到關注。其中氧化鋅（ZnO）中的鋅最大的優點就是成本較低、資源豐富且不具有毒性。大部分研究主要以在 ZnO 摻雜 Al、Ga 等元素，摻雜後之氧化鋅不但可提高導電度且增加高溫穩定性，並且已有大批研究人才投入氧化鋅薄膜的相關研究。

由近年的研究得知，ZnO 的導電機制分別為鋅間隙（Zinc Interstitial）與氧空缺（Oxygen Vacancies），本實驗是以製鍍氧化鋅系列中的氧化鋅鋁透明導電膜，探討改變製程參數對透明導電膜性質之影響。製鍍方式是使用離子束濺鍍系統（Ion Beam Sputter System）以共鍍（co-sputtering）的方式鍍製氧化鋅鋁薄膜。然而離子束濺鍍相較於其他系統鍍製出來的膜質更為緻密，無論長期置放在大氣中或使用高能量雷射照射時，薄膜的特性也較不易改變。特別的是本實驗離子束濺鍍系統將兩個 4N 的鋅靶與鋁靶並排，在室溫下用離子束以一個固定轟擊面積比率同時轟擊兩個靶材，改變氧分壓的參數來研究 AZO 透明導電膜在光學性質、結構特性與電性特性。[1-4]

表 1 離子束濺鍍系統之參數

離子束轟擊靶材的角度	離子束電流	離子束電壓	放電電壓
45°	20 mA	1000 V	43 V

2. 實　驗

本實驗使用的基材是型號為 B270 的玻璃基板，玻璃基板的大小為 1.3 cm×1.3 cm。鍍製薄膜於基材之前，務必先將基材做完善的事前清洗動作，否則在基材表面上易有氧化物或者有碳化物，這些都會直接影響薄膜生成的品質，或是減少薄膜之附著

性。在基板架設完畢之後，將真空腔抽氣至背景壓力為 6×10^{-6} Torr，先固定靶高為 2.8 cm（圖 1），也就是鋁佔轟擊全部面積比例的 12 %，接著在腔體中通入不同的氧氣分量，然後在離子槍中通入氬氣做為工作氣體。鍍製時固定離子束濺鍍系統之參數（表 1）鍍製本實驗之所有 AZO 透明導電膜，而薄膜的物理厚度以石英監控器監控在 140 nm，而實際利用橢圓偏振儀量測出來的厚度為 220±7.5 nm。實驗中 AZO 薄膜氧分量的不同，樣品以 AZO-*K* Torr 來表示，*K* 代表的是在鍍製過程中所通入的不同氧分量的氧分壓，實驗對以下幾個參數的樣品進行鍍製並且分析，分別是：AZO-1.0×10^{-4} Torr、AZO-1.3×10^{-4} Torr、AZO-1.7×10^{-4} Torr、和 AZO-2.0×10^{-4} Torr。最後，把鍍製好的樣品分別作量測。在光學分析上，使用光譜儀在波長 200 nm ～ 2000 nm 量測薄膜的穿透光譜，再藉由穿透光譜計算能隙，最後，分別在紫外光區、可見光區與紅外光區上做光學特性分析。在結構特性上，利用 X-Ray 繞射儀（XRD）去了解氧分壓的不同所造成的結構上的改變，並由 XRD 計算晶粒尺寸（grain size）與晶格平面間距（*d-space*）。在電性方面，使用霍爾量測探討不同的鋁摻雜量與電阻率、載子濃度與電子遷移率的關係。

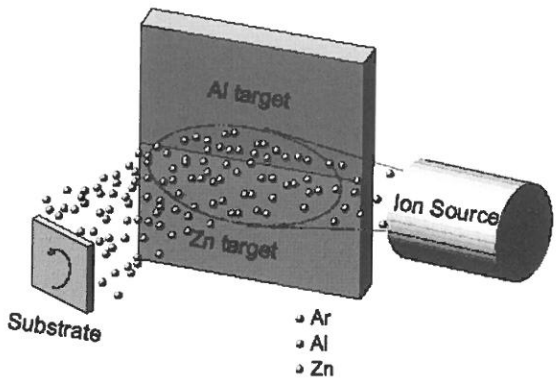

圖 1 離子源、靶材與基板的相對關係圖

3. 實驗結果與討論

研究氧分壓與 AZO 薄膜特性關係

本實驗依據先前的研究[5]，將靶高固定在 2.8 cm，也就是鋁佔轟擊全部面積比例的 12 %。搭配不同的氧分壓來探討 AZO 透明導電膜對其光學特性、結構性質與電性特性有何影響。

研究不同氧分壓 AZO 薄膜之光學特性

一般而言，ZnO 理論上其結構能隙約為 3.3 eV，當入射光線之能量大於其能隙時會被吸收，而入射光小於能隙時會有穿透、反射與吸收的情形發生。因此，在可見光區域 AZO 薄膜容易穿透。圖 2 是經由 Varian Cary 5E 光譜儀量測不同氧分壓下的 AZO 薄膜之穿透光譜圖。

在可見光（380 nm ～ 780 nm）區域內，隨著氧分壓的增加，穿透光譜並沒有明顯的改變，皆有平均 80%以上的穿透率。而在波長比 380nm 短的紫外（UV）區，在氧分壓 1.0×10^{-4} Torr 逐漸增加至 1.3×10^{-4} Torr 時，吸收邊緣有稍微向短波長偏移（blue shift）的趨勢。將本研究不同氧分壓求得之各 AZO 薄膜膜層厚度（d）及穿透光譜（T），帶入公式並把數據作圖找出能隙（band gap）的大小，如圖 3。

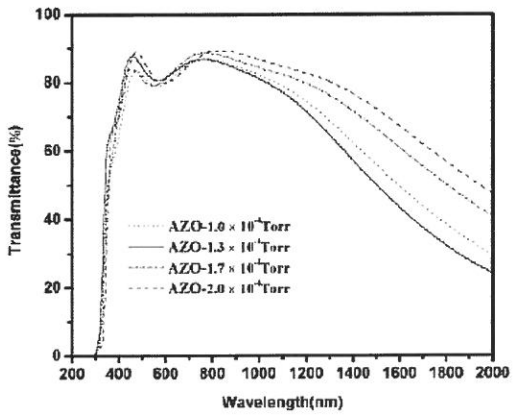

圖 2 不同氧分壓 AZO 薄膜之穿透光譜圖

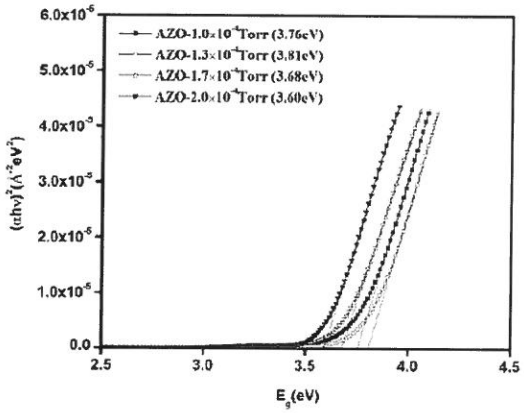

圖 3 不同氧分壓 AZO 薄膜之能隙圖

由表 2 知氧分壓 1.0×10^{-4} Torr 逐漸增加至 1.3×10^{-4} Torr 時，能隙亦會從 3.76 eV 逐漸增加至 3.81 eV，然而能隙的增加導致吸收邊緣往短波的地方偏移，這是因為柏斯坦－摩斯偏移 [6] 所造成。而當氧分壓再從 1.3×10^{-4} Torr 逐漸增加至 2.0×10^{-4} Torr 時，吸收邊緣又會稍微往長波的方向偏移。那是因為當氧分壓逐漸增加的時候，載子濃度由 1.72×10^{21} /cm^3 大幅下降至 8.59×10^{20} /cm^3（載子濃度可由表 2 得知），導致能隙明顯從 3.81 eV 降至 3.6 eV。依照能隙寬（ΔE_g）與載子濃度之公式 [7]，可以發現當 AZO 薄膜載子濃度降低時，其能隙寬亦會減少。所以當氧分壓增加時，載子濃度的下降剛好與『紅移』的現象相符合，因此穿透光譜的吸收邊緣會稍微的往長波偏移。最後在波長比 780 nm 長的紅外（IR）區，穿透光譜會有不同的反射現象，最主要的原因是載子濃度的改變所導致 [8]。當氧分壓從 1.0×10^{-4} Torr 至 1.3×10^{-4} Torr 時，載子濃度有增加的趨勢，因此從穿透光譜發現樣品 AZO-1.3×10^{-4} Torr 相較於樣品 AZO-1.0×10^{-4} Torr 有更大的反射現象產生，因此穿透率有較大的下降。然後氧分壓從 1.3×10^{-4} Torr 至 2.0×10^{-4} Torr 時，載子濃度反而逐漸的降低至 8.59×10^{20} /cm^3，因此明顯的從穿透光譜可以發現氧分壓逐漸增加後，其反射的現象會漸漸的降低。由穿透光譜發現載子濃度的多寡不僅影響到 AZO 薄膜的電性，也直接影響到薄膜的光學特性。

表 2 不同氧分壓 AZO 薄膜之能隙與載子濃度

	AZO-1.0×10^{-4} Torr	AZO-1.3×10^{-4} Torr	AZO-1.7×10^{-4} Torr	AZO-2.0×10^{-4} Torr
能隙（eV）	3.76	3.81	3.68	3.6
載子濃度（/cm^3）	1.22×10^{21}	1.72×10^{21}	1.04×10^{21}	8.59×10^{20}

研究不同氧分壓 AZO 薄膜之結構特性

本研究是以 X-Ray 繞射儀對不同氧分壓所鍍製出來的 AZO 薄膜做結構上的量測與結晶性的研究。由 X-Ray 全角度掃描 θ-2θ 發現，除了量測到 B270 基板和載具的訊號以外，在角度大約 34.16° 的地方皆能量測到氧化鋅（002）的晶向，如圖 4 所示。當氧分壓從 1.0×10^{-4} Torr 增加到 1.3×10^{-4} Torr 時，明顯看到 AZO 薄膜的繞射強度有很大的提升。而樣品 AZO-1.0×10^{-4} Torr 的晶向性會比 AZO-1.3×10^{-4} Torr 差，那是因為在鍍製時氧氣的不足，會導致薄膜缺少同質性，而造成晶體的缺陷，因此當氧分壓逐漸增加到 1.3×10^{-4} Torr 時，剛好是氧氣的最佳參數，因此有最佳的晶向性；之後再提升氧分壓至 2.0×10^{-4} Torr，繞射強度又會有大幅度的下降趨勢，而樣品 AZO-1.7×10^{-4} Torr 與 AZO-2.0×10^{-4} Torr 的繞射強度差不多。

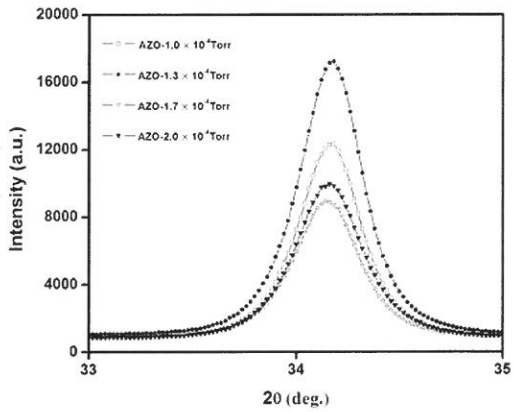

圖 4 不同氧分壓 AZO 薄膜之 XRD 圖

把改變氧分壓 XRD 的 AZO 薄膜繞射角度與入射光波長（$\lambda = \lambda_{CuK\alpha} = 1.54055$ Å），代入布拉格定律（Bragg's law）公式，可得知晶格平面間距。其變化是由於 AZO 薄膜繞射角度所影響。因此從 XRD 圖譜（圖 4）中，當氧分壓從 1.0×10^{-4} Torr 逐漸增加至 2.0×10^{-4} Torr 時，其繞射角度分別是 34.16°、34.17°、34.15° 與 34.16°；所以 (002) 晶格平面間距分別是 2.623、2.622、2.624 與 2.623 Å。因此從圖 5 中，發現當氧分壓逐漸增加時，其晶格平面間距並沒有改變。而由文獻得知[9]，由於 Al^{3+}（53 ～ 67.5 pm）的離子半徑小於 Zn^{2+}（74 ～ 104 pm）的離子半徑，因此當有較多的鋁（Al）原子去取代鋅（Zn）原子時，晶格平面間距會變比較小。所以由圖 5 中發現，當氧分壓逐漸增多時，晶格平面間距沒有明顯改變，由此得知，在氧分壓增多的期間，並沒有更多或更少的鋁原子去取代鋅原子。

而這邊的半高寬（FWHM）是利用 OriginPro 8 應用程式以高斯（Gauss）方程式所逼合（fitting）出來。由圖 5 發現，當氧分壓逐漸增加時，AZO 薄膜之半高寬（FWHM）會漸漸的增加的趨勢。一般而言，當半高寬比較小其薄膜的晶向性會比較佳[10]。因此 XRD 圖譜（圖 4）印證，樣品 AZO-1.0×10^{-4} Torr 與 AZO-1.3×10^{-4} Torr 有比較小的半高寬，因此有較佳的晶向性。晶粒尺寸（grain size）是將入射光波長（$\lambda = \lambda$ CuK $\alpha = 1.54055$ Å）、峰值之半高寬（β）與繞射角度帶入史瑞爾方程式（Scherrer equation）計算出來的結果。由圖 5 得知，當氧分壓逐漸增加時，其半高寬有增加的趨勢，而晶粒尺寸則會以相反比例逐漸減小。

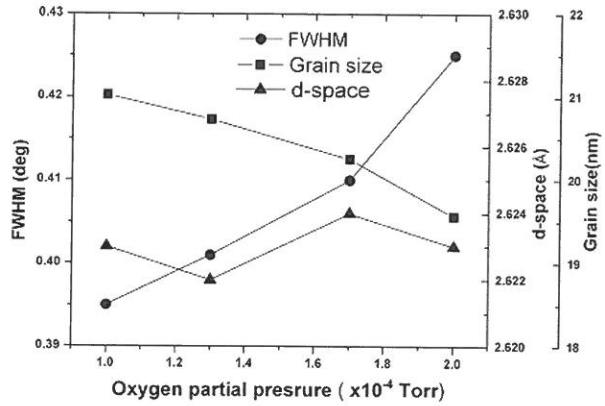

圖 5 不同氧分壓 AZO 薄膜之晶粒尺寸、晶格平面間距晶粒尺寸與半高寬比較圖

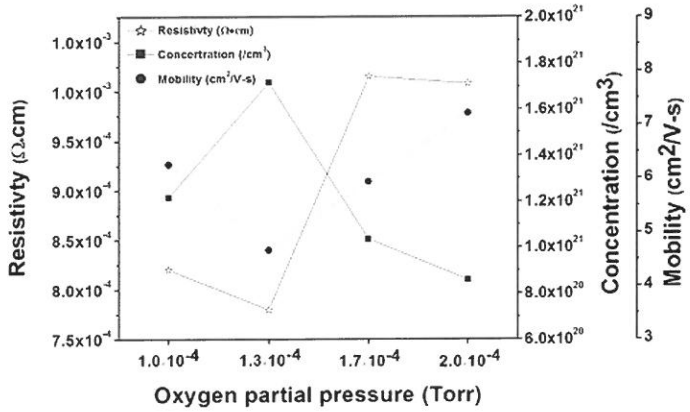

圖 6 不同氧分壓 AZO 薄膜之電阻率、載子濃度與遷移率

研究不同氧分壓 AZO 薄膜之電性特性

在氧分壓實驗中，所有的 AZO 透明導電薄膜經由 Hall effect 量測皆是 n-type。圖 6 為不同氧分壓下其電阻率、載子濃度與電子遷移率的相關圖。因為透明導電膜 AZO 的導電機制是利用鋁離子置換鋅離子及氧空缺的形成來提升載子濃度，因此，過低的氧分壓會使薄膜仍屬於金屬膜並大幅降低其穿透率；然而，提高氧分壓會減少氧空缺而減少載子濃度造成電阻率的升高。由圖 6 得知，當氧分壓從 1.0×10^{-4} Torr 增加到 1.3×10^{-4} Torr 時，電阻率會從 8.2×10^{-4} Ω · cm 下降到 7.8×10^{-4} Ω · cm。持續增加氧分壓至 2.0×10^{-4} Torr 時，電阻率會大幅提升至 1.0×10^{-3} Ω · cm。因此，當氧分壓為 1.3×10^{-4} Torr 時，AZO 薄膜有最低電阻率 7.8×10^{-4} Ω · cm 與最佳的晶向性（由圖 4 得知）。在氧分壓從 1.0×10^{-4} Torr 增加到 1.3×10^{-4} Torr，因為薄膜中的氧空缺增加，造成載子濃度的增加，使得電阻率下降，因此在 1.3×10^{-4} Torr 有最小的電阻率 7.8×10^{-4} Ω · cm。而且，藉由圖 5 得知，因為在氧分壓逐漸增加的同時，AZO 薄膜本身晶格平面間距並沒有明顯改變。所以，可以推論在氧分壓 1.0×10^{-4} Torr 增加到 1.3×10^{-4} Torr 時，載子濃度會增加並不是因為有更多的鋁原子去取代鋅原子，而是因為氧空缺的增加導致載子濃度提升。持續增加氧分壓（> 1.3×10^{-4} Torr），電阻率會有大幅度增加的趨勢，那是因為 AZO 薄膜中的氧空缺減少，以至於載子濃度大幅降低（由圖 7 得知）。而導電性質的第二個決定因素是載子的遷移率，由圖 7 得知，當氧分壓由 1.0×10^{-4} Torr 增加到 1.3×10^{-4} Torr 時，其載子遷移率會逐漸的下降至 4.66 cm^2/V-s。持

續增加氧分壓至 2.0×10^{-4} Torr，載子遷移率會呈線性的趨勢逐漸上升至 7.22 $cm^2/V\text{-}s$，而載子遷移率會受到散射機制的影響。

而在本研究的 AZO 透明導電膜中，由表 3 知，氧分壓逐漸增加，其晶粒尺寸會由 21.02 nm 減少到 19.56 nm。然而經由平均自由徑（L）公式 [11]

$$L=(3\pi^2)^{\frac{1}{3}}(he^{-2})\rho^{-1}n^{-\frac{2}{3}}$$

h 為普朗克常數；e 為電子電荷；ρ 為電阻率；n 為載子濃度。

表 3 不同氧分壓 AZO 薄膜之晶粒尺寸與平均自由徑

	AZO-1.0×10^{-4} Torr	AZO-1.3×10^{-4} Torr	AZO-1.7×10^{-4} Torr	AZO-2.0×10^{-4} Torr
晶粒尺寸（nm）	21.02	20.73	20.25	19.56
平均自由徑（nm）	8.56	7.16	7.70	8.79

由公式知，載子的平均自由徑會受載子濃度的影響，所以載子遷移率應該和載子濃度有關。n 型透明導電膜（transparent conductive oxide film, TCO）中，摻雜物在提供自由電子後，便以正離子型態存在於晶體內。因為摻雜物離子與自由電子間有庫倫力，所以摻雜物在提供電子的同時，也會成為電子的散射中心，阻礙電子的移動 [12]。由圖 7 發現，當氧分壓從 1.0×10^{-4} Torr 增加到 1.3×10^{-4} Torr 時，載子濃度增加而載子遷移率下降；當氧分壓持續提升至 2.0×10^{-4} Torr，其載子濃度則會呈現下降的趨勢，相對地，載子遷移率會有逐漸上升的現象發生。而且由文獻 [13] 得知，摻雜過的 ZnO 薄膜其載子濃度在 $10^{19}\sim10^{20}$ cm^{-3}，影響其載子遷移率有可能是晶界散射和摻雜物離子散射（ionized impurity scattering）；然而，若載子濃度在 $10^{20}\sim10^{21}$ cm^{-3}，則最主要影響其載子遷移率是摻雜物離子散射。因此可以推論本實驗主要影響載子遷移率的是摻雜物離子散射。

因此由氧分壓實驗得知，當氧分壓為 1.3×10^{-4} Torr 時，有最佳的電阻率 7.8×10^{-4} Ω · cm 以及最佳的晶向性和最大的載子濃度 1.72×10^{21} cm^{-3}，並有最小的載子遷移率為 4.66 $cm^2/V\text{-}s$。

4. 結　論

本實驗是固定靶材高度，也就是鋁佔轟擊全部面積比例的 12%。以改變氧分壓來探討氧分壓與 AZO 薄膜的特性關係。在光學分析上，所有樣品皆在可見光區域都有 80%以上的穿透率。紫外光區域中，氧分壓從 1.0×10^{-4} Torr 增加至 1.3×10^{-4} Torr，因為載子濃度增加使得能隙亦增加，根據柏斯坦－摩斯效應，吸收邊緣會逐漸往短波偏移。當氧分壓持續增加（$>1.3\times10^{-4}$ Torr），因為載子濃度降低造成能隙寬變小，因此吸收邊緣會有紅移的現象。紅外光區域中，整體的反射率會隨著載子濃度的增加而增加，當載子濃度越大穿透率下降會越大，反之亦然。在結構特性上，所有 AZO 薄膜樣品在角度大約 34.16° 的地方皆有氧化鋅（002）的晶向。在氧分壓為 1.3×10^{-4} Torr 時樣品有最佳的晶向性，但持續增加氧分壓（$>1.3\times10^{-4}$ Torr），其晶向性有變差的趨勢。在電性特性上，當氧分壓為 1.3×10^{-4} Torr 時，AZO 薄膜有最小的電阻率 7.8×10^{-4} Ω・cm 以及最佳的晶向性。因為從氧分壓實驗得知，氧分壓的改變並沒有使晶界距離有所改變，從中印證有最小的電阻率是因為氧空缺的增加，使的薄膜中載子濃度的提升，並不是有更多的鋁原子去取代鋅原子。而從晶粒尺寸與平均自由徑中發現，造成電子遷移率下降的最主要原因是摻雜物離子散射。因此由本實驗得知，樣品 AZO-1.3×10^{-4} Torr 有最小的電阻率 7.8×10^{-4} Ω・cm、最佳的晶向性，且有較大的載子濃度 1.72×10^{21} /cm^3 以及電子遷移率 4.66 cm^2/V-s。

參考資料

1. H. Sheng, N. W. Emanetoglu, S. Muthukumar, B. V. Yakshinskiy, S. Feng, and Y. Lu, "*Ta/Au ohmic contacts to n-type ZnO*", J. Electron Mater 32, 935-938（2003）.
2. H. K. Kim, S. H. Han, and T. Y. Seong,"*Low-resistance Ti/Au ohmic contacts to Al-doped ZnO layers*", Appl. Phys. Lett. 77, 1647-1649（2000）.
3. H. K. Kim, K. K. Kim, S. J. Park, and T. Y. Seong,"*Formation of low resistance nonalloyed Al/Pt ohmic contacts on n-type ZnO epitaxial layer*", J. Appl. Phys. 94, 4225-4227（2003）.
4. Y. G. Wanga, S. P. Laua, X. H. Zhangb, H. H. Hngc, H. W. Leea, S. F. Yua, and B. K. Taya , Journal of Crystal Growth 259, 335-342（2003）.
5. 白曜緯，*"以離子束濺鍍共鍍法研究 AZO 透明導電膜之組成、結構、溫度對電阻之影響"*，輔仁大學物理系碩士論文（2009）.
6. Z. C. Zin, I. Hamberg, and C. G. Granqvist, "*Optical properties of sputter-deposited ZnO:Al thin films*", J. Appl. Phys. 64, 5117-5131（1988）.
7. F. Urbach, "*The Long-Wavelength Edge of Photographic Sensitivity and of the Electronic Absorption of Solids*", Phys. Rev. 92, 1324-1324（1953）.
8. K. L. Chopra, S. Major, and D. K. Pandya, "*Transparent conductors-A status review*", Thin Solid Films 102, 1-46（1983）.
9. Y. Y. Chen, J. C. Hsu, P. W. Wang, Y. W. Pai, C. Y. Wu, and Y. H. Lin,"*Dependence of resistivity on structure and composition of AZO films fabricated by ion beam co-sputtering deposition*", Appl. Surf. Sci. 257, 3446-3450（2011）.
10. L. Li, L. Fang, X. M. Chen, J. Liu, F. F. Yang, Q. J. Li, G. B. Liu, and S. J. Feng, *"Influence of oxygen argon ratio on the structural, electrical, optical and thermoelectrical properties of Al-doped ZnO thin films"*, Physica E 41, 169-174（2008）.
11. C. Kittel, *Introduction to solid state physics*（8th ed., Wiley, New Caledonia, UK, 2005）.
12. 楊明輝，透明導電膜（藝軒出版社，台北，2008）.
13. T. Minami, S. Suzuki, and T. Miyata,"*Transparent conducting impurity-co-doped ZnO:Al thin films prepared by magnetron sputtering*", Thin Solid Films 53, 398-399（2001）.

Received October 31,2011
Revised December 29,2011
Accepted January 9,2012

AZO Thin Film Fabricated by Ion Beam Sputter Deposition in Various Partial Pressures

Jin-Cherng Hsu [*1,2], Yun-Yu Chen [2], Chung-Yi Lee [1]

[1] *Department of Physics, Fu-Jen Catholic University*
[2] *Graduate Institute of Applied Science and Engineering, Fu-Jen Catholic University*

Abstract

In this study, zinc oxide doped Al (AZO, ZnO:Al) films were co-sputtered by ion-beam sputter deposition in various oxygen partial pressure at room temperature. The optical, structural and electrical properties of the films were investigated. Optical ellipsometer and spectrometer were used to find the optical bind gaps. The AZO film structure was measured by XRD. And, the electric resistivity, carrier concentration and mobility were determined by Hall effect. Moreover, the AZO film deposition at oxygen partial pressure of 1.3×10^{-4} Torr had the least resistivity of 7.8×10^{-4} Ω・cm and optimum crystallinity; it had the largest amount of carrier concentration of 1.72×10^{21} /cm^3 and electronic mobility of 4.66 cm^2/V-s.

Key words: AZO transparent conducting film, ion-beam co-sputtering, Hall effect

A Current Sensing Circuit for the Average Current Mode DC to DC Buck Converter

Chih-Kang Liu and Ding-Lan Shen*

Departement of Electrical Engineering
Fu Jen Catholic University, Hsin Chuang 242, Taipei, Taiwan

Abstract

This paper proposes an average-current sensing circuit applied to the dc to dc buck converter. The circuit utilizing a single rail to rail input amplifier with negative feedback forces the drain source voltage between the Power MOS and the mirrored transistor in equilibrium to sense the inductor current in different working periods. This sensing circuit is fabricated with TSMC 2P4M 0.35μm CMOS technology. Experimental results indicate that the inductor current is sensed through the sensing circuit in the switching frequency between 200 kHz to 1 MHz at the input voltage of 3.6V.

Key words: Current Sensing, Average Current Mode, DC to DC Buck Converter.

*Corresponding author: Tel: (02)2905-3739
E-mail address: dlshen@ee.fju.edu.tw

1. Introduction

The demand for consumer electronics and the advance of integrated circuit manufacturing process dominate power supply technology with high efficiency, light weight, small size switching approaches. Buck switching converters include voltage mode[1-7] and current mode feedback architecture [8][9]. Voltage mode operation means that the sensed voltage moves through the resistor divider. The difference between the sensed voltage and the reference voltage is amplified through the error amplifier. Then the amplified result is compared with a sawtooth ramp to control the switching duty of the buck converter to obtain the demanded voltage. Another current mode is coupled with a current loop to compensate the output of the error amplifier in the buck converter. This additional loop can effectively speed up the dynamic response in closed-loop operation.

Current modes are divided into three types. The first peak current mode [10-13] detects the positive half cycle of the inductor current into voltage with the output of the error amplifier to the pulse width modulation (PWM) to achieve the demanded output voltage. The drawback is that when the duty cycle is greater than 0.5, the harmonic distortion is induced. This distortion requires adding a slope compensation signal to moderate the undesired effects. The second hysteresis current mode [14] is sensing inductor current and pre-generated hysteresis current for comparison to obtain the corresponding duty cycle of the output voltage. The drawback is that when the input voltage and loading current has a great variation, there will be a pre-set voltage or current limitation. The third average current mode senses the inductor current of both positive and negative half cycles. This sensed signal accompanying with the deviation signal from the voltage-error amplifier is compared with a fixed frequency sawtooth ramp through the PWM comparator. Then the controlled pulse duty achieves the desired output voltage.

Fig. 1 shows the DC to DC buck converter with an application of average current sensing circuit. The average current mode has the following advantages [15]. The current sensing circuit suppresses the switching noise of the Power MOS. Because the Power MOS is ON, the input of A_2 amplifier is away from the input voltage signal of PWM comparator when the slope is decreased. Compared with the peak current mode, the stability requirement

of loop gain limitation in average current mode needs no slope compensation circuit when the switching duty is greater than 0.5. This paper presents an average current sensing circuit with a signal negative feedback amplifier in inductor current sensing which is applied to a current-mode buck converter.

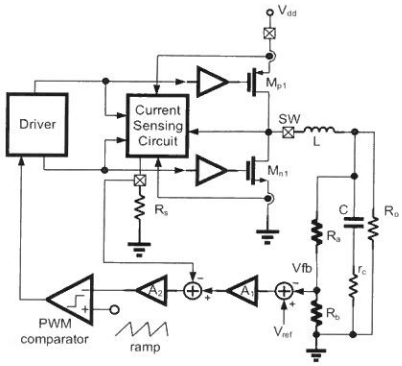

Figure 1.The average current mode DC to DC buck converter.

2.The average switch current sensing circuit

2.1.The average current sensing circuit of a synchronous buck conversion

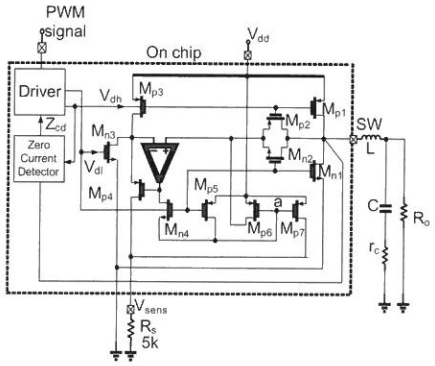

Figure 2.The average current sensing circuit of a synchronous buck conversion.

This paper proposes an average current sensing circuit for the DC to DC switching buck conversion as shown in Fig. 2. To avoid adding a small resistor to detect the inductor current in change-pump path, the circuit utilizes a rail to rail operational amplifier (op) in feedback structure to sense the inductor current. As the input voltage range is between 2.5V to 5V, a single full input range operational amplifier with negative feedback senses the inductor current to save the area and power consumption.

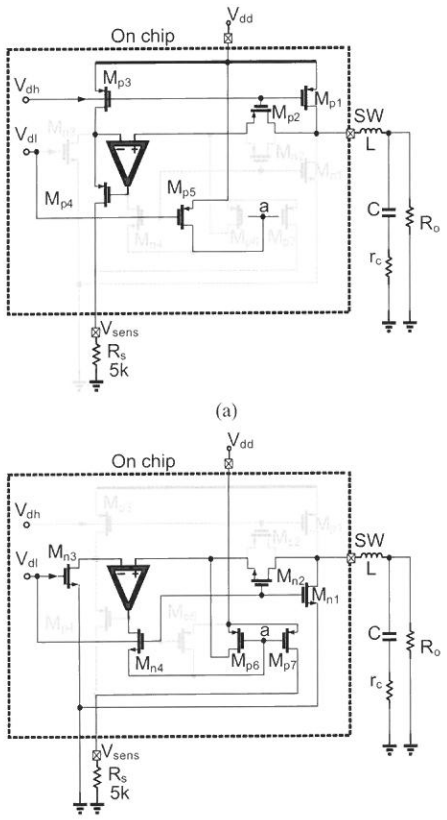

Figure 3.(a) M_{p1} conducting sensing circuit diagram, and (b) M_{n1} conducting sensing circuit.

Fig. 3 (a) shows that when driving circuit generated V_{dl} and V_{dh} go low, the high-side Power PMOS (M_{p1}) is ON. Then IM_{p1} performs inductive energy storage. The inductor current is equal to the IM_{p1} of Mp1. And the low-side switch of the Power NMOS (M_{n1}) is OFF. Drain current, I_d, of the Power PMOS operating in the linear region is as in (1).

$$Id = \frac{1}{2}\mu pCox\left(\frac{W}{L}\right)\left[2\left(Vsg - \left|Vtp\right|\right)Vsd - V_{sd}^2\right] \tag{1}$$

When M_{p2}, M_{p3}, M_{p5} are ON, the node, a, is pulled to V_{dd} through M_{p5}, and then M_{p6}, M_{p7} turns OFF. Because both ends of the positive and negative input of OP are virtual short, V_{ds} of M_{p1} and M_{p3} are the same. The designed size of M_{p1} and M_{p3} is at the ratio of N_p:1, then the relationship between I_{Mp1} and I_{Mp3} is given in (2). If the charging path of M_{p1} is connected in series with a conventional resistor as R_{sensp}, the relationship between sensing resistor, R_s, and R_{sensp} are shown in (3). The sensed current, I_{Mp3}, flow through R_s to generate sensed voltage, V_{sens}. As shown in (4), if select R_s / N_p = 1, the sensed voltage is equivalent to the inductor current.

$$\frac{I_{M_{p1}}}{I_{M_{p3}}} = \frac{\frac{1}{2}\mu_p C_{ox}\left(\frac{W}{L}\right)_{M_{p1}}\left[2\left(V_{sg} - \left|V_{tp}\right|\right)V_{sd} - V_{sd}^2\right]}{\frac{1}{2}\mu_p C_{ox}\left(\frac{W}{L}\right)_{M_{p3}}\left[2\left(V_{sg} - \left|V_{tp}\right|\right)V_{sd} - V_{sd}^2\right]} = N_p \tag{2}$$

$$R_{sensp} = \frac{R_S}{N_p} = \frac{\left(\frac{W}{L}\right)_{M_{p3}}}{\left(\frac{W}{L}\right)_{M_{p1}}} \cdot R_S \tag{3}$$

$$V_{sens} = I_{M_{p1}} \cdot R_{sensp} = I_{M_{p3}} \cdot R_S = \frac{I_{M_{p1}}}{N_p} \cdot R_S \tag{4}$$

Similarly in Fig. 3 (b), when M_{p1} is OFF, I_{Mp1} can not continue the inductive energy storage. Therefore the inductor current provides energy to the capacitor while the low-side switch of the Power NMOS (M_{n1}) is ON. The inductor current is equal to I_{Mn1} of Power NMOS (M_{n1}) plus the I_{Mn2} flowing into M_{n2}. As V_{dl} is high, M_{n3} and M_{n4} are ON, the amplifier

regulates the gate of M_{p6} to force the V_{ds} of M_{n2} equal to the V_{ds} of M_{n1}. Current I_{Mn1} and I_{Mn2} have the relationship of (5) as the size ratio of M_{n1} and M_{n2} is N_n:1. When Nn is larger than 1, the inductor current is approximately equal to I_{Mn1}. The equivalent resistor of the inductor current sensing circuit is given by (6). Since Vgss of M_{p6} and M_{p7} are identical, M_{p7} duplicates the current of M_{p6} to the sensing resistor, R_s. Therefore, $I_{Mn2} = I_{Mp6} = I_{Mp7}$. Consequently, the voltage across R_{sensn} is equal to I_{Mp7} times R_s, as shown in (7).

$$\frac{I_{Mn1}}{I_{Mn2}} = \frac{\frac{1}{2}\mu_n C_{ox}\left(\frac{W}{L}\right)_{M_{n1}}\left[2(V_{gs}-V_{tn})V_{ds}-V_{ds}^2\right]}{\frac{1}{2}\mu_n C_{ox}\left(\frac{W}{L}\right)_{M_{n2}}\left[2(V_{gs}-V_{tn})V_{ds}-V_{ds}^2\right]} = N_n \tag{5}$$

$$R_{sensn} = \frac{R_S}{N_n+1} \approx \frac{R_S}{N_n} = \frac{\left(\frac{W}{L}\right)_{M_{n2}}}{\left(\frac{W}{L}\right)_{M_{n1}}} \cdot R_S \tag{6}$$

$$V_{sens} = I_{M_{n1}} \cdot R_{sensn} = I_{M_{n2}} \cdot R_S = I_{M_{p7}} \cdot R_S = \frac{I_{M_{n1}}}{N_n} \cdot R_S \tag{7}$$

Using the same amplifier for sensing the positive and negative half cycle of inductor current in the switching buck converter, which effectively saves the circuit area and power consumption.

2.2.Rail to rail input folded cascode amplifiers

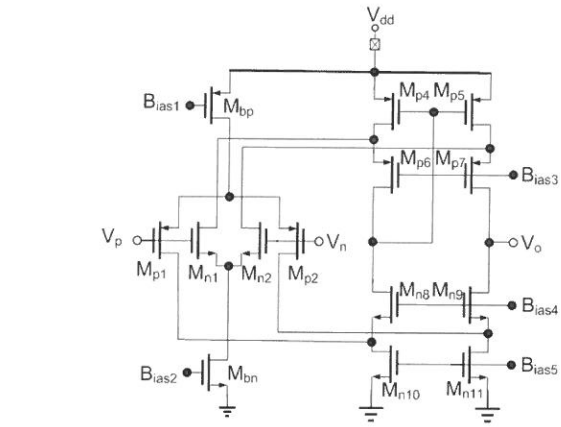

(a)

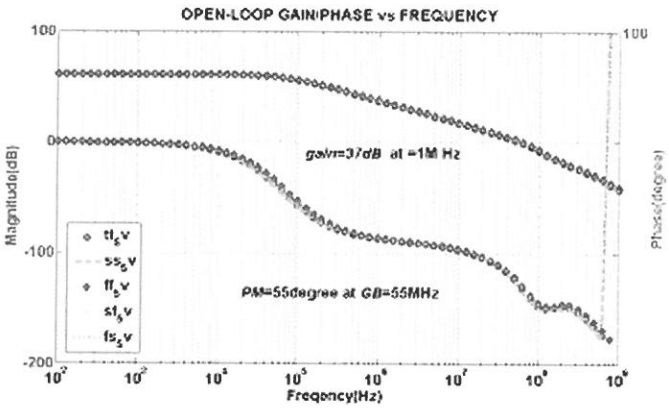

(b)

Figure 4.(a) A rail to rail folded cascode op circuit. (b) Vdd=3.6V Bode-plot simulation.

Since the average current sensing circuit requires a high-gain amplifier with full input swing, the rail to rail folded cascode amplifier [16-18] in Fig. 4(a) is adopted. The PMOS and NMOS input pairs enlarge the input range of the amplifier. When the input is at high potential (V_{dd}), the NMOS input pair is ON and the PMOS input pair is OFF. Conversely, as the input is at low potential (gnd), the PMOS input pair is ON and the NMOS input pair is OFF. In the switching power converter applications, the amplifier input is normally high potential (V_{dd}) and low potential (gnd), so both PMOS and NMOS input pairs do not conduct at the same time. Therefore, the constant transconductance biasing circuit is eliminated to simplify the amplifier design. Fig. 4(b) shows that as V_{dd} = 3.6V, 0.5pF capacitive loading case, the DC gain of the

amplifier is about 60dB in the post-simulated Bode plot. In the (TT, SS, FF, SF, FS) five corners, voltage gain of the amplifier is 37dB with a phase margin 50 at 1MHz input signal.

2.3.Driving circuit

The driving circuit is shown in Fig. 5(a). The applied synchronous buck conversion uses non-overlapping signals to prevent the large current from the simultaneous conduction of Power PMOS and NMOS. In Fig. 5(b), control signals V_{dh} and V_{dl} generated from the PWM signal, prohibit the Power PMOS and NMOS conducting at the same time. The Z_{cd} is the zero-current-detection signal [2]. As the inductor current is less than zero, the Z_{cd} is high. Then driving circuit turns M_{n1} OFF to prevent the reverse current. When V_{dh} is low, Z_{cd} is pulled to low at the end of the zero-current detection region.

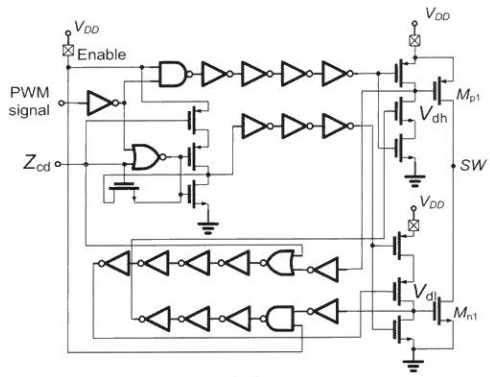

(a)

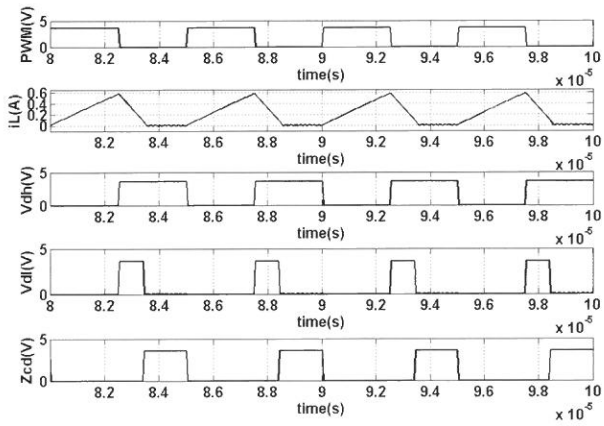

(b)

Figure 5.(a) Zero-current synchronous rectification control driving circuit. (b) Simulated zero current detection waveform .

3.Experimental Results

In this paper, the average current sensing circuit is fabricated with a TSMC 2P4M 0.35 μm CMOS technology. Fig. 6 shows the microphotograph of this current sensing circuit with power MOSs. The area occupation is about 1300 μm x 700 μm.

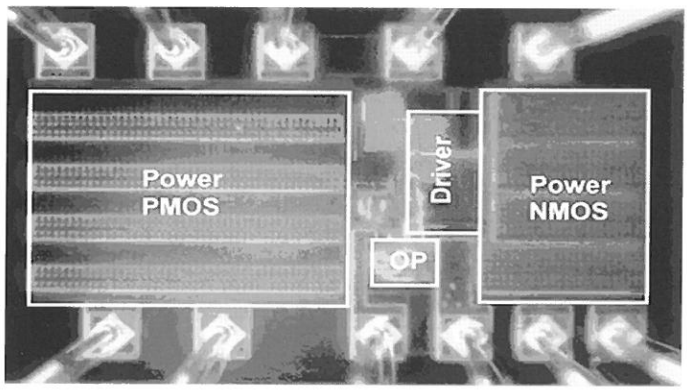

Figure 6.Chip microphotograph.

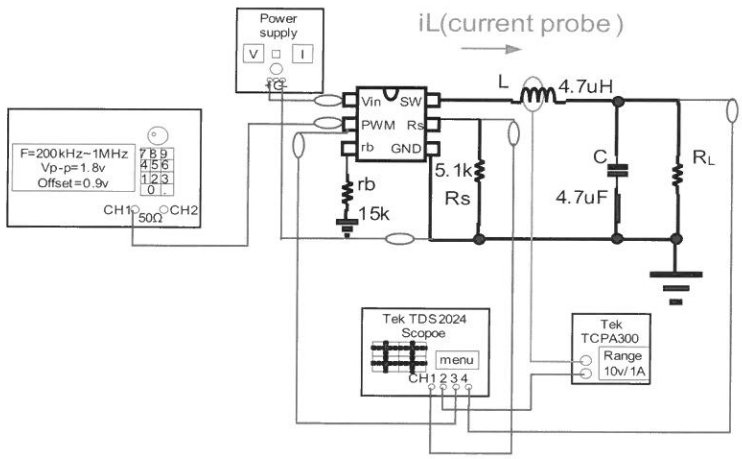

Figure 7.Test setup.

Fig. 7 demonstrates chip test setup. The inductor current sensing circuit realized in this paper senses the current of Power PMOS and Power NMOS at the ratio of 4500/1 and 5000/1, respectively. Accordingly, the designed ratio of sensed voltage, $V_{sens\ p\text{-}p}$, and the inductor current, $i_{Lp\text{-}p}$, is about unity as follows:

$$R_{sensp} = \frac{R_s}{N_p} = \frac{\left(\frac{W}{L}\right)_{M_{p3}}}{\left(\frac{W}{L}\right)_{M_{p1}}} \cdot R_s = \frac{\frac{20\mu}{0.5\mu}}{\frac{90000\mu}{0.5\mu}} \cdot 5.1k \cong 1 \ ,$$

$$\Rightarrow V_{sens} = I_{M_{p1}} \cdot R_{sensp} \approx I_{M_{p1}}$$

$$R_{sensn} = \frac{R_s}{N_n + 1} \approx \frac{R_s}{N_n} = \frac{\left(\frac{W}{L}\right)_{M_{n2}}}{\left(\frac{W}{L}\right)_{M_{n1}}} \cdot R_s = \frac{\frac{9\mu}{0.5\mu}}{\frac{45000\mu}{0.5\mu}} \cdot 5.1k \approx 1 \ ,$$

$$\Rightarrow V_{sens} = I_{M_{n1}} \cdot R_{sensn} \approx I_{M_{n1}}$$

The sensing resistor, R_s, is equal to 5.1 kΩ. The output inductor and the output capacitor is designed to 4.7 μH and 4.7 μF, respectively. The PWM signal is provided with the function generator and the input voltage, V_{in}, is provided with the DC power supply. The equivalent sensed current is measured in voltage, $V_{sens\ p\text{-}p}$, from the top node of R_S and the output current, $i_{Lp\text{-}p}$, is measured from the output inductor through the current probe. The loading resistor, R_L, is selected as 6.2Ω.

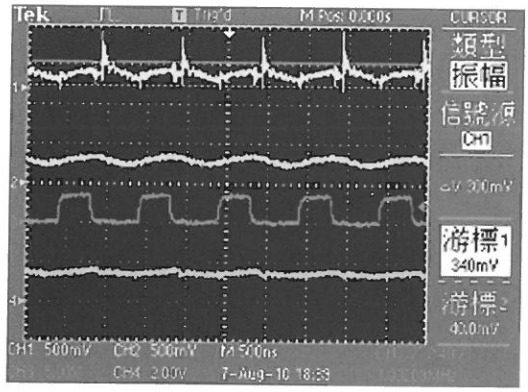
Tek
CURSOR
類型
振幅
信號源
CH1
游標1
340mV
游標2
CH1 500mV
CH2 500mV
M 500ns
CH4 200V
7-Aug-10 18:59

(a)

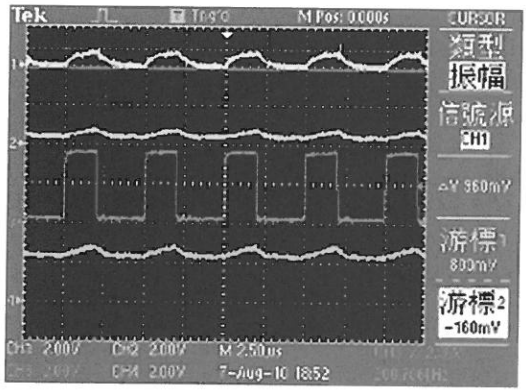
Tek
CURSOR
類型
振幅
信號源
CH1
游標1
800mV
游標2
-160mV
CH1 200V
CH2 200V
M 250ns
CH4 200V
7-Aug-10 18:52

(b)

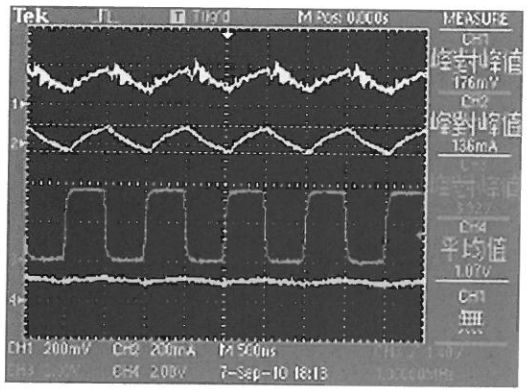
Tek
MEASURE
CH1
峰對峰值
176mV
CH2
峰對峰值
136mA
CH4
平均值
1.07V
CH1
無
CH1 200mV
CH2 200mA
M 500ns
CH4 200V
7-Sep-10 18:13

(c)

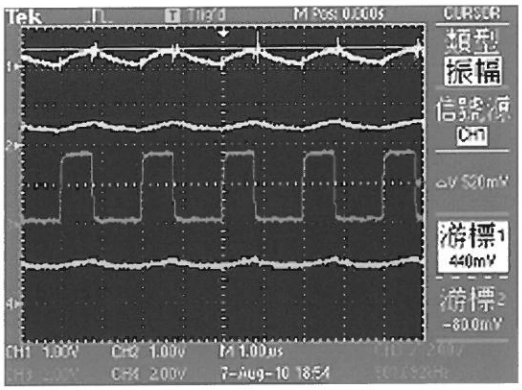

(c)

Figure 8. Measured waveforms. (The corresponding signals is $V_{sens\ p\text{-}p}$, $i_{Lp\text{-}p}$, PWM and V_o from upper part to lower part in the same scope.)

Table 1. Corresponding Experimental Results

V_{in}=3.6V	Figure 8(a)	Figure 8(b)	Figure 8(c)	Figure 8(d)
$V_{sens\ p\text{-}p}$	300mV	960mV	176mV	520mV
$i_{Lp\text{-}p}$	280mA	400mA	136mA	200mA
PWM	1MHz	200kHz	1MHz	501.1kHz
V_o	1.8V	2.4V	1.07V	2V
R_L	6.2Ω	6.2Ω	6.2Ω	6.2Ω

Table 2. Specification Summary

Technology	TSMC 2P4M 0.35µm
Input Voltage	3.6V
PWM Input Frequency	1MHz(Max)
Chip Area (including Pads)	1300µm x 700 µm
Power Consumption	1.92W(Max)

Table 3. Comparison of Current Sensing Technique

	[9]	[10]	[11]	[12]	[13]	[14]	This work
Technology (m)	N/A BiCMOS	TSMC 0.35μ	AMS 0.6μ	AMS 0.6μ	AMS 0.6μ	TSMC 0.35μ	TSMC 0.35μ
Input voltage (V)	N/A	2.7~5	3~4.2	3~5.2	1.2~2	3~6	3~5
Maximum load current (A)	1000m	500m	300m	450m	120m	750m	300m
Switching frequency (Hz)	N/A	1M	0.3M~1 M	0.3M~1 M	0.5M	1.8M	0.2M~1 M
Maximum power dissipation (W)	N/A	900m	N/A	N/A	N/A	2.442	1.92
Close loop Feedback	N/A	Yes	No	Yes	Yes	Yes	No
Sensing rise current	Yes	Yes	Yes	Yes	Yes	Yes	Yes
Sensing fall current	No	No	No	No	No	Yes	Yes
Chip area (including pads) (mm^2)	N/A	1.88	2.03*	2.87	4.87	2.16	0.91*

*only current sensing circuit

The experimental results are shown in Fig. 8 and Table 1. As V_{in} is set to 3.6V, the operating frequency is test within 200 kHz to 1 MHz. Though the ratio of the measured $V_{sens\ p\text{-}p}$ and the measured $i_{Lp\text{-}p}$ is larger than unity, the waveforms are similar in shape. This difference may be induced form the second ordered effect of the MOS transistors and the approximation of the designed parameters in the circuit. Such phenomenon causes the gain error but can be compensated in the closed-loop application of the averaging current mode buck converter. The chip specification is summarized in Table 2. The maximum input frequency of PWM is 1 MHz, and the maximum power consumption of this sensing circuit including the Power MOSs is about 1.92W at the input voltage of 3.6V. The comparison of the current sensing technique is summarized in Table 3.

4.Conclusion

This paper presents an average current sensing circuit for the switching buck converter. Because the positive half cycle and negative half cycle do not occur at the same time in switching buck converter, the Power PMOS and Power NMOS do not turn ON simultaneously. Using this property, this circuit applies a single rail to rail amplifier with negative feedback to equal the source and drain voltage of Power MOSs and mirrored transistors for current sensing. This approach saves the area and power dissipation of the sensing circuits.

Acknowledgment

The authors thank the support of National Science Council under the grant NSC 99-2221-E-030-021- , the chip fabrication assistance of National Chip Implementation Center (CIC), and Taiwan Semiconductor Manufacturing Company Limited (TSMC).

References

1. A. Pressman, K. Billings, and T. Morey, "Switching Power Supply Design," 3rd Ed., McGraw-Hill, 2009.
2. D. W. Hart, "Introduction to Power Electronics," Prentice Hall, 1997.
3. P. T. Krein, "Elements of Power Electronics," New York: Oxford University Press, 1998.
4. M. Brown, "Practical Switching Power Supply Design," San Diego, CA: Academic, 1990.
5. K. Billings, and T. Morey, "Switch mode Power Supply Handbook," 3rd Ed., McGraw-Hill. 1999.
6. N. Mohan, T. M. Undeland, and W. P. Robbins, "Power Electronics: Converters, Applications, and Design," John Wiley & Sons, Inc., 2003.
7. R. W. Erickson, and D. Maksimovic, "Fundamentals of Power Electronics," 2nd Ed., Springer, 2001.
8. R. Ridley, "Current mode or voltage mode?" Switching Power Magazine, pp. 4-5 Oct. 2000.
9. M. Corsi, "Current sensing schemes for use in BiCMOS integrated circuits," Proc. IEEE Bipolar/BiCMOS Circuit and Technology Meeting, pp.55-57, New York, 1995.

10. T. H. Liu and K. H. Chen, "High performance and minimized external pins in current mode DC-DC buck converter," Master thesis, NCTU, Hsinchu, 2006.
11. C. F. Lee and P. K. T. Mok, "On-chip current sensing technique for CMOS monolithic switch-mode power converter," Proceedings, IEEE Int. Symp. Circuits and Systems, vol. 5, pp. 265-268, May 2002.
12. C. F. Lee, and P. K. T. Mok, "A monolithic current-mode CMOS DC-DC converter with on-chip current-sensing technique," IEEE Journal of Solid-State Circuits, vol 39, pp.3-13, Jan. 2004.
13. C. Y. Leung, P. K. T. Mok, K. N. Leung, and M. Chan, "An integrated CMOS current-sensing circuit for low-Voltage current-mode buck regulator ," IEEE Transactions on Circuit and Systems II: Express Brief, vol 52, pp. 394-397, 2005.
14. J. J. Chen, F. C. Yang, C.C. Chen, "A new monolithic fast response buck converter using spike reduction current sensing circuit," IEEE Transactions. on Industrial Electronic, vol. 55, no. 3, Mar. 2008.
15. L. Dixon, "Average current-mode control of switching power supplies," Unitrode Power Supply Design Seminar Manual, 1990.
16. J. Huijsing, R. Hogervorst, and K-J. de Langen, "Low-power low-voltage VLSI operational amplifier cells," IEEE Transactions on Circuits and Systems, vol. 42, no. 11, pp. 841-852, Nov. 1995.
17. B. Razavi, "Design of Analog CMOS Integrated Circuits," McGraw-Hill, 2001.
18. P. R. Gray, P. J. Hurst, S. H. Lewis, and R. G. Meyer, "Analysis and Design of Analog Integrated Circuits," 5th Ed., John Wiley & Sons, Inc., 2010.

Received September 30,2010
Revised March 3,2011
Accepted April 11,2011

適用於平均電流模式直流對直流降壓轉換器的電流感測電路

劉至剛　沈鼎嵐

輔仁大學 電機工程學系

摘　要

本文提出一個適用於平均電流模式直流對直流降壓轉換器的電流感測電路。此電路在不同的工作時段，使用單一個操作在負迴授的軌對軌放大器迫使金氧半功率電晶體與鏡射電晶體的汲源極電壓相等，因而感測出電感電流。此感測電路採用 TSMC 2P4M 0.35 μm CMOS 製程技術製造。實際量測結果顯示，在切換頻率從 200 kHz 到 1 MHz 之間及輸入電壓為 3.6V 的情況下，電感電流可由感測電路感測出相對應的電流。

關鍵字：電流感測，平均電流模式，直流對直流降壓轉換器。